

A NEW BRAZILIAN ENERGY PORTFOLIO: THE CASE FOR SUN AND WATER

By

Erik Jacob Brown

A DISSERTATION

Submitted to  
Michigan State University  
in partial fulfillment of the requirements  
for the degree of

Mechanical Engineering – Doctor of Philosophy

2021

## ABSTRACT

### A NEW BRAZILIAN ENERGY PORTFOLIO: THE CASE FOR SUN AND WATER

By

Erik Jacob Brown

The Amazon is a delicate ecosystem that has global-scale environmental and climatological impact, and is at risk of overdevelopment, over-modification and destruction. Issues associated with the installation and operation of traditional reservoir-dam systems in the Amazon are examined, and it is suggested to supplement the current Brazilian energy portfolio and replace future dam plans with hybrid in-stream generator and photovoltaic systems to provide for distributed renewable microgrids as well as on-grid power needs. These systems can be installed at various scales, from a single-household off-grid implementation, up through and including offsetting or replacing current and future planned large-scale dams for on-grid use. This solution offers a socially and environmentally safer alternative to dams, by reducing or eliminating several issues with reservoir-based dams: deforestation for reservoirs, flooding from reservoirs, displacement of local families, inhibition of sediment and marine life transport, and greenhouse gas emissions. The financial and energetic feasibility of the proposed system is compared, including transmission costs, to several common electrification methods. Other supporting topics are also investigated, such as the fish-friendly design of in-stream devices, and the maximum reach of the proposed hybrid microgrid system relative to the in-stream deployment sites.

This is dedicated to my darling wife Kathryn, to our cherished children who are here and on their way, and to all of those who helped and supported me along the way.

## ACKNOWLEDGEMENTS

I would like to thank my NSF project sponsors for the wonderful opportunity to take part in this project. A special thanks to Dr. Müller for recognizing and providing me with the project, time, and wisdom you shared throughout my degree.

## TABLE OF CONTENTS

LIST OF TABLES . . . . .	viii
LIST OF FIGURES . . . . .	ix
CHAPTER 1 INTRODUCTION . . . . .	1
1.1 Environmental and Social Issues with Dams . . . . .	4
1.1.1 Environmental Issues with Dams . . . . .	4
1.1.1.1 Deforestation and Flooding . . . . .	4
1.1.1.2 Sediment Transport Blockage . . . . .	5
1.1.1.3 Greenhouse Gas Emissions . . . . .	5
1.1.2 Ecological Impact . . . . .	6
1.1.3 Social Issues with Dams . . . . .	6
1.1.3.1 Displacement by Flooding . . . . .	7
1.1.3.2 Displacement by Food Source Change . . . . .	7
1.1.3.3 Displacement by Modernization . . . . .	7
1.1.3.4 Awareness of Local Issues . . . . .	7
1.2 Drivers . . . . .	8
CHAPTER 2 SUGGESTED ENERGY PORTFOLIO . . . . .	9
2.1 Current Brazilian Amazon Basin Energy Situation . . . . .	9
2.1.1 Current Energy Portfolio . . . . .	9
2.1.2 Generation Plants Distribution . . . . .	10
2.1.3 Amazonian Energy Potential . . . . .	11
2.1.3.1 Hydraulic Energy Potential . . . . .	11
2.1.3.2 Photovoltaic and Eolic Energy Potential . . . . .	12
2.1.3.3 Bio-Energy Potential . . . . .	12
2.2 Recommended Energy Enhancement . . . . .	14
2.2.1 Local Communities: Off-Grid Solution Methodology . . . . .	14
2.2.1.1 Load Development . . . . .	17
2.2.1.2 Equipment selection and preliminary financial analysis . . . . .	22
2.2.1.3 Generation Determination and Detailed Financial Analysis . . . . .	25
2.2.1.4 Off-grid microgrids: the natural reach of rivers . . . . .	46
2.2.2 Financial Interests: On-Grid Solution Methodology . . . . .	49
2.2.2.1 Load Development . . . . .	50
2.2.2.2 Generation Determination . . . . .	50
2.2.2.3 Financial Analysis and Discussion . . . . .	52
CHAPTER 3 ENHANCEMENT OF GRID STABILITY WITH FLOATING SOLAR PANELS . . . . .	55
3.1 Background . . . . .	55
3.2 An Overview of the Current Brazilian Electric Power System . . . . .	59

3.2.1	Underproduction of Dams . . . . .	60
3.2.2	Wind and PV Power in Brazil . . . . .	62
3.3	Environmental and Social Impact of Dams . . . . .	66
3.4	Floating PV Systems on Hydropower Dam Reservoirs . . . . .	67
3.5	Generation Adequacy Assessment . . . . .	69
3.6	System Modeling . . . . .	70
3.6.1	Wind Turbine Output Power . . . . .	71
3.6.2	Output Power of PV Systems . . . . .	72
3.6.3	Generation Model . . . . .	73
3.6.4	Load Model . . . . .	74
3.6.5	Generation Reserve Model . . . . .	75
3.7	Case Studies . . . . .	76
3.7.1	Capacity factor of PV system at the proposed locations . . . . .	76
3.7.2	Attributes of PV power to the peak load shaving . . . . .	77
3.7.3	System adequacy . . . . .	78
3.7.3.1	System reliability indices—current system—2018 . . . . .	83
3.7.3.2	System reliability indices—2023 projection . . . . .	84
3.7.4	Results and Discussion . . . . .	85
3.8	Conclusion . . . . .	86
CHAPTER 4 IN-STREAM TURBINES AS FISH-FRIENDLY TECHNOLOGY . . . . .		88
4.1	Background . . . . .	88
4.2	Turbine Installation . . . . .	89
4.2.1	Dam Turbine . . . . .	89
4.2.2	Run-of-River Turbine . . . . .	90
4.2.3	In-Stream Turbine . . . . .	90
4.3	Fish Injury Mechanisms . . . . .	92
4.3.1	Physical Strike . . . . .	92
4.3.2	Pressure Changes . . . . .	94
4.3.3	Shear . . . . .	96
4.3.4	Turbulence . . . . .	97
4.3.5	Current Traditional Configuration Fish-Friendly Designs . . . . .	97
4.3.6	Sound . . . . .	98
4.4	Fish Safe Turbine Design . . . . .	98
4.4.1	Physical Strike . . . . .	99
4.4.2	Pressure Change, Shear, and Turbulence . . . . .	101
4.4.3	Sound . . . . .	102
4.4.4	Bypasses and Ladders . . . . .	104
4.4.5	In-Stream Turbines in Farms . . . . .	106
4.4.6	Electromagnetic Emissions . . . . .	106
4.5	Marine Safety and Aquatic Health . . . . .	107
4.6	Literature Summary . . . . .	107
4.7	Design . . . . .	108
4.8	Simulation . . . . .	111
4.8.1	Model and Mesh . . . . .	111

4.8.2	Setup . . . . .	111
4.8.3	Results . . . . .	116
4.8.3.1	Power Coefficient . . . . .	117
4.8.3.2	Pressure . . . . .	118
4.8.3.3	Strain Rate . . . . .	119
4.8.4	Postprocessing Routine . . . . .	121
4.8.4.1	Method . . . . .	121
4.8.4.2	Output . . . . .	122
4.8.4.3	Discussion . . . . .	123
4.8.5	Conclusion . . . . .	127
CHAPTER 5 CLOSING REMARKS AND GLOBAL IMPLICATIONS . . . . .		130
APPENDICES . . . . .		131
APPENDIX A	GIS File Sources . . . . .	132
APPENDIX B	MATLAB Sample Script . . . . .	133
APPENDIX C	Excel VBA Sample Script . . . . .	163
BIBLIOGRAPHY . . . . .		187

## LIST OF TABLES

Table 2.1: Cables used as basis for investigation . . . . .	46
Table 3.1: Current installed power capacities and projection of capacity planning increase by year 2023 . . . . .	60
Table 3.2: Dams underproduction . . . . .	63
Table 3.3: Installed PV capacity and the horizontal solar irradiation for different countries . . . . .	65
Table 3.4: Brazilian system data . . . . .	81
Table 3.5: Annual reliability indices of IEEE-RTS . . . . .	81
Table 3.6: Annual reliability indices of the system before and after adding FPV system	83
Table 3.7: Annual reliability indices of the system with load increase . . . . .	83
Table 3.8: Annual reliability indices of the system with load increase <i>2023-projection</i>	84
Table 3.9: SRIF considering different reliability indices . . . . .	85
Table 4.1: Turbine Design Parameters . . . . .	110

## LIST OF FIGURES

Figure 1.1: The Amazon Basin and the Amazon Extended or Legal Basin . . . . .	2
Figure 1.2: The Amazon Extended or Legal Basin and major South American rivers	3
Figure 2.1: The 2017 Power Capacity of the Brazilian SIN (source: [126]) . . . . .	10
Figure 2.2: The current and future power lines of the SIN (source: [125]) . . . . .	11
Figure 2.3: Brazilian isolated system locations (source: [125]) . . . . .	12
Figure 2.4: Snapshot of Brazilian energy balance (source: [123]) . . . . .	13
Figure 2.5: Operational Generation Plants in Brazilian Amazon (source: [9]) . . . . .	14
Figure 2.6: Operational Hydraulic Plants and Transmission Lines in Brazilian Amazon (source: [9]) . . . . .	15
Figure 2.7: The Legal Amazon and major Brazilian sub-basins . . . . .	16
Figure 2.8: The hydraulic potential in Brazil (source: [7]) . . . . .	17
Figure 2.9: The direct normal solar irradiation potential in the Amazon, assuming an overall 12% conversion efficiency (data source: [111]) . . . . .	18
Figure 2.10: The eolic potential in the Amazon at 50 meter height, assuming an overall 45% conversion efficiency (data source: [111]) . . . . .	19
Figure 2.11: Amazonian energy solution portfolio . . . . .	20
Figure 2.12: Pictorial comprisal of assumed off-grid load with one possible scenario of usage times . . . . .	20
Figure 2.13: Temporal curve of assumed off-grid load . . . . .	21
Figure 2.14: Option for possible load by utilizing smart load management system . . .	22
Figure 2.15: Developed load models 1-8. The y-axis is the power consumption, in watts, and the x-axis is the time of day, in hours. The green curve represents the optimal total generation calculated, comprised of the yellow (PV) and blue (in-stream) curves, that meet or exceed the load (the black curve). . . . .	23

Figure 2.16: Potential “excess power” available for future load reduction . . . . .	23
Figure 2.17: Developed load models 1-8. The y-axis is the power consumption, in watts, and the x-axis is the time of day, in hours. The green curve represents the optimal total generation calculated, comprised of the yellow (PV) and blue (in-stream) curves, whose integrated power-time area meets that for the load (the area under black curve). . . . .	24
Figure 2.18: Single household load profile with suggested generation profiles . . . . .	29
Figure 2.19: Curve of base cost over the investigated range of flow velocities, costs calculated over a 30 year equipment lifespan . . . . .	29
Figure 2.20: Locations of sample sites overlaid on top of river paths, with markers representing the river velocity available at that location, based on $Q_{90}$ . . . . .	38
Figure 2.21: Comparison of proposed UPC solution (green diamonds) with several common energy generation and distribution methods. The costs associated with the electric grid extension is shown by the purple range, a diesel generator is shown by the brown range and the 2019 Brazilian North region residential and rural tariffs are shown by the black range. The x-axis is the distance from the community to the nearest existing transmission line, in km, and the y-axis is the calculated cost in USD/kWh over 30 years. . . . .	39
Figure 2.22: Comparison of proposed UPC solution (green diamonds) with several common energy generation and distribution methods. Dam construction with distribution lines is shown by the gold range, with no underreporting factor included; the other ranges are the same as 2.21. The x-axis is the distance from the community to the optimal in-stream generation site, in km, and the y-axis is the calculated cost in USD/kWh over 30 years. . . . .	40
Figure 2.23: Comparison of proposed UPC solution (green diamonds) with several common energy generation and distribution methods. A new dam construction with distribution lines is shown by the gold range, with an underreporting factor of 1.96 USD/USD included, a diesel generator is shown by the brown range and the 2019 Brazilian North region residential and rural tariffs are shown by the black range. See Figure 2.22 for axes. . . . .	41

Figure 2.24: Comparison of proposed PC solution (green diamonds) with several common energy generation and distribution methods. The costs associated with the electric grid extension is shown by the purple range, a diesel generator is shown by the brown range and the 2019 Brazilian North region residential and rural tariffs are shown by the black range. See Figure 2.21 for axes. . . . .	42
Figure 2.25: Comparison of proposed PC solution (green diamonds) with several common energy generation and distribution methods. A new dam construction with distribution lines is shown by the gold range, with no underreporting factor included, a diesel generator is shown by the brown range and the 2019 Brazilian North region residential and rural tariffs are shown by the black range. See Figure 2.22 for axes. . . . .	43
Figure 2.26: Comparison of proposed PC solution (green diamonds) with several common energy generation and distribution methods. A new dam construction with distribution lines is shown by the gold range, with an underreporting factor of 1.96 USD/USD included, a diesel generator is shown by the brown range and the 2019 Brazilian North region residential and rural tariffs are shown by the black range. See Figure 2.22 for axes. . . . .	44
Figure 2.27: Reach of lossless cables at various goal cost of energy levels . . . . .	49
Figure 2.28: Load model development process for on-grid system . . . . .	51
Figure 2.29: Load model development process for on-grid system . . . . .	53
Figure 2.30: Load model development process for on-grid system . . . . .	54
Figure 3.1: Brazilian interconnected system [130]. . . . .	61
Figure 3.2: Direct normal irradiation in Brazil from 1999–2015 [193]. . . . .	64
Figure 3.3: Global horizontal irradiation in Brazil from 1999–2015 [193]. . . . .	65
Figure 3.4: Potential of average Photovoltaic power in Brazil from 1999–2015 [193]. . . . .	66
Figure 3.5: Percentage of potential wind power in Brazil [193]. . . . .	67
Figure 3.6: Integrated PV system with hydropower installed capacity worldwide. . . . .	68
Figure 3.7: Floating PV system on reservoir in which marine life and fishing activity are not disrupted by placing PV systems on the reservoir. . . . .	69

Figure 3.8: Capacity factor of PV system at several dam locations—A . . . . .	77
Figure 3.9: Capacity factor of PV system at several dam locations—B . . . . .	78
Figure 3.10: Capacity factor of PV system at several dam locations—C . . . . .	79
Figure 3.11: Capacity factor of PV system at several dam locations—D . . . . .	80
Figure 3.12: Contribution of grid-connected PV system to daily peak shaving . . . . .	80
Figure 3.13: Attribution of grid-connected PV system to assist Hydropower peak load shifting . . . . .	81
Figure 4.1: Canonical fish injury risk mechanisms (from: [36]) . . . . .	89
Figure 4.2: Schematics of turbine configurations (a) cross-section of a dam or run- of-river housing, (b) traditional dam, (c) run-of-river, (d) in-stream turbine	91
Figure 4.3: Survival of rainbow trout ( <i>Oncorhynchus mykiss</i> ) based on strike speed (modified from: [6]) . . . . .	93
Figure 4.4: Dose-Response chart of mortality vs. pressure for juvenile Chinook salmon, in terms of the ratio of acclimation to minimum pressures, and the natural log of the ratio on the bottom axis (modified from: [32]) . . . . .	95
Figure 4.5: Experiment to quantify tolerable shear stresses on fish (from: [112]) . . . . .	96
Figure 4.6: A Moon Wrasse ( <i>Thalassoma lunare</i> ) evading an in-stream turbine (from: [79]) . . . . .	99
Figure 4.7: Pressure Traces at Various Radii along a Tidal Stream Turbine. The legend shows the radial distances in terms of the ratio of a given radius to the tip radius. (modified from: [198]) . . . . .	102
Figure 4.8: Shear rate of tidal stream turbine (from: [198]) . . . . .	102
Figure 4.9: Sound levels measured in the Mississippi River near Memphis, 75 meters away from the barge and 21 meters from the turbine, shown by the solid lines without markers. The lines with markers show the hearing ability of certain fish. (from: [21]) . . . . .	104
Figure 4.10: Ducted rotor model from three views: flow direction, oblique and top . . . . .	112

Figure 4.11: Cross-section of the in-stream generator, with a simplified rim-drive generator. The black blocks are bearings, the dark blue blocks are magnets (rotating with the blades), and the red blocks are the stator windings and core (stationary with shroud). . . . .	113
Figure 4.12: In-stream generator in a river channel . . . . .	113
Figure 4.13: Numeric domain . . . . .	114
Figure 4.14: Ducted rotor mesh: domain side view . . . . .	114
Figure 4.15: Ducted rotor mesh: rotor blade view . . . . .	115
Figure 4.16: Massflow rate difference between inlet and outlet normalized by inlet massflow rate over iteration count . . . . .	116
Figure 4.17: Torque coefficient over iteration count . . . . .	117
Figure 4.18: Plot of power coefficient over tip speed ratio, based on the rotor and duct areas . . . . .	118
Figure 4.19: Plot of pressure ratio over tip speed ratio, at three acclimation pressures: 1 atm, 1.5 atm, and 2 atm . . . . .	119
Figure 4.20: Plot of maximum negative pressure rate of change over tip speed ratio. . . . .	120
Figure 4.21: Plot of maximum domain strain rate over tip speed ratio . . . . .	121
Figure 4.22: Plot of percent of blade surrounding volume above criteria of 495 1/s over tip speed ratio . . . . .	122
Figure 4.23: Designed triangle velocities over blade span . . . . .	123
Figure 4.24: Designed blade angle difference across blade over blade span . . . . .	124
Figure 4.25: Comparison of designed blade triangle velocities with CFD output . . . . .	124
Figure 4.26: Spanwise profiles of angular difference between design and CFD output . . . . .	125
Figure 4.27: Relative flow velocity vectors and contours at 10% square radial span . . . . .	125
Figure 4.28: Relative flow velocity vectors and contours at 50% square radial span . . . . .	125
Figure 4.29: Relative flow velocity vectors and contours at 90% square radial span . . . . .	126

Figure 4.30: Relative flow velocity streamlines and contours at 10% square radial span	126
Figure 4.31: Relative flow velocity streamlines and contours at 50% square radial span	126
Figure 4.32: Relative flow velocity streamlines and contours at 90% square radial span	127
Figure 4.33: Relative flow velocity vectors and contours at 10% square radial span, using nodal values . . . . .	127
Figure 4.34: Relative flow velocity vectors and contours at 50% square radial span, using nodal values . . . . .	128
Figure 4.35: Relative flow velocity vectors and contours at 90% square radial span, using nodal values . . . . .	128

# CHAPTER 1

## INTRODUCTION

The Amazon Basin is the largest drainage basin in the world, with an area of 7.8 million square kilometers [197]. The Amazon is made up of eight countries: Brazil, Bolivia, Peru, Ecuador, Guyana, Venezuela, and Suriname. Within Brazil, which accounts for around 64% of the Amazon Basin's area [197], eight states are within the bounds of the Amazon: Amazonas, Para, Maranhao, Rondonia, Roraima, Acre, Amapa, Mato Grosso, and also a ninth state, Tocantins, if the so-called 'Legal Amazon' is considered (see Figures 1.1 and 1.2 for visuals of the regions of interest, with and without rivers shown, and Appendix A for shapefile sources). The Amazon Basin also contains the world's largest rainforest, covering 6.7 million square kilometers, and is home to tens of thousands of species of mammals, fish, insects, and plant life [40]. Often referred to as "Earth's lungs", the Amazon region is a crucial ecosystem, whose health can largely determine the environmental and climatological health of the rest of Earth as well. Due to Brazil containing most of the area of the Amazon, the policies and actions of the Brazilian government and peoples have a large effect on the overall health of the Amazon. Misuse of the natural resources of the Brazilian Amazon have been a historical issue, and still persist. Misuse can have several forms: deforestation for land use, poaching and wildlife trading, excessive mining, water and air pollution, and introduction of overly-invasive power generation systems. Due to the intense public effort of the Brazilian government over the last 15 years to increase its citizens' quality of life and protection against misuse of the natural resources within their borders, focusing on the Brazilian portion of the Amazon, called the Brazilian Amazon Basin from here on, can be an effective indicator of the Amazon as a whole. The Brazilian government and related individual institutions release several crucial datasets with information on: population, national power grid (called the National Interconnected System, or SIN from the Portuguese wording), deforestation, energy availability, and utilization of natural resources. With the aforementioned information, it is



Figure 1.1: The Amazon Basin and the Amazon Extended or Legal Basin

possible to make conclusions about what the current and possible future energy resources and needs are in the Brazilian Amazon Basin, which can act as a proxy for the rest of the Amazon, where data may not be as readily available.

The questions of interest here are: who needs (and wants) electric power, how much do they need, how to get them power, and at what cost (financially, socially, and environmentally)? The Brazilian government addressed some these issues in 2003 with the start of the Light for All program (Luz para Todos, or LPT, in Portuguese). The goal of LPT was, similar to its predecessor, Luz para Campo, to increase rural electrification in Brazil, headed by the Ministry of Mines and Energy (MME) department. According to the 2010 Brazilian census, LPT reached approximately a 98.7% electrification rate in Brazil [86]. The increase in electrification rate was achieved primarily in two ways: increasing the stock of large-scale

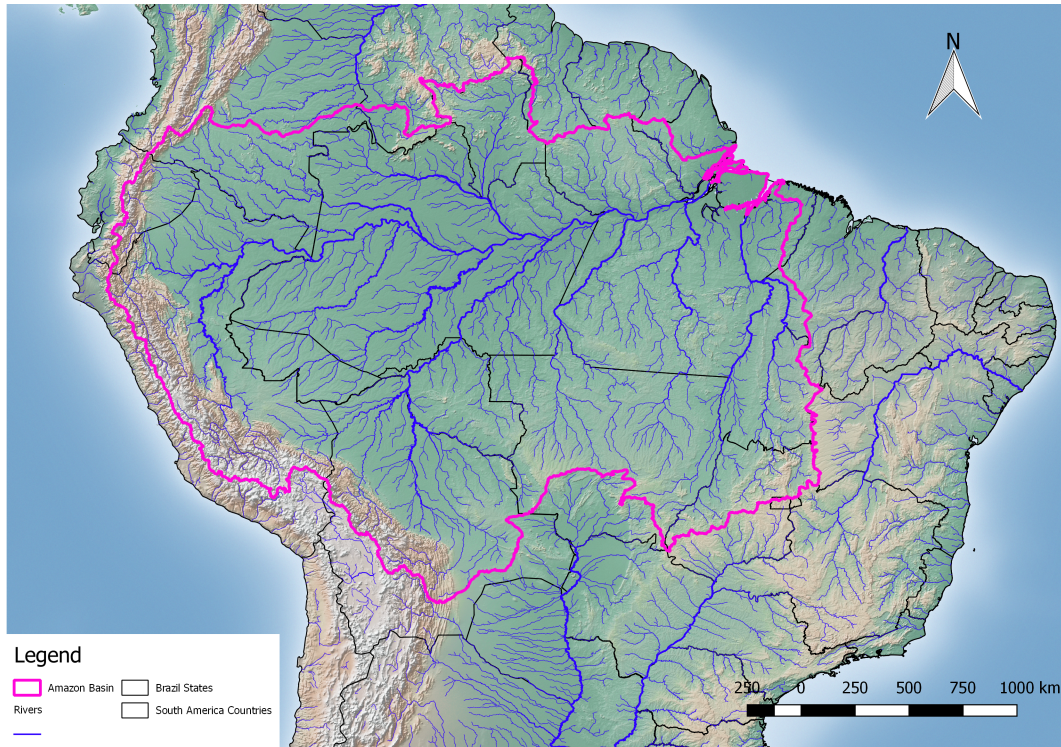


Figure 1.2: The Amazon Extended or Legal Basin and major South American rivers

hydraulic power, and providing small thermal generators for off-grid communities. Though this methodology may have partially solved the issue of getting power to the people in need, it did not answer the question of what social and ecological costs the solution has. Some of the costs associated with the large scale hydropower and distributed thermal systems are: displacement of families and communities from reservoir construction, disruption of sediment and ecological transport, enhanced greenhouse gas emission, and risk of environmental spill while transporting thermal stock. These issues are reviewed in Section 1.1.

With these social and environmental costs in mind, naturally another question arises of how should the increase in power demand be met in the future? Should Brazil continue with the same methodology, or change to a new outlook for energy generation? Authors such as [115] recommend changing to a “biomimetic” viewpoint, meaning modeling practices and resource utilization with natural processes. These ‘natural’ systems can include: solar, wind, biomass, and in-stream (also called hydrokinetic) turbines. The generation systems

that are not considered to embody the spirit of “biomimicry” can include traditional reservoir-based hydropower dams and thermal systems that require risky fuel transport or harmful environmental emissions. In Brazil, the non-‘natural’ methodology has been traditionally employed, with large dam hydropower leading the country’s energy market.

Future installed power generation systems should be sized and located carefully for a realistic and reasonable use of the produced power. In other words, there needs to be separate consideration for power “for the people” and power that is required by big industry and metropolis. For individual families or communities in the Amazon, small systems (on the order of 500 Watts per person/household) should be implemented, and for big industry or financial interests, scaled-up versions of similar systems can be utilized. In particular, in-stream turbines and photovoltaic systems are examined here as flexible and friendly options at both scales, which can reduce or eliminate further social and environmental implications of energy generation in Brazil. This will be discussed further in Chapter 2.

## **1.1 Environmental and Social Issues with Dams**

### **1.1.1 Environmental Issues with Dams**

It is a commonly held belief that all hydropower is completely ‘green’ and ‘friendly’, however, it is not entirely true. Dam (and thus reservoir) based hydropower systems present several environmental issues: deforestation and flooding, sediment transport blockage, greenhouse gas emission, as well as several ecological issues, such as fish migration blockage, marine life injury risk due to the turbines, and also behavior changes due to the presence of the dam and turbines.

#### **1.1.1.1 Deforestation and Flooding**

In order to produce the elevation change designed to drive the turbines in a dam at a given water flow rate, and to help combat low water levels during water shortage events, reservoirs

are dug from the ground and are filled up from the supplying river. The material removal process often requires nearby forest and fauna to be removed along with the soil, resulting in deforestation that is proportional to the area of the reservoir. The area of excavation will then flood with water from the river that will stagnate at the dam. Depending on the season and on the climatological conditions, the water level will rise and fall, resulting in a partially filled reservoir, or depending on the efficacy of the planning for the maximum flooded volume, could result in the local area becoming inundated with flood water that spilled out of the reservoir. The modified landscape of the new water-land interface will also shift over time, due to the motion of the water in the reservoir flowing towards the dam and over the nearby land, causing more deforestation; the trees, fauna, and loosened sediments will be introduced into the reservoir, where they will either sink to the bottom and build up over time, or will continue downriver over the spillway.

#### **1.1.1.2 Sediment Transport Blockage**

Due to their generally higher density compared to water, sediments tend to sink to the bottom of rivers and reservoirs, and will travel near to the riverbed. Without the presence of a dam, the sediments that move along the riverbed would transport towards the ocean where they would be buried. With dams installed, however, these sediments cannot pass by as easily, and instead they build up in the reservoir in front of the dam.

#### **1.1.1.3 Greenhouse Gas Emissions**

Tropical biomes such as the Amazon, containing most of the world's wetlands, are major producers, transporters, and sinks of carbon due to their high temperatures, precipitation rates, humidity, stocks of biomass, among other factors [120]. The vast areas of wetlands and rivers in the Amazon have been found to be major contributors in the global carbon cycle, contributing an estimated 470 Tg of carbon (C) from carbon dioxide (CO<sub>2</sub>) riverine evasion [148] and 42.7 Tg of methane (CH<sub>4</sub>) each year [132]. This large potential for carbon emission

in the natural carbon cycle has been hypothesized to be disrupted by the introduction of dams. It has been shown that the deforestation associated with the creation of the dam reservoirs leads to enhanced greenhouse gas emissions to the atmosphere [74]. Showing whether reservoir-based dams in general lead to a net source or sink of carbon (in the form of CH<sub>4</sub> and CO<sub>2</sub>) has not been made concrete in the literature yet. Measurements have been taken to calculate the gross emissions once dams are installed, however, net emissions require measurements from before and after the dams were installed, which has been performed on only one tropical dam: the Petit Saut project in French Guiana [1]. Another issue with the current literature is that not every source of carbon was considered in each experiment: for a full, consistent comparison at each dam, diffusion and ebullition (bubbling) of both CH<sub>4</sub> and CO<sub>2</sub>, both upstream and downstream of the dam need to be measured [65].

### **1.1.2 Ecological Impact**

Dams present several ecological risks to local marine life:

- Habitat and migration blockage
- Physical injury
- Behavior impact

These impacts will be reviewed in detail in Chapter 4.

### **1.1.3 Social Issues with Dams**

Along with the environmental issues associated with dam-based hydropower, there are also several social issues: household displacement by flooding, food source changes, or by local changes to the social or physical infrastructure (‘modernization’), as well as diverting awareness of local issues away from the area, such as for access to electricity.

### **1.1.3.1 Displacement by Flooding**

The most immediate issue for households near to dam projects is flooding. When the reservoir is created, nearby land might have to be converted to flooded area to provide for the dam required height, depending on the dam design and the local landscape. Additionally, the dam designers may not have accounted for the extremity of seasonal changes in climate and river hydraulics or the exact contour of the land surrounding the reservoir that should not be flooded, which may result in a larger area becoming flooded than originally planned.

### **1.1.3.2 Displacement by Food Source Change**

As was mentioned in Section 1.1.1, one of the environmental issues with dams is the blockage of migrating fish. The communities that rely on the marine life may lose their common fishing spots, and would have to move further away from home, allowing less time each day to collect food [38].

### **1.1.3.3 Displacement by Modernization**

A generally slower developing, but equally concerning issue with the development of dams is the social transformation of the area local to the project site. The transformations can include, but are not limited to: conversion of undeveloped areas into tourist sightseeing locations, settling of local area by project workers, or constrictive purchase of lands surrounding existing communities for project or public use [64].

### **1.1.3.4 Awareness of Local Issues**

With the introduction of dams, it is possible that the outside view of the local people may shift; it could be seen that because they are close to a large power producing structure, that they do not need further assistance for access to electricity; it could even go as far as being viewed as wealthy or well-off, simply due to being close to a dam. However, the reality is

that even in well-developed areas, the communities close to a dam and transmission line may still not have access to electricity, and may rely on traditional means for daily life, such as kerosene lamps instead of electric lights [60].

## 1.2 Drivers

The Brazilian Energy Research Company (EPE in Portuguese) estimated that there is almost 2 GW of traditional hydropower planned to be built in the Brazilian Amazon Basin between 2018 and 2027, as well as over 3000 km of powerlines planned [51]. The amount of planned hydropower increases to over 8 GW when considering hydropower that are in various other stages of planning, that could be accepted into the Brazilian ten-year plan at any time [9]. It can be shown that at the 2010 Brazilian electrification rate, it is possible to provide electricity to all households that were reported to be without energy by installing or providing grid connections of approximately 500 MW of rated power (see Section 2.2.1). This difference in planned versus needed power for the people demonstrates the need to ask questions posed in Section 1, namely, where is the planned power going and who is it benefitting? The goal of this work is to suggest and investigate alternatives to current centralized dam-based power plans, in order to provide the greatest benefit to both the local communities in need of electricity access, as well as the growing financial interests in the Amazon while also to reducing or eliminating environmental and social impacts.

## CHAPTER 2

### SUGGESTED ENERGY PORTFOLIO

## 2.1 Current Brazilian Amazon Basin Energy Situation

### 2.1.1 Current Energy Portfolio

As of 2017, there are two dominating power generation sources in Brazil; 68% of the energy feeding into Brazil's national power grid is from hydropower, and 22% is from thermal systems (oil, gas, biomass, etc.) as is shown in Figure 2.1 [126]. The remaining 10% is from all other forms of energy: wind, solar, nuclear, and others. The most dramatic change in power plans for the future is for solar: there is a nearly 4-fold planned increase in the solar capacity for the grid. The planned increase in solar is still relatively small compared to the 11 GW of possible dam-based hydropower planned over the same time frame. To distribute the generated power to the country, the current national electric grid extends eastward and southward from the cities of Porto Velho and Manaus, towards the eastern border and southern tip of Brazil. The area between and westward of those two cities and also north of Manaus is nearly devoid of grid connections, as can be seen in Figure 2.2. The area between Manaus and Porto Velho is shown to have no plans for transmission line extension; however, it is unlikely that this will remain undeveloped in the future, due to the high hydraulic potential in the Madeira and Tapajós rivers. There are also off-grid systems (called isolated systems by ONS, the Brazilian electric grid operating government agency) to provide power for the people who were not given a connection to the current electric grid. These off-grid systems can comprise one or more of the following: thermal or gas generators, water turbines, solar panels, or wind turbines. Brazil provides power to at least 246 of these off-grid sites, almost all of which are supplied by thermal and diesel generators, servicing approximately 760,000 citizens [128]. A visualization of the locations of the off-grid systems

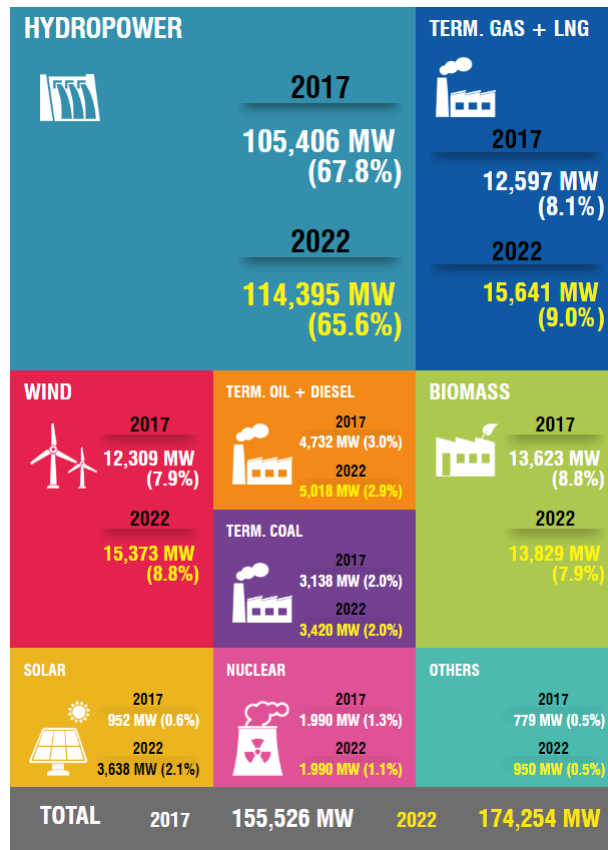


Figure 2.1: The 2017 Power Capacity of the Brazilian SIN (source: [126])

in 2009 can be found in Figure 2.3. It is to be noted that although Figure 2.2 shows that there are plans to extend the national grid from Manaus northward into Roraima, Brazil currently does not classify the state of Roraima as being ‘on-the-grid’, and all power in Roraima is generated by off-grid means.

### 2.1.2 Generation Plants Distribution

The power for the grid comes from various plants throughout Brazil, and is redistributed among the different regions of Brazil (North, South, etc.), as is shown in Figure 2.4. The excess energy is then exported to neighboring countries. It can be inferred from Figure 2.2 that Brazil intends to increase their energy trade with other South American countries, due to the planned transmission line leading north into Venezuela. The possible future electric

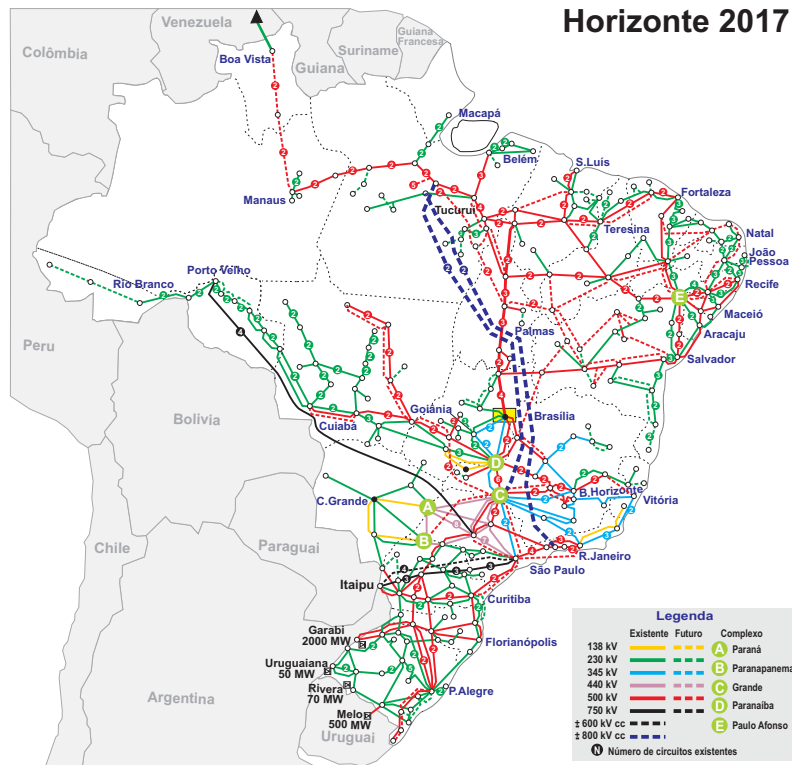


Figure 2.2: The current and future power lines of the SIN (source: [125])

grid system, called the “Arc of the North,” would aim at increasing electric exportation. All of the operational generation plant locations for Brazil are shown in Figure 2.5, and all of the operational Amazonian hydraulic plant locations are shown in Figure 2.6.

## 2.1.3 Amazonian Energy Potential

### 2.1.3.1 Hydraulic Energy Potential

Three of the most energy-important sub-basins within the Amazon Basin are the Madeira, Tapajós and Xingu sub-basins (Figure 2.7), due to their large hydraulic potentials, shown in Figure 2.8. Each of these three sub-basins, shown in dark blue, have around 15-30 GW of hydraulic potential, most of which is untapped into.

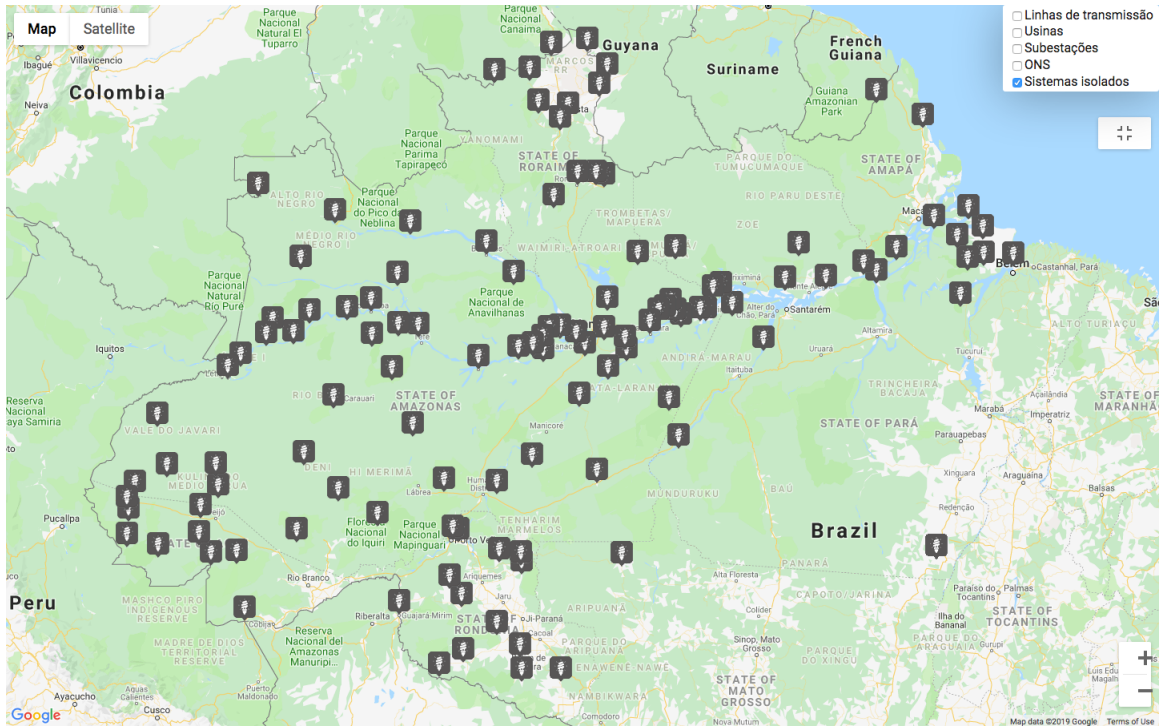


Figure 2.3: Brazilian isolated system locations (source: [125])

### 2.1.3.2 Photovoltaic and Eolic Energy Potential

The photovoltaic (PV, or solar) and eolic (wind) potential energy densities are shown in Figures 2.9 and 2.10. The solar to eolic potential ratio for most of the Amazon is around 9, showing that for most of the Amazon, wind is not a viable option. There are locations near the ocean borders and further away from the forested areas of the Amazon that are more suited for wind; the eolic potential is relatively low in the interior of the Amazon at heights below 50 meters.

### 2.1.3.3 Bio-Energy Potential

There are several options to pursue biomass energy systems that have been reviewed in literature. Traditional methods of utilizing dedicated biomass crops and their associated wastes are not considered as an option here due to the likely outcome of increased deforestation in the Amazon and the conversion of rich, greenhouse gas absorbing land into degraded fields

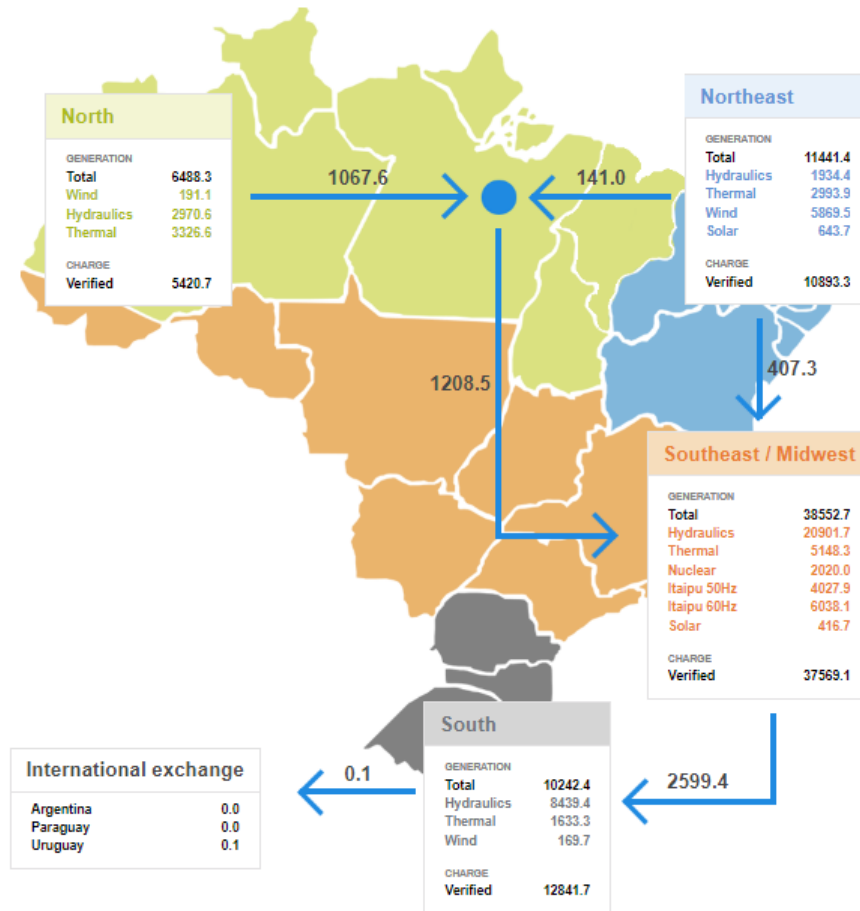


Figure 2.4: Snapshot of Brazilian energy balance (source: [123])

[56]. However, there are several alternative sources for feed stock that have been presented in the literature. For example, [13] suggests using floating wood from the Madeira River to power biomass generators. Others suggest using municipal solid waste to produce various chip or pellet biomass forms [68]. It is recommended that existing biomass sources in Brazil be pursued, such as on-site conversion of farm-based animal or existing crop waste products, and not to pursue options that could lead to further destruction of the natural land use of Brazil or the Amazon.

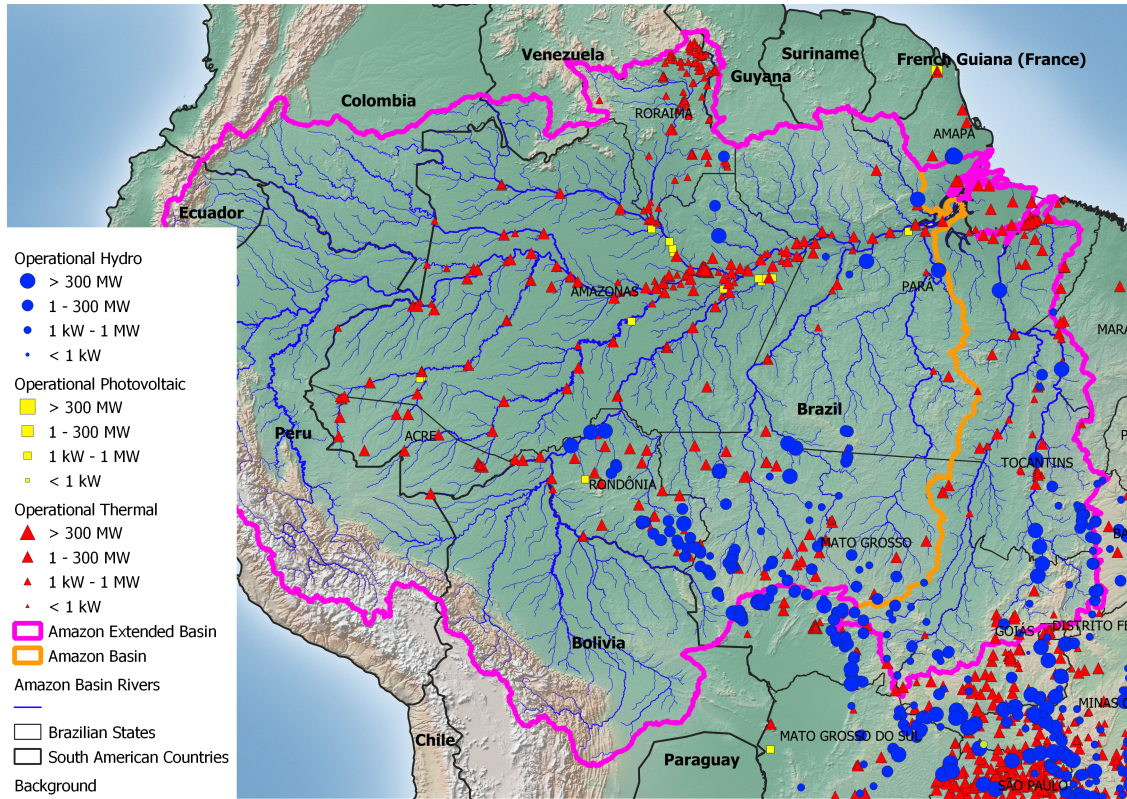


Figure 2.5: Operational Generation Plants in Brazilian Amazon (source: [9])

## 2.2 Recommended Energy Enhancement

For the Brazilian Amazon Basin, there are several parties to consider with varying degrees of interest and polarized directions of needs. Figure 2.2 shows the categories of Amazonian energy beneficiaries and the suggested energy solution that is recommended to satisfy their needs. The first split of scale-of-interests is between off-grid and on-grid: the off-grid needs or the needs of the local communities, examined in Section 2.2.1, are smaller in scale than the on-grid needs, examined in Section 2.2.2, which are the needs of the country, or of growing financial interests.

### 2.2.1 Local Communities: Off-Grid Solution Methodology

The questions of who needs power as well as how much they need are naturally accompanied by the question: why do they need power? There are two main answers to this question:

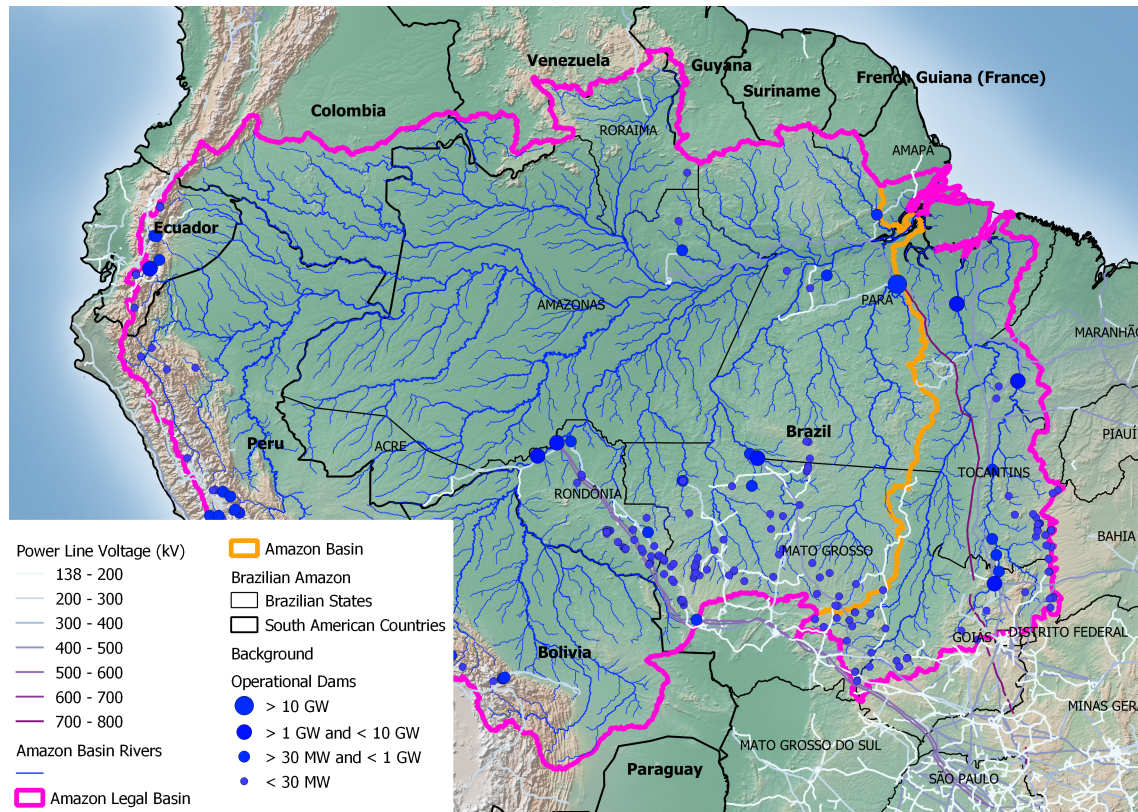


Figure 2.6: Operational Hydraulic Plants and Transmission Lines in Brazilian Amazon (source: [9])

the first answer being that, simply, the household has little to no access to power and would like to have accommodations for lights, refrigeration, etc. The second answer is expanding financial interests: industrial and commercial needs for power to increase manufacturing, distribution, and/or efficiency. The needs of those who would answer with either the first or the second response are fundamentally the same, i.e. they need power, but the method to provide power and the amount needed can be very different. This difference is polarized in the Amazon, due to a portion of the population living in rural regions of the Amazon, possibly deep within the rainforest itself, far away from any city. The distribution of power to these people who live far from the national grid becomes difficult and costly, in terms of both infrastructure investment and landscape modification. For the people who are far away from the current grid, it makes more sense to utilize the natural resources in the nearby region to produce the power locally. For the communities and households that are close

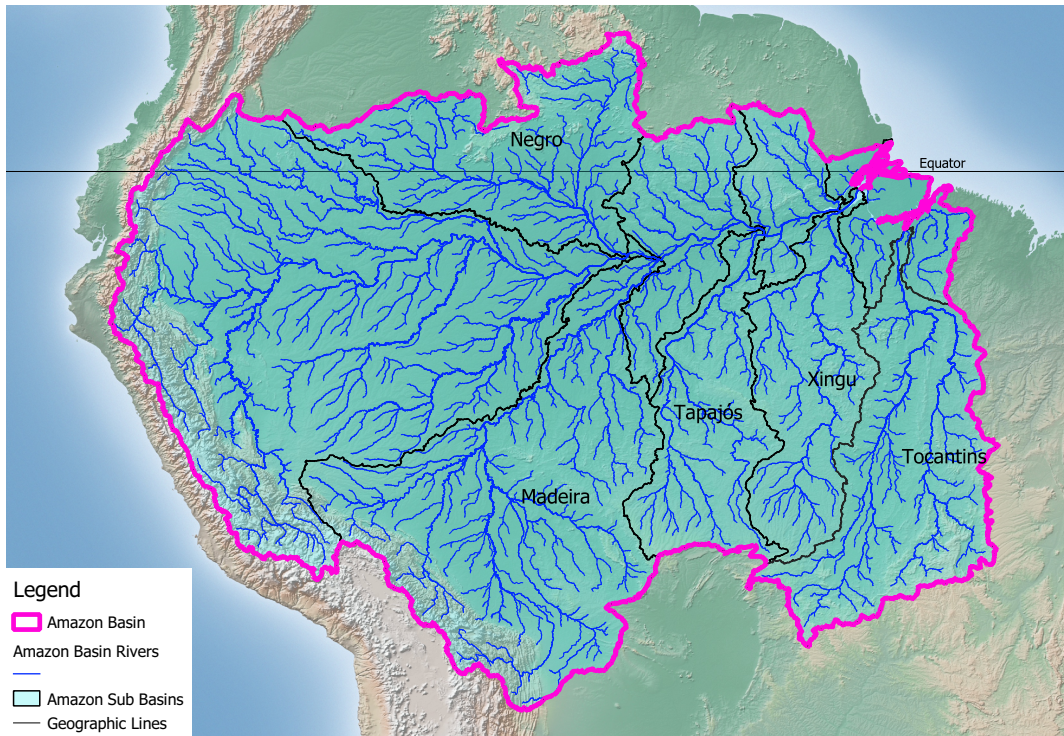


Figure 2.7: The Legal Amazon and major Brazilian sub-basins

to the current electric grid, or those who will be close to the future line extensions, it is recommended to simply provide them with a direct tie-in to the grid. For those who do not fit into these categories, an off-grid solution is necessary. The process for developing a solution for future off-grid systems was as follows:

1. Develop a load model for an individual household
  - Pick common household devices
  - Assume daily usage habits
  - Provide smart load-management concepts to reduce maximum load
  
2. Determine generation to meet load
  - Determine ‘sunny hours’ that solar energy is available, as well as its potential
  - Determine the maximum ‘non-sunny’ load to be met with in-stream turbines

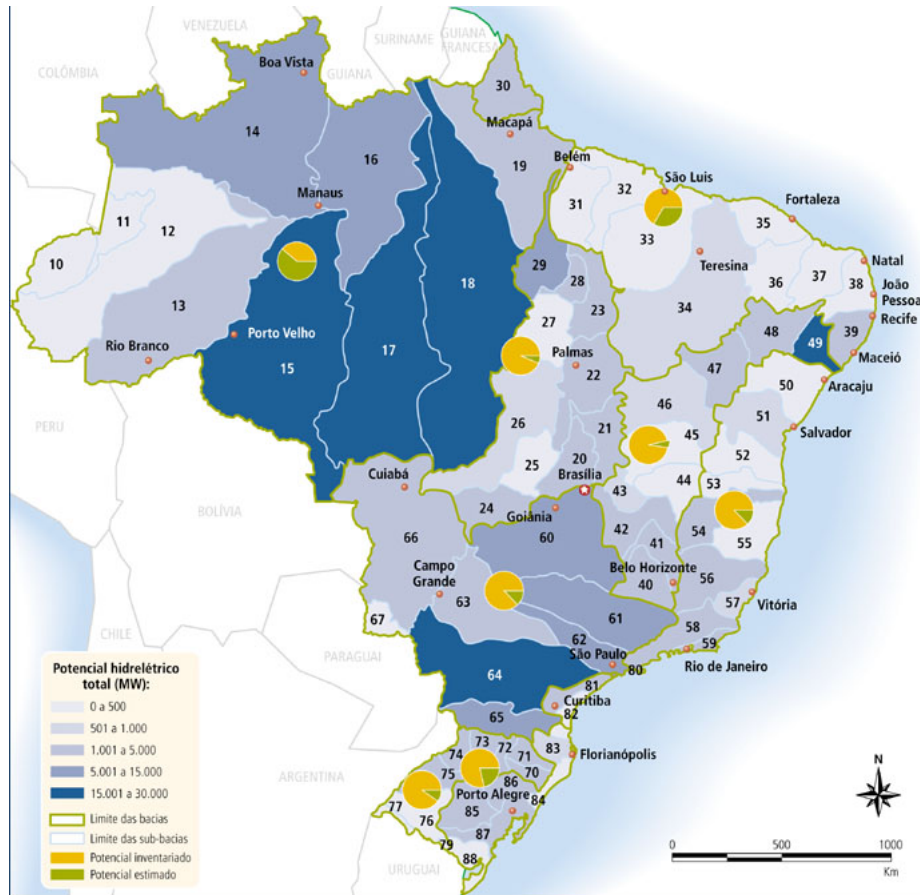


Figure 2.8: The hydraulic potential in Brazil (source: [7])

- Size PV to meet difference between hydro and peak load

3. Scale solution up to number of households of interest

4. Perform financial analysis

### 2.2.1.1 Load Development

The first stage of developing a load model is to select the devices that are ‘common necessities’ for the communities of interest. For the case of the Amazon off-grid communities, the following devices were chosen to constitute the load model:

1. Refrigerator
2. Lights

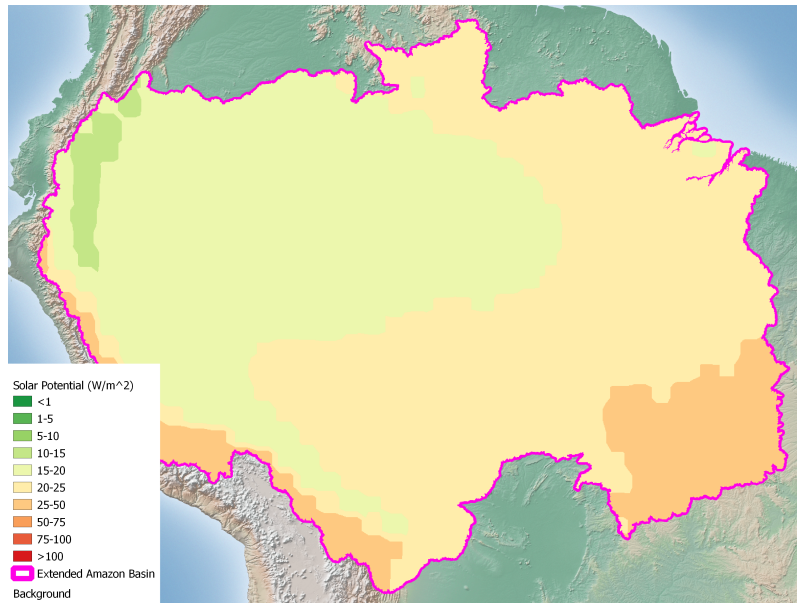


Figure 2.9: The direct normal solar irradiation potential in the Amazon, assuming an overall 12% conversion efficiency (data source: [111])

3. Fans

4. Television

5. Small standalone freezer

With the devices known, the next step is to assume device instantaneous power requirements and daily usage habits for the devices. The simplest case, as well as the worst case scenario, is to assume that all devices are used at 100% capacity for 24 hours each day. Another possibility is to assume that the refrigerator and freezer are the only devices that run all day, in order to keep food preserved, and that the other devices follow the load curve shown in Figure 2.12 and 2.13. This load model assumes that households are out working, playing, and any other daily activity during the hours that the sun is out, and that the household needs lights and fans during the evening and morning hours when the family is in the house. Additionally, the model assumes that the household watches TV for a couple hours once the sun begins to set.

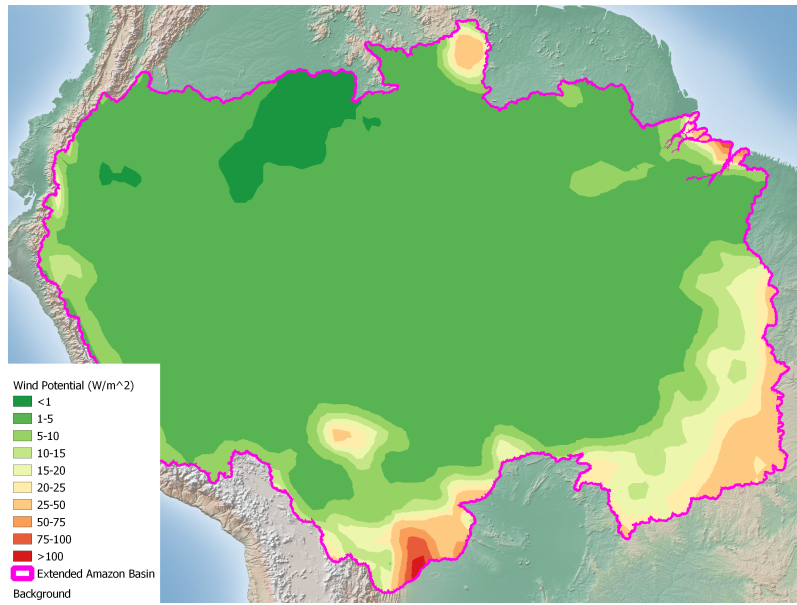


Figure 2.10: The eolic potential in the Amazon at 50 meter height, assuming an overall 45% conversion efficiency (data source: [111])

Another possible case for the load model is to introduce smart load management systems that can reduce the maximum constant load and/or the peak load. One example of a smart load management system would be to utilize a simple timing circuit on the more consistently used devices, particularly the higher power devices like the refrigerator, to only run when needed. For the case of the refrigerator, this could mean only turning it on for a few hours in the evening when the door will be open for usage, and to keep it on just long enough to keep the contents cool until the next day, see Figure 2.14.

Along with these two load models, several others were developed, all of which are shown together in Figures 2.15 and 2.17, for loads met with and without batteries, respectively. Load models 1-4 represent needs that are likely more aligned with the off-grid communities that have not yet had electric access: these communities likely have lower power expectations, and could simply enjoy having access to daily needed/desired devices. Load models 5-8 would likely be enjoyed by any community, previously powered or not, however, these load models are better suited for previously powered communities. This is due to the inclusion of more devices included that these communities could be already used to having at least part-time

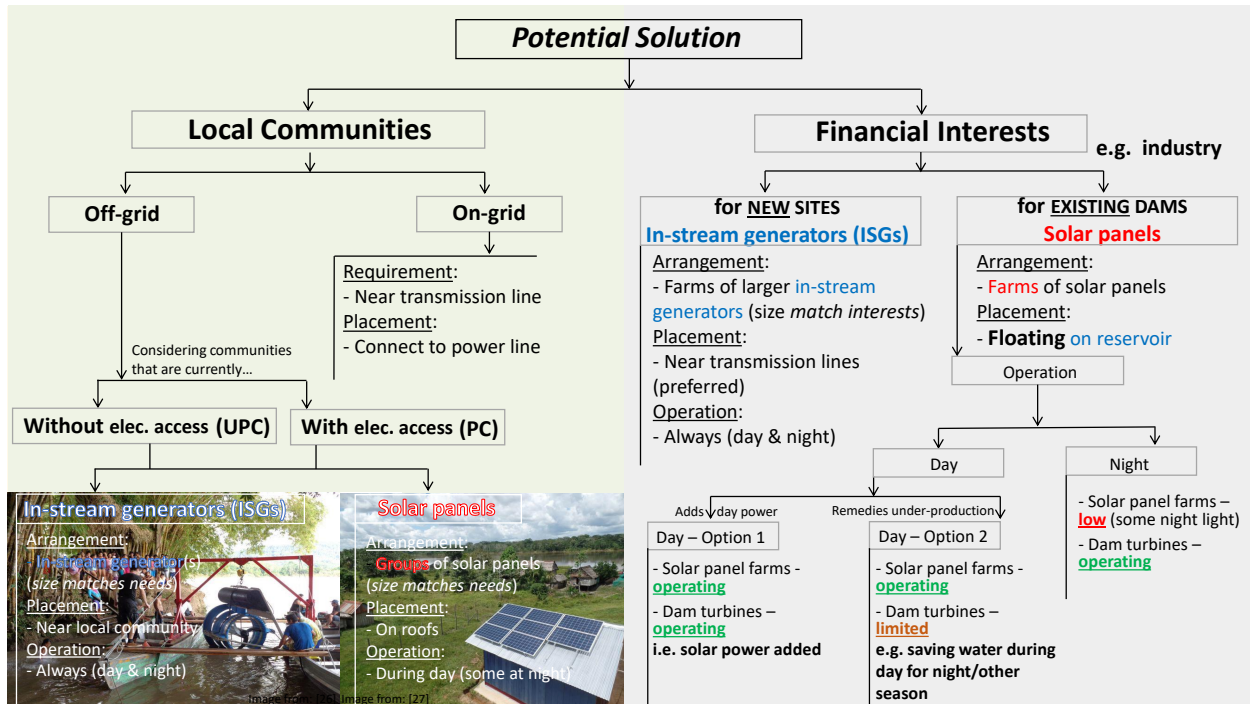


Figure 2.11: Amazonian energy solution portfolio

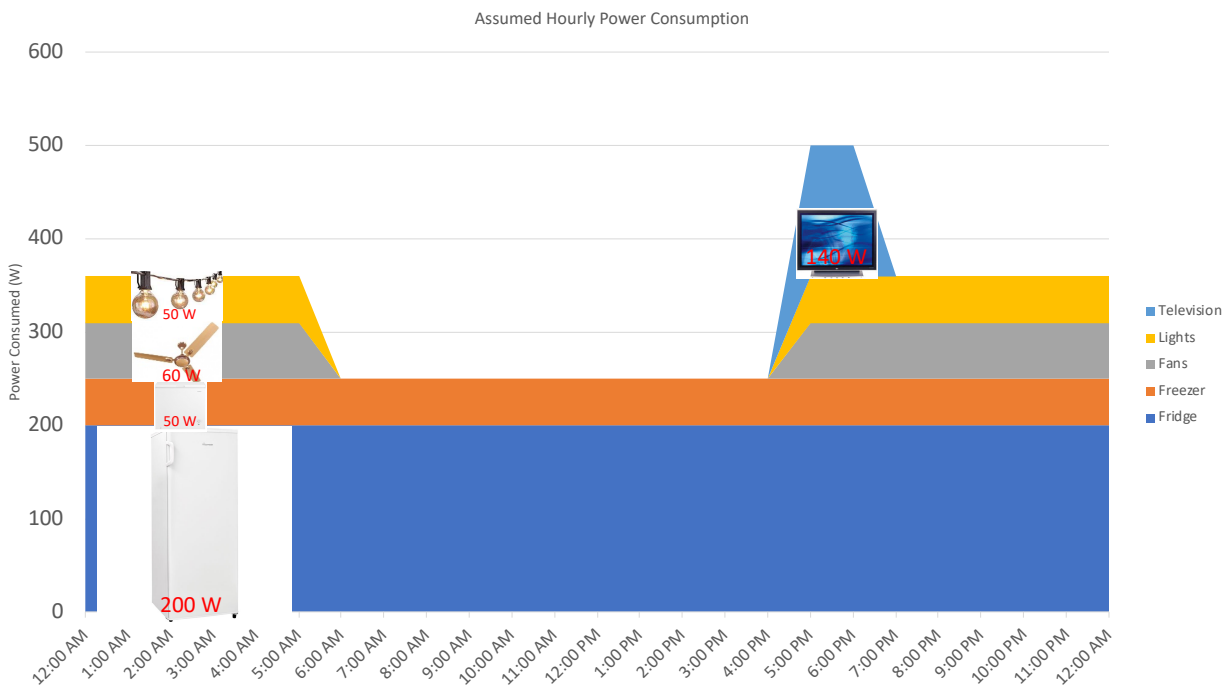


Figure 2.12: Pictorial comprisal of assumed off-grid load with one possible scenario of usage times

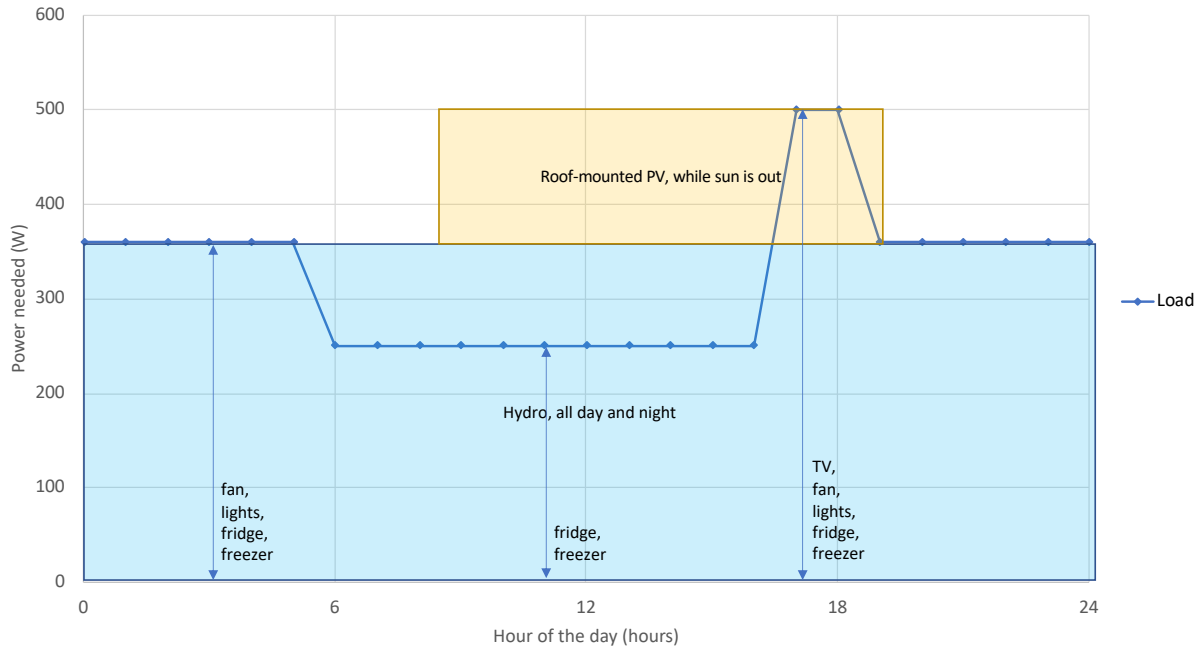


Figure 2.13: Temporal curve of assumed off-grid load

(such as air conditioning), but will be more expensive and thus possibly more difficult to persuade the funding bodies to accept.

The load models are shown with their optimally-low equipment cost generation curves (see Section 2.2.1.3 for details). It can be seen for the profiles that have an optimum generation mixture consisting of both PV and IST (as opposed to pure IST), that there is often more energy delivered when compared to the load. This overshoot leads to an excess in power that will be unused without battery or grid storage; however, this energy can be repurposed, such as providing household cooling using the freezer with a split A/C system, as shown in Figure 2.16 as an equivalent reduced load. It is recommended to not use batteries, if possible, from both a financial and environmental perspective. Environmentally-safe batteries, such as salt water-based technology, can be very expensive to purchase, and cheaper, standard lead-acid batteries, can be environmentally damaging to dispose of at the end of their life. The lead-acid batteries in that they can be left in the dirt or water locally if easy disposal procedures are not planned for or acted on.

### 2.2.1.2 Equipment selection and preliminary financial analysis

The financial analysis begins with pricing components. For the off-grid solar system, the following items were chosen as a financial reference setup:

- Peimer SG33OP panels (0.504 USD/Watt)
- Solarland SLB0103 universal tilt bracket (0.172 USD/Watt)
- Schneider Conext SW4024 inverter (0.440 USD/Watt)
- Assumed approximately 0.1 USD/Watt for cabling and couplings

The Peimar panels are rated at 330 Watts, and have 72 cells. The panels output at a maximum of 36.4 Volts DC (VDC), but likely at normal operating conditions (NOCT) will output closer to 30 VDC, which is within the 20-34 VDC input required for the Schneider inverter, without the assistance of a voltage transformer. The Schneider inverter allows for 120 or 240 V output, which can fit the needs of most existing off-grid devices. These items yielded

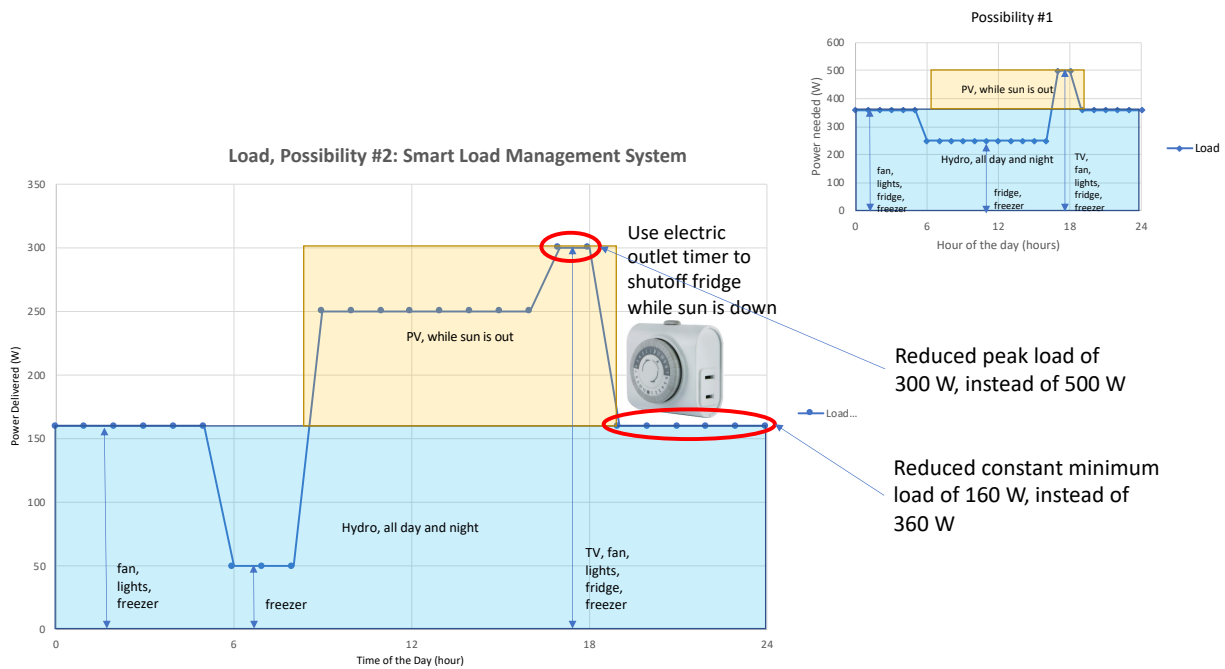


Figure 2.14: Option for possible load by utilizing smart load management system

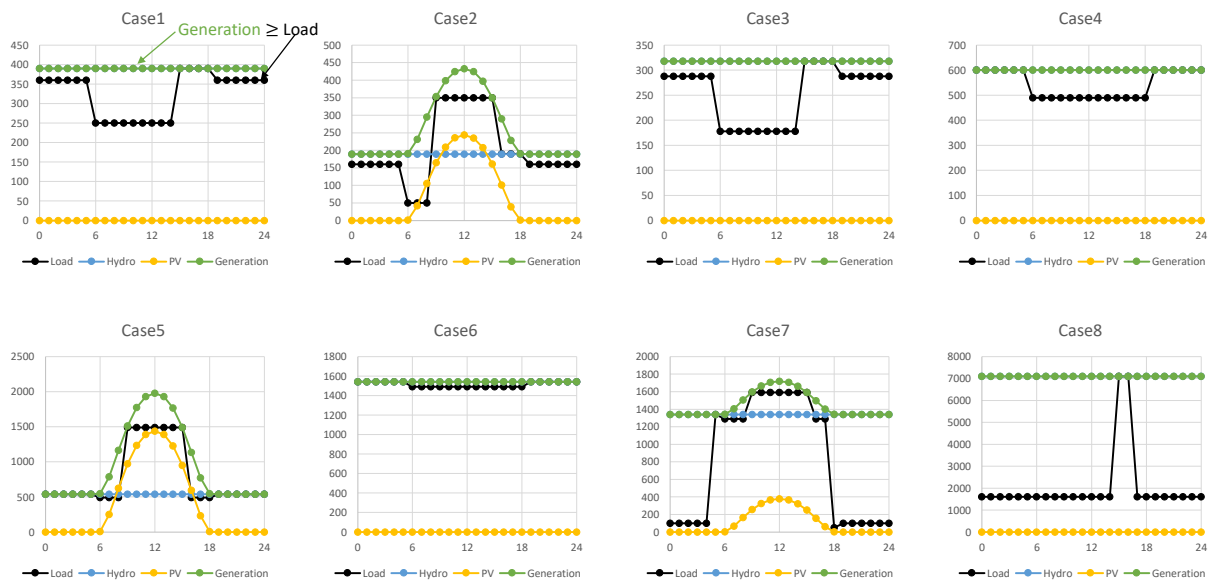


Figure 2.15: Developed load models 1-8. The y-axis is the power consumption, in watts, and the x-axis is the time of day, in hours. The green curve represents the optimal total generation calculated, comprised of the yellow (PV) and blue (in-stream) curves, that meet or exceed the load (the black curve).

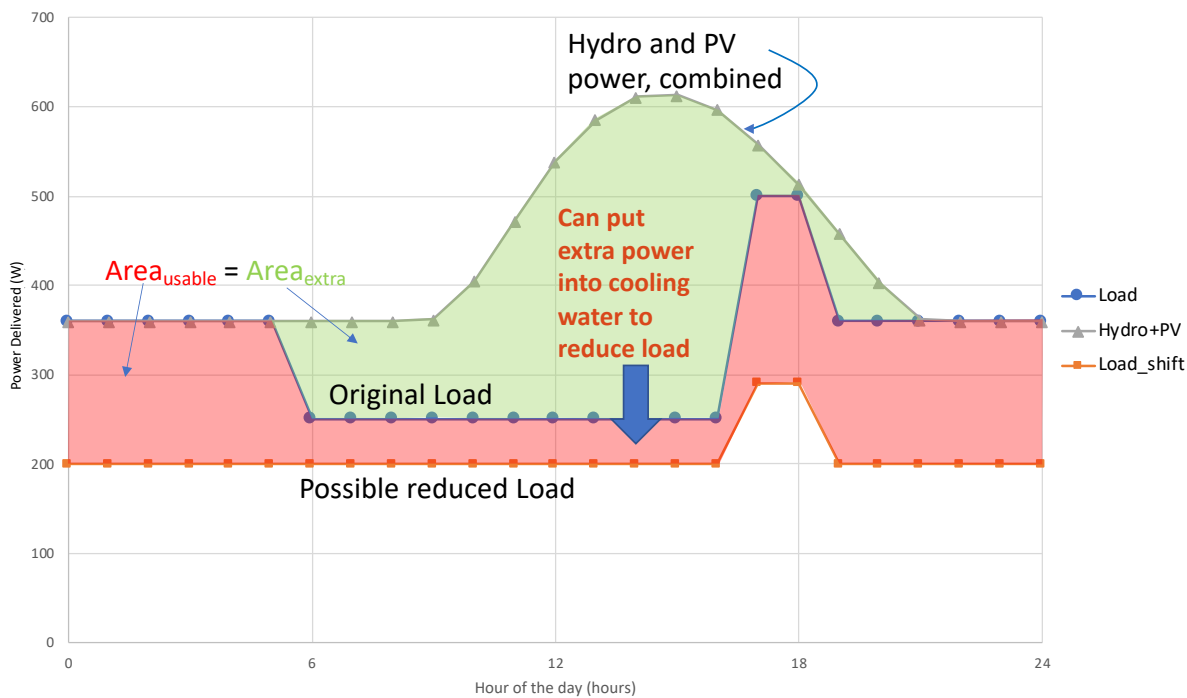


Figure 2.16: Potential “excess power” available for future load reduction

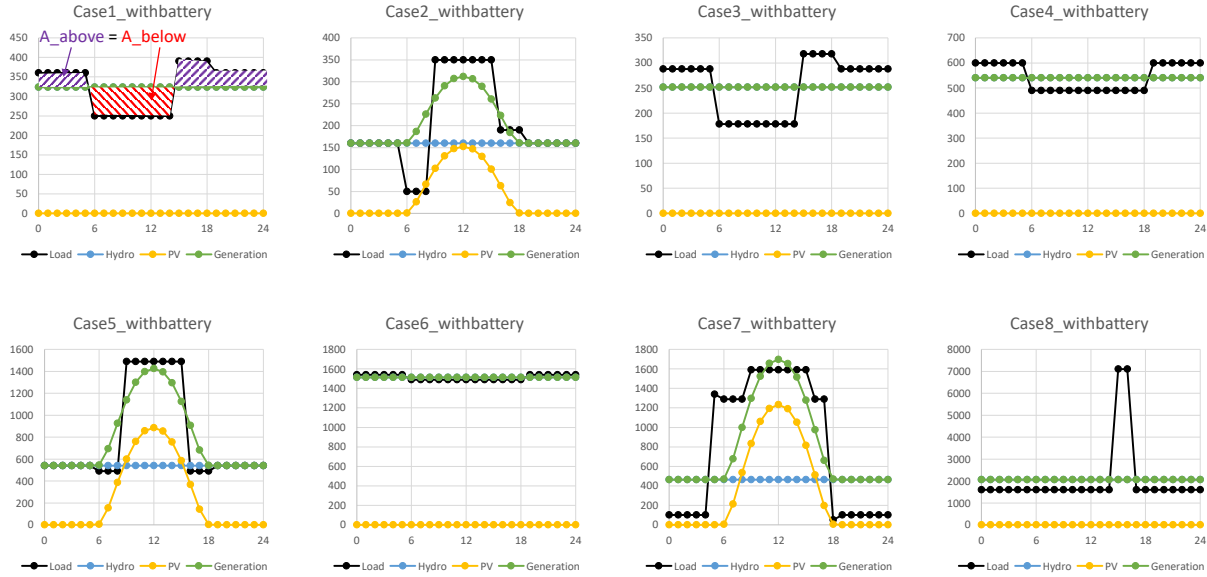


Figure 2.17: Developed load models 1-8. The y-axis is the power consumption, in watts, and the x-axis is the time of day, in hours. The green curve represents the optimal total generation calculated, comprised of the yellow (PV) and blue (in-stream) curves, whose integrated power-time area meets that for the load (the area under black curve).

a PV system cost of 1.04 USD/Watt. At the time of developing this solution, little data is available on the price of in-stream technology. In industry, only one ready-from-the-shelf price data point was found: SmartHydro, based in Germany, offers a complete off-grid IST package for 12,490 Euro or 14,580 Euro, depending on the available flow velocity and desired mooring configuration [173]. This price can be equated to, at maximum generator output, 2.69-3.44 USD/Watt. At a similar time, [48] commented that the cost of IST technology is around 2.5 USD/Watt, also noting the benefit of being environmentally safe. Combining the IST and PV systems costs, and scaling by the unit load, it is calculated that the cost of the off-grid solution is between 1.34 and 3.01 USD/Watt. The cost for all reported dams in the Amazon Basin is 3.67 USD/Watt, and even higher for the Brazilian Amazon approximately 5.50 USD/Watt [70]. Comparing the costs, it is shown that the solution proposed here can be economically viable and advantageous over dams; a more detailed analysis is presented to determine the spatial extent and span of this statement, see Section 2.2.1.3.

### 2.2.1.3 Generation Determination and Detailed Financial Analysis

After the load models were developed, the generation required to meet that load is determined. Due to the energy potentials discussed in 2.1.3 for the Amazonian region, it is recommended to utilize hydraulic (with in-stream turbines) and solar energy sources, as was shown in Figure 2.2. The number of in-stream turbines depends on the maximum load during ‘non-sunny’ hours as well as constraints from the river: the average depth and transverse flow velocity profiles, the intermittency of availability of the flow velocity, the depth and width of the river, and the distance from the river to the community. The ISTs are to be placed in the nearest, highest velocity river stretches to the community, and the power shared and distributed to the households and common buildings. The number of PV panels depends on the difference between the constant hydro-met load and the peak load, the time of day of the maximum difference between the two, and the specific coordinate location in the Amazon. The PV panels are suggested to be placed on the roofs of the individual households or on top of central community buildings, both of which will provide the communities with the most convenient solution, and hopefully provide the strongest feeling of ‘self-ownership’ for the solution; the individual people and families can feel that they were considered and cared for directly.

To evaluate the detailed financial analysis, a Microsoft Excel VBA-based script was developed to be able to test a wide range of conditions, to automatically extract data from an internet source [136], to logically locate and tabulate river conditions from a provided dataset [41], and to facilitate rigid solver input-output, and to be able to more easily and consistently adapt to the solution output signals, see Appendix C. The script is organized with the following logic: user input is provided on an Excel sheet, which will be referred to alphabetically here, “A”, which is then passed onto sheet “B” that will serve as the output for the final script results. From sheet “B”, the coordinates of interest are passed through, along with the number of community households, and an optional community name; the coordinates are used to look up the hourly solar data over one year using another excel VBA

script provided by Renewables.ninja [136] that pulls from sheet “C”. On sheet “C” are the following variables: the user’s renewables.ninja APID, the coordinates of interest, the size of the PV plant to design(1 kW), the desired solar model (MERRA-2), the tilt and azimuth of the planned panels ( $0^\circ$ ), and the additional system loss (10%). For each community’s coordinate set, the PV data is extracted from sheet “C” to sheet “D”, with an assumed plant size of 1 kW. The year of hourly data is averaged for each hour of the day, which will be scaled by the required hourly PV rated power at the current solver iteration on sheet “D”. The PV rated power is used as a scaling factor over the 1 kW script input plant size because the solar data estimates the relative efficiency of the panel, utilizing a parameterized energy performance model presented by [85], Equation (2.3). The solar script uses the MERRA-2 global reanalysis data to extract the location-specific 2-meter displacement height (T2M, zero wind log-profile velocity), air temperature and irradiance to estimate the module temperature via an empirical relationship to calculate the module heating and relative efficiency. The relative power performance equation presented by [85] is then solved, using the free-standing module temperature rise coefficient, Equation (2.2), which is reproduced here as Equations (2.1) - (2.4).

$$T_{mod} = T_{amb} + c_T * G \quad (2.1)$$

$$c_T = 0.035^\circ CW^{-1} m^2 \quad (2.2)$$

$$\eta_{rel} = 1 + k_1 \ln(G') + k_2 [\ln(G')]^2 + T' \left[ k_3 + k_4 \ln(G') + k_5 [\ln(G')]^2 \right] + k_6 T'^2 \quad (2.3)$$

$$P = P_{STC} * \frac{G}{G_{STC}} * \eta_{rel} \quad (2.4)$$

Where  $G' = \frac{G}{G_{STC}}$ ,  $T' = T_{mod} - T_{mod_{STC}}$ ,  $G_{STC} = 1000W/m^2$ ,  $T_{mod_{STC}} = 25^\circ C$ ,  $G$  is the in-place irradiance, and  $T_{amb}$  is T2M and  $k_1 - k_6$  are found from experimental data.

Once the PV data is imported, the approximately 30-year average river flow rate and flow velocity was retrieved from a tabulated sheet of coordinate data, sheet “E”, at the nearest river location to the community coordinate (found by using automated logic to search for nearest reasonably-high flow rate,  $\mathcal{O}(100 - 1000)$ ). The river flow and cross-sectional area

data comes from a leaf-hydro-flood (LHF) hydraulic model, carried out at a 2 km resolution for the entirety of the Amazon River basin [41]. Once the nearest “large” river has been found, then the highest river velocity in the surrounding tabular region (found by using similar logic to the previous step to find tabular direction of river) is passed back to sheet “D” where the solver setup and iteration can proceed. The turbine delivered power is calculated from the river velocity found previously via use of a curve fit from data available on the SmartHydroPower website [173], or equal to the rated 5000 W at the full-rated 2.8 m/s. Equation (2.5) shows the power curve fit, where  $P_{IST}$  is the generator-included power of the in-stream unit, and  $C_{\infty}$  is the free-stream velocity found for the given river location. The in-stream unit is assumed to be able to operate at the calculated level 24/7, on average throughout the year.

$$P_{IST} = \begin{cases} 196.43 * C_{\infty}^{3.1336}, & \text{if } C_{\infty} < 2.8 \text{ m/s} \\ 5,000, & \text{if } C_{\infty} = 2.8 \text{ m/s} \end{cases} \quad (2.5)$$

A nonlinear Generalized Reduced Gradient (nGRG) algorithm was utilized within the VBA environment, using Microsoft Excel’s solver to evaluate the generation to meet the load while minimizing cost. The nGRG method is a “...nonlinear extension of the simplex method for linear programming” [97]. According to [96] and [97], this algorithm seeks to solve a series of simplified, or reduced equations, which are summarized in Equations 2.6 - 2.13:

$$\text{minimize} \quad F(x) \quad (2.6)$$

$$\text{subject to} \quad l < x < u \quad (2.7)$$

where  $F(x)$  is the reduced objective function and  $l$  and  $u$  are the upper and lower bounds of variable  $x$ .  $F(x)$  is the reduced form of the original function that is being sought to optimize,  $f(X)$ , with the basic variables ( $y$ ) written in terms of the nonbasic ( $x$ ):

$$f(y(x), x) = F(x) \quad (2.8)$$

At each iteration, the reduced gradient,  $\nabla F(x)$  is solved via:

$$\pi = \frac{\partial f^T}{\partial y} B^{-1} \quad (2.9)$$

$$\frac{\partial F}{\partial x_k} = \frac{\partial f}{\partial x_k} - \pi \frac{\partial g}{\partial x_k} \quad (2.10)$$

Where  $k$  indicates an iteration count, and  $\bar{X}$  refers to a set of variables that satisfy the original constraints, which can be written as  $g(y,x) = 0$ ,  $B$  is an  $m \times m$  nonsingular basis matrix when evaluated at  $\bar{X}$ :

$$B = \frac{\partial g}{\partial y} \quad (2.11)$$

The reduced gradient is used to calculate a direction  $\bar{d}$  to evaluate:

$$\text{minimize} \quad F(\bar{x} + \alpha \bar{d}), \text{ for } \alpha > 0 \quad (2.12)$$

Where  $\alpha$  is chosen to satisfy the bounds on the original constraints. In the original function form, this is equivalent to solving:

$$f(y, \bar{x} + \alpha_i \bar{d}) = 0 \quad (2.13)$$

where only  $y$  is unknown (the "basic" or "bound" constraints), which can be solved with the Newton-Raphson root-searching method.

The generation costs were calculated over the range of 1-2.8 m/s of river flow speed, with 2.8 chosen as the maximum for the in-stream generator's rated maximum power level, assuming that there is cut-out control. The results are shown in are shown in Figures 2.18 and 2.19. If the load profile is modified then the results above will change accordingly. For example, if the peak load is increased then the total cost will also likely increase, likewise for increasing the maximum load during 'non-sunny' hours (in other words, there are two peak loads to consider: sunny and non-sunny). The magnitude of effect of the change will be dependent on the severity of the load change, as well as the flow velocity in question: at high flow velocity, changing the peak non-sunny load will have less of an effect on total cost due to the hydraulic potential being higher than at low velocity. Another change that

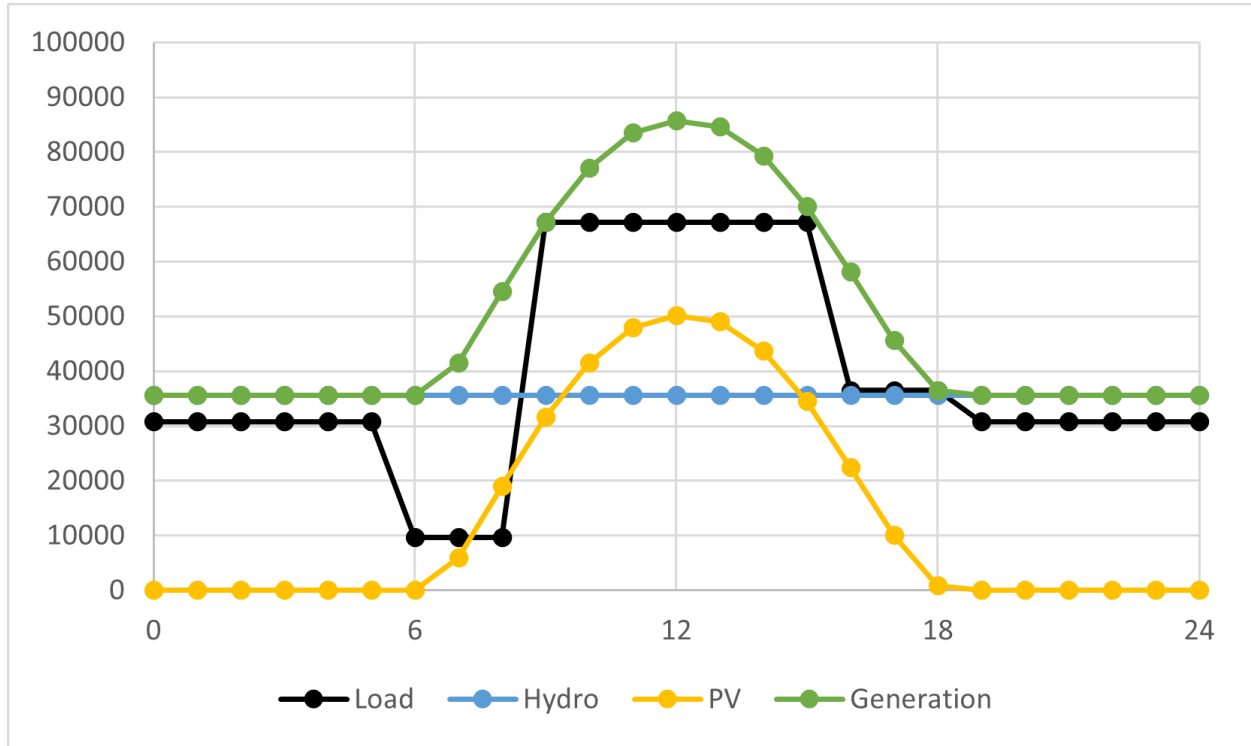


Figure 2.18: Single household load profile with suggested generation profiles

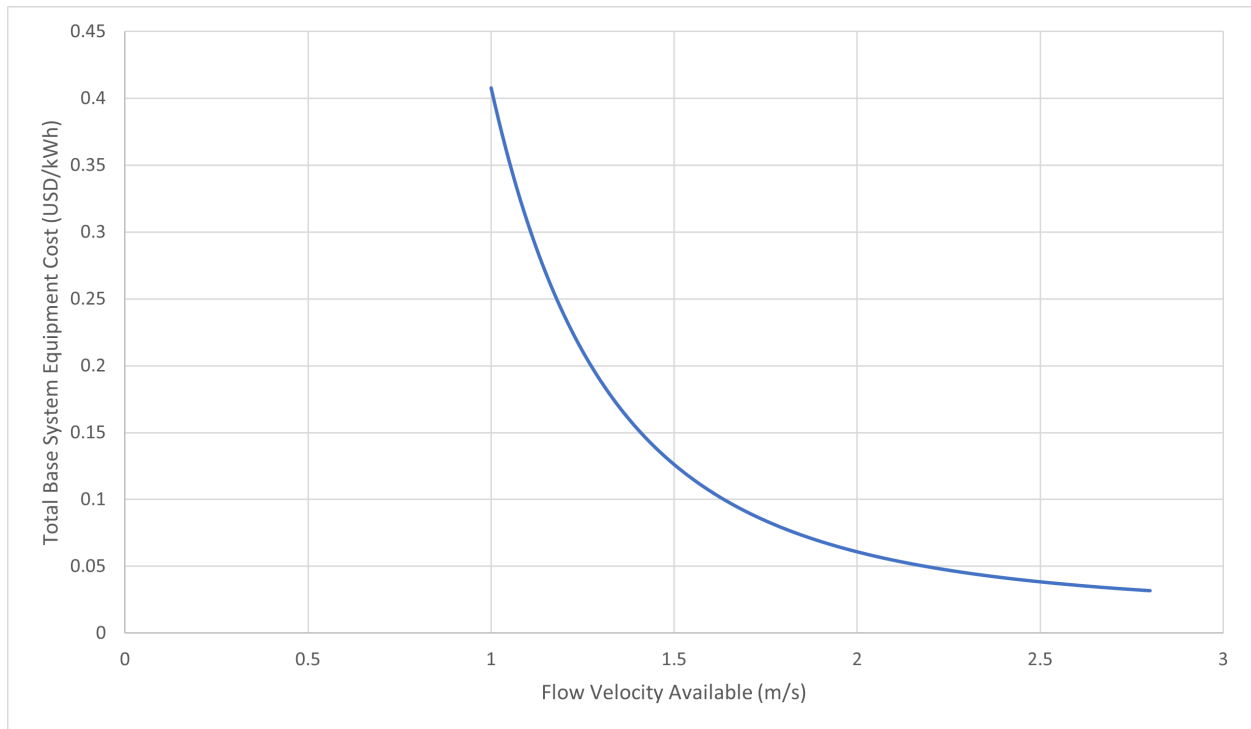


Figure 2.19: Curve of base cost over the investigated range of flow velocities, costs calculated over a 30 year equipment lifespan

will have a significant effect on the above result is the temporal usage of the devices: PV is used to shave the peak load, so if too many devices (namely, high power devices like the refrigerator) are used around sunrise/sunset then the costs will likely increase, as PV does not have enough potential at a reasonable scale to shave the peak load without batteries.

The next step was to calculate the cable costs associated with the particular optimal generation case to meet the load. The SmartHydroPower unit comes with 50 meters of cabling, which may be sufficient if the generator is not far from shore right near to the community. Requiring the turbine to be right next to the community is convenient, but not necessarily always the most energetically or financially feasible option. The optimal scenario would be that the community has high flow velocity water within approximately 50 meters of the water's edge, where at minimum the cabling provided could transmit power to shore. However, as it is possible that most communities are not right next to river locations with high flow velocity, allowing the in-stream devices to be placed further away and transmit the power over longer cables is a possible solution to keep costs low and power capacities closer to rated levels. With longer cables, costs will also increase in proportion to the turbine system rating as well as the distance to the nearest high-velocity river location. To calculate the cable costs, the following is assumed: a maximum distance of 60 km between the community and the ISG deployment site was allowed in the script (approximately half of a typical medium voltage line maximum length), and a 10 American Wire Gauge (AWG) off-the-shelf spool would be used as a basis for costs (ranging from 0.82 to 1.18 USD/meter, which was approximated as 1 USD/m). The cable cost range examined here is 1,000-6,000 USD/km, representing using only a cable bundle (or more likely, multiple cables) up to a low-cost distribution network (transformers, external conductors, and other electrical components). It is noted that the PV system is not under consideration when examining the cabling due to the proposed placement of the PV panels being on the roofs of the community, thus, will always be a short distance away from where the power is used. See Section 2.2.1.4 for further details and results on the theoretical maximum distance that can be serviced at a given cost

of energy goal. It is assumed that the 50 meters of cable is sufficient to reach from the turbines to the shore, where conversion (from  $3\phi$  to  $1\phi$ ) and transformation (from generator voltage to 120 or 240V) can take place, and then the power transmitted to the community (which can then be rectified if necessary), or, the generator phases can be “tricked” into single phase (connecting to one of the three phases and the neutral line, or by using two live phases), for low power situations, and then transmitted to the community.

To have a basis for comparison with the calculated cost of the proposed solution, several possible common Brazilian energy generation or distribution methods were estimated: an extension of the current national electric grid, the building of a new dam with distribution lines, using a diesel generator, and also the 2019 Brazilian North region tariffs. Though the tariffs represent the average charge for electricity while interconnected to the national grid, it is recognized that this rate may not be accurate for communities that are far from the grid without the aid of extra government incentive programs, due to the large costs incurred to extend the grid over a long distance. Regardless, the tariffs act as a “golden standard” guide for the cost effectiveness of a project, in that if a proposed system could meet or be lower cost than the tariffs, it could be a strong incentive for further examination by the government (ANEEL, EPE, ONS, MME, etc.) for utilization even beyond off-grid communities.

The first mode of energy provision is an extension of the national grid via a new transmission/distribution line network. To calculate the grid extension costs, two major perspectives to calculate the line costs were developed: 1) use Brazilian government reported data as a situational absolute; if the current method to supply any region with power is to build 230 kV line up to the point of distribution, then that is likely how it will be done for grid stability and reliability, and so the perspective is an accurate basis or 2) use a range of electrical component (high voltage (HV), medium voltage (MV), and low voltage (LV) lines, transformers, etc.) pricing from the literature to model a transmission system. For both scenarios a wide possible range of line costs were found, from approximately 6,000 USD/km, attempting to develop a cheaper low-to-medium voltage distribution/transmission line, [55] up to 80,000 -

410,000 USD/km, calculated from existing and planned HV transmission lines in the Brazilian Amazon region ([129], [127], [122]). It is unclear at this time which value would be most representative of extending a transmission line deeper into the heart of the Amazon, where existing roadways and construction right-of-ways have not yet been established, the terrain may be highly variable, and native lands and protected areas may be present that prevent “shortest route” building, etc., thus a range of possible costs is considered.

The Brazilian line costs were used on their own as total cost per kilometer, due to no additional information being provided about whether or not these are total project costs, or some subset of the total. Thus, the Brazilian cost estimates will be dubbed “total line” costs, as the line costs are assumed to capture all transmission costs, as opposed to just a “line” cost, which here is meant to refer to the cost of the cable alone. Additionally, substation costs were also not included, assuming that the distances and loads will not be significant enough for substations to be required. From Brazilian data, it is calculated that an HV line could extend anywhere from 4 to 168 km (on average  $\sim 77$  km) ([129], [127], [122]) between substations. As long as the HV line does not extend far outside of the approximate range of 77-160 km, the assumption of not pricing a substation should hold. Equation (2.14) shows the calculation of absolute grid extension costs in USD:

$$C_{ONS_{tot}} = CC * L \tag{2.14}$$

where  $C_{ONS_{tot}}$  is the total grid extension cost based on data from the Brazilian government entity ONS,  $CC$  is the cable cost per kilometer calculated from the data, and  $L$  is the length of cable extension.

The literature component costs were used differently: instead of assuming that the cable cost is the “total line” cost, the cable costs are only one component of the whole system, which is built up from the following:

- HV, MV, and LV cable costs
- transformers

- household conversion equipment and connection costs

The LV line costs are calculated from an assumed inter-house distance of 25 meters [155] with a cable cost between 10,611 USD/km and 12,000 USD/km ([133],[155]), and the MV line is assumed to carry the power over a “typical” maximum distance of 120 kilometers to the community [46] at a cost between 6,000 USD/km and 30,580 USD/km ([55], [99]) at which point the HV line makes up the remaining distance, with a cost ranging from 90,000 USD/km to 192,000 USD/km, depending on operating voltage [46]. The transformers are assumed to cost between 39 and 1,000 USD per rated kW ([133], [155]), the household equipment is assumed to cost between 263 and 367 USD per household ([133], [155]), and the household connection cost is 149 USD per household [133]. The operation and maintenance costs are assumed to be between 2-3% for the transformers and cables, respectively ([133], [155]). The transformers are assumed to have 18% losses and a 10 year lifespan [133]. The total cable length can be calculated by Equation (2.15), and the total grid extension costs were calculated with Equation (2.16).

$$L_{total} = L_{LV} + L_{MV} + L_{HV} \quad (2.15)$$

Where  $L_-$  is the length of cable for a particular voltage category, or total length.

$$C_{COMP_{tot}} = \begin{cases} (1 + OM_{MV}) * CC_{MV} * L_{MV} + ... \\ (1 + OM_{LV}) * CC_{LV} * HH * d_{ihs} + ... \\ (1 + OM_{tr}) * (1 + LF_{tr}) * (T/t_{tr}) * (C_{tr} * P_{peak} * HH), & \text{if } L_{MV} \leq 120km \\ CC_{HV} * L_{HV} + (1 + OM_{MV}) * CC_{MV} * 120 + ... \\ (1 + OM_{LV}) * CC_{LV} * HH * d_{ihs} + ... \\ (1 + OM_{tr}) * (1 + LF_{tr}) * (T/t_{tr}) * (C_{tr} * P_{peak} * HH), & \text{otherwise} \end{cases} \quad (2.16)$$

Where  $OM_-$  is the operation and maintenance cost of the particular equipment in percent of cable cost,  $CC_-$  is the cable cost of a given voltage category found in literature in USD/km,  $HH$  is the number of households examined,  $d_{ihs}$  is the inter-household distance,  $LF_{tr}, t_{tr}, C_{tr}$  are the loss factor, lifetime, and unit cost of the transformers in percent, years, and USD/kW, respectively, and  $P_{peak}$  is the peak rated load power level.

The next mode of energy provision to compare the proposed solution to is the construction of a new full-scale dam with transmission lines built to bring the power to the community. Equation (2.17) shows the total estimated cost calculation of dam construction and power transmission.

$$C_{damtot} = C_{dam} * UR * P_{peak} * HH + OM_{dam} * P_{MWh} + CC_{BR} * L \quad (2.17)$$

Where  $C_{dam}$  is the average calculated cost of dam construction (5.5 USD/W) in the Amazon Basin and Brazil ([135], [189]),  $UR$  is the average global dam construction cost typical underreporting ratio (values of either 1 USD/USD or 1.96 USD/USD [10] were considered here),  $P_{peak}$  and  $P_{MWh}$  are the peak power and energy usage over a year in W and MWh, respectively,  $OM_{dam}$  is the operation and maintenance for a dam (2.31 or 5.8 USD/MWh) [87],  $CC_{BR}$  is the cable cost for transmission, assuming that the current Brazilian method for power transmission applies, and HV cables will be used for most of the distance, and  $L$  is the distance of cable. As was mentioned for the grid extension calculation, the Brazilian transmission line costs are used at the total line cost, assuming that all costs are included (right-of-way, projected operation and maintenance, etc.), due to a lack of information on project cost components. Both the grid extension and the dam construction use the Brazilian line costs, because unlike with a decentralized microgrid, the reliability of the national systems (whether it is a new dam or the grid itself) is under closer scrutiny by any interests-at-large, and so it is assumed here that the traditional HV line will be installed to reduce risk of outages if the load spikes become too large. Similar to the grid extension, a transmission network was also calculated from components in literature, which yields a cost calculated by

Equation (2.18).

$$C_{dam_{tot}} = \begin{cases} C_{dam} * UR * P_{peak} * HH + OM_{dam} * P_{MWh} + ... \\ (1 + OM_{MV}) * CC_{MV} * L_{MV} + ... \\ (1 + OM_{LV}) * CC_{LV} * HH * d_{ihs} + ... \\ (1 + OM_{tr}) * (1 + LF_{tr}) * (T/t_{tr}) * (C_{tr} * P_{peak} * HH), \quad \text{if } L_{MV} \leq 120km \\ \\ C_{dam} * UR * P_{peak} * HH + OM_{dam} * P_{MWh} + ... \\ CC_{HV} * L_{HV} + (1 + OM_{MV}) * CC_{MV} * 120 + ... \\ (1 + OM_{LV}) * CC_{LV} * HH * d_{ihs} + ... \\ (1 + OM_{tr}) * (1 + LF_{tr}) * (T/t_{tr}) * (C_{tr} * P_{peak} * HH), \quad \text{otherwise} \end{cases} \quad (2.18)$$

The rating of a “full-scale” conventional dam that could be installed in the same river location as the in-stream site is calculated by Equations (2.19) and (2.20) were utilized along with the hydraulic data used to calculate the river velocity. The total head is calculated from the sum of the static head (water height,  $h_-$  and elevation,  $z_-$ ) across the site, and the kinetic head at the site. This is converted into an equivalent total pressure and multiplied by the flow rate ( $Q_{90}$ ) at the site to obtain the maximum theoretical extractable riverine power.

$$H_{total} = (h_2 + z_2) - (h_1 + z_1) + \frac{C_{\infty}^2}{2g} \quad (2.19)$$

$$P_{dam} = \rho * g * H_{total} * Q_{90} \quad (2.20)$$

Only a portion of the total power calculated will be diverted towards the community, whereas most of the power is assumed to be directed to the existing electric grid. It is assumed that the community would then be charged only for the power utilized, equivalent to the cumulative community loads,  $P_{community} = \frac{HH * P_{peak}}{P_{dam}} P_{dam}$ .

One major difference between the grid extension and the dam construction is the risk of flooding and associated community displacement once the reservoir is filled. To estimate

the reach of the reservoir, the average reservoir radius was calculated with respect to the nameplate capacity of each dam:

$$R_{res} \approx \sqrt{1.58 * P_{nameplate} / \pi} \quad (2.21)$$

Where  $P_{nameplate}$  is the calculated theoretical capacity of the dam in MW, and 1.58 is the calculated average conversion for Brazilian Amazon dams in  $km^2/MW$ . With the reservoir area determined, a constant radius circular shape is assumed, neglecting the local topography, allowing for simple calculation of the reach of flooding. If the community is within the radius of the calculated reservoir, then it is concluded that it is possible that there is a risk of flooding for that community, and installing a full-scale dam at the in-stream site could lead to displacement of that community. The sites at risk of flooding are marked with a red ‘x’ in Figures 2.22-2.23 and 2.25-2.26 .

The last mode of energy provision examined is a diesel generator. To calculate the cost of energy of a diesel generator, typical usage from an Amazonian community in the state of Amapa was calculated. From [144], using the power rating (90 kW) and yearly allotted fuel consumption (27,600 liters), an estimated average load of 75% was calculated using power-consumptions curves/tables for similarly sized diesel generators (80-100 kW) at a fuel rate of  $\sim 4.99$  gal/hr. From this generator load, the number of households that the device could equivalently support was calculated, based on a UPC peak load of 350 W and 1,490 W for PC, yielding 192 and 45 households, respectively. There are two usage cases considered for a diesel generator: meeting the same load pattern as the proposed solution, and meeting an all-day constant, all-devices load (500 W for 135 households and 1,540 W for 43 households, for UPC and PC, respectively). The latter is considered as the “best-case scenario” for having constant access to all devices all day; however, the fuel costs would likely be too expensive for many households, and as was mentioned in [144], would not be funded in the fuel allowance (likely to be granted enough fuel for approximately 4 hours per day of usage, not 24), and so this case is considered as a theoretical lower limit for the given examined conditions. The diesel generator was quoted to cost 44,151.52 USD [144]. To calculate the fuel costs, the

Brazilian 2019 average diesel cost [14] was converted into USD, which was found to be 2.60 USD/gal. The cost of diesel generator is shown in Equation (2.22).

$$C_{dieseltot} = C_{generator} + CR_{fuel} * 2.60 * 8760 * T \quad (2.22)$$

Where  $CR_{fuel}$  is the consumption rate of diesel fuel by the generator.

To explore the possible range of the proposed solution costs in the Amazon, several sample sites were chosen, based on currently planned dams, as well as a few of planned dams that were halted for environmental/social reasons, with the addition of a few extra sites to distribute the locations more evenly among the three sub-basins shown in Figure 2.20. These sites act as proxies for communities that could be present at these locations, and can serve as locational case studies for examining the proposed solution as being a viable alternative for full-sized large scale dams providing local power. Figures 2.21-2.26 show the results of the microgrid sizing calculation by comparing the calculated proposed solution costs against the calculated costs for an electric grid extension (Figures 2.21 and 2.24) and against a new dam construction with distribution lines (Figures 2.22-2.23 and 2.25-2.26), where a red x symbolizes a possible community flooding/displacement, depending on the reservoir built for the dam. The costs are shown in terms of USD/kWh, which was calculated by dividing the total costs by the load energy usage per household (hh) per year, 1,544 kWh/hh or 7,048 kWh/hh for UPC and PC, respectively, with the exception of the low-cost diesel, which has a yearly usage at 4,380 kWh/hh, and then multiplying by the number of households in question.

Figure 2.21 examines several cable costs on the feasibility of the proposed solution as compared to an extension of the current electric grid, a diesel generator, and the 2019 tariffs for a previously unpowered community (UPC). The sample sites show that a range of costs were calculated, depending on the local river velocities, and their distance to the community. At the extrema, for the low end of cable costs (1,000 USD/km), there are two sample sites whose river velocities are 0.74 and 0.84 m/s that have costs above the high diesel generator

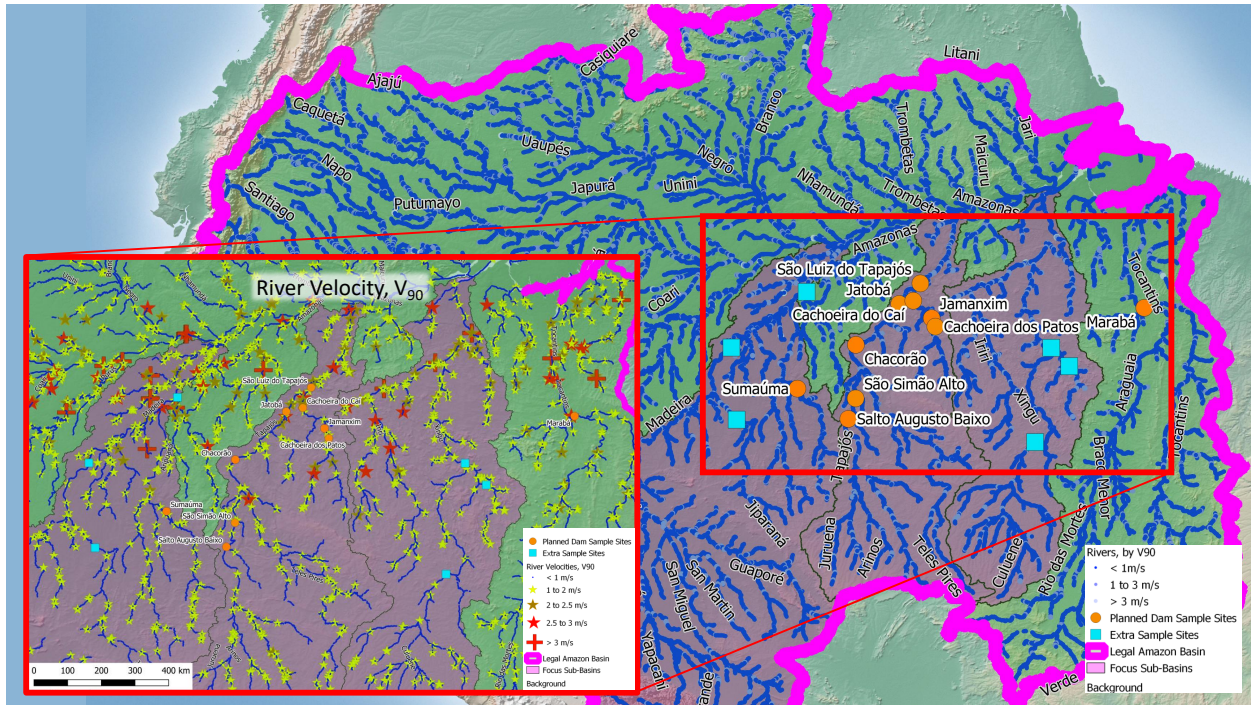


Figure 2.20: Locations of sample sites overlaid on top of river paths, with markers representing the river velocity available at that location, based on  $Q_{90}$ .

level, therefore these may not benefit from the proposed mix as much as other sites, and there are around seven sites that have a lower cost than the 2019 rural tariff, which seems to associate with river velocities above 1.54 m/s that are also generally close to high-velocity river locations, that may most consistently benefit from the proposed energy mix. Three of these seven sites also are within  $\sim 90$  km from a current transmission line, so could also potentially receive a grid connection, if the low extension costs can be met, and no major substation or electrical supporting structure needs to be built to support the additional load. There are another three sites whose costs are in between the two tariffs, that could also benefit from the energy mix, with the exception of one site that is  $\sim 100$  km from an existing transmission line, that could also benefit from a low-cost grid connection. The remaining sites have costs that lie somewhere in between the 2019 residential tariff and the high cost of diesel lines, and are thus competitive with the current diesel generator method of supplying power to off-grid communities; the communities that still need power could benefit

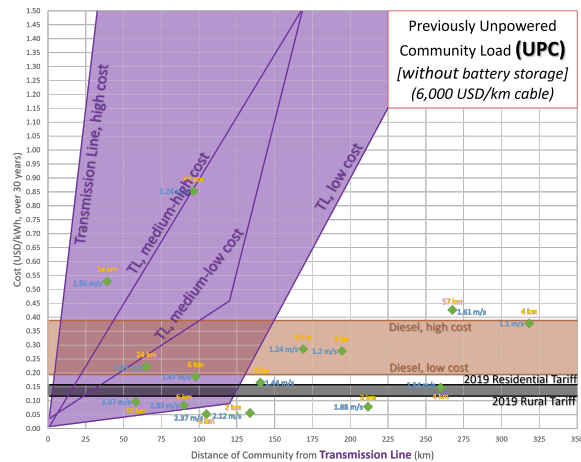
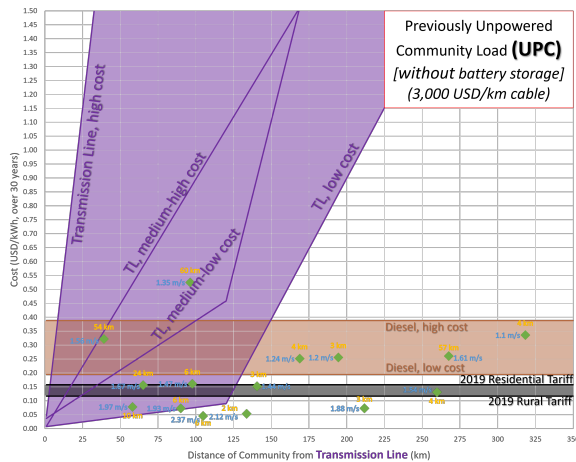
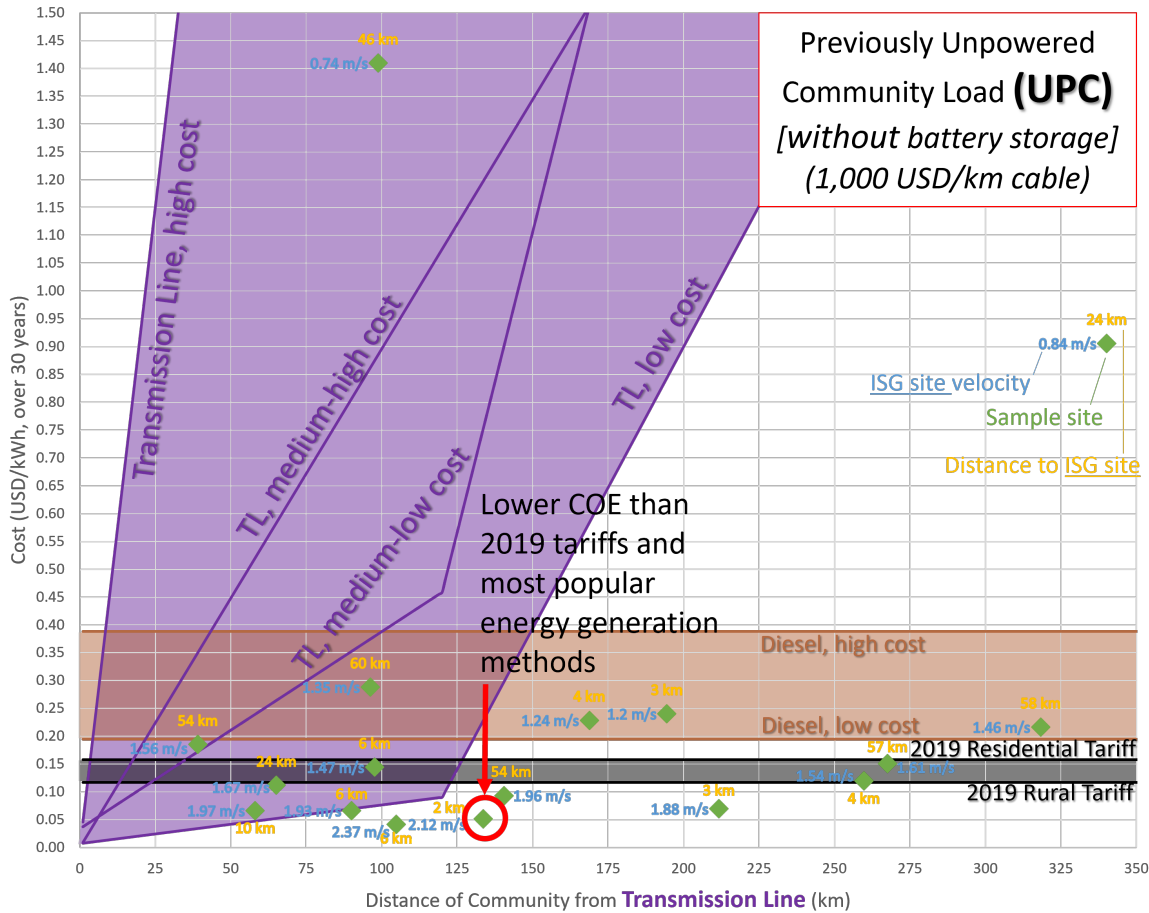


Figure 2.21: Comparison of proposed UPC solution (green diamonds) with several common energy generation and distribution methods. The costs associated with the electric grid extension is shown by the purple range, a diesel generator is shown by the brown range and the 2019 Brazilian North region residential and rural tariffs are shown by the black range. The x-axis is the distance from the community to the nearest existing transmission line, in km, and the y-axis is the calculated cost in USD/kWh over 30 years.

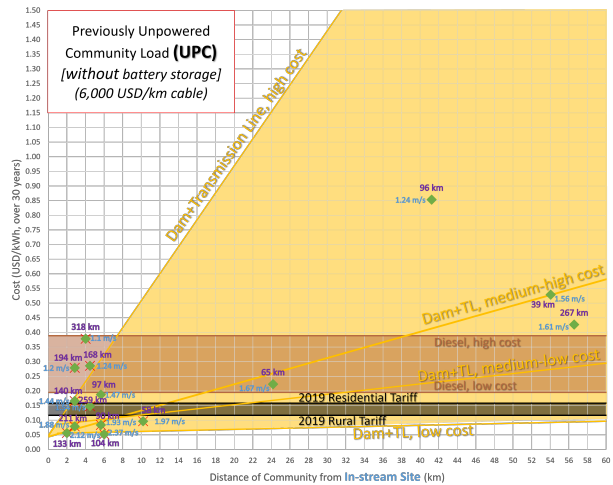
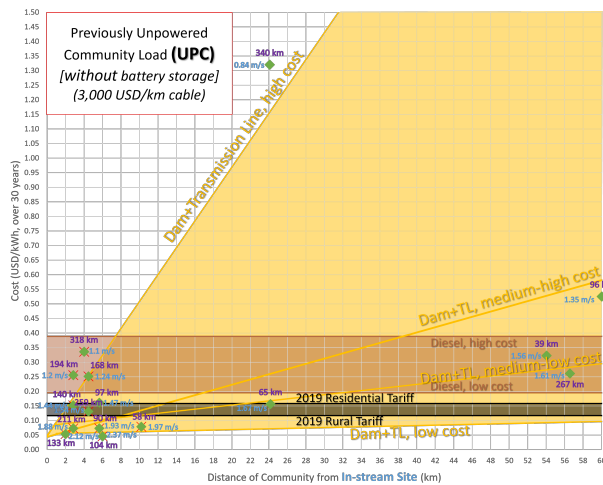
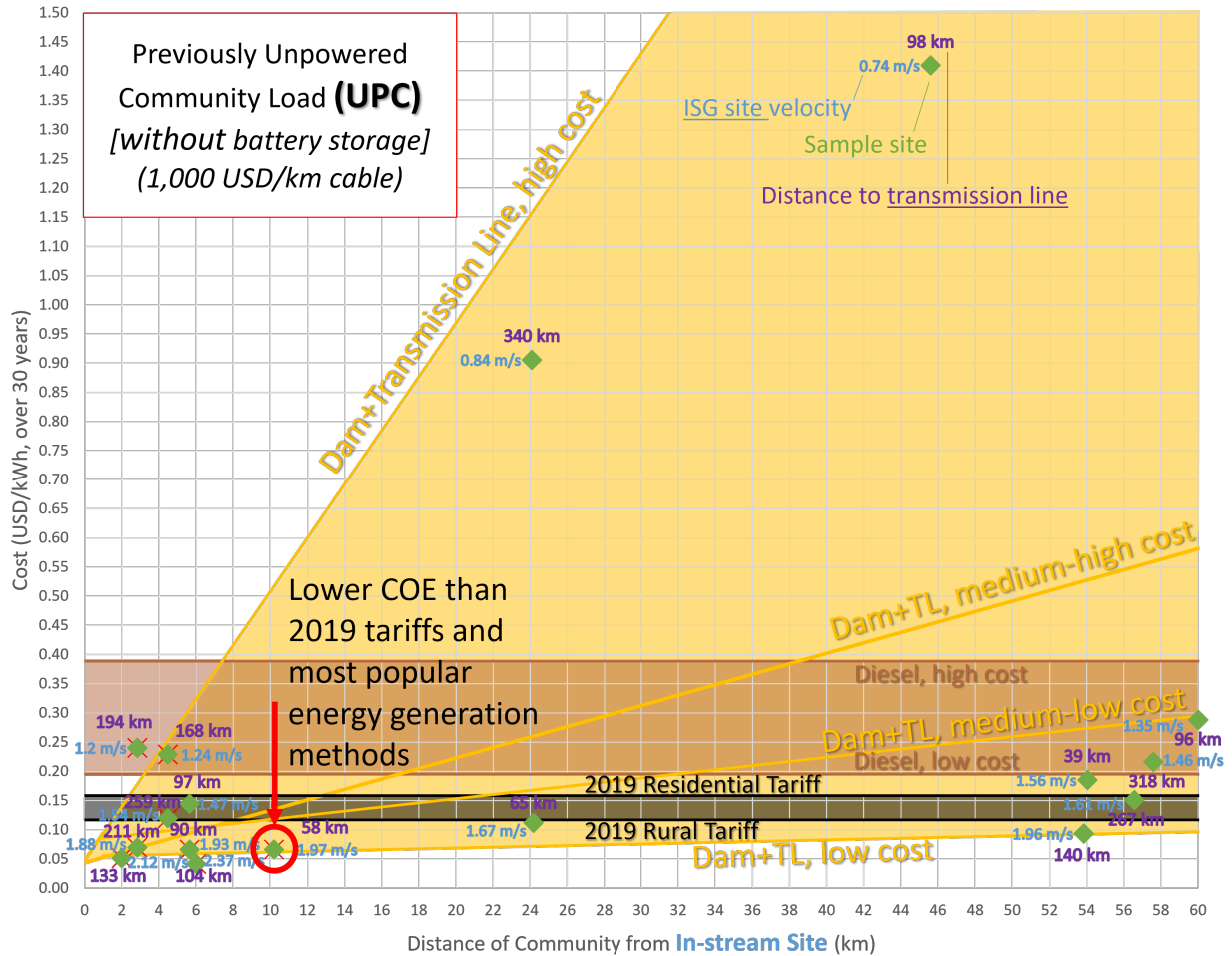


Figure 2.22: Comparison of proposed UPC solution (green diamonds) with several common energy generation and distribution methods. Dam construction with distribution lines is shown by the gold range, with no underreporting factor included; the other ranges are the same as 2.21. The x-axis is the distance from the community to the optimal in-stream generation site, in km, and the y-axis is the calculated cost in USD/kWh over 30 years.

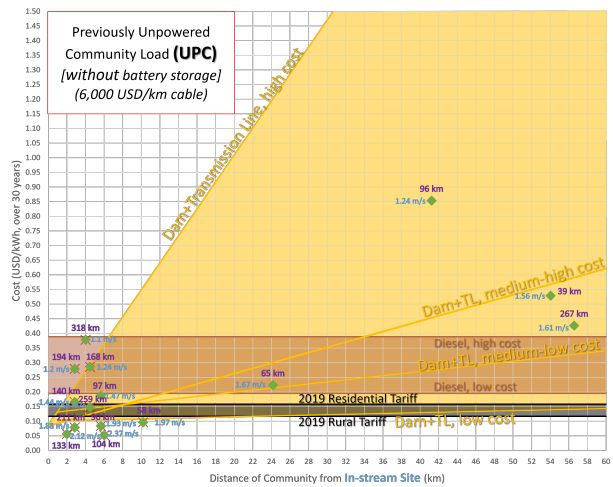
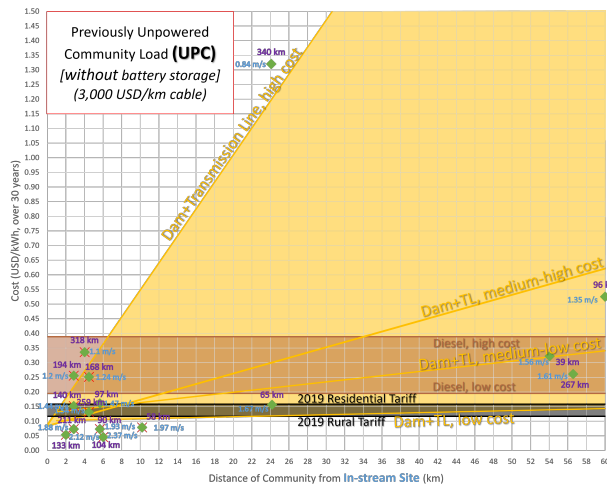
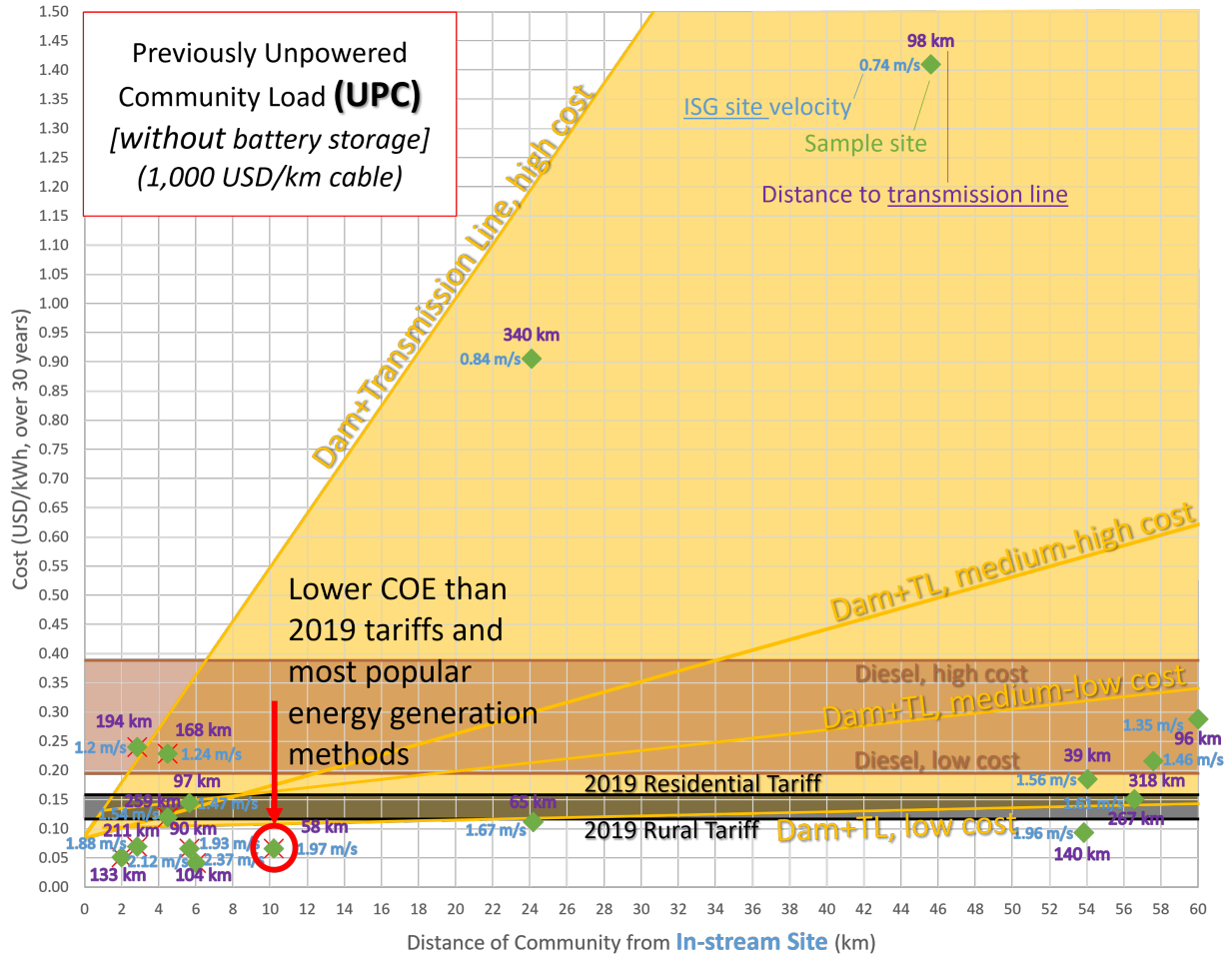


Figure 2.23: Comparison of proposed UPC solution (green diamonds) with several common energy generation and distribution methods. A new dam construction with distribution lines is shown by the gold range, with an underreporting factor of 1.96 USD/USD included, a diesel generator is shown by the brown range and the 2019 Brazilian North region residential and rural tariffs are shown by the black range. See Figure 2.22 for axes.

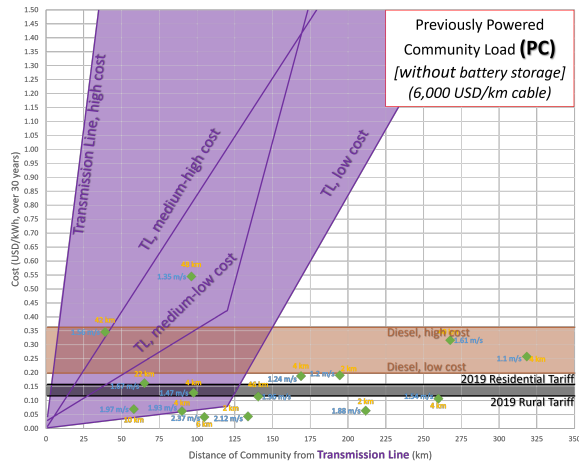
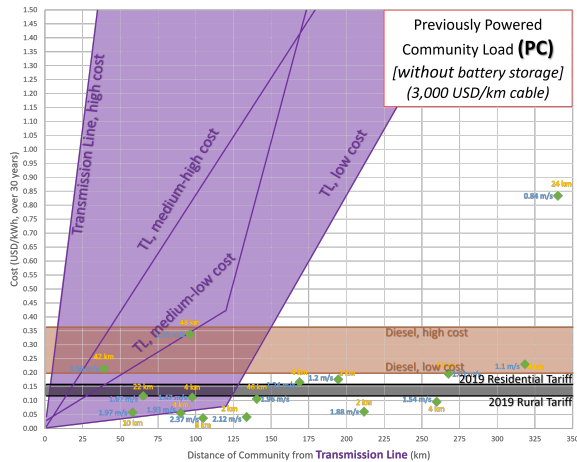
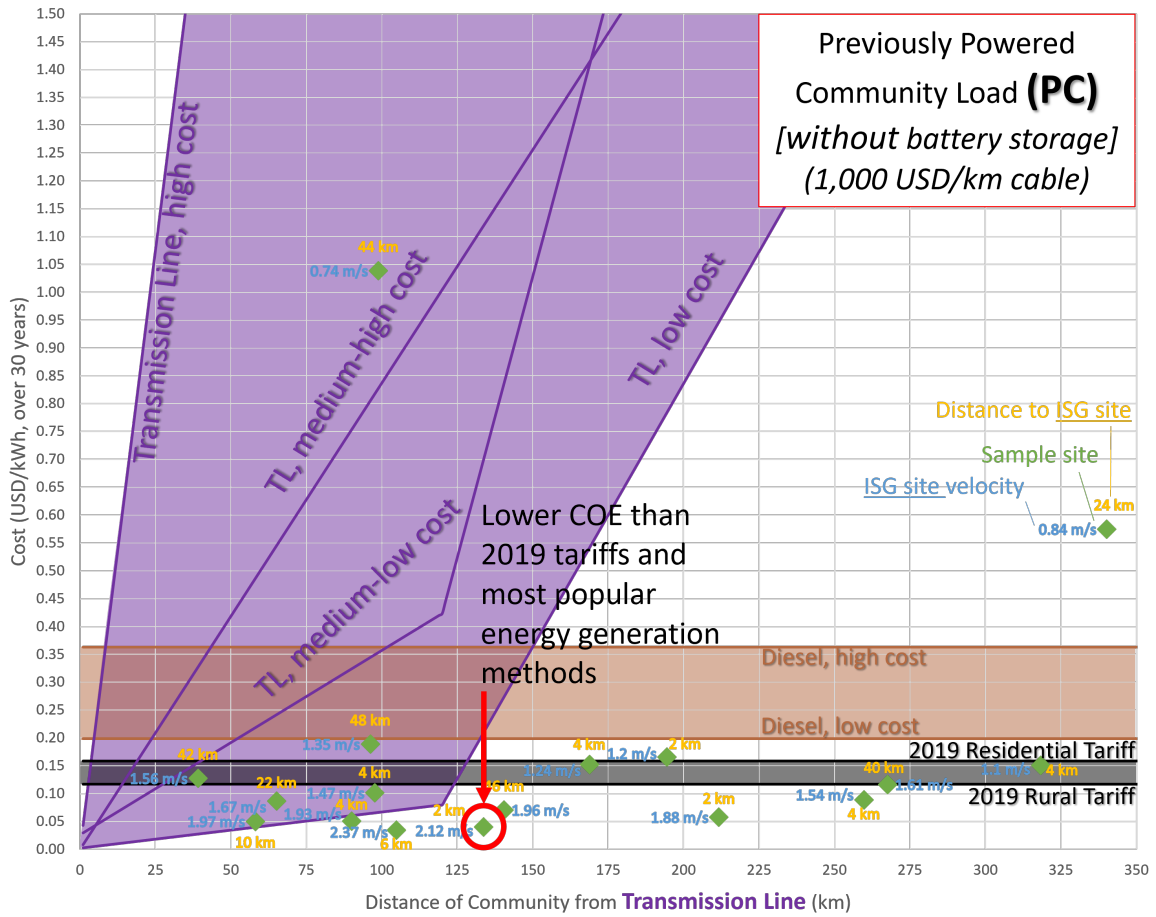


Figure 2.24: Comparison of proposed PC solution (green diamonds) with several common energy generation and distribution methods. The costs associated with the electric grid extension is shown by the purple range, a diesel generator is shown by the brown range and the 2019 Brazilian North region residential and rural tariffs are shown by the black range. See Figure 2.21 for axes.

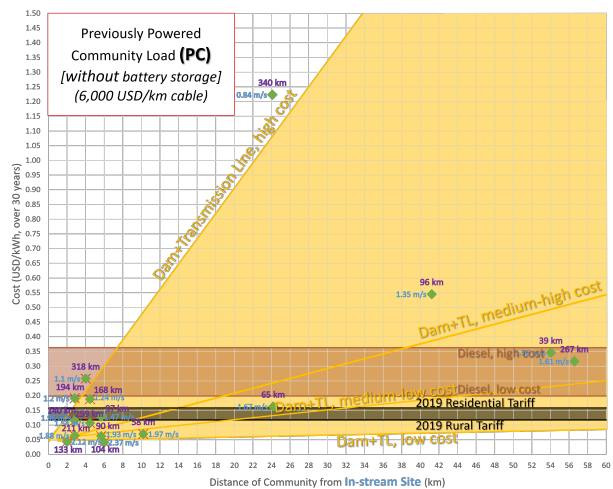
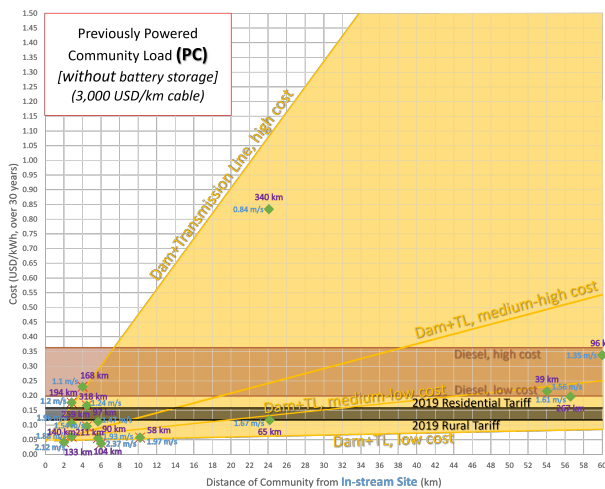
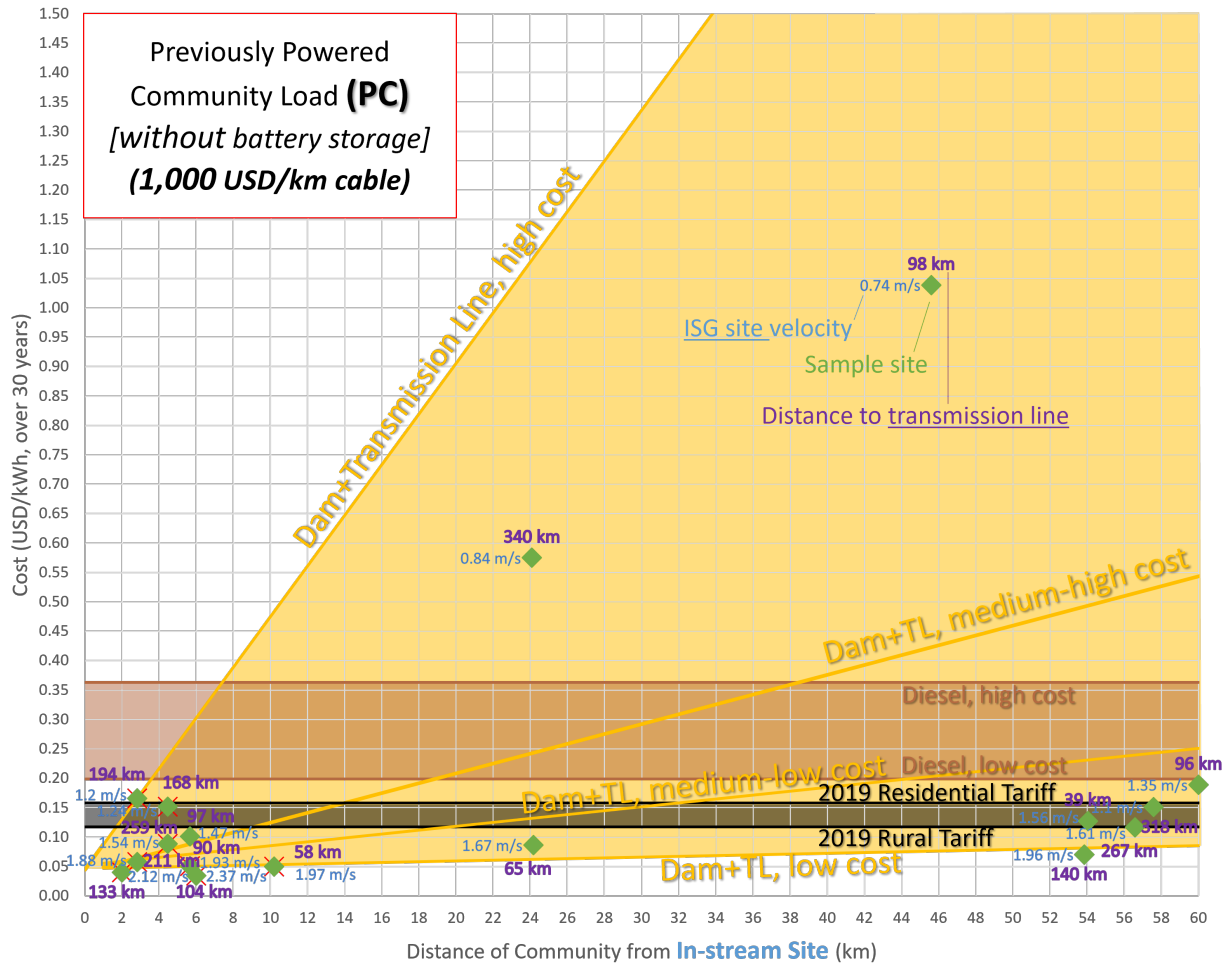


Figure 2.25: Comparison of proposed PC solution (green diamonds) with several common energy generation and distribution methods. A new dam construction with distribution lines is shown by the gold range, with no underreporting factor included, a diesel generator is shown by the brown range and the 2019 Brazilian North region residential and rural tariffs are shown by the black range. See Figure 2.22 for axes.

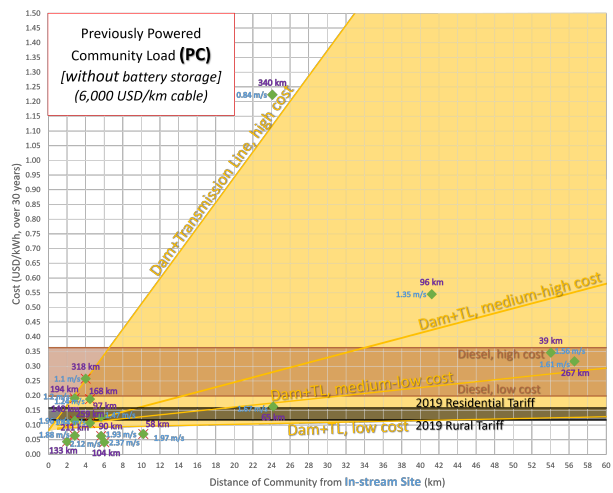
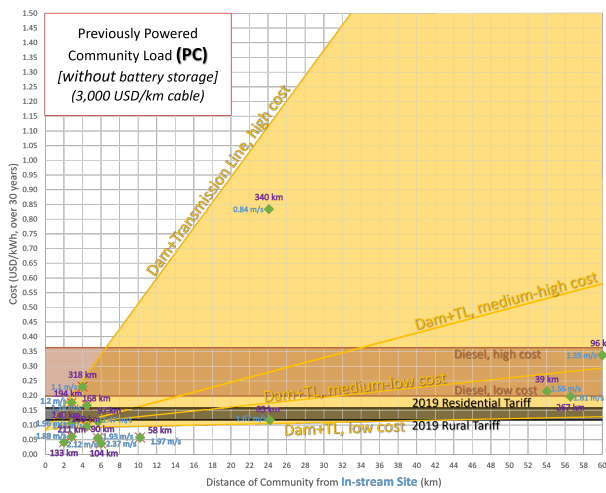
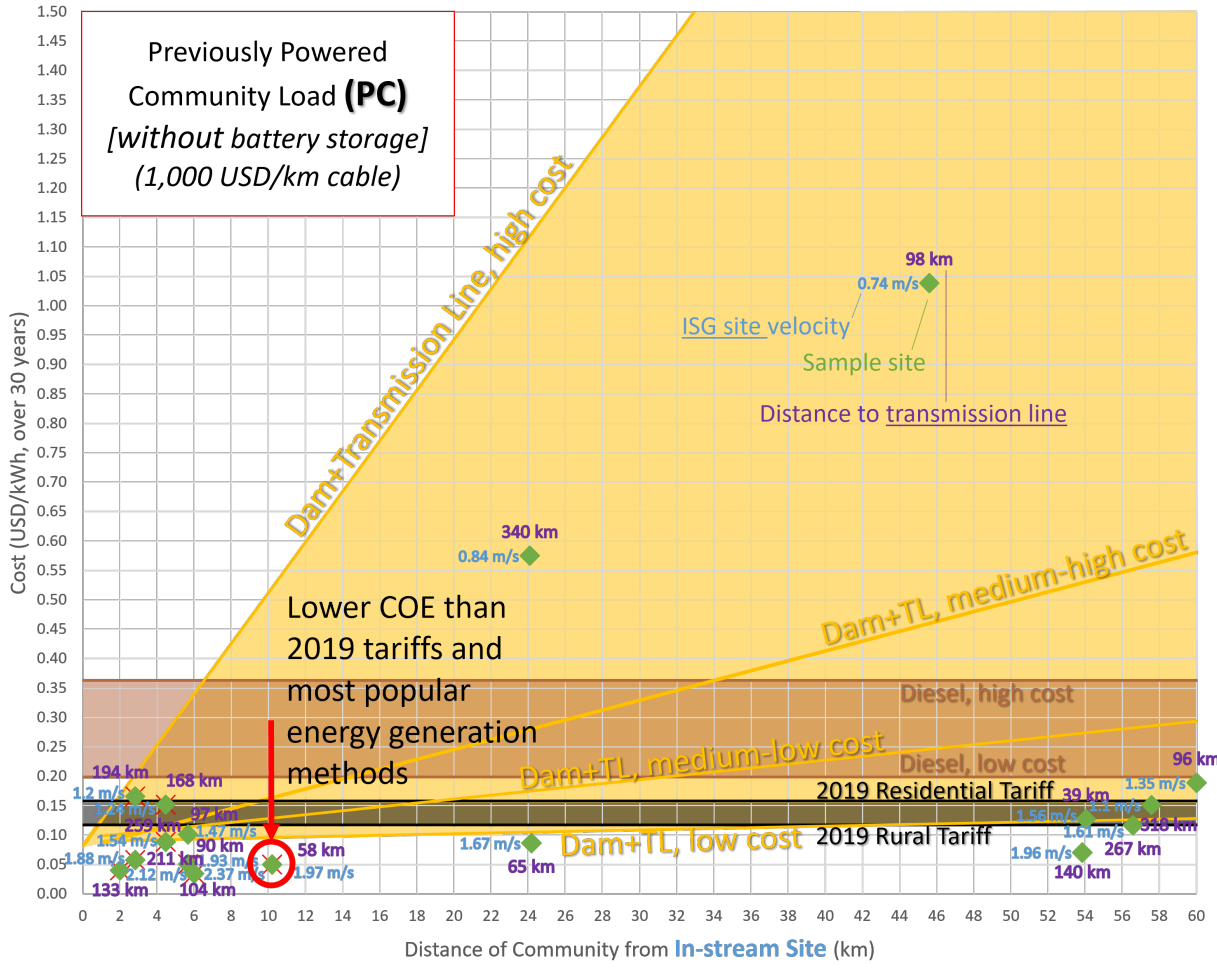


Figure 2.26: Comparison of proposed PC solution (green diamonds) with several common energy generation and distribution methods. A new dam construction with distribution lines is shown by the gold range, with an underreporting factor of 1.96 USD/USD included, a diesel generator is shown by the brown range and the 2019 Brazilian North region residential and rural tariffs are shown by the black range. See Figure 2.22 for axes.

from the proposed solution, and not need to depend on fossil fuels or government fuel credits. Increasing the cable cost from 1,000 USD/km to 3,000 and 6,000 yields the expected result of the costs associated with the in-stream generation to increase, and without the presence of a battery, the total project cost increases. The two sites that had calculated costs above the high diesel generator line increase in cost to a point where they are no longer shown on the higher cable cost plots, but for the sites that have costs that were comparable to the tariffs or diesel generator, the grouping of points remains consistently in the cost-competitive range over the cable costs considered here.

Figures 2.22 and 2.23 examine several cable costs on the feasibility of the proposed solution as compared to the construction of a new full-scale dam, a diesel generator, and the 2019 tariffs for a previously unpowered community. As it was found from Figure 2.21, there is a range of costs and thus feasibility of the proposed solution over the sample sites. The distribution of results for the sites is consistent with the aforementioned results, with the exception some sites across the examined cable cost range that are not as financially feasible as the others: these sites have a higher cost than the full-scale dam, but are at risk for flooding. For these sites, comparing the costs to a diesel generator leads to the conclusion that the proposed energy mix is competitive, even if not more cost-effectively than a dam, where the environmental and social safety compared to the full dam or diesel generator could be considered to make up the difference. Again increasing the cable costs from 1,000 USD/km to 3,000 and 6,000 yields two responses from the sample site costs: sites that were less competitive become even less competitive (some sites have costs that are high to be shown in the range of the figures), and the rest remain fairly well grouped in the competitive range. Results for a previously powered community (PC) indicate very similar trends to the UPC case, but at a slightly more cost-effective rate (see Figures 2.24 to 2.26). The results also remain consistent over the cost of cabling considered. The examined values of underreported costs for dam also did not change the overall resulting trend: the lower cost rate solutions (those around or below the tariffs) are financially beneficial with the 1.96

Table 2.1: Cables used as basis for investigation

Cable	V (V)	I (A)	USD/m
1	600	15	0.849
2	600	30	5.157
3	600	95	10.335
4	600	325	12.830

underreporting ratio (thought more so than compared to the factor of unity), and the sites that have higher costs are still less competitive comparatively.

#### 2.2.1.4 Off-grid microgrids: the natural reach of rivers

Another perspective on providing power to the local communities is instead of asking how economically they can receive power, asking how far can the community be from a high-enough velocity river and receive electricity at a given goal cost of energy? Conversely, the question could also be “high enough” river velocity to reach a certain distance? To find the maximum distance of service, there are two paths that could be used: coupled and uncoupled solution procedures. The coupled solution involves including the cable cost directly within the script used to determine the optimal river location simultaneous with the generation determination, minimizing distance and (and thus, cable cost) and maximizing river velocity available. For this study, the uncoupled method is used for a simplified examination of cable cost decoupled from the generation system costs. For this method, the generation system is sized to meet the load and then the cable costs are calculated based on the output. The cables used in the analysis are several “off-the-shelf” spools: the diameters are 18AWG, 16AWG, 12AWG, and 250MCM, ranging in cost from approximately 0.8 to 12.8 USD/meter, see Table 2.1 for details of each cable. The power carrying capability of the cable is calculated from the maximum rated voltage and the typical amperage carrying ability for that cable, assuming a power factor of unity (voltage in phase with current, or the real power is equal to the electric power,  $I * V$ ).

To calculate the effective range of the generation system, the cost levels of 0.40 USD/kWh

and 0.12 USD/kWh are used as a basis, corresponding to a diesel generator meeting the same load profile as the suggested energy portfolio and the 2019 North Region Brazilian rural tariff [8], respectively. The cost and carrying capacity of the cables are used to calculate the theoretical power transmission cost, up to a typical medium voltage line usage of 120 km [47]. After 120 km, it is assumed that a high voltage line has to be utilized, increasing the cable cost for the distances greater than 120 km to 90 USD/m [47]. It is assumed that for the size of community examined, an additional device for high voltage transformation will be required, but that the price will be small in proportion to the assumed total system costs. For a much smaller or larger community, this assumption will not hold as strongly, and high voltage transformer(s) would have to be added to the costs.

The following system of constraints (Equations 2.23 - 2.25) are solved, and then an analytical equation for maximum extension distance is solved (Equation 2.26):

$$\text{Minimize } (C_{b,eq}) \quad (2.23)$$

Where  $C_{b,eq}$  is the total system equipment cost without cabling, in USD, and is calculated as:  $C_{b,eq} = UC_{ISG} * P_{r,ISG} + UC_{PV} * P_{r,PV}$ . Where  $W, r$  is the rated power of the ISG or PV systems.

$$P_{ISG}(t) + P_{PV}(t) \geq Load(t) \quad (2.24)$$

Where  $P$  is the instantaneous power delivered by the ISG or PV systems at time-of-day  $t$ .

$$N_{ISG} \geq 0 \ \& \ N_{PV} \geq 0 \quad (2.25)$$

Where  $N$  is the number of ISG or PV generating units.

$$D_{MV} = \frac{gCoE * kphy * HH * T - C_{b,eq}}{CC_{MV} * TF} \quad (2.26)$$

Where  $D_{MV}$  is the distance of extension using a medium or low voltage line (LV or MV, simply named MV here) in km.  $gCoE$ ,  $kphy$ ,  $HH$ ,  $T$ ,  $CC_{MV}$ , and  $TF$  are: the goal cost of energy in USD/kWh, the load kWh/year per household, the number of households, the

number of years for the lifetime of the equipment, the cable cost of the MV line in USD/km, and the turbine factor, respectively. The turbine factor is a ratio of the designed ISG rated power to the theoretical maximum power that the line can carry. If the extension distance  $D_{MV}$  is found to be greater than 120 km, then a second equation is used:

$$D_{HV} = \frac{gCoE * kphy * HH * T - C_{b,eq} - CC_{MV} * 120 * TF}{CC_{HV}} \quad (2.27)$$

Where  $D_{HV}$  is the distance of extension using a high voltage (HV) line. It follows that if Equation 2.27 is used, then the total distance of reach of the system is  $D_{total} = D_{HV} + 120$ .  $CC_{HV}$  is the cable cost of a high voltage line, in USD/km. The turbine factor is not included in the high voltage line calculation assuming that for the system rated power in question for a typical off-grid community will be well-below the capacity of an HV line.

As can be seen from Figure 2.27 the behavior of the curves before the extension distance reaches 120 km is generally well-behaved, in that a simple conceptual simplification can be made: as a higher flow velocity is available, the farther that the generation mix can reach at a given price point. After the 120 km crossover, there is a change in the magnitude of slope the curves being dependent on the cost basis and cable of interest; however, the overall trend stays consistent: the higher the flow velocity available, the farther away from the river that the community can be located and have power provided in a financially-incentive manner. For several cables, there is another slope change around 1.6 m/s (cable #4) or 2.3-2.4 m/s (cables #1 or 3), which is caused by the assumption of TF not being able to go below unity, in other words, at least one full cable has to be sized, and not a fraction of one. This yields a curve that increases more slowly in extension distance over flow velocity, when compared with a curve that would allow the TF to fall below unity. The maximum renewable grid service distance is found to be approximately 150 km in the flow range investigated. At a distribution distance of 150 km from a river location that has a flow velocity greater than 2.6 m/s, approximately 43.6% of the Amazonian area could benefit from the service and meet the 0.40 USD/kWh goal cost of energy, or 35.5% for the Northern rural tariff.

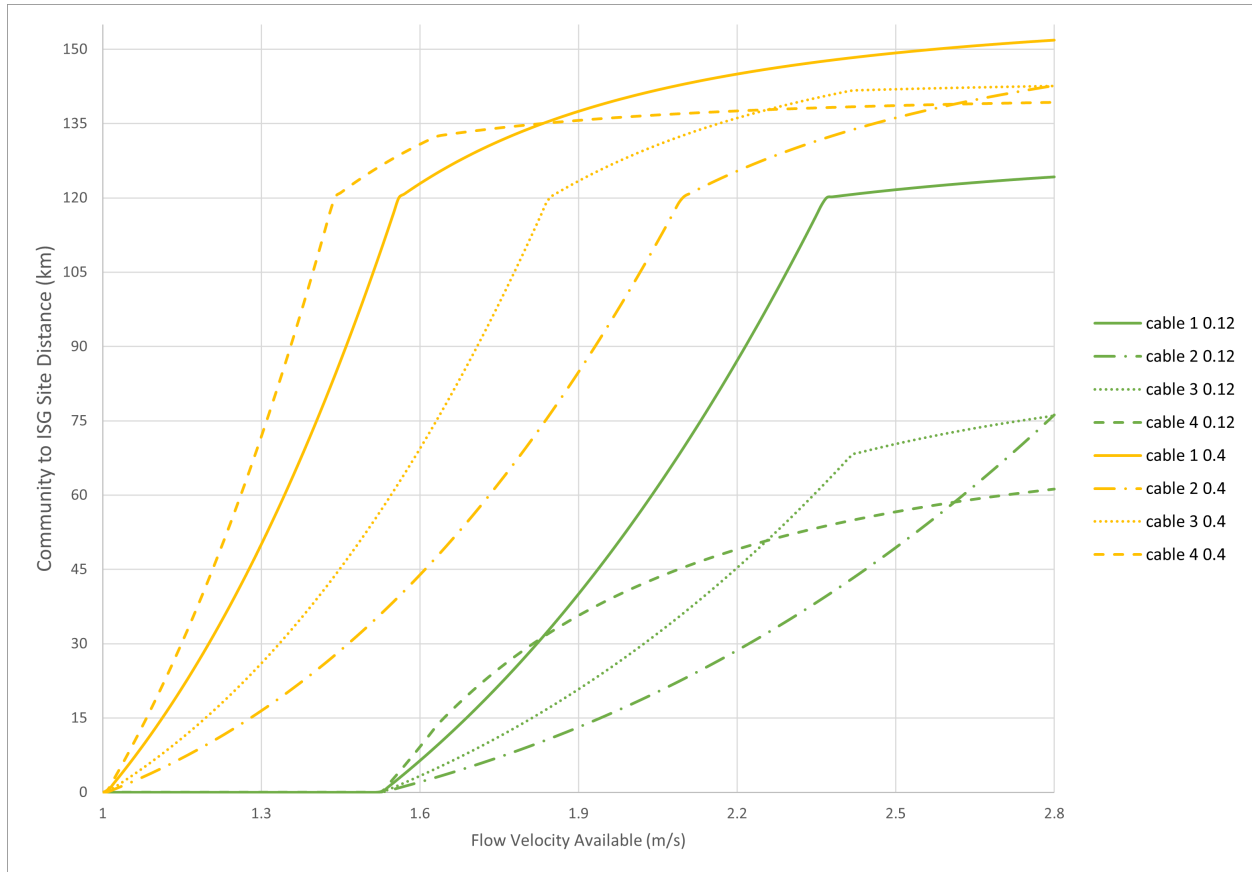


Figure 2.27: Reach of lossless cables at various goal cost of energy levels

### 2.2.2 Financial Interests: On-Grid Solution Methodology

Similar to the process for developing the off-grid solution, the on-grid solution is comprised of the following steps:

1. Develop a load model
  - Determine rated power to replace
    - Underproduction of current dams
    - Replacing planned dams
  - Scale rated power to current grid trend
  - Confirm that rated power is met
2. Determine generation to meet load

### 3. Perform financial analysis

#### **2.2.2.1 Load Development**

The first stage is to develop a load model, which represents the power needs of the country in contrast to individual communities. The load model is chosen as one that estimates the contributions to the grid from the future planned hydropower, as well as making up for current dam underproduction. However, it is not sufficient for a load model in this analysis to be equal to a constant over time, because it is an unrealistic assumption that the load (and thus, the load-following hydro) will be constant at all times. Instead, the net underproduction and planned power (approximately 12 GW) are used as a scaling factor, with load and generation data from ONS being the reference basis for scaling. The process for scaling is shown in the input-output structure in Figure 2.28. The nameplate capacity of the installed hydropower as well as the time history of actual supplied generation is reported by ONS [124]. The yearly average actual generated hydropower is calculated via a temporal integral, which is then used to calculate the ratio of the average power delivered to the average nameplate capacity for the year. This ratio, as well as the ratio of average actual delivered hydropower to the assumed average load (the modeled delivered power to the grid), are used to scale the net load curve for the solution. The load curve will have the same temporal shape as the actual grid hydropower generation. This load curve represents an expectation of how the installed on-grid components could be utilized in replacement of the planned dams and offset of underproduced power, in the scenario that the load injection is temporally curtailed so that it follows the existing grid load behavior.

#### **2.2.2.2 Generation Determination**

As was suggested for the off-grid systems, is it recommended to meet the modeled load for the on-grid system with a mixture of in-stream turbines and solar panels. One of the major differences between the two solutions is scale: the on-grid will have a much higher power

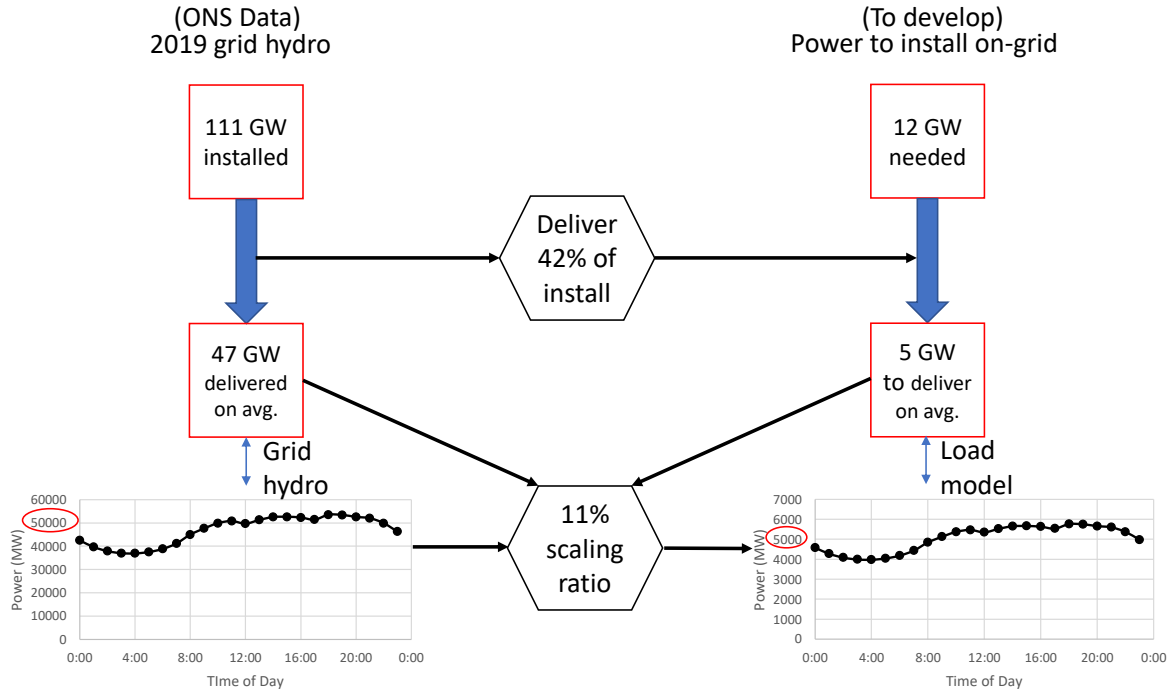


Figure 2.28: Load model development process for on-grid system

requirement for generation, due to the large dam plans for and the underproduction from several large dams. Another difference between the two solutions is that it is recommended that the solar panels be installed to float on existing dam reservoirs, instead of within communities on rooftops. There are several countries that are beginning to develop floating solar power: China, Japan, the United Kingdom, and Brazil, due to several noted positive effects over standalone solar and hydro systems, if designed with adequate spacing [77]:

- Increased panel output due to increased cooling
- increased water saving due to decreased reservoir evaporation
- Decreased algal blooms, and increased water quality
- Decreased greenhouse gas emissions from reservoir
- Decreased plant cost of energy and resulting tariffs

For further discussion and investigation into floating solar panels, see Chapter 3.

Unlike the off-grid solution, the on-grid case is a more “open-ended” problem to solve, as the need to minimally meet a load is not an explicit condition; Brazil routinely sells power to neighboring countries, and has also had issues with severe localized outages, thus Brazil could benefit from an increased grid reliability from the increased number of generators. As such, the calculated load profile serves as a soft guide, rather than a hard limit, meaning that the generation designed to meet the load has increased flexibility. Using the same panels for the off-grid case, covering only 1% of the reservoirs of underproducing dams, the floating PV system could generate and deliver 7 GW out of the 12 GW designed. The 1% coverage equates approximately  $72.7 \text{ km}^2$  out of  $7,262 \text{ km}^2$  total available surface area (a total of  $13,565 \text{ km}^2$  was found, but the Chave do Vaz reservoir was ignored, due to its unrealistic reported area versus the power and size of the dam). ISGs make up the difference of 6 GW at the full-rated  $V_{90}$  of 2.8 m/s. The generation that was calculated to meet (and likely exceed) the load model is shown in Figure 2.29. For this generation scenario, an extra 66.1 GWh is added to the grid. Another possibility for a generation mixture can be found by assuming the grid acts as a battery for the system, and so any “extra” power generated will be stored by the grid, effectively reducing the total MWh needed to meet the required load. Shown in Figure 2.30, this reduces the required in-stream rated capacity (the number of devices), where the floating PV system still covers only 1% of the existing reservoir surfaces.

### 2.2.2.3 Financial Analysis and Discussion

For the PV system, it is recommended that the panels be installed floating on existing reservoirs, which is reported to add 18% cost over traditional land-based systems [164]. The cost of the proposed energy mixture for on-grid usage was calculated to be 0.017-0.019 USD/kWh, over 30 years (assuming 365 days per year operation). The dams that could be sized to meet the same load (12 GW of rated power), assuming the same yearly usage as the proposed solution and installation cost of 5.5 USD/W, were calculated to operate at 0.052 USD/kWh, showing that the on-grid solution could be an economically viable portfolio

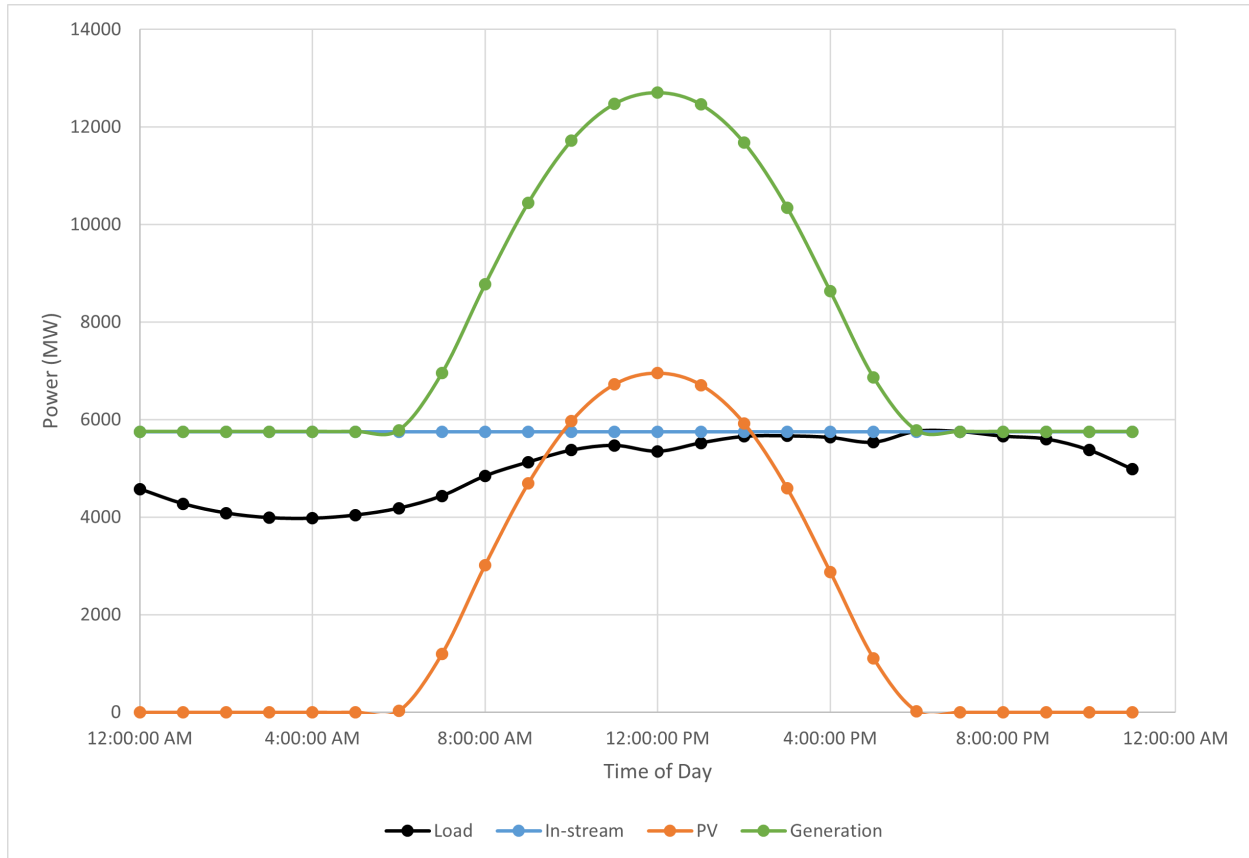


Figure 2.29: Load model development process for on-grid system

addition for Brazil. Due to the basin-scale distribution of the reservoirs and rivers in question, cabling costs were not included in the on-grid financial analysis, but would be a crucial detail to include in future work to decide financial feasibility, or at least, the most cost-effective magnitude of power to produce at (at the shown 10 GW, or at 100 GW, etc.). To estimate an equivalent value compared to the replaced dams, the flow velocity of approximately 1.73 m/s was found to yield a similar cost per kWh of electricity supply. From hydraulic data, assuming that rivers are represented by flow rates of greater than  $100 \text{ m}^3/\text{s}$ , this minimum velocity criterion is present in approximately 5,353 km worth of equivalent river length in the grid cells. The found river lengths can provide sufficient spacing to fit the 5.26 million turbines (with a 10 diameter spacing in between turbines) even if only a single one meter diameter turbine is placed in each row. This warrants another optimization problem, where

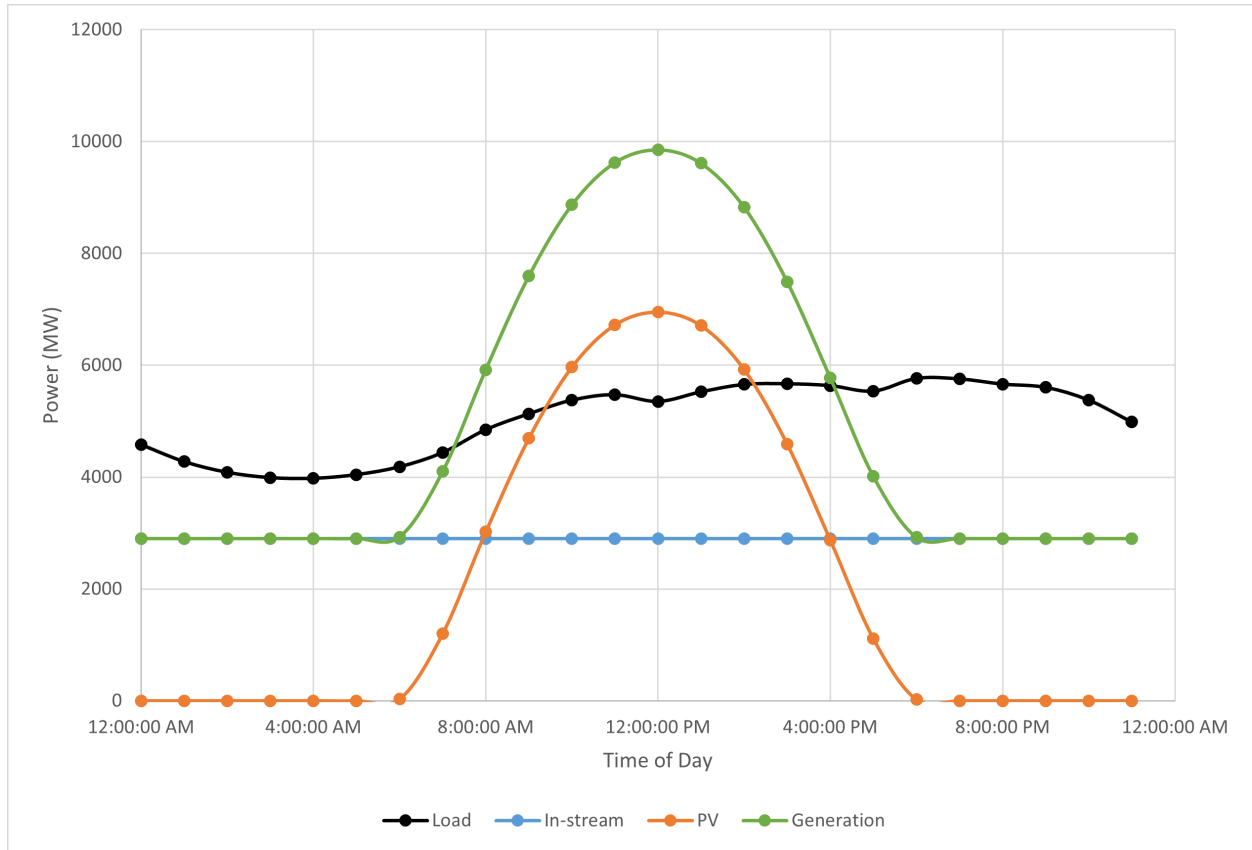


Figure 2.30: Load model development process for on-grid system

the number of turbines in each row can be increased (or an equivalent blockage ratio), as well as the diameter of each turbine, balanced against the possible hydraulic effects on the marine environment as well as the cable costs associated with transferring power from that location to the national electric grid.

## CHAPTER 3

### ENHANCEMENT OF GRID STABILITY WITH FLOATING SOLAR PANELS

This chapter has been reproduced as originally published: Samer Sulaeman, Erik Brown, Raul Quispe-Abad, Norbert Müller. Floating PV system as an alternative pathway to the amazon dam underproduction. *Renewable and Sustainable Energy Reviews*, Volume 135, 2021. 110082. ISSN 1364-0321, <https://doi.org/10.1016/j.rser.2020.110082>.

#### 3.1 Background

One of the numerous, and perhaps most transformative, changes that the power grid is undergoing is the inclusion of renewable energy resources. In recent years, the penetration of grid-level renewable resources such as wind power and photovoltaic (PV) systems has tremendously increased due to political, environmental, and economical incentives. The rapid investment toward increasing the penetration level of renewable energy sources has become one of the possible solutions to reduce greenhouse gas emissions, among other social-environmental issues related to electric power production, aiming to replace the need for fossil-fueled generators. Globally, the investment toward installing large wind and PV farms, and hydropower plants (dams) have increased in the recent years, largely because of the believed benefit over fossil fuel generation systems in regards to: environmental concerns, global warming awareness, and economic incentives. Wind power, PV systems, and hydropower plants have received more attention especially in regions where the output power of these sources is potentially high. In the US, the projection of wind power and PV system integration is assumed to reach 35% and 19% respectively by 2050 [186]. In other countries such as Brazil about 68% of the electrical energy is currently coming from large dams, while the contribution of other energy sources is around 32% [130]. However, the Brazilian government is planning to build more dams to meet the future increased power demand [130].

On the other hand, many environmental and social concerns associated with hydropower plants expansion in the Amazon region are still of concern, some of these concerns have already been studied and extensively addressed in the literature [72, 98, 169, 177, 20, 178]. The utilization of an additionally balanced mix of energy sources may potentially provide an alternative pathway to avoid the environmental and social impact of dam expansion in Brazil while meeting the increasing power demand.

One of the promising applications of a generation mix that has gained attention recently is the integration of floating PV (FPV) systems on the reservoir of dams. Some countries such as China have already aggregated as much as 150 MW of FPV systems on flooded mining sites and connected to the national grid [154, 194]. Other countries such as Japan already have installed 22.66 MW of FPV systems; while countries such as Canada, Singapore and India contribute to a small amount of worldwide installation of PV system alongside hydropower plants [154, 194]. In the US, despite the fact that investment toward implementing FPV system is limited, a study by Spencer et al. [175] shows that the investment of FPV systems on man-made water bodies could potentially produce up to 10% of current national power supply. In Brazil, where most of the electrical energy is currently coming from large dams, installing FPV systems on the reservoirs of hydropower plants is still in its early stages. Recently, FPV pilot projects were announced by the Brazilian government for the reservoirs of the hydroelectric power plants of Balbina (State of Amazonas) and Sobradinho (State of Bahia) [71]. Although the main goal of these pilot projects is to evaluate the performance of FPV systems under different climatic conditions, the current experiences with the installed FPV systems worldwide reveal some advantages of hybrid system deployment, especially on reservoirs of dams. Such a hybrid system already offers a higher power dispatch flexibility that PV power provides especially during high demand times (i.e., day time when the output of PV system is potentially high), and adding more flexibility to the operator to dispatch power generated by hydropower plants as such to be used during night and early morning hours [154, 194].

In the literature, several authors have evaluated possible scenarios that can be implemented to minimize the environmental and social impacts associated with reservoirs in the Amazon Basin as a result of building new large hydropower plants. In [12], the authors evaluated the Brazilian electric network expansion considering replacing large dams with wind power plants. The authors' findings suggest that wind power has limited potential as the investment toward more wind power installation increases. With the limited deployment of PV systems in Brazil, several authors have also discussed the potential electrical benefits of PV systems in both grid-connected and off-grid applications, as well as the potential social and environmental benefits, especially in rural and off-grid communities. In [17, 18, 16], the authors have evaluated the transmission expansion and location-based marginal price along with other issues such as energy import/export between Brazil and neighboring countries. Others [168, 42, 114] have evaluated the deployment of PV systems in the rural areas where the main grid is too far away to allow for economically-feasible expansion.

Large-scale deployment of PV systems in Brazil also has been investigated with regard to grid-connected and building-integrated systems and their potential benefits to the electric grid [103, 153, 11]. In [145], a literature review of FPV system configuration, application, and its impact on water evaporation and CO<sub>2</sub> reduction have been discussed. It has been concluded that using the FPV system has a high potential of reducing CO<sub>2</sub> emissions and water evaporation. In [179], a sustainable hydro-solar model is proposed as an alternative to the current model of power production in Brazil. [121] evaluates different FPV technologies and their performance, and the authors conclude that the FPV system performance is mainly dependent upon the technology used and the location of the PV system. Another benefit is that the deployment of FPV could also lead to more favorable policies towards future consideration of large-scale deployment of PV systems in Brazil. [200] also has shown that a hybrid FPV-hydropower system improves the energy efficiency of the hydropower plant. In [151], the electrical and economic benefits of installing a FPV system on the tropical Gavião reservoir in Northeast Brazil have been evaluated. The authors have that is it eco-

nomically viable, besides the environmental benefits, it is also economically viable. Further, [137] examines the environmental and socio-economic impacts of large-scale deployment of photovoltaic systems in Brazil. In [170], a case study on the hydroelectric plants of the São Francisco River basin has been presented, wherein the technical and economical procedures for sizing the FPV system and the coordination with hydroelectric plant operation have been evaluated. Besides the environmental gain, the results also indicate installing FPV could potentially increase the hydroelectric plant production flexibility by 76% and the capacity factor by 17.3% on average.

A utilization of mixed generation resources may potentially provide an alternative approach that can be fully implemented and utilized to avoid the environmental and social impact of dam expansion in Brazil while meeting the increased power demand. The work presented here focuses on assessing the contribution of FPV to the adequacy of generating capacity of the Brazilian electric system. The capacities of FPV systems are designed to offset the hydropower dam underproduction and an alternative pathway to large dam expansion is proposed. FPV systems are installed and integrated alongside the existing dams to offset the current underproduction capacities, enhance the existing power sources and provide an alternative pathway to meet the increasing power demand. System adequacy is evaluated by calculating system reliability indices before and after adding FPV systems. Further, the correlation between PV output and system load is evaluated, and the environmental and social concerns associated with dam expansion in the Amazon Basin are briefly discussed. This work evaluates the benefits of adding FPV systems on the system adequacy and is not intended for security assessment. The main contributions of this work are: 1) Evaluating the potential contribution of floating PV systems to the Brazilian power grid. 2) Investigating the enhancement the existing power sources by installing FPV on existing reservoirs to provide an alternative pathway to meet the increasing power demand. 3) Evaluating the correlation between FPV output and system load. 4) Evaluating the contribution of large-scale deployment of FPV systems to the system adequacy. System adequacy is evaluated

with respect to the current underproduction of dams and the required capacities of FPV systems that are needed to offset the current underproduction of dams. In addition, reliability assessment is used to evaluate the potential benefits toward installing FPV systems on the reservoirs on the overall system reliability. Adequacy of generating capacity of the Brazilian electric system is evaluated in several case studies with different scenarios. System reliability improvement, in terms of reliability indices, is also evaluated with and without the addition of a FPV system. Metrics commonly used for reporting bulk power system reliability are utilized in this work: loss of load probability (LOLP), Loss of Energy Expectation (LOEE), expected demand not supplied (EDNS), and loss of load frequency (LOLF). Also, the environmental and social concerns associated with dam expansion in the Amazon Basin are briefly discussed.

The remainder of this paper is organized as follows. Section 3.2 presents an overview of the current power system in Brazil. Section 3.3 discusses the environmental and social impact of hydropower dam expansion. Section 3.4 discusses an alternative pathway to dam expansion and the proposed solution. Section 3.5 describes the adequacy of power system and evaluation of reliability indices. Section 3.6 presents system modeling. Section 3.7 provides several case studies, results, and discussions thereof. Section 3.8 provides concluding remarks.

## **3.2 An Overview of the Current Brazilian Electric Power System**

The Operator of the National Electricity System (ONS), which is responsible for the coordination and control of the generation and transmission installations in the National inter-connected system of Brazil under the supervision and regulation of the National Electric Energy Agency (ANEEL) has listed the current installed power capacities including transmission line expansion need to meet the increasing demand [30]. These statistics are listed in Table 3.1.

Currently, the largest power source in the Brazilian power network is the hydropower dams, with an installed capacity exceeds 109 GW and it is projected to increase to 114.395

Table 3.1: Current installed power capacities and projection of capacity planning increase by year 2023

Power source	Installed Capacity (2018) (GW)	Projected Capacity (2023) (GW)	Percentage of Capacity Increase (%)
Hydro	109.058	114.449	4.710
Thermal+Gas	12.821	17.780	27.890
Oil-Diesel	4.614	4.900	5.830
Coal	2.672	3.0170	11.430
Biomass	13.696	14.028	2.370
Nuclear	1.980	1.980	0.000
Wind	14.142	17.177	17.670
Solar (PV)	1.780	3.630	50.960
Others	0.779	1.000	22.100
Total	161.552	177.961	9.220

GW by the year 2023 [130]. Other resources such as wind and PV power contribute to a smaller percentage comparing with hydroelectric power plants as indicated in Table 3.1. Currently, solar power contributes to only 1% of the system total installed capacity, on the other hand, wind contribute to around 9%. However, the projection of PV power in the year 2023 will increase by 51% while wind power is projected to increase by 17.7%. However, the Brazilian government has recently previewed several pilot-projects on floating PV (FPV), this largely because of the high incidence of solar radiation that powers PV systems [103, 114, 42, 11]. With the need for more generating capacity expansion, the Brazilian government is planning to expand the existing transmission lines to meet the grown demand, especially with the largest power sources (hydropower dams) being located far away from the major loads. Fig. 3.1 shows the interconnected system of Brazil as adopted from [130].

### 3.2.1 Underproduction of Dams

Dams with reservoirs act as natural hydraulic batteries that resist high-frequency changes to water levels. The reservoirs, however, can not adjust sufficiently for long-term or severe

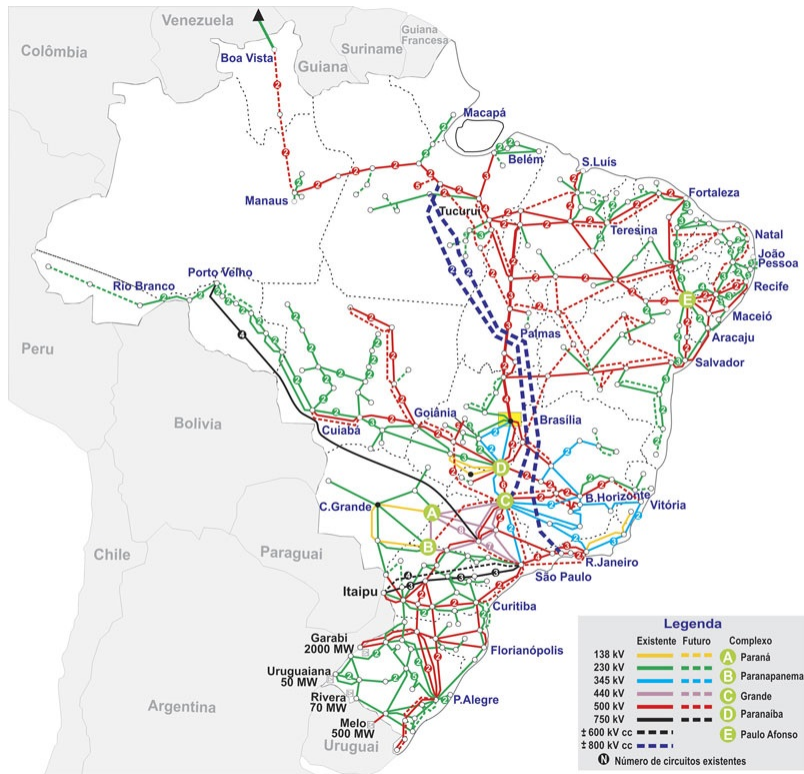


Figure 3.1: Brazilian interconnected system [130].

changes in rainfall or other climatological factors. As a result, dam systems cannot always produce their average rated power when water levels are below an acceptable level to produce the head drop necessary for the installed turbines. Another factor that can affect the ability of the dam system to produce power is economic feasibility; depending on the load on the electric grid system at a given time of the day, it may not be profitable to run the turbines at high load or possibly at all. Water estimations for the Amazon Basin indicate a drying trend in the Southern and Eastern regions [178, 110]. This is decreasing the water supplies and affecting the reliability of power generation [178, 110]. The Jirau dam and Santo Antonio dam on the Madeira River in Brazil, completed in 2013, are estimated to generate only a fraction of the projected power (3 GW each) due to the smaller storage capacity of run-of-the-river reservoir [178, 167]. Belo Monte dam on the Xingu River, completed in 2016, is also estimated to produce only 4.46 MW of the projected power (11.23 GW) [100, 167, 110]. Another factor affecting the power generation is the deforestation in the Amazon River Basin, which is being

investigated by [178]. In the Xingu Basin, the location of the Belo Monte dam, with changes in rainfall, the projections of forest loss could reach 40% by 2050, and could potentially lead to 25% reduction of the current power capacity [178, 116]. In Brazil, it can be estimated that there is around 12 GW of underproduction of rated capacity considering operational dams [30]. The nominal capacities of the dams, fiscal power production and underproduction percentage as calculated from the reported values in 2018 by [30] are shown in Table 3.2.

### 3.2.2 Wind and PV Power in Brazil

In Brazil, the largest state in the Amazon is the state of Amazonas, with a large surface area of 1,559,148  $km^2$ . As shown in Figures 3.2–3.4, the Amazon region has a strong solar radiation and high potential of PV power output [193]. Despite the seasonal variation and climate characteristics along the Brazilian territory, the total daily average value of solar irradiation as recorded for 16 years (1999–2015) shows that the global irradiation is fairly uniform with a maximum daily average value reaches 46.2  $kWh/m^2$ . Further, the daily average of PV potential power as recorded for the same period of time along the Brazilian territory ranges between 3.8–4.8  $kWh/kWp$ , with yearly average ranges between 1387–1753  $kWh/kWp$ . The amount of solar radiation and potential of PV along Brazilian territory is considerably high comparing to the majority of the European countries where more investments towards PV power installation have gained a great momentum [22]. Although Brazil has on average a high PV power potential compared to some leading countries, such as Japan with GHI of 1022–1607 with a total installed capacity of 56,162 MW, Germany with GHI of 949–1241 with a total installed capacity of 45,452 MW and France with GHI of 494–1680 with a total installed capacity of 10,562 MW as shown in Table 3.3, Brazil has only accumulated 2,296 MW of PV system so far [104]. According to [130], Brazil is planning to increase the investment towards PV installations to bring the total projected capacity to 4,241 MW by the year 2024. However, wind power has received more investments in Brazil along the coastal areas where the potential of wind speed is high as shown in Fig. 3.5. Noticeably,

Table 3.2: Dams underproduction

Dam Name	Nominal Capacity (MW)	Fiscally Reported Power (MW)	Percent under Rating (%)	Dam Name	Nominal Capacity (MW)	Fiscally Reported Power (MW)	Percent under Rating (%)
Ado Popinhaki	22.600	16.950	25.0	Pedrinho I	16.200	16.040	1.0
Alto Benedito Novo	6.500	2.192	66.3	Pereira Passos	99.900	99.110	0.8
Balbina	250.000	249.750	0.1	Piabanha	20.000	9.000	55.0
Bariri	143.100	136.800	4.4	Porto Colômbia	320.000	319.200	0.3
Belo Monte	11233.100	3938.570	64.9	Primavera	25.700	24.740	3.7
Bugres	24.120	11.120	53.9	Rio Fortuna	6.990	6.850	2.0
Cachoeira do Ronca	0.900	0.340	62.2	Ronuro	1.040	0.874	15.9
Calheiros	19.528	19.000	2.7	Santa Cruz	0.550	0.364	33.8
Canastra	44.800	42.500	5.13	Santa Cruz	1.500	1.400	6.7
Capigui	4.470	3.760	15.8	Santa Luzia Alto	29.250	28.500	2.6
Capivari	18.738	18.090	3.5	Santa Rosa	1.580	1.400	11.4
Cedros	8.400	7.280	13.3	Santana	0.650	0.500	23.1
Celso Ramos	12.816	5.600	56.3	Santo Antonio	3150.400	2286.100	27.4
Chave do Vaz	1.600	0.680	57.5	São Domingos II	24.660	24.300	1.5
Paranoá	30.000	29.700	1.0	São Lourenço	29.990	29.100	3.0
Passo de Ajuricaba	6.200	3.200	48.3	São Manoel	700.000	175.000	75.0
Passo do Inferno	4.900	1.332	10.6	São Pedro	2.160	1.500	30.5
Coaracy Nunes	78.000	76.952	1.3	Tudelândia	2.547	2.400	5.8
Venâncio	3.820	1.600	58.1	Walter Rossi	16.500	15.780	4.4
Congonhal I	1.816	1.616	11.0	Ypê	30.000	27.400	8.7
Cristo Rei	1.800	0.960	46.6	Mello	10.680	9.540	10.7
Ernestina	4.960	4.800	3.2	Nilo Peçanha	380.030	378.420	0.4
Estreito	1050.000	1048.000	0.2	Mascarenhas	198.000	189.000	4.5
F	3.972	3.792	4.5	Marumbi	9.600	4.800	50.0
Ferraria Gomes	252.000	168.000	33.3	Marco Baldo	16.750	16.550	1.2
Fontes Nova	131.900	130.300	1.3	Jirau	3750.000	2100.000	44.0
Forquilha	1.118	1.0000	10.5	Itiquira	157.400	156.000	0.9
Glória	13.800	11.360	17.7	Itapebi	462.000	456.000	1.3

as mentioned in Section 3.2, solar power has more potential than wind power especially in the Amazon region largely due to: wind power having less potential power especially in the

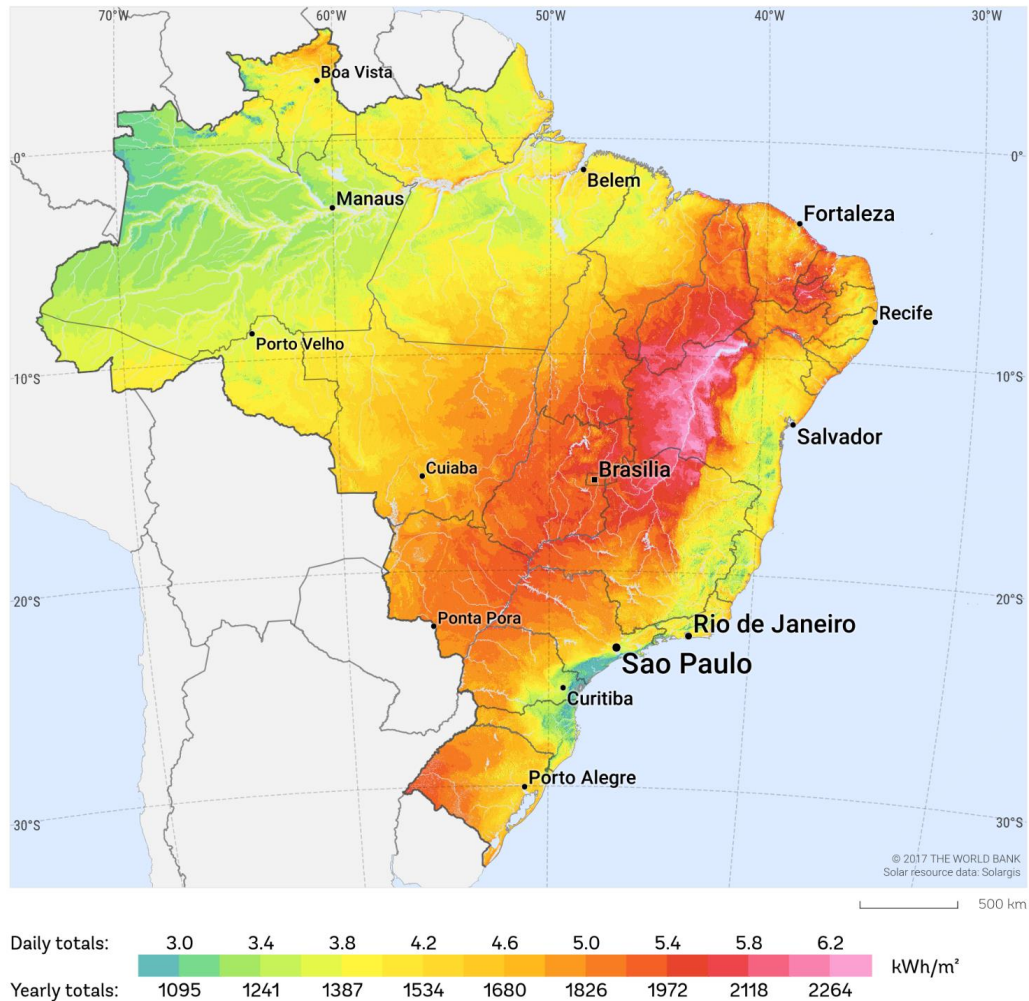


Figure 3.2: Direct normal irradiation in Brazil from 1999–2015 [193].

Amazon region where the tall, dense forests and low-pressure gradients are concentrated, high potential of PV power within the Brazilian territory, and changing policies toward a more balanced generation mix investment [103, 114, 42, 11]. Therefore, in this work, wind power is not considered as an alternative solution to dam expansion in the Amazon Basin. However, adequacy assessment of Brazilian power network is evaluated for generation mix including the existing wind farms and PV systems.

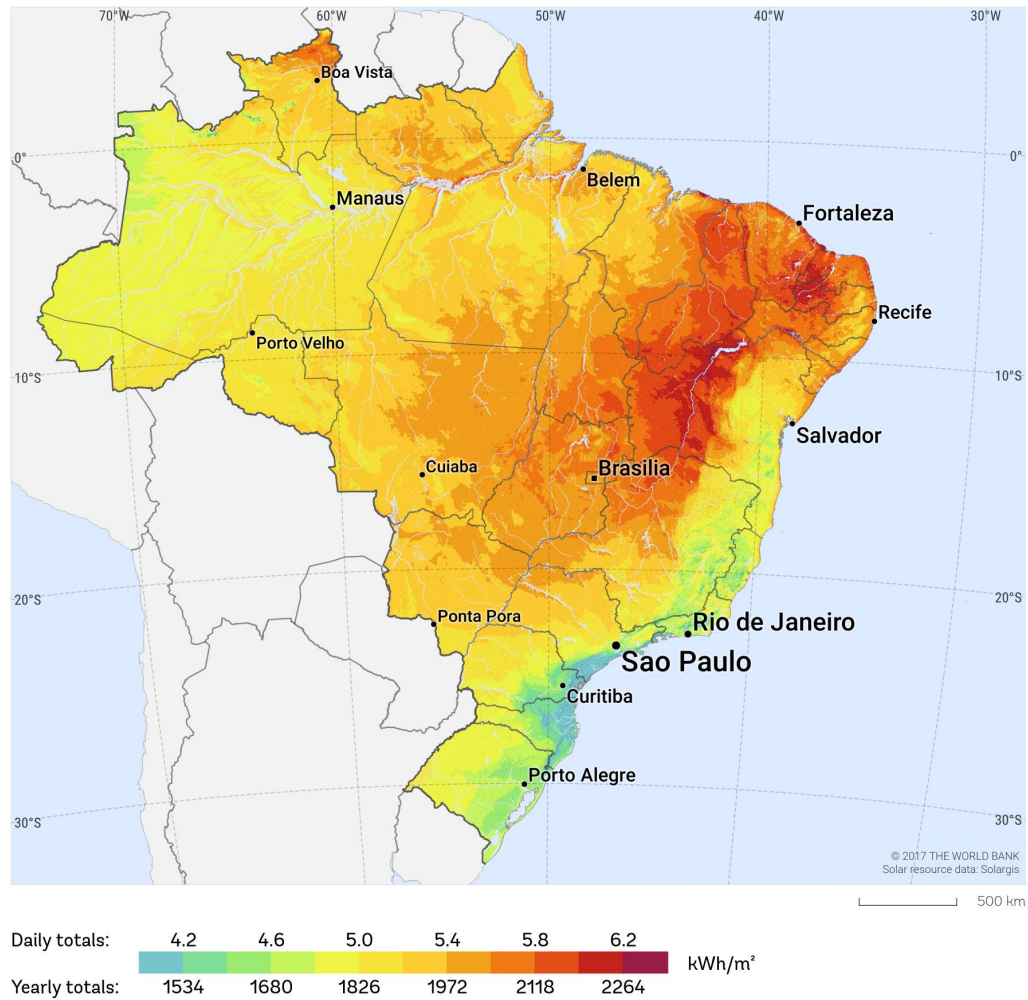


Figure 3.3: Global horizontal irradiation in Brazil from 1999–2015 [193].

Table 3.3: Installed PV capacity and the horizontal solar irradiation for different countries

Country	Yearly Average GHI ( $kWh/m^2$ )	Installed Capacity (MW)	Grid-connected (MW)	Off-grid (MW)
China	949–2118	175,400	175,032	368
Japan	1022–1607	56,162	55,989	173
U.S.A	330–2191	62,498	62,498	—
Germany	949–1241	45,452	45,402	50
India	1241–2264	34,831	34,831	—
Italy	1022–1899	20,107	20,107	—
Australia	1387–2264	10,953	10,669	284
France	494–1680	10,562	10,532	30
South Korea	1241–1461	10,505	10,505	—
Spain	1095–1972	5,659	5,513	146
Brazil	1387–1753	2,296	1796	500

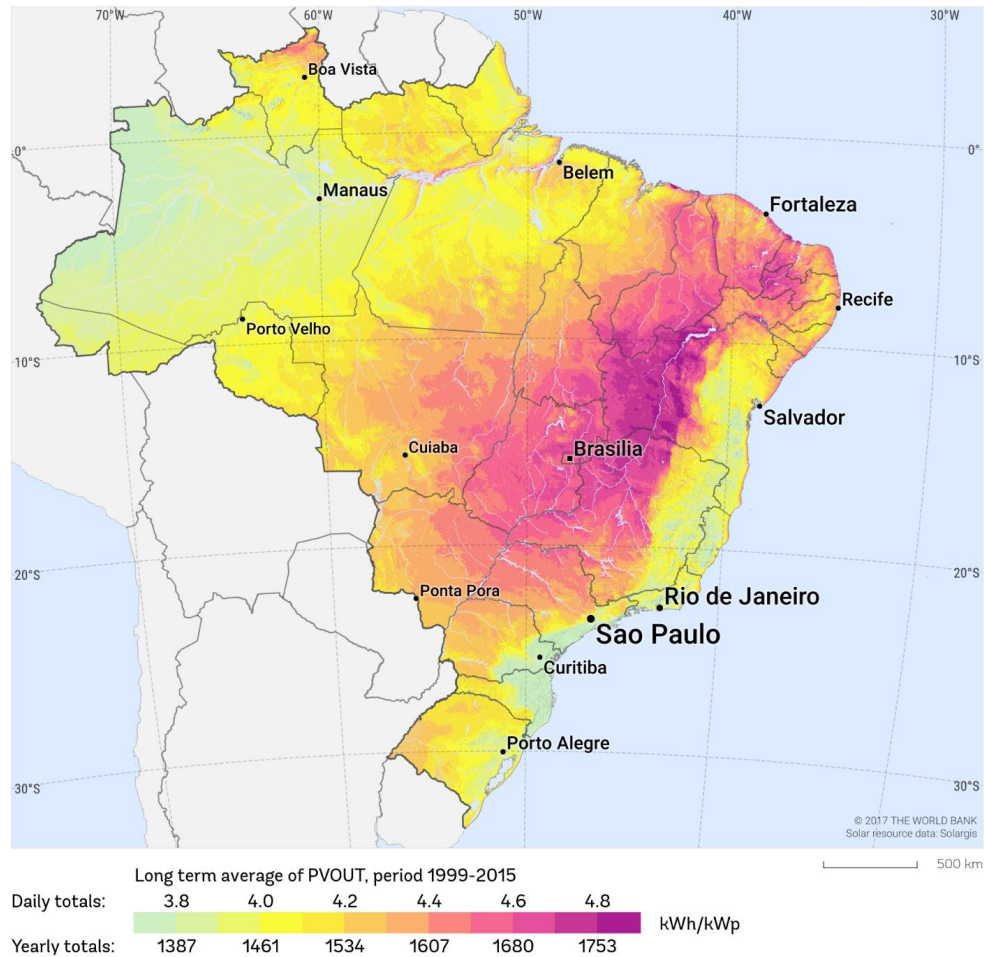


Figure 3.4: Potential of average Photovoltaic power in Brazil from 1999–2015 [193].

### 3.3 Environmental and Social Impact of Dams

Contrary to popular belief, the notion of hydraulic dams with reservoirs being completely green is inaccurate. Dams cause environmental and social issues, some of which are: increase greenhouse gas emission [176, 66, 63, 59, 58, 57], increase likelihood of toxic methylation [180, 62], increase evaporation of river water [58], interruption or complete blockage of waterborne animal migration and natural living patterns, and deforestation and unnatural levels of flooding for the dam reservoir. These environmental issues are also simultaneously social issues, with the addition of forced relocation of local peoples for the introduction of the dam



Figure 3.5: Percentage of potential wind power in Brazil [193].

and reservoir via the destruction of the local area for the reservoir itself, or from the resulting flooding from filling the reservoir [61].

### 3.4 Floating PV Systems on Hydropower Dam Reservoirs

The addition of off-grid PV systems and grid-level PV systems floating on the reservoir of dams can help prevent social and environmental issues associated with dams from worsening in the future by offsetting the planned need for power from dams. Integrating grid-level FPV systems to existing dams add more flexibility to the operation of large dams by allowing large dams to operate not following base-load but rather load following approach. The investment toward integrating such alternative systems open up more opportunities for deployment of environmentally- friendly and yet efficient power sources that can supply the current and future power needs of the country, both on and off of the grid. Despite the fact that the deployment of large scale grid-connected FPV systems are still in early stages, the deployment of PV systems alongside existing dams or floating on the reservoirs has been recently

gaining more attention. As depicted in Fig. 3.6, globally, China and Japan are leading on PV systems installation with total capacity of 376.50 MW and 22.66 MW, respectively. Other countries such as Canada (0.0005 MW), Singapore (0.005 MW) and India (0.06 MW) contribute to a small amount of world wide installation of PV system along side hydropower plants. Meanwhile, other countries such as Afghanistan, Azerbaijan, Colombia, Ghana, and the Kyrgyz Republic, development of FPV systems projects are under progress [154, 194]. This is largely because of the fact of high potential and efficiency of FPV system installed on the reservoir of dams and the ability to provide a natural storage system that can be utilized and dispatched to provide a balance to the system operation including the intermittent sources. Further more, FPV systems can help reduce environmental issues due to the fact that the FPV systems providing shade that minimize water evaporation, improve water quality and help fish and other water species' population stability but also symbiotically increasing the PV system efficiency by providing a natural cooling system [196, 39, 152].

Considering the environmental and social concerns associated with the dam expansion in Brazil as mentioned in Section 3.3 and herein, the proposed solution aims to minimize such concerns by installing grid level FPV systems (*floating on the reservoir area*) alongside the existing dams. The FPV system design facilitates local fishing activities and the cohabitation of marine life when PV arrays are presented as depicted in Fig. 3.7.

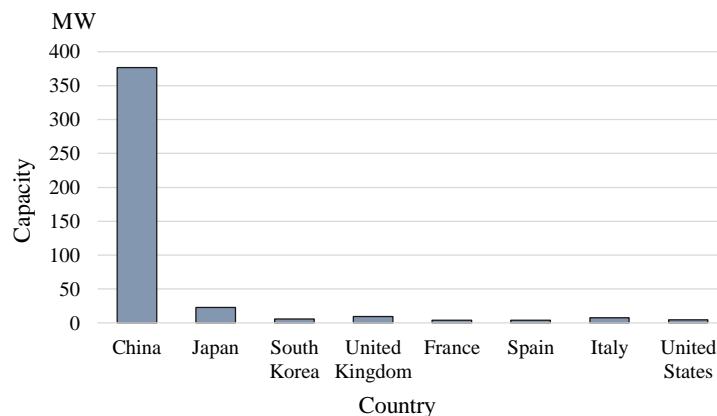


Figure 3.6: Integrated PV system with hydropower installed capacity worldwide.

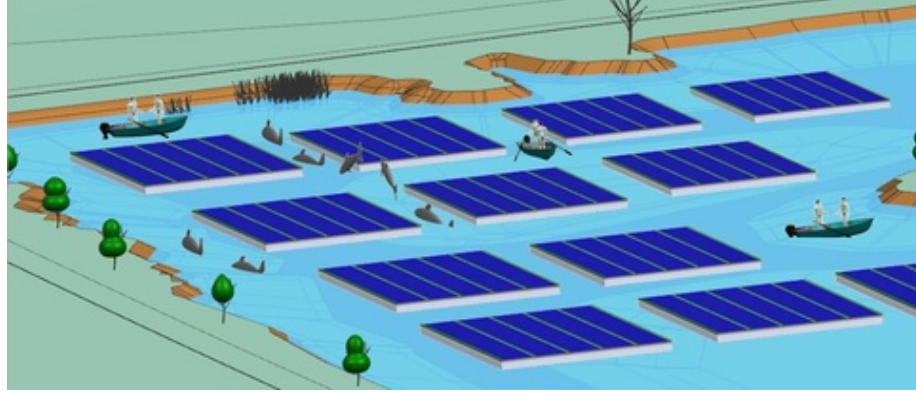


Figure 3.7: Floating PV system on reservoir in which marine life and fishing activity are not disrupted by placing PV systems on the reservoir.

### 3.5 Generation Adequacy Assessment

In general, generation adequacy assessment is used to evaluate short-term and long-term power generation capacity planning studies. Probabilistic methods are commonly used in power system adequacy studies as they take into account the stochastic nature of system behavior, such as component failures and load-level changes [23, 156, 3, 29, 181]. For power system planning projects, probabilistic methods are used to examine the ability and the adequacy of the total generating system to meet the demand [3]. In addition, power system reliability assessment has played a major role in evaluating the contribution of variable energy resources to the adequacy of generation system for both operation and planning process [181]. In this work, an analytical method is used to evaluate system adequacy and calculate reliability indices. Reliability indices such as but not limited to; *loss of load probability (LOLP)*, *Loss of Energy Expectation (LOEE)*, *Expected Demand not Supply (EDNS)* and *Loss of Load Frequency (LOLF)* are among the most commonly used indices as a metric to measure the contribution of additional generation resources to adequacy of the system [26, 25]. These indices are briefly defined as follows [106]:

- A Loss of Load (LOL) event is one in which a system is unable to meet its total demand.

- Loss of Load Probability (LOLP) is the probability of encountering one or more LOL events during a given time period.
- The EDNS index is the sum of the products of probabilities of failure states and the corresponding load curtailments. It is expressed in MW/year or GW/year.
- Loss of Load Expectation (LOLE) is the expected number of LOL hours during a given time period. It is expressed in hr/year.
- Loss of Energy Expectation (LOEE) is the expected energy that the system is unable to serve as a result of LOL events during a given period. It is calculated as the weighted sum of the energies curtailed during the LOL events, the weights being the probabilities of the corresponding LOL events. It is expressed in MWh/year or GWh/year.
- Loss of Load Frequency (LOLF) is the expected frequency of encountering one or more LOL events during a given time period.
- Loss of Load Duration (LOLD) is the expected duration of LOL events occurring during a given time period.

### 3.6 System Modeling

Due to the complexity of the power system, the reliability assessment of the bulk power system has mainly been applied in three different hierarchical levels [3]. The assessment of generation adequacy, known as hierarchical level-I (HL-I). At HL-I studies, the transmission lines are considered highly reliability able to transfer the generated power to all load points. Whereas, when both generation units and transmission systems are considered in the reliability evaluation, its known as the reliability of composite system or Hierarchical level-II (HL-II) studies. Further, the reliability evaluation at Hierarchical level-III (HL-III) considers the entire system. However, due to the complexity of power system and high computation time, reliability evaluation at the HL-III level is rarely attempted. Instead, power

system reliability is evaluated at three different levels separately: generation system level (HL-1), composite power system level (HL-2), and distribution level [3, 49]. In this work, reliability evaluation at HL-I is considered. In this process, the failures of generating units are considered to be independent events, so that the probability of failure of a generation unit can be modeled as Markovian components with two states, *up* and *down* states with known failure and repair rates,  $\lambda$  and  $\mu$  respectively ( $\lambda$  is the failure transition rate from an up state to a down state, and  $\mu$  is the repair transition rate from a down state to an up state).

### 3.6.1 Wind Turbine Output Power

Wind turbine power curve provides a quantitative relationship between wind speed and the output power. It describes the operational characteristics of a wind turbine generator (WTG).

The output power that can be extracted from WTGs can be calculated as follows [89].

$$P = \frac{1}{2}C_p\rho Av^3 \quad (3.1)$$

where  $P$  is the output power (Watts),  $\rho$  is the air density ( $\text{kg}/\text{m}^3$ ),  $v$  is the wind speed ( $\text{m}/\text{sec}$ ),  $A$  is the swept area of the turbine ( $\text{m}^2$ ), and  $C_p$  is the power coefficient.

The output power curve combines (3.1) with the physical constraints in the system. The output power curve including the physical constraints can be expressed as follows.

$$P = \begin{cases} 0 & \text{if } v < v_{cut-in} \\ \frac{1}{2}\rho AC_p v^3 & \text{if } v_{cut-in} \leq v < v_r \\ P_r & \text{if } v_r \leq v < v_{cut-out} \\ 0 & \text{if } v_{cut-out} \leq v \end{cases} \quad (3.2)$$

where  $v_{cut-in}$  is the designed cut-in speed,  $v_{cut-out}$  is the designed cut-out speed,  $v_r$  is the rated speed and  $P_r$  is the rated power of the wind turbine.

### 3.6.2 Output Power of PV Systems

The maximum output power ratings of PV-systems are provided by the manufactures and usually are expressed in peak-watt ( $W_P$ ). The current-voltage characteristics ( $I - V$  characteristics) under the standard test conditions (the radiation level of  $1\text{kW}/\text{m}^2$  is given for temperature of  $25\text{C}^o$ ) can be calculated using the following relationship [93]:

$$I = S [I_{sc} + K_I(T_c - 25)], \quad (3.3)$$

$$V = V_{oc} - K_V T_c, \quad (3.4)$$

where  $S$  is the radiation level,  $I_{sc}$  is the short circuit current,  $K_I$  is the short circuit current temperature coefficient in  $\text{A}/\text{C}^o$ ,  $V_{oc}$  is the open circuit voltage,  $K_V$  is the open circuit voltage temperature coefficient in  $\text{V}/\text{C}^o$  and  $T_c$  is the cell temperature in  $\text{C}^o$  which can be expressed as follows [93].

$$T_c = T_a + S \left( \frac{T_{no} - 20}{0.8} \right), \quad (3.5)$$

where  $T_a$  is the ambient temperature and ( $T_{no}$ ) is the nominal operating temperature of the cell ( $\text{C}^o$ ).

The output power ( $P_{pv}$ ) for a given radiation level, ambient temperature and the current-voltage characteristics can be calculated using the following relationships [93]:

$$P_{pv} = N \times FF \times I \times V, \quad (3.6)$$

where  $N$  is the number of panels and  $FF$  is the fill factor, which depends on the module characteristics, and can be expressed as follows [93].

$$FF = \frac{V_{mpp} I_{mpp}}{V_{oc} I_{sc}}, \quad (3.7)$$

where  $V_{mpp}$  and  $I_{mpp}$  are the current and voltage at the maximum power point.

### 3.6.3 Generation Model

Based on the FOR (*forced outage rate is the failure probability*) of generation units, the CO-PAFT (*Capacity outage probability and frequency table*) can be built using the unit addition algorithm. This is a recursive algorithm that starts with the distribution of one unit and successively convolves with it the distributions of the remaining units, one unit at a time. The FOR is defined as follows [23].

$$FOR = \frac{\lambda}{\lambda + \mu} = \frac{r}{m + r} \quad (3.8)$$

where  $m$  is the mean time to failure (*MTTF*):  $MTTF = \frac{1}{\lambda}$ ,  $r$  is the mean time to repair (*MTTR*):  $MTTR = \frac{1}{\mu}$ .

In general, when adding a new unit of capacity  $C$ , the cumulative probability and frequency of an outage of  $X$  MW can be determined by the following expression: [23].

$$P(X) = \bar{P}(X)(1 - q) + \bar{P}(X - C)q, \quad (3.9)$$

where  $P(X)$  and  $\bar{P}(X)$  denote the cumulative probabilities of the capacity outage state before and after the units are added respectively. Equation (3.9) is initialized as follows.

$$P(X) = \begin{cases} 1, & \text{if } X \leq 0 \\ 0, & \text{otherwise,} \end{cases}$$

The cumulative probability  $P(X)$  for a forced outage of  $X$  MW or greater can be in general calculated using (3.10).

$$P(X) = \sum_i P(X_i), \quad \forall \sim X_i \leq X, \quad (3.10)$$

where

$$\bar{P}(X) = 1, \quad \forall \sim X \leq C,$$

In the case of multi-state generating units, (3.9) can be modified as follows.

$$P(X) = \sum_i^n P(i) \times \bar{P}(X - C_i). \quad (3.11)$$

The cumulative frequency of capacity outage of  $X$  MW can also be calculated using the same approach using (3.12).

$$F(X) = F_i(1 - q) + F_jq + (P_j - P_i)q\mu, \quad (3.12)$$

where  $q$  and  $\mu$  are respectively the probability of failure and repair rate of the new added unit;  $P_i$ ,  $P_j$ ,  $F_i$ , and  $F_j$  are determined from the old COPAFT (prior to adding the new unit);  $i$  is the index of the existing capacity outage state,  $C_i = X$ , and  $j$  is the index of existing capacity outage state,  $C_j$ , such that  $C_j = X - C$ .  $F_i$  and  $F_j$  are cumulative frequencies of states  $i$  and  $j$  respectively.

#### 3.6.4 Load Model

The load model is usually expressed in the form of probability and frequency distribution of the random variable that represents system load [23, 24]. The load model can be constructed by scanning the hourly load data of the system over the time period of study, usually one year. In general, the load model can be built in terms of load level  $L_i$  with its commutative probability and frequency as follows [23, 24].

$$P_L(L \geq L_i) = \frac{H(L \geq L_i)}{T}, \quad (3.13)$$

$$F_L(L \geq L_i) = \frac{\Gamma(L < L_i \rightarrow L \geq L_i)}{T}, \quad (3.14)$$

where  $H(L \geq L_i)$  is the number of hours that the hourly load is greater than or equal to the load level  $L_i$ ,  $T$  is the number of hours in the interval,  $P_L(L \geq L_i)$  is the commutative probability of the load level  $L_i$ ,  $\Gamma(L < L_i \rightarrow L \geq L_i)$  is the number of transitions from  $(L < L_i)$  to  $(L \geq L_i)$ , and  $F_L(L \geq L_i)$  is the commutative frequency of  $L_i$ .

### 3.6.5 Generation Reserve Model

The generation reserve margin has been used to estimate the reliability indices. The generation reserve margin model consists of the probability and frequency of a random variable  $M$ , which represents the difference between the available generation and load [23, 24]. Though the rigorous derivation of the generation reserve margin model will not be reproduced here, some expressions will be presented and briefly explained. The reserve margin model can be expressed in terms of generation and load model as follows [23, 24].

$$M = C_C - C_O - L, \quad (3.15)$$

where  $C_O$  is the capacity outage,  $L$  is the system load, and  $C_C$  is the net available generation capacity for commitment which can be expressed as follows.

$$C_C = C_i - C_{OP}, \quad (3.16)$$

where  $C_i$  is the installed capacity,  $C_{OP}$  is the capacity on planned outage.

For each generation reserve margin level,  $M_i$ , the cumulative probability and cumulative frequency can be calculated using (3.17) and (3.18) respectively.

$$P(M \leq M_i) = \sum_{j=1}^{n_G} [P_G(C_j) - P_G(C_j + 1)] \times P_L(C_C - C_j - M_i), \quad (3.17)$$

$$F(M \leq M_i) = \sum_{j=1}^{n_G} [F_G(C_j) - F_G(C_j + 1)] P_L(m_{ij}) + [P_G(C_j) - P_G(C_j + 1)] F_L(m_{ij}). \quad (3.18)$$

where  $n_G$  is the number of states in the generation model (COPAFT),  $C_j$  is the capacity outage level,  $m_{ij} = C_C - C_j - M_i$ , and  $P_G(\bullet)$  and  $F_G(\bullet)$  are the cumulative probability and frequency of generation reserve model respectively.

## 3.7 Case Studies

Brazilian power system is a large power network that has a total of 4587 generating units with installed capacity around 161 GW, with total peak demand exceeds 85 GW as reported in 2018 [30]. In this work, the system adequacy is evaluated with and without FPV system. These case studies are more detailed in the following sections.

### 3.7.1 Capacity factor of PV system at the proposed locations

In general, the capacity factor of a power plant is used to measure actual power generated comparing to its rated output during a specific period of time. For PV systems, the capacity factor measures total amount of energy the PV system produced during a period of time to the total amount of energy that the PV system would have produced at full capacity. In general it can be calculated using (3.19).

The capacity factor of PV system at different dam locations where the underproduction is reported is calculated using (3.19) and shown in figures 3.8–3.11. It can be seen that the capacity factor of the PV systems have values that range from 0.38 to 0.52 with an 0.42 overall average capacity factor for all locations, based on daytime hours. This indicates a high potential of PV system at the amazon region as shown in figures 3.3–3.4 and discussed in Section 3.6.2.

$$\text{C.F} = \frac{\sum_{n=1}^T PV_{power}}{T \times NC} \quad (3.19)$$

where C.F is the capacity factor of PV system,  $T$  is the length of time period where the actual output is recorded,  $PV_{power}$  is the actual output of PV system produced over that period of time and  $NC$  is the nameplate capacity of PV system installed.

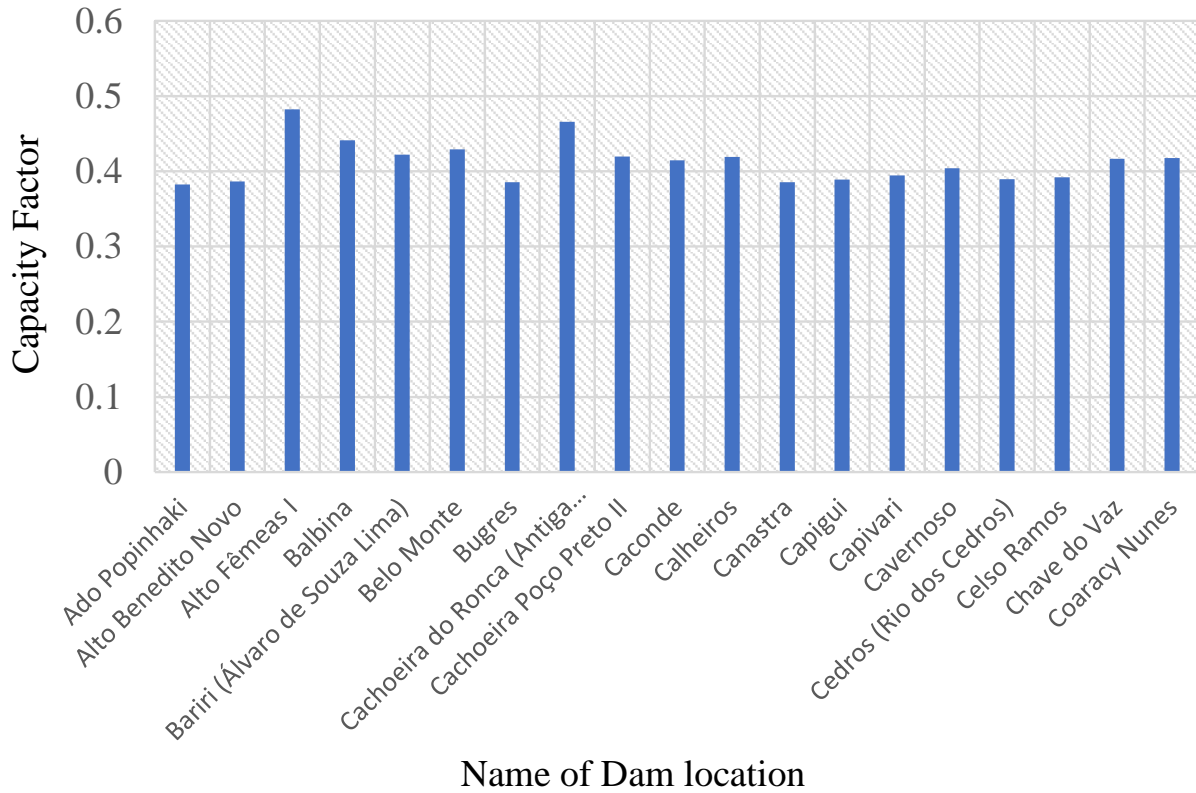


Figure 3.8: Capacity factor of PV system at several dam locations—A

### 3.7.2 Attributes of PV power to the peak load shaving

In Brazil, the majority of power comes mainly from large hydropower dams, and the contribution of solar power to the total power capacity is currently less than 2.0%. Until recently, most of the photovoltaic applications are limited to a small-scale deployment. However, the potential of solar power in Brazil has been investigated by several authors [103, 153, 11, 84], in which investigations reveal that solar power has high power potential and economically viable. In this work, the correlation between the system load and PV output is evaluated. As shown in Fig. 3.12, the correlation between the system load and PV output is significantly high especially during peak hours. As shown in Fig. 3.13, grid-connected PV systems not only assist in peak load reduction especially during peak hours but also indicate that the grid-level FPV systems could potentially add more flexibility to the operator to dispatch

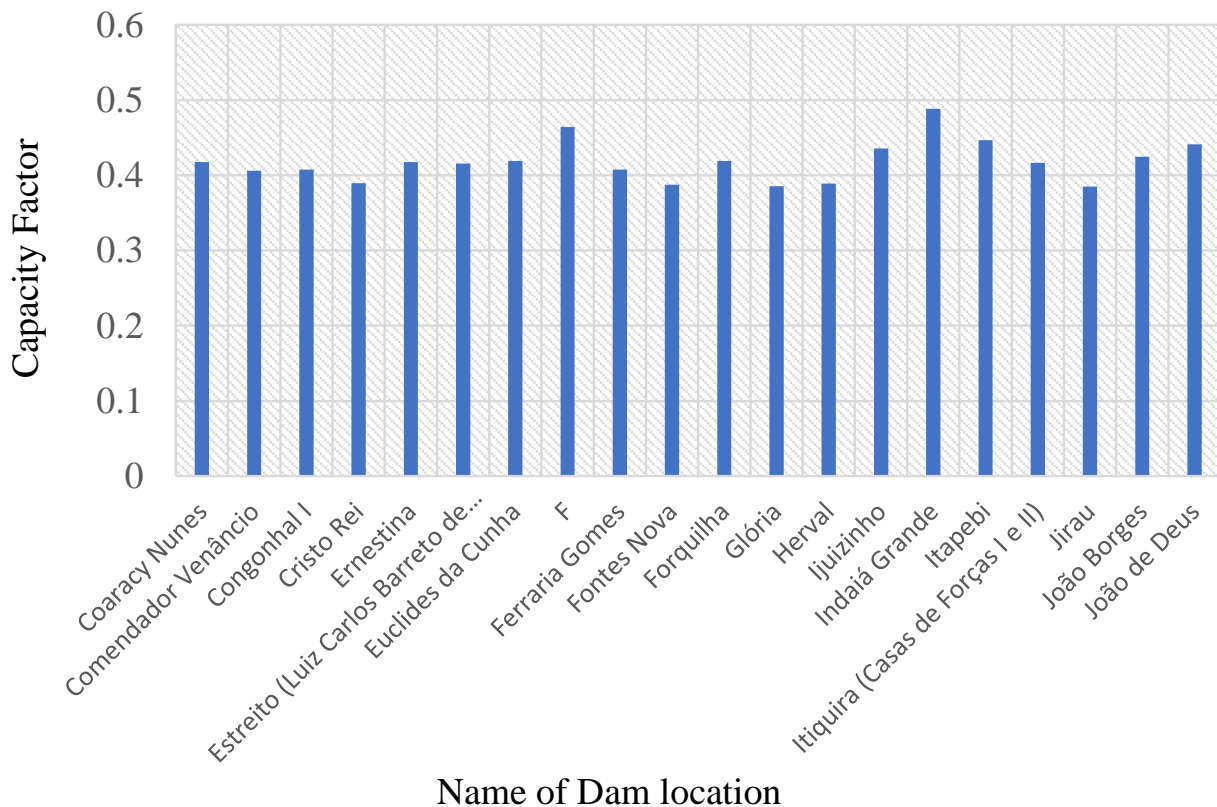


Figure 3.9: Capacity factor of PV system at several dam locations—B

power generated by hydropower plants during off-peak hours. Installing FPV systems alongside the existing dams not only offsets the current underproduction capacities but also takes advantages of the fact that the existing dams offer large capacities that can be used as natural energy storage that can be dispatched to compensate for the uncertainty and fluctuations associated with variable energy sources such as PV power.

### 3.7.3 System adequacy

The objective of this case study is to evaluate the contribution of large-scale deployment of FPV systems to the system adequacy. In order to perform such analysis, mean time to failure (MTTF) and mean time to repair (MTTR) for different types of generating units are needed. Since the Brazilian system is quite large and consist of hundreds of different

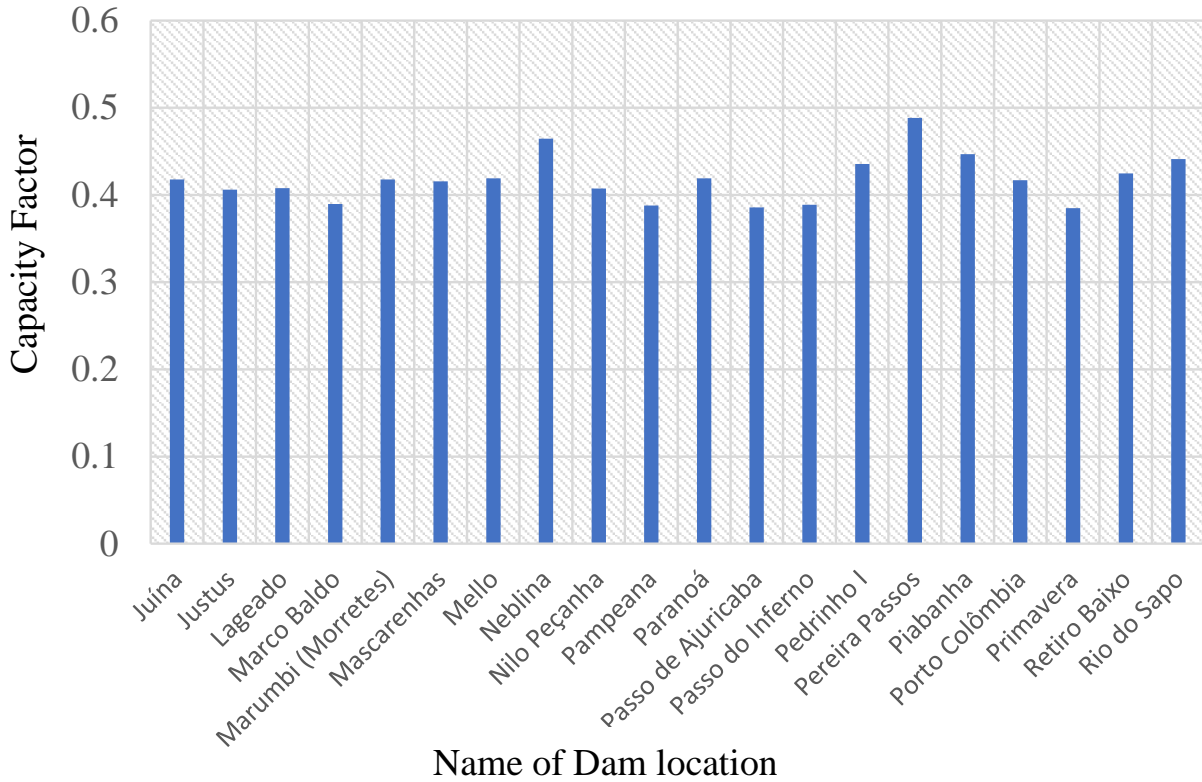


Figure 3.10: Capacity factor of PV system at several dam locations—C

generating units, such data are not fully available to the public. Therefore, in order to evaluate system adequacy, system data shown in Table 3.4, and MTTF and MTTR for different generating units obtained from [88, 158, 157] are used in this work. Due to the complexity of the Brazilian power network, several authors have discussed the protocols and procedures regarding establishing a reliability benchmark for the Brazilian power system [166, 146, 165, 161]. The authors used IEEE-RTS test system (*IEEE-RTS has 32 generating units, with a total installed capacity of 3045 MW and a peak load of 2850 MW*) to compare and discuss the protocols, the conversion criteria, and the computation time to evaluate the reliability indices of the entire Brazilian power grid. Therefore, with the lack of a reliability benchmark for the Brazilian system and to validate the mathematical model and to ensure accuracy with the presented model, the mathematical model presented in this work is scripted

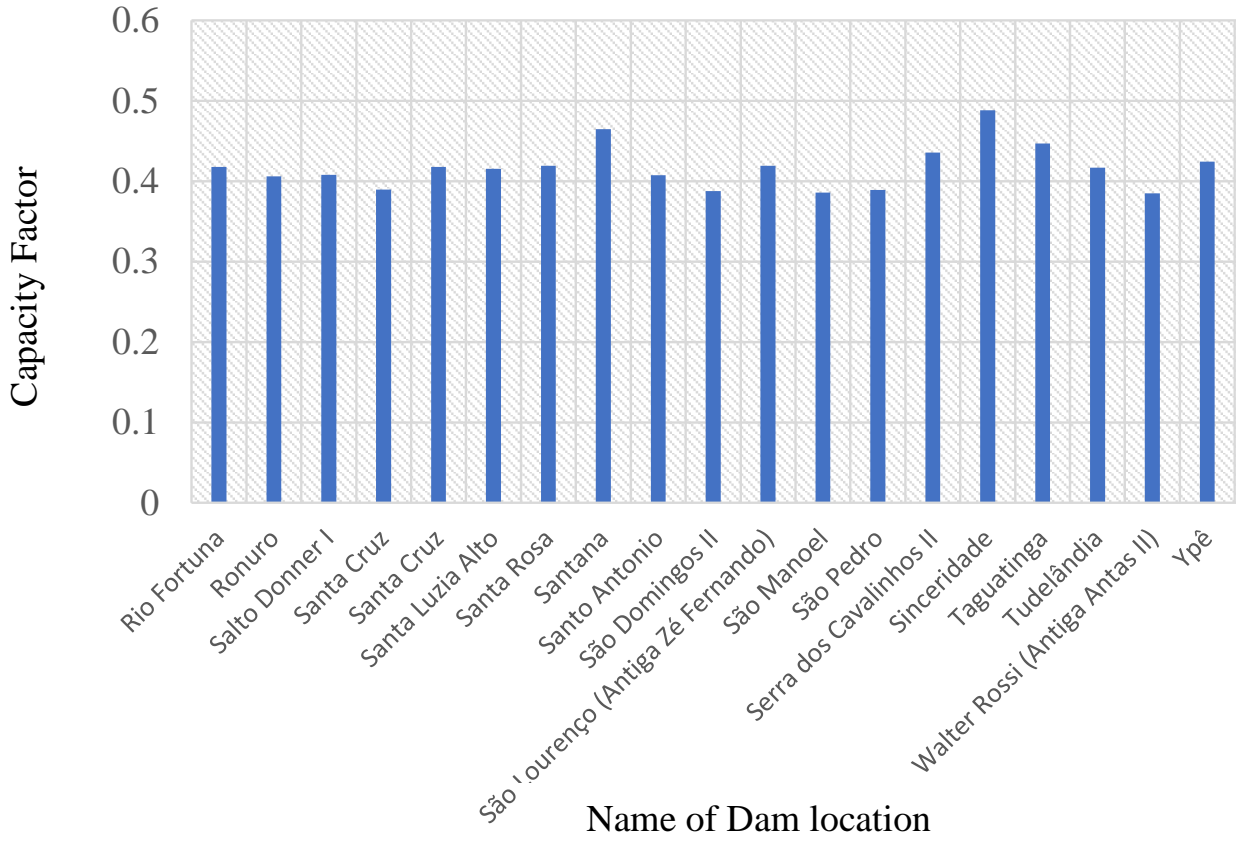


Figure 3.11: Capacity factor of PV system at several dam locations—D

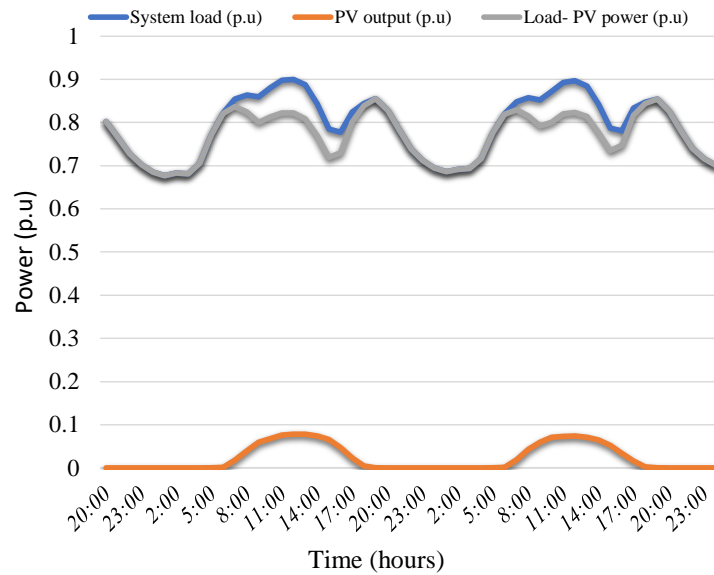


Figure 3.12: Contribution of grid-connected PV system to daily peak shaving

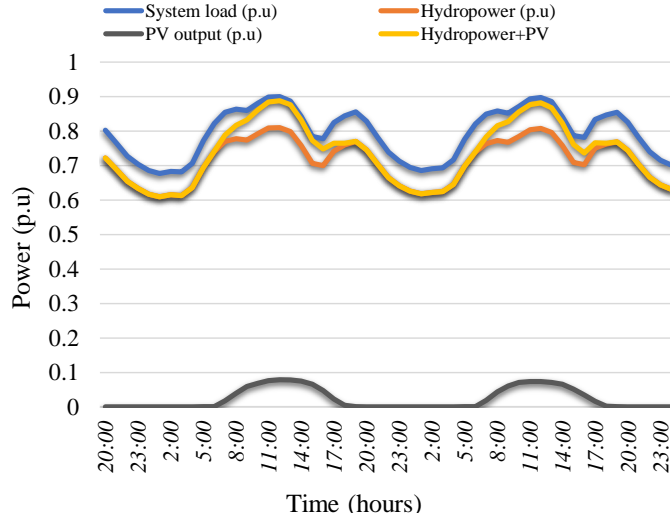


Figure 3.13: Attribution of grid-connected PV system to assist Hydropower peak load shifting

Table 3.4: Brazilian system data

Type of Energy Source	Num. of Operational Units/Farms	Power Capacity (MW)
Nuclear	2.000	19900.000
Thermal+others	2545.000	35622.063
wind	502.000	12296.439
solar	252.000	1302.599
hydro	1286.000	107536.960
Total	4587.000	158748.052

Table 3.5: Annual reliability indices of IEEE-RTS

Case	LOLP	EDNS MW/yr	LOLD hr	LOLF occ./yr	LOEE MWhr/yr	LOLE hr/yr
Reported [88]	0.001069	0.1348396	4.64723	2.01600	1181.1950	9.36
Obtained	0.001069	0.1348396	4.64722	2.01600	1181.1949	9.36

using MATLAB environment and the obtained results are compared to those reported for IEEE-RTS as shown in Table 3.5. Then Brazilian generation and load system data are incorporated in the script and used to calculate reliability indices. It is worth mentioning that the focus of this work is to evaluate the potential benefits of adding FPV systems to the Brazilian power grid, and not an attempt to establish a benchmark for system adequacy.

In this work, the random behavior of generation units is represented by two-state Markovian models [28, 171]. The hourly wind power and PV power for the existing wind farms and PV system are calculated based on the installed capacities for each location (i.e., 252 location for PV system, and 502 wind farms). Using the historical data obtained from [147] for each wind farm and PV system location, the output power is calculated as described in Section 3.5. In addition, for the locations where the underproduction of dams is reported as shown in Table 3.2, a total of 12 GW of floating PV power to be added to the simulated system. The FPV systems are installed on existing dam reservoirs for all locations with rated capacity equal to the reported underproduction capacities. Due to the complexity of the system in terms of large number of generators, the following are assumed:

1. Given the nominal capacities of existing dams, the existing transmission lines are capable of transmitting the maximum power generated by power sources.
2. Regardless of the point of insertion, the power produced by variable energy resources (*i.e., Wind farms and PV systems*) will be accepted by the network.
3. For a large system such as Brazilian network with very low penetration of wind power, the contribution of wind turbine failure to the system adequacy is insignificant, especially when the observed wind speed tends to have low profile [27].

In this work, the following case studies are considered:

1. System reliability indices are evaluated with and without adding FPV system (*for the current system—2018*).
2. System reliability indices are evaluated with adding FPV to the system and peak load is increased.
3. System reliability indices are evaluated with and without adding FPV system (*projection of generation capacity increase—2023*).

Table 3.6: Annual reliability indices of the system before and after adding FPV system

LOLP	EDNS MW/yr	LOLD hr	LOLF occ./yr	LOEE MWhr/yr	LOLE hr/yr
<i>Base case—2018</i>					
0.004177	20.5699	4.35	8.397	179698.7	36.496
<i>Base case after adding FPV system—2018</i>					
0.001859	7.67593	3.69	4.402	67056.9	16.243

Table 3.7: Annual reliability indices of the system with load increase

Load Increase	LOLP	EDNS MW/yr	LOLD hr	LOLF occ./yr	LOEE MWhr/yr	LOLE hr/yr
8%	0.003671	17.937	3.96	8.079	156669.9	32.06
16%	0.006396	36.293	4.23	13.20	317058.6	58.76
24%	0.010129	65.779	4.51	19.63	574636.5	65.78

### 3.7.3.1 System reliability indices—current system—2018

The generation adequacy of the Brazilian system is evaluated by calculating the reliability indices of the system before and after adding floating PV to the system. The annual reliability indices of the system before and after adding FPV systems are shown in Table 3.6. It can be seen from the obtained results that the system reliability indices have improved significantly. The improvement of system reliability indices after adding PV power can be attributed to a high capacity factor of PV power, correlation with load and high potential output during the high demand times.

To evaluate the effect of peak load increase on the reliability of the system, the system peak load is increased by 4% annually. The annual reliability indices in the case of peak load increase with FPV system added to the system (*biannually*) are shown in Table 3.7. As expected, the system reliability indices deteriorated when the system load increased. This indicates that after 5 years of load increase, additional power sources are may be needed to meet the increasing demand.

Table 3.8: Annual reliability indices of the system with load increase *2023-projection*

LOLP	EDNS MW/yr	LOLD hr	LOLF occ./yr	LOEE MWhr/yr	LOLE hr/yr
<i>Base case—2023 projection</i>					
0.015121	107.71	5.000	26.435	941009.45	132.09
<i>Base case with FPV—2023 projection</i>					
0.008133	49.454	4.369	16.262	432034.52	71.056

### 3.7.3.2 System reliability indices—2023 projection

In this case study, the projection of power demand and the power capacity increase shown in Section 3.2, Table 3.1 are evaluated in two cases;

- Annual reliability indices without adding FPV system (*Base case—2023 projection*).
- Annual reliability indices after adding FPV to the system (*Base case with FPV—2023 projection*).

For the two case studies, the power demand is assumed to increase by 4% annually. The annual reliability indices for the system before and after adding FPV system are shown in Table 3.8.

The results shown in Table 3.8 indicate that adding FPV to the system improves overall system reliability. However, to better assess the contribution of FPV systems to generation adequacy, system reliability improvement factor (SRIF) is introduced. SRIF can be calculated as follows;

$$\text{SRIF} = \frac{ARI_B - ARI_A}{ARI_B} \quad (3.20)$$

where  $ARI_B$  is the annual reliability index before adding PV system, and  $ARI_A$  is the annual reliability index after adding PV system.

Table 3.9 shows the SRIF of the system using different reliability indices for two scenarios; I) the SRIF is calculated for the current system after adding FPV system (Scenario—I—

Table 3.9: SRIF considering different reliability indices

SRIF (LOLP)	SRIF (EDNS)	SRIF (LOLF)	SRIF (LOEE )	SRIF (LOLE)
<i>Scenario—I—2018</i>				
0.5550	0.6270	0.4760	0.6270	0.5550
<i>Scenario—II—2023</i>				
0.4620	0.1279	0.3848	0.1281	0.4620

2018), and II) the SRIF is calculated for the system after adding FPV system (Scenario—II—2023).

### 3.7.4 Results and Discussion

The results obtained in this work show that Brazil has high solar radiation and high potential of PV power output even with the amazon region where most hydropower dams are located. As shown in Fig. 3.12 and Fig. 3.13, large scale deployment of PV system contributes significantly to daily peak load shaving and adds more flexibility to hydropower plant operation. Mainly because of the high correlation between the PV system and system load, especially during peak times. Results also showed that the capacity factor of PV systems is significant, with an overall average capacity factor of 42%. The generation adequacy of the Brazilian system is evaluated by calculating reliability indices before and after adding floating PV to the system. The annual reliability indices of the system before and after adding FPV systems are shown in Table 3.6. It can be seen from the obtained results that the system reliability indices have improved significantly. The improvement of system reliability indices after adding PV power can be attributed to the high capacity factor of PV power, correlation with load, and high potential output during the high demand times. Further, the effect of the peak load increase on the reliability of the system in the presence of the FPV system is also evaluated. As shown in Table 3.6 and Table 3.7, the system reliability indices are improved in both the 2018 scenario and the 2023 projection scenario. As shown in Table 3.9, in both situations, SRIF indicates a significant improvement in system reliability when the

FPV system is introduced. It can be seen, for instance, the SRIF based on LOLP and LOLE indices indicates a 55.5% improvement of system reliability after adding the FPV system, while the system reliability improved by 62.70% when EDNS and LOEE indices are used as a criterion. In contrast, when the LOLF index is used as a criterion, the reliability of the system is only improved by 47.60%. The results also show that installing FPV systems on the reservoirs of existing dams enhances system reliability. e.g., the LOLP index increases by 55.5% for the current system and by 46.2% for the 2023 projection case when the FPV system is introduced. However, it is up to the planner to decide a proper index; for instance, if the priority is to minimize power interruption, the LOLF index can be used. On the other hand, if expected load curtailment is given importance in the planning process, the LOLE index can be used instead. The results indicate that the utilization of large-scale floating PV systems alongside the existing hydropower plants provides an efficient power source to meet the increasing demand and a pathway to minimize the environmental and social impact of dam expansion in Brazil while meeting the increased power demand.

### **3.8 Conclusion**

Considering the environmental and social concerns associated with hydropower plant expansion in the Amazon region, an alternative solution to meet power needs due to the underproduction of hydropower dams is proposed and evaluated. The utilization of mixed generation resources may potentially provide an alternative approach that can be implemented to minimize the environmental and social impact of dam expansion in Brazil while also meeting the increased power demand. The work presented here has focused on assessing the contribution of FPV to the adequacy of generating capacity of the Brazilian electric system, with the capabilities of the FPV systems designed to offset the hydropower dam underproduction. Several cases were considered to evaluate system adequacy by calculating reliability indices before and after adding FPV systems. The results show that installing FPV systems on the reservoirs of existing dams improves system reliability. e.g., the LOLP

index improves by 55.5% for the current system and by 46.2% for the 2023 projection case. FPV systems installed on a large scale can make up for a significant portion of dams' underproduction and can decrease the level of underproduction of existing dams by enhancing the natural ability of the reservoir to store water for hydropower production. The results also suggest that installing FPV systems on the reservoirs of existing dams improves system reliability, enhancing the natural ability of the reservoir to store water and preventing a more significant negative impact on the society and environment by offsetting the planned power need in the future. In addition to the positive outcome for mitigating environmental concerns, a large scale FPV system could add more flexibility to the power system operator in terms of dispatchability and minimize load curtailment during high demand times. The PV systems can also be installed locally on the roofs of family homes or on common-use buildings for a community in place of the current diesel generators, which can provide power for local communities or individual families. A PV system is a more environmentally friendly option than the current diesel generator systems due to the absence of greenhouse gas emissions from burning fuel, and less risk of spilled fuel while transporting to the various locations.

## CHAPTER 4

### IN-STREAM TURBINES AS FISH-FRIENDLY TECHNOLOGY

#### 4.1 Background

This paper considers traditional dam configuration and in-stream turbines. The traditional dam configuration blocks a body of water to create a reservoir providing an increased head for the turbine in the dam, where head directly relates to the difference of the total pressure that is theoretically available across the turbine. As an alternative, an in-stream turbine is placed directly into the flowing body of water without significantly increasing the water level in front of the turbine nor blocking the passage as typically results from a dam. There are also “run-of-river” configurations that divert a portion of a major flow through its turbines. Dams, unlike in-stream turbines and run-of-river plants, are generally built across the entire span of the body of water and develop high residence times, blocking fish from being able to migrate naturally. While there are concepts like fish ladders and bypasses meant to mitigate the blockage of migrating marine life by a dam, these often are found to be insufficient or ineffective in configuration, number, and size, leaving the majority of fish to retreat or attempt to pass through the turbine ([2], [45], [117], [188], [105]).

Fish passing through a traditional turbine configuration encounter several canonical key mechanisms for injury or mortality: physical strike, pressure change, shear, and turbulence [52], as visualized in a traditional turbine system in Figure 4.1. Another mechanism that can have a negative impact on fish, but may not directly lead to injury or mortality, is the sound emitted from the device. These and other mechanisms are examined individually, compiled and discussed here. Consequently, a list of recommendations for fish-safe design criteria is formulated.

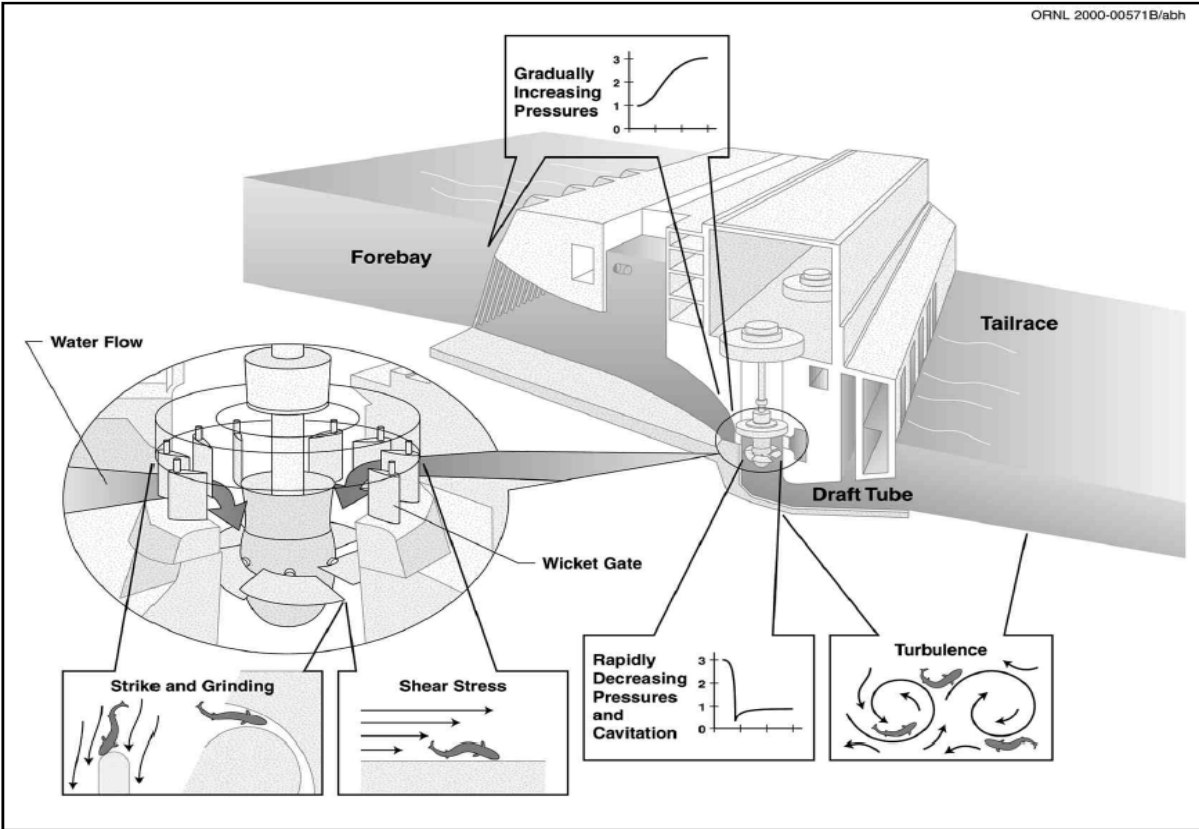


Figure 4.1: Canonical fish injury risk mechanisms (from: [36])

## 4.2 Turbine Installation

The power of a turbine is directly related to the product of the flow rate through the turbine rotor and the total pressure drop across it. This applies for any turbine in any configuration (Figure 4.2), thus the main difference between in-stream, dam, and run-of-river turbines is the magnitude of the total pressure drop across the rotor.

### 4.2.1 Dam Turbine

A dam turbine relies on a considerable water level difference between an upper and a lower reservoir or outlet. The difference in the height of the free reservoir surface and the outlet surface constitutes a potential energy at the inlet to the penstock that is partially converted into a kinetic energy within the penstock itself. The flow encounters resistance due to the

presence of the rotor, which builds up a static pressure difference across the turbine, driving flow through. The total pressure, made up of the static pressure from flow resistance and the kinetic contribution from the flow, is thus related to the ability of the rotor to produce the static pressure drop and also to the height of the dam. Of the three turbine configurations, dams will generally have the highest total pressure drop, due to their large height differences, the most notable case being the tallest dam in the world: the Jinping-1 in China, at over 300 meters in height [195].

#### **4.2.2 Run-of-River Turbine**

A run-of-river turbine has similarities to both in-stream and dam turbines, in that there is low flow residence times similar to an in-stream turbine, but there is an appreciable developed head drop like a dam. The height of a run-of-river is typically lower than that of dams, in the range of 1-5 meters [183], where the reservoir is often called a ‘headpond’ due to its smaller size than a traditional dam reservoir. The operating principle for a run-of-river turbine is the same as for a dam, but with a smaller total pressure drop, resulting in lower power capacities.

#### **4.2.3 In-Stream Turbine**

An in-stream turbine extracts energy from the flow via conversion of kinetic energy to the rotational mechanical work of the turbine, without needing to convert the kinetic energy into potential head energy in a reservoir or artificial channel. The terms ‘hydrokinetic’ and ‘marine current’ come from this ability to extract energy directly from the flowing water. Another term that has also been used in the literature to describe in-stream turbines, ‘zero-head’ turbines, due to the absence of external head-producing infrastructure, such as a dam. In-stream turbines can be designed with various rotor types, sizes, and with the option of adding guide vanes, nozzles and/or diffusers. The two main types of in-stream turbines are vertical axis (‘cross-flow’) and horizontal axis (‘axial’) turbines. There also exist in-stream

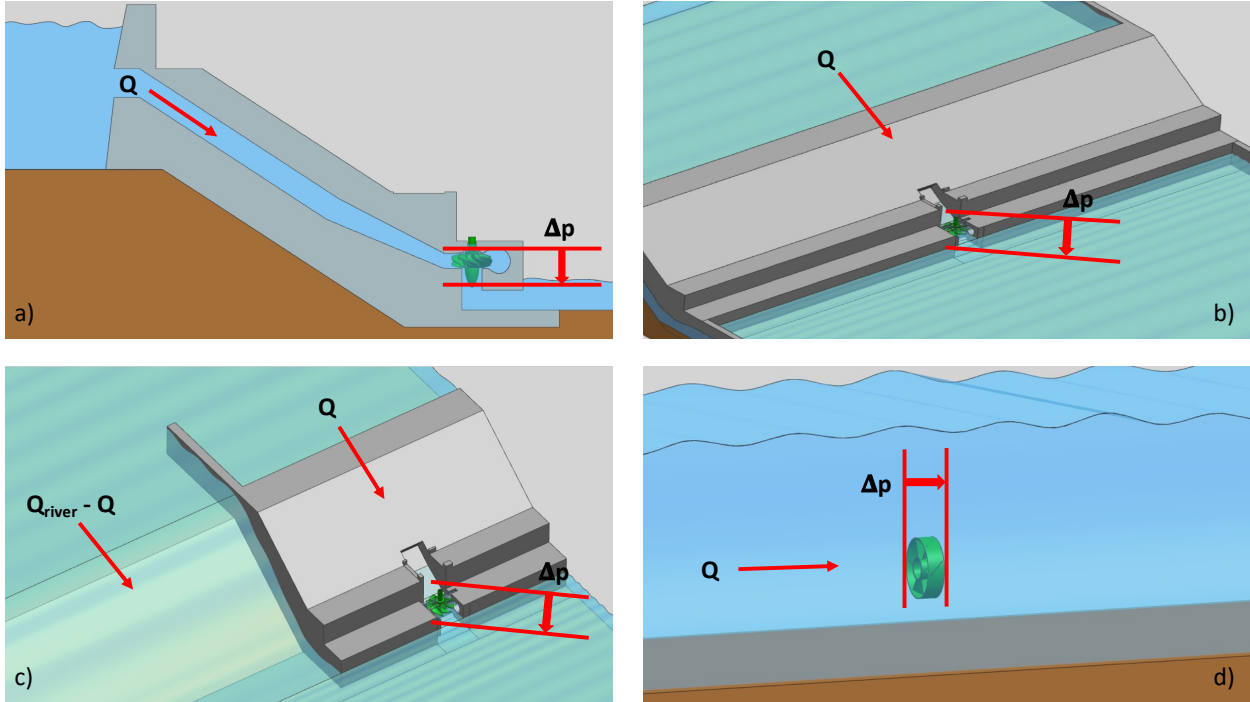


Figure 4.2: Schematics of turbine configurations (a) cross-section of a dam or run-of-river housing, (b) traditional dam, (c) run-of-river, (d) in-stream turbine

turbine designs that are in between the two main types, such as the linear turbine (a conveyor belt with blades along the periphery that can pivot about an axis normal to the flow).

The principle of operation for an in-stream turbine is the same as for the dam and run-of-river turbines: the rotor and any associated structure partially block and resist the flow of the river, building up a higher static pressure in front of the rotor, driving flow through the turbine at a designed flow rate. The definition for power of the product of flow rate and total pressure drop is not the commonly reported form, which is usually the product of the mass flow rate and the kinetic energy of the flow through an orifice that is the diameter of the rotor tip (or the largest diameter, if using a nozzle/diffuser). The kinetic energy definition has roots in the canonical work done to quantify the theoretical maximum extractable energy of the flow, known as Betz limit (or the Lanchester-Betz limit in some literature, see [73]). The Betz limit dictates that a bare turbine in an infinitely large flow field (so that there are no wall effects) can extract a maximum of 59.3% of the kinetic energy in the flow that is in

a duct with the same diameter as the turbine rotor. This value and nature of this limit has been examined in the literature ([73], [90], [75]). It has been found that the Betz limit can be generalized for two important cases for in-stream turbines: including nozzles/diffusers in the turbine design and placing multiple turbines in a finite sized channel.

### 4.3 Fish Injury Mechanisms

In this section, the damage and disturbance mechanisms encountered by marine life while passing through traditional dam-turbine configurations are examined, as have been noted from canonical literature, and are shown graphically in Figure 4.1 [36]. The issues are examined, and relevant parameters drawn from the literature with respect to a ‘fish-friendly’ turbine design are noted.

#### 4.3.1 Physical Strike

An injury from physical strike is considered to be when contact is made (either sliding or impact) with walls or structures that are associated with the turbine rotor, support piers or stator vanes. Injury from physical strike occurs when the relative velocity between the fish and a physical barrier induces a shear or pressure that is greater than the material moduli in question, where the scales, skin or organs are then sheared or ruptured. There are several important factors involved in risk of physical strike:

- Fluid velocity
- Fish velocity (may be different than fluid velocity)
- Wall velocity (nonzero for rotor blades)
- Wall geometry
- Fish geometry
- Gaps between moving and stationary walls or structures

These factors together will determine the strike risk and possible extent of damage for a fish. Experiments have been performed to examine fish behavior and strike risk, in an attempt to quantify the effect of some of these variables ([52], [35], [5]). To minimize the risk of fish injury, it can be concluded that:

- Blade strike velocities should be kept below 5 m/s, assuming that the fish in question are longer than the blades are thick ( $L/t > 1$ ) (see Figure 4.3)
- Blade leading edges should be kept as thick and rounded as possible
- Blade spacing should be kept high
- Gaps between rotor blades and outer walls should be minimized
- Gaps between rotor blades and gates or vanes should be maximized

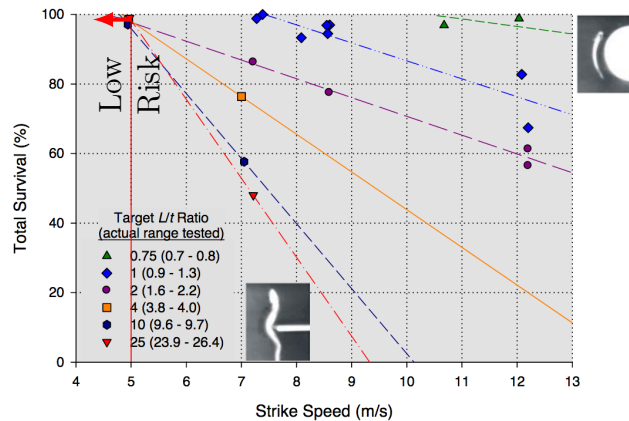


Figure 4.3: Survival of rainbow trout (*Oncorhynchus mykiss*) based on strike speed (modified from: [6])

An alternative recommendation in the literature is 6-12 m/s peripheral blade speed for minimal fish strike risk [118]. This range could have higher risk than originally thought at the higher velocities, based on new data on rainbow trout of lengths 110 to 163 and 182 to 236 mm, yielding a length to blade thickness ratio ( $L/t$ ) of approximately 1.14 and 2. [5] showed that at strike speeds of 10 and 12 m/s, if the fish impacts the blades at an angle

above 45 and 30 degrees relative to the blade surface, respectively, the survivability of fish drops to and below 67% and 4.2%. Further, at 7 m/s, the tested fish survived at 98% or more at varying degrees of impact with the blade surface (30,60, and 90 degrees) [5]. The 5 m/s criteria is used here as a conservative measure, allowing for larger than a 2 L/t ratio between the fish and the blades (longer fish and/or thinner blades); however, the strike speed could approach 10 m/s depending on the fish present and blade design developed.

### 4.3.2 Pressure Changes

Traditional dam-turbine configurations rely on small to large head differences, which is converted into extractable energy through a static pressure drop across the turbine at a designed flow rate. As fish enter the turbine intake, they experience an increasing pressure above atmospheric (depending on the depth of the intake below the surface of the reservoir), and then they experience a rapid decrease in fluid pressure as they move through the turbine section, that can approach a ratio of 4 ([149], [182]) to over 10 [118] from the gates to after the runner blades for typical turbines. A low nadir pressure relative to the pressure that the fish is adjusted to gives rise to several issues:

- Low pressures can disrupt the function of the swim bladder, allowing for easy predation
- Low minimum pressures can rupture organs, such as swim bladders and eyes
- Pressures below the working vapor pressure can cause cavitation, which can cause physical damage to fish, as well as the above issues

[32] showed that the most important factor for juvenile Chinook salmon (*Oncorhynchus tshawytscha*) is the ratio of acclimation pressure to minimum pressure, when compared to rate of pressure change, condition factor of the fish, and total dissolved gas content of the water. It can be seen from the same work that if the minimum pressure does not fall below around half of the acclimation pressure for a given fish (an acclimation to minimum pressure ratio of 2), there is a low probability of injury or death as is shown in Figure 4.4. [32]

also concluded that the juvenile Chinook salmon that were studied responded well to slow decompression, however, it has been commented in literature that other fish species might not respond well to even slow decompression [143].

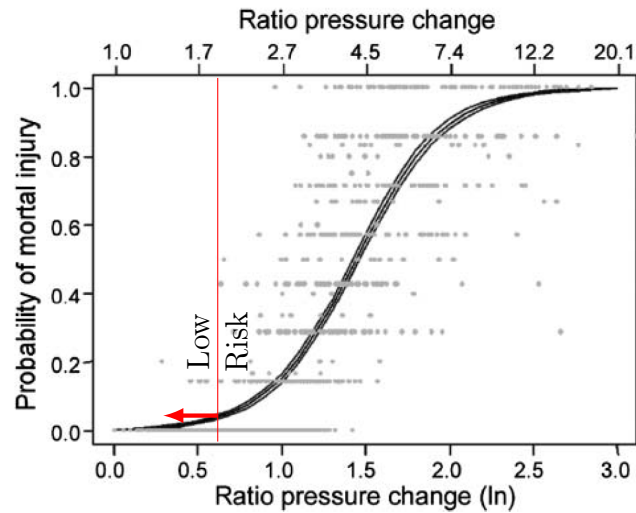


Figure 4.4: Dose-Response chart of mortality vs. pressure for juvenile Chinook salmon, in terms of the ratio of acclimation to minimum pressures, and the natural log of the ratio on the bottom axis (modified from: [32])

A lower-pressure criteria found in the literature is allowing the minimum pressure to drop to 30% of adjusted pressure (a pressure ratio of 3.33) [118]. The author cites a figure from [34], justifying the criteria by shifting focus away from non-anadromous (bass and crappie) data points. The original cited work recommends a criteria of not allowing a minimum pressure below 60% of adjusted pressure (a pressure ratio of 1.67) [34]. The studies performed to gather the data for these two recommendations is commented by the original author as being "...old, poorly documented, have inadequate or no controls, and used only small numbers of fish" [34], and thus newer, well-explored and well-documented data is used in substitute to come to the criteria used here.

### 4.3.3 Shear

Similar to physical strike, damage due to shear is due to relative velocity, but the velocity in question is of the fluid instead of a physical wall. According to experiments and simulations, around 1-2% of a typical conventional turbine dam configuration will have a shear rate (often referred to as ‘strain rate’) greater than  $495 \text{ 1/s}$ , which is reported as the point where injuries to fish will tend to increase ([112], [35]). These regions are mostly areas associated with wakes behind structures, such as support piers or stationary gates or vanes, though the turbine rotor can also produce high shear rates near the tips, depending on the design and loads. The strain limit can be converted to an equivalent shear stress of slightly less than  $1600 \text{ Pa}$  (calculated from  $517 \text{ 1/s}$ ) [35]. The schematic of the experimental setup by [112] to determine the tolerable shear rate is shown in Figure 4.5, where a nozzle is used to accelerate fluid in a jet, and then the fish are introduced into the stream.

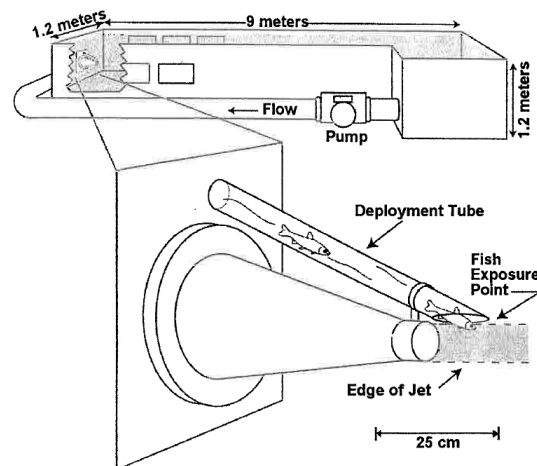


Figure 4.5: Experiment to quantify tolerable shear stresses on fish (from: [112])

Other literature uses a lower strain rate criteria of  $180 \text{ 1/s}$  [118]. This lower value is used for examining the “bulk” flow through a turbine passage, and not the entirety of the turbine rotating region. Most of the flow through a passage should be well-behaved and will not have as high of strain rates as would be found in the boundary layer near to solid surfaces, and so a lower criteria can be used to evaluate this region. [118] also comments that in the

boundary layer, where the strain rate is highest, the probability of physical strike is also at its highest, and so assumes that in the near-wall region, if physical strike risk is mitigated (through design blade velocity), then that region could be considered ‘safe’. However, to examine the individual effects of each safety risk, using a criteria that can serve as a basis for the entire turbine flow region, the higher criteria of 495 1/s cited here is more suited to evaluate the design.

#### **4.3.4 Turbulence**

Driven by shear, the velocity gradients associated with turbulence can have two main effects on fish:

- Physical shear damage of fish body
- Disorientation by large scale vortical structures (eddies)

Experiments with a controlled level of turbulence induced by generated shear stress can be performed, an example of which attempted to estimate the risk of mortality of small fish and larvae by a ship’s propeller ([94], [95]). The study concluded that a linear relationship between shear developed by a boat’s propeller and larval, egg, and juvenile fish mortality can be predicted. It was shown that for the investigated life cycle stages, the larval fish being were most sensitive to shear. It is postulated that turbulence can also enhance predation by inducing disorientation if the turbulence intensity is high enough, but quantifying ‘disorientation’ is not simple, so no explicit criteria has been found as to an acceptable level of turbulence. It has been noted that turbulence and disorientation can also affect the fish’s ability to eat, swim, as well as where they choose to make a habitat [174].

#### **4.3.5 Current Traditional Configuration Fish-Friendly Designs**

A few novel designs for ‘fish-friendly’ turbines for traditional turbine configurations have been developed; the most prominent and well-documented of these designs are the Alden

turbine, the Minimum Gap Runner (MGR), and the Very Low Head turbine (VLH). The Alden turbine's main features are a runner that rotates with its outer shroud, eliminating relative velocity between the blade tip and the outer wall, and also has only three blades to reduce the probability of strike. The Minimized Gap Runner (MGR) design alleviates some of the issues associated with blade strike risk to fish, namely, minimizing the gap between the runner blade root and tip regions as well as the hub and outer wall, lowering the risk of fish becoming trapped and injured ([6], [83]). MJ2 set out to develop a very low head (VLH) turbine that can minimize civil works costs, as well as being 'fish-friendly' [108]. Other companies have also developed their own 'fish-friendly' concepts, working to increase the ease for fish to pass through the gate and runner sections without harm, such as GE and Natel ([190], [31]).

#### **4.3.6 Sound**

Though not necessarily a direct injury mechanism, the emitted sound from a turbine can still have an effect on fish. It has been known since at least the 1980s that sound can affect how fish will interact with regions around dam turbines [50], though the level of behavior change was not quantified at that point in time. More recently, fish passage efficiency has been quantified in regards to directing sound pressure waves at certain locations and in certain directions with respect to the dam ([159], [78]). This issue will be examined further in section 4.4.3, where it is used as one of the considerations for 'fish-friendly' in-stream turbine design.

### **4.4 Fish Safe Turbine Design**

It has been noted that in-stream turbines have a relatively small environmental impact, and can be considered to be very low risk devices, even when in small array configurations ([43], [150], [131]).

#### 4.4.1 Physical Strike

For low-head turbines in a traditional dam configuration, it has been reported that blade strike is the most critical issue for fish safety [4]. The issue of impact with the rotor blades themselves is the same among in-stream and traditional dam-turbine configurations. However, in-stream turbines allow the fish to pass around the turbine or retreat at any point up until the fish reaches the rotor blades themselves (see Figure 4.6), giving the fish more time and space to react to the turbine. For fish passing through the turbine rotating section, in-stream turbines have the advantage of generally being lower solidity than their traditional counterparts, allowing for more space between the blades for fish to pass through [76].



Figure 4.6: A Moon Wrasse (*Thalassoma lunare*) evading an in-stream turbine (from: [79])

For in-stream turbines, there could exist a critical RPM of the rotor that can increase the chance of fish survival; the common design RPM for “low-speed” devices is around 15-40 RPM ([79], [134], [163], [109], [52]). There is a design choice, however, to design the turbine at one end or the other of the aforementioned range, due to the different ecological phenomena or design constraints. At the low end of the range, rotating at very low RPM can be seen as safer than higher RPM in the case of fish impact with the rotating blades, due to low RPM designs being associated with large turbine diameters, such as the Cape Sharp turbine (6-8 RPM) [37]. These large diameter, slow rotating turbines can allow for

large gaps between the blades and also provide the fish with more time to maneuver around the blades, facilitating more effective fish passage. Towards the higher end of the range, rotating above 20 RPM has been noted as being the point where fish tend to avoid the local area around the turbine, and thus would not attempt to pass through the turbine [199], which could also reduce the risk for strike, though this may introduce migration route and habitat choice changes. [79] showed that of all of the observations of fish encountering a vertical axis in-stream turbine in a real river channel, while the rotor was spinning only two individual fish entered the rotor (out of approximately 150 measurable fish passings with the rotor present), and only when the current speed (approximately 0.25 m/s) and rotor speed were low (17 RPM).

This RPM phenomena could have varying importance to the fish attempting to pass through depending on the species, channel geometry, time of day, number of fish in the group, among other variables, as was shown by work from various authors. For example, [185] noted an approximately 0.477 probability of fish entering an Ocean Renewable Power Company (ORPC) Turbine Generating Unit (TGU) in a tidal channel during the combined night and day, when it was rotating at an average of 21.4 RPM. It was also shown that the probability of fish entering during the day was much lower than at night, as has been indicated throughout the literature in regards to fish response to light stimuli ([187], [33]), particularly, only approximately 4% of the observed fish passed through the turbine during the day while it was rotating. [54] also showed that certain species of fish may still choose to pass through a runner that is rotating above 20 RPM, as was shown by the avoidance of only 33% for hybrid striped bass (*Morone saxatilis* x *Morone chrysops*), while much closer to 100% for the other tested species (86-100%). Much like the way light affects the behavioral response of fish via the visual sensory system, the reason for the critical speed being around 20 is presumably due to the nature of the interaction between the turbine emitted sound waves and the fish auditory sensory systems: the inner ear, and the lateral line. [192] commented that the low frequency stimuli results in an elongated ‘near field radius’, allowing the fish to

sense the flow disturbance from much farther away, which could lead to increased likelihood of avoidance maneuvers. The influence of turbine sound on fish will be examined further in section 4.4.3.

#### **4.4.2 Pressure Change, Shear, and Turbulence**

From computational simulations of a 5-meter radius turbine rotating at 21.5 RPM (2.25 rad/s), it has been shown that in-stream turbines can have pressure drops of one order of magnitude or more less than a typical high-head dam-turbine configurations; the maximum ratio of total pressure change was shown to be approximately 1.1 near the blade tip in Figure 4.7 [198]. The relatively high minimum pressure corresponds to a high survival rate of fish in regard to pressure effects, as well as a low risk of cavitation damage. The time of decompression is also noted as an important factor in [198], which is shown to be approximately of the same order for in-stream turbines as tradition dam-turbine configurations when considering a full blade resolved geometry (BRG) CFD model; however, the author notes that the time for decompression is longer based on the results of Blade Element Momentum (BEM) CFD simulation.

Similarly, shear and turbulence produced by a typical in-stream turbine have been shown to be low in most of the turbine. The shear rate is shown to peak around 300 1/s (from blade resolved geometry CFD simulation), which is less than the 495 1/s criteria for fish safety [198]. The numerical investigation concluded that the only region of issue for shear is very near to the tip (within 0.01 m, shown in Figure 4.8); however, it is unlikely that fish would swim near the tip, and this could be further mitigated with the introduction of a shroud or nozzle/diffuser around the periphery of the rotor, as it would be even more difficult for fish to encounter this region. The turbulence length scale was shown to reach the peak of 1.7 m at the end of the domain (approximately 300 to 400 meters after the turbine), and the largest turbulent kinetic energy eddies behind the blade tips have a length scale of approximately 10 cm. For small fish with swim bladders, this could cause disorientation, and thus employing

strategies to mitigate fish access to the blade tips would be beneficial in design.

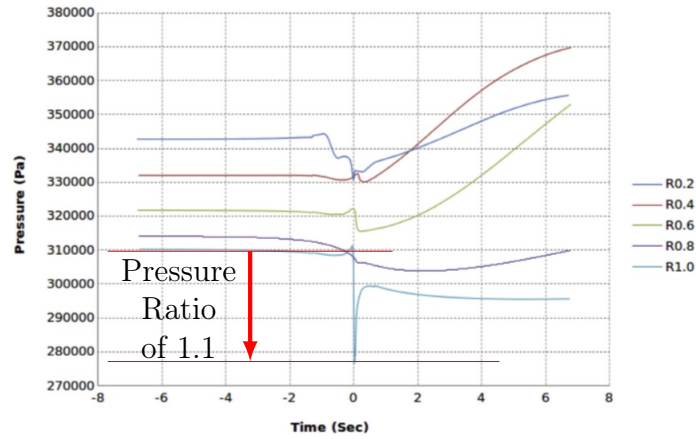


Figure 4.7: Pressure Traces at Various Radii along a Tidal Stream Turbine. The legend shows the radial distances in terms of the ratio of a given radius to the tip radius. (modified from: [198])

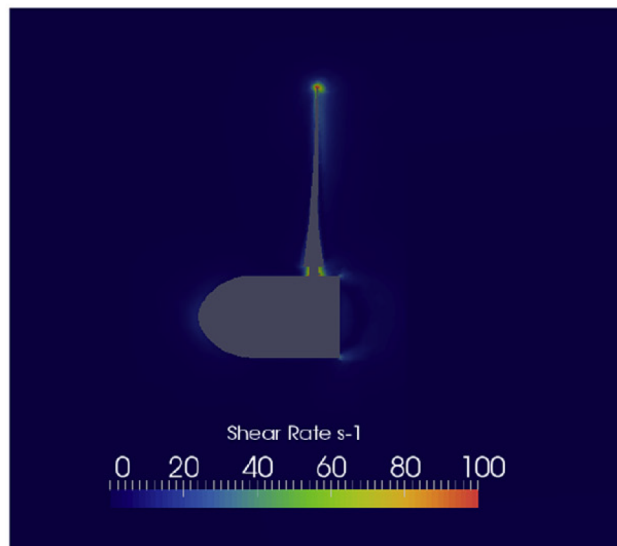


Figure 4.8: Shear rate of tidal stream turbine (from: [198])

#### 4.4.3 Sound

Fish have two main acoustic sensing systems: the inner ear and the lateral line [140]. The two systems work in concert to produce a complete flow disturbance image in the fish's brain,

by analyzing near-field (approximately 1 to 2 fish body lengths away) and far-field (greater than 2 body lengths; the maximum range varies with the fish species) acoustic waves. The inner ear generally is used for far-field hearing, in the frequency range of 50 to over 2000 Hz, whereas the lateral line is used for near-field sensing, in the frequency range of 1 to 200 Hz [140]. According to [172], producing external interference to the natural frequencies emitted and heard by fish can affect:

- Distribution of fish
- Growth and reproduction (or ‘fitness’)
- Predator-prey relationships
- Communication

Any external noise source could affect these natural interactions of fish, to a degree that depends on the frequency spectrum emitted by the source. Manmade disturbances can emit loud acoustic disturbances, from boats, barges, and underwater machines. Underwater noise emitted from a dam-turbine configuration has been of little focus in the literature, though it can be an important study in an attempt to minimize fish entrainment through hydropower plants ([107], [113]). With minds geared towards fish safety and gaining an insight into fish behavior relative to underwater machinery, investigations have been conducted to quantify sound produced from in-stream turbines. [21] in particular concluded that the sound level produced by a TidGen turbine is about the same as the natural environment at high water velocity (by utilizing a cylindrical sound spreading model), and slightly higher. The author also states that at a distance of 21 meters away, it is likely that some species of fish cannot hear the turbine, as shown in Figure 4.9. This means that the turbine will not interfere with fish interactions except possibly close to the turbine itself, where the fish could likely avoid due to the pressure sound level produced by the turbine rotation. It has been noted, however, that using the individual classic spreading models (spherical or cylindrical) can lead

to an underestimate of the sound levels from the source ([139]). In another investigation, [162] concluded that there is a measurable change to fish behavior from short- and long-term playback of a pre-recorded turbine soundtrack, but for the fish species studied, the behavioral changes in an experimental setup were not statistically significant enough to determine behavior in the case of an actual in-stream turbine in nature.

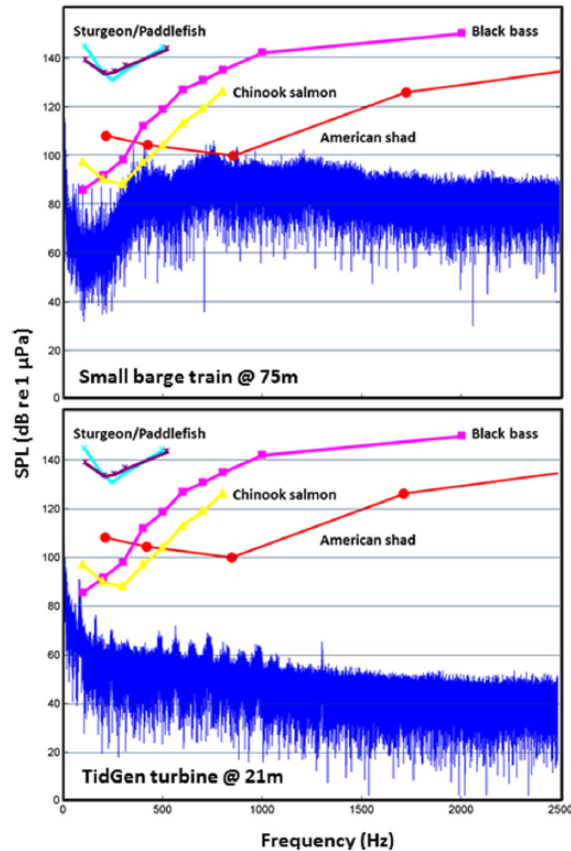


Figure 4.9: Sound levels measured in the Mississippi River near Memphis, 75 meters away from the barge and 21 meters from the turbine, shown by the solid lines without markers. The lines with markers show the hearing ability of certain fish. (from: [21])

#### 4.4.4 Bypasses and Ladders

Traditional dam configurations should have systems in place that attempt to allow fish to bypass the turbine intake and safely continue swimming up or downstream. However, these systems can be ineffective, not allowing all fish to pass through, due to their geometric setup

and location ([2], [45], [117], [188], [105]). Unless the specific species is particularly adept at jumping over obstacles, or laterally altering their path of motion to seek open routes, many of the fish bypasses or ladders can block migration and normal fish behavior. Several authors have investigated alternatives to current fish bypass configurations to increase their effectiveness ([191], [67], [92], [119]). Unfortunately, most of these efforts have been made after large dams have been constructed in major waterways, and in all likelihood, would not be implemented due to cost. Utilizing ineffective fish bypass systems, modern dams provide only two main options to migrating fish: retreat or attempt to pass through the turbine.

A ladder is defined here as a structure designed to allow fish to pass upstream across the dam. In contrast, a bypass is defined as a structure designed to allow fish to choose to avoid to enter the turbine penstock and can continue swimming downstream past the dam. These two categories will be referred to in general and called “fish passage” systems. There are five main types of fish passage systems: pool/weir ladders, vertical slot ladders, chute fishway ladders (also called “baffle” ladders), culverts, and elevators [142]. The pool/weir type is the oldest of the ladder technologies, made up of a long ramp with “buckets” or “boxes” for the fish to jump in and out of (or through, for an orifice/port type) to move up and down the ramp, similarly to a lock for a boat. The chute or “baffle” ladder is similar to the vertical slot ladder, in that they both include structural protrusions that are designed to produce a flow behavior that is advantageous for the fish to travel through with respect to flow speed, orifice sizes, areas for rest, etc. The culvert-type ladder is a duct of some sorts that allow natural flow through it (such as through a road or dam), and can include internal baffles to keep the flow velocity from becoming too high for fish passage. Lastly, the fish elevators are the most unique of the passage technologies, in that the fish are collected in a holding area, and are transported via an elevator over the dam. Other types of passage systems exist, such as removing the barrier to flow (dam removal), as well as the newer-coined “nature-like” or biomimetic bypasses, which attempt to mimic natural rapids or river sections [160]. The last method is to collect the fish and transport them in barges or trucks to move them to

the other side of the dam, or transporting them in helicopters, giving them the name “flying fish” [141]. The question arises whether these are implemented sufficiently in number and scale for current dam systems.

#### **4.4.5 In-Stream Turbines in Farms**

Another difference between in-stream and dam-turbine configurations, is that to obtain large amounts of power, the in-stream turbines generally need to be designed in larger numbers of units. This is due to the fact that in-stream turbines are near-zero head turbines, and thus rely heavily on flow kinetic energy to convert to mechanical shaft energy. Placing turbines in farms, however, could possibly lead to issues with the natural aquatic environment, if the spacing between turbines is made too small (in both the streamwise and the crossflow directions). If the cross-stream spacing between turbines is too small, aquatic life might have a more difficult time maneuvering around the turbines, and the blockage effect could become too great, reducing the total power output of the turbine array [184] and the ability of the river to recover its natural flow conditions [91]. The optimum number of turbines and their spacing will depend on the channel geometry, flow characteristics, individual turbine design, and the type and quantity of aquatic life present.

#### **4.4.6 Electromagnetic Emissions**

The possible issue with electromagnetic fields (EMFs) emitted from generators and power transfer cables is interference with navigation, foraging, or development by aquatic life, particularly fish that are dependent on or sensitive to magnetic or electric fields, such as sharks, salmonoids, sea turtles, and whales and dolphins ([44], [53]). In current literature, there have been no findings that indicate that EMF from single devices will negatively affect aquatic life [15]. The level of EMF will locally increase with the number of generators and cables in the water, however, no current literature has been found to quantify the compounding effect of the EMF on aquatic life.

## 4.5 Marine Safety and Aquatic Health

Depending on the location of the turbine, marine life may be comprised of much more than only fish: mammals, crustaceans, and insect and plant life all may use the waterways for food, reproduction, or migration. The behavior of each species will differ, so designing for as many different reactions and needs as possible may prove to be a challenge. From possibly modifying the behavior of mammals and birds ([19], [80], [69]) to disrupting crab metamorphosis [138], turbines can affect marine life in various ways. Monitoring the response of marine life to the existence and operation of the turbine, and the hydrodynamics and sound produced can be difficult, even with current active acoustic technology [101].

Along with the life supported by the riverine environment, the organic and inorganic materials transported by the flow also play an important role in the ecosystem. The sediments, comprised of organic and inorganic components of soils, silts, sands, and solids, as well as trapped gases and un-dissolved compounds are needed by plankton, farmland, and marine life throughout the river. The sediments provide nutrients, a balance of water quality, and habitat for aquatic life. It has been shown that in-stream turbines affect the sediment dynamics of a river by changing the local bedform from scouring below the turbine and depositing sediment towards the outside of the channel and downstream ([81], [82]) depending on the shape of the river and the flow velocity. The severity of the influence of the turbine on the sediment dynamics is related to the blockage ratio of the turbine device(s), though no existing literature was found to provide a functional relationship between them.

## 4.6 Literature Summary

The canonical injury mechanisms of dam-turbine configurations have been reviewed, and applied to fish safe turbine design with the addition of RPM and sound considerations. It has been shown that in-stream turbines can operate with low risk to the surrounding aquatic environment with respect to physical strike, pressure, shear, and turbulence if the following are included in the design process:

- Keep tip strike velocity below 5 m/s (balance of RPM, free stream velocity, and rotor radius)
- Operate at low RPM (at or below 20 RPM)
- Long blade chord and gaps between blades large (depending on size of largest fish present in waterway)
- Eliminate or minimize gap distances between stationary and moving parts
- Keep distance between turbines as large as possible, if placed in farms
- Mitigate fish access to blade tip region
- Keep strain rate less than 495 1/s
- Keep pressure ratio less than 2

It is to be noted that these design criteria are from the available data in the literature, corresponding to the studied species in question: future experiments will show how well these parameters will hold for other fish species. It is recommended that in-stream technology be further investigated, particularly examining in-situ marine interaction with the turbine. One of the main gaps in the current knowledge is the effect of the sound produced by a single real installed turbine and by a farm of turbines. It is recommended to perform short and long term experiments before and after the installation of real turbine unit(s) to fully understand the local temporal effects on aquatic life as well as to monitor the behavior change in native marine species. Acceptable criteria for safe sound levels should then be established to minimize the interference with the local aquatic life and should be included in the suggested list of design criteria for fish-friendly design.

## 4.7 Design

The lessons from Section 4.4 were applied in the preliminary design process for an in-stream turbine. One of the most simple ways to design a turbine is a parametric approach;

important and restricting parameters are chosen by or set for the designer, that when combined with basic turbomachinery and fluid dynamic principles allow for the calculation of blade shape at the mean radial location (generally, the area-averaged mean). These important parameters will depend on the scope of the intended use of the turbine, but could likely include: rotor tip maximum diameter (in the form of the minimum flow depth), rated power extraction, mean flow velocity (or flow rate, knowing channel bathymetry), and rotor RPM. Once the mean blade angles are calculated from the parameters, the designer picks a radial distribution of loading or specific work on the blade, with the common initial choice for a traditional blade being a “free-vortex”, meaning that the swirl (or circumferential) velocity is scaled from the mean as inversely proportional to the radius. For the particular design discussed here, the preliminary parameters that determined the mean blade angles are:

- Maximum strike speed less than 5 m/s
- Rotation rate equal to 20 RPM
- Flow velocity equal to 1 m/s

Where the strike speed is used here as the hypotenuse of the triangle formed by the rotational velocity and the rotor inlet velocity, which assumes that the fish is moving in the river by simply following the flow at the same speed as the mean flow velocity. In other words, the strike speed is equal to the blade inlet relative velocity, which is assumed to be the maximum velocity at which the fish will risk contacting the blade surface. The maximum strike speed, along with the RPM and flow velocity, determines the maximum diameter of the turbine. The flow velocity is chosen as what would be typical for the river of interest, in this case the Amazon River. The RPM is chosen in this case to be the hypothesized critical point for fish safety, favoring low impact velocity in the event of fish contact with the rotor blades.

The initial estimation of rated power extraction is determined by the aforementioned parameters, as well as the mean circumferential velocity (chosen as the outlet blade angle at the average radius). The mean circumferential velocity is scaled in the radial direction using

a free-vortex profile assumption (4.1),

$$K = \text{constant} = C_\theta * r \quad (4.1)$$

and all other blade angles are calculated at each radial location. The blade outlet circumferential velocity is calculated as the value at which the Betz limit is reached for a bare rotor (4.2),

$$P_{Betz} = \dot{m} * KE_\infty = 0.5 * \rho * C_\infty^3 * A_{turbine} \quad (4.2)$$

assuming that there is no pre-swirl into the rotor (4.3), and that the rotor has 100% blade efficiency (relative to Betz) (4.4). In other words, the mean blade swirl is determined when the resulting power from the Euler turbine equation matches the power reported from the ideal Betz equation.

$$P_{bare rotor} = \omega * U * r * C_\theta, \text{ where values are calculated at } r_{mean} \quad (4.3)$$

$$P_{bare rotor} = \eta * P_{available} = P_{Betz}, \text{ if } \eta = 100\% \quad (4.4)$$

The rotor is encased in a duct, mainly to mitigate fish access to the blade tips, as well as increasing the rated power extraction of the turbine over a bare rotor. The design is evaluated in open-water efficiency as well as the maximum strain rate and minimum pressure are found numerically with a CFD simulation in an infinite media environment, see Section 4.8. The turbine design is summarized in Table 4.1.

Table 4.1: Turbine Design Parameters

<i>Turbine Design</i>	
<b>Parameter</b>	<b>Value</b>
Tip Diameter	1.25 m
Hub Diameter	0.4 m
RPM	20 RPM
Mean Outlet Blade Angle	25.8°
Rated Power	325 W

## 4.8 Simulation

### 4.8.1 Model and Mesh

The aforementioned turbine design was modeled in BladeGen and Siemens NX, and imported into ANSYS Workbench for meshing and Computational Fluid Dynamics (CFD) simulation. The mesh comprised of a mixture of 12.5 million tetrahedral and hexahedral elements for the turbine, shroud, and flow domain. The mesh quality was measured in terms of the skewness and the orthogonal quality: the maximum element skewness was equal to 0.851 and the minimum orthogonal quality was equal to 0.182. The geometric model and simulation mesh are shown in Figures 4.10 to 4.15.

This rotor is designed to be hubless, and instead drives a generator at the rim, such is shown in 4.11. The hubless design is chosen due to the possible benefit that if any fish or debris manage to resist the natural bypass flow and make it past the trashrack (not shown), that the open center as well as the backward-leaned blades can help to pass the fish or debris through without contacting the blades.

Excluding a possible trashrack, electrical cables, and a mooring device (a float or cables), the in-stream device is shown in a river in 4.12.

### 4.8.2 Setup

The turbine was simulated in a transient, full-wheel 3D flow environment. The turbulence closure problem was handled with the  $k - \omega$  Shear Stress Transport (SST) model, in order to enhance the accuracy of the turbulence modeling near to the blade walls as well as far out into the fluid. This is done by combining the standard  $k - \epsilon$  and  $k - \omega$  closure models, and blending them between wall and free-stream regions. Equations (4.5) through (4.8) show the set of equations that are solved in ANSYS Fluent, with the  $k - \omega$  SST closure model. The difference between the standard  $k - \omega$  and the SST model is in the functional form of the turbulent viscosity  $\mu_t$  and the turbulent Prandtl numbers  $\sigma_k$  and  $\sigma_\omega$  that are used to

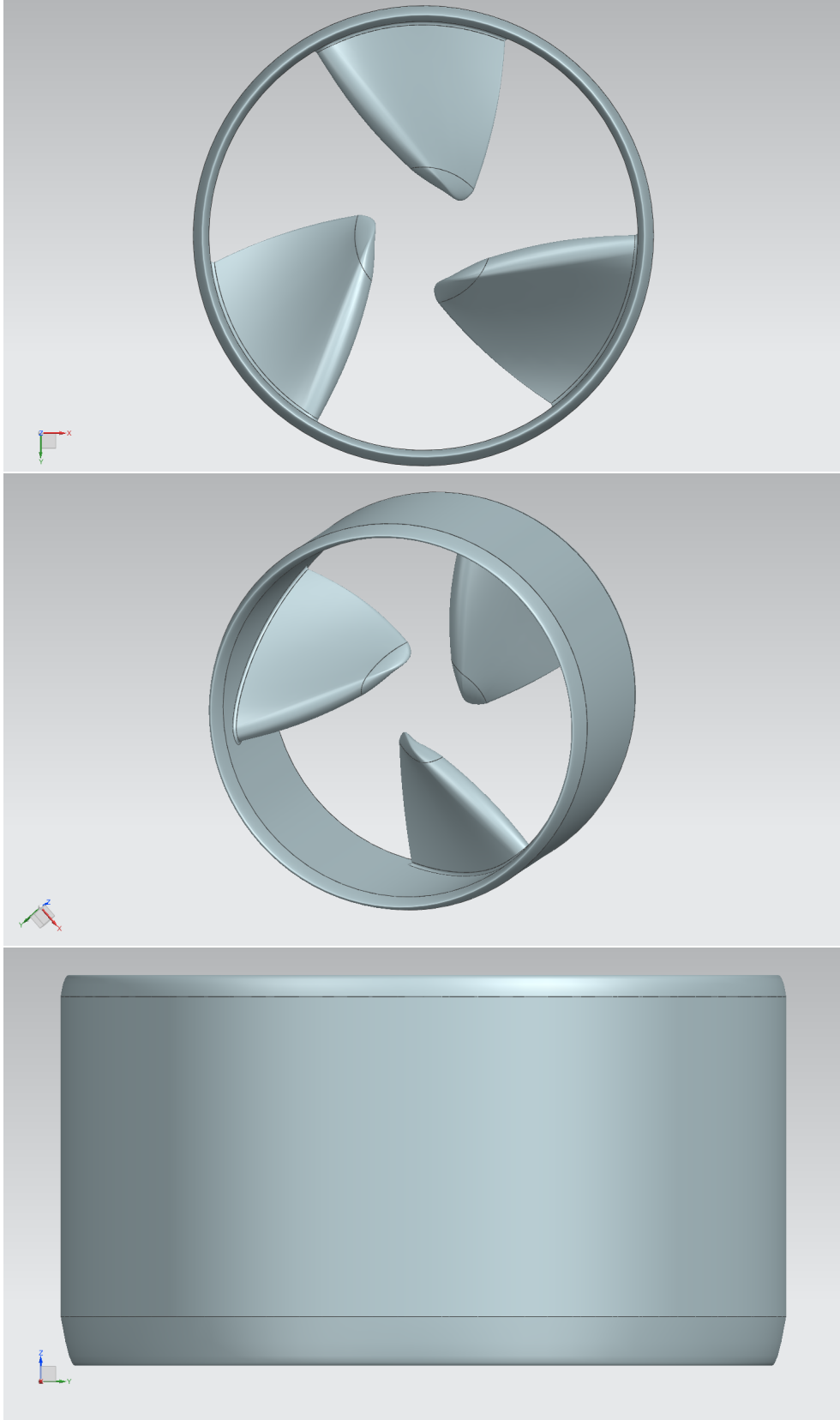


Figure 4.10: Ducted rotor model from three views: flow direction, oblique and top

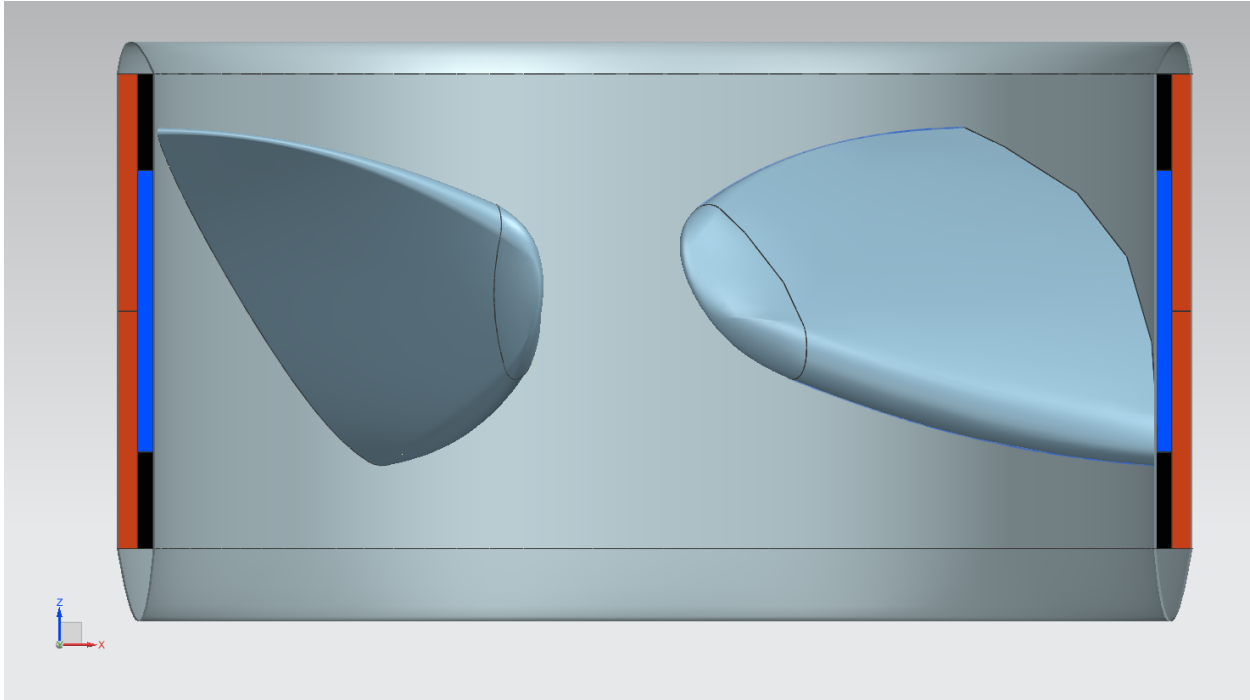


Figure 4.11: Cross-section of the in-stream generator, with a simplified rim-drive generator. The black blocks are bearings, the dark blue blocks are magnets (rotating with the blades), and the red blocks are the stator windings and core (stationary with shroud).

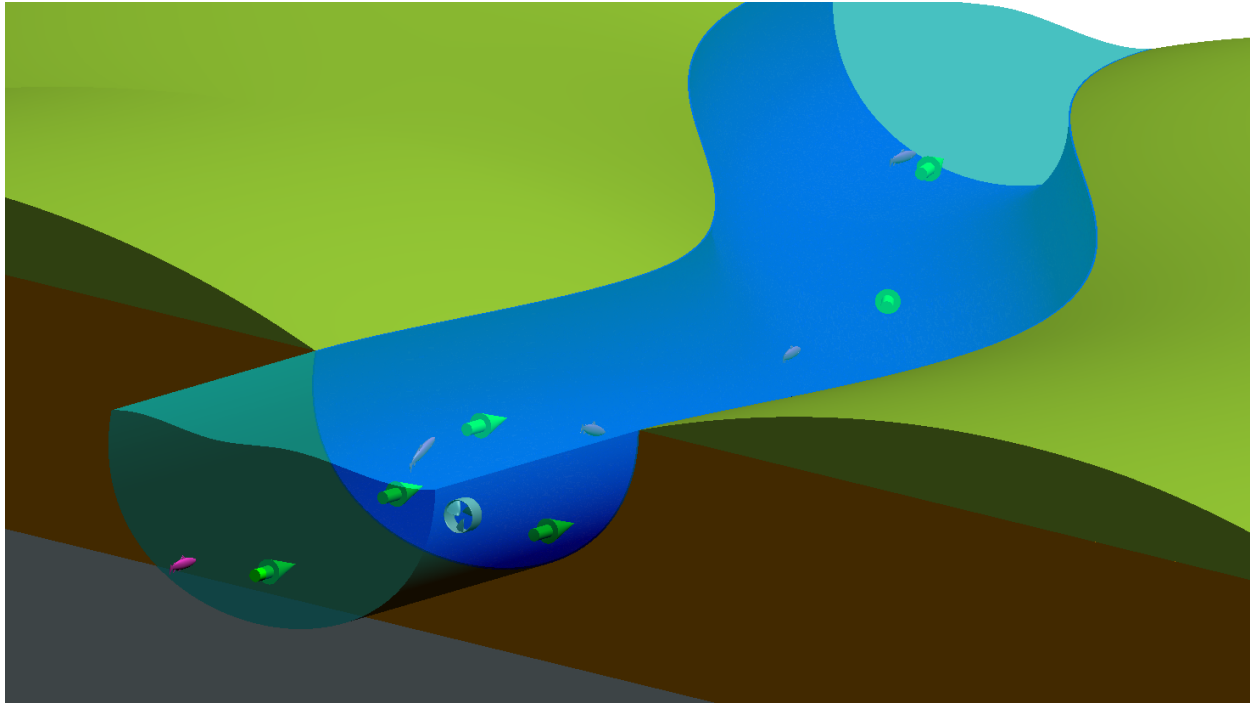


Figure 4.12: In-stream generator in a river channel

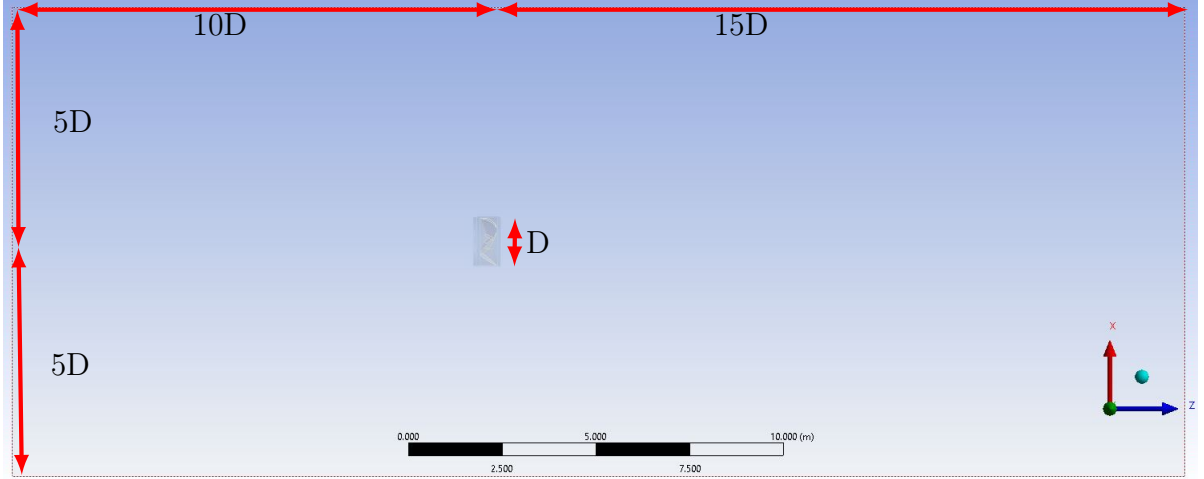


Figure 4.13: Numeric domain

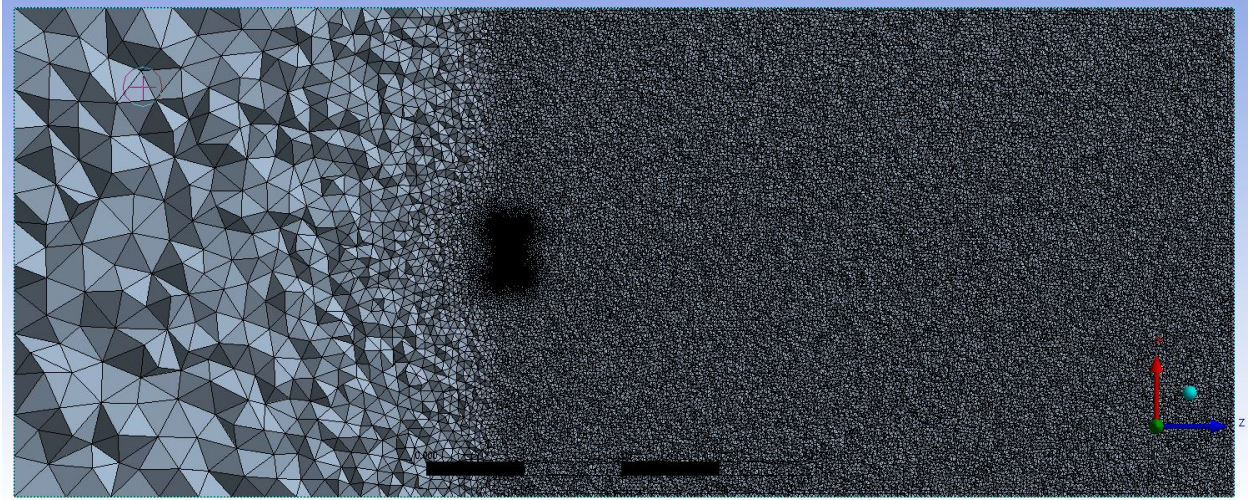


Figure 4.14: Ducted rotor mesh: domain side view

calculate  $\Gamma_k$  and  $\Gamma_\omega$  in (4.7) and (4.8). The SST model used a hyperbolic tangent function to blend  $k - \omega$  and  $k - \epsilon$ , instead of purely using  $k - \omega$ . The production (G), dissipation (-Y), and user source terms (S) for both  $k$  and  $\omega$  are similar among the standard and SST  $k - \omega$  models, with a few constants and calculation logic components that set them apart.

$$\frac{\partial \rho}{\partial t} + \nabla \cdot (\rho \vec{v}) = S_m \quad (4.5)$$

$$\frac{\partial}{\partial t}(\rho \vec{v}) + \nabla \cdot (\rho \vec{v} \vec{v}) = -\nabla p + \nabla \cdot (\bar{\tau}) + \rho \vec{g} + \vec{F} \quad (4.6)$$

$$\frac{\partial}{\partial t}(\rho k) + \frac{\partial}{\partial x_i}(\rho k u_i) = \frac{\partial}{\partial x_j}(\Gamma_k \frac{\partial k}{\partial x_j}) + \tilde{G}_k - Y_k + S_k \quad (4.7)$$

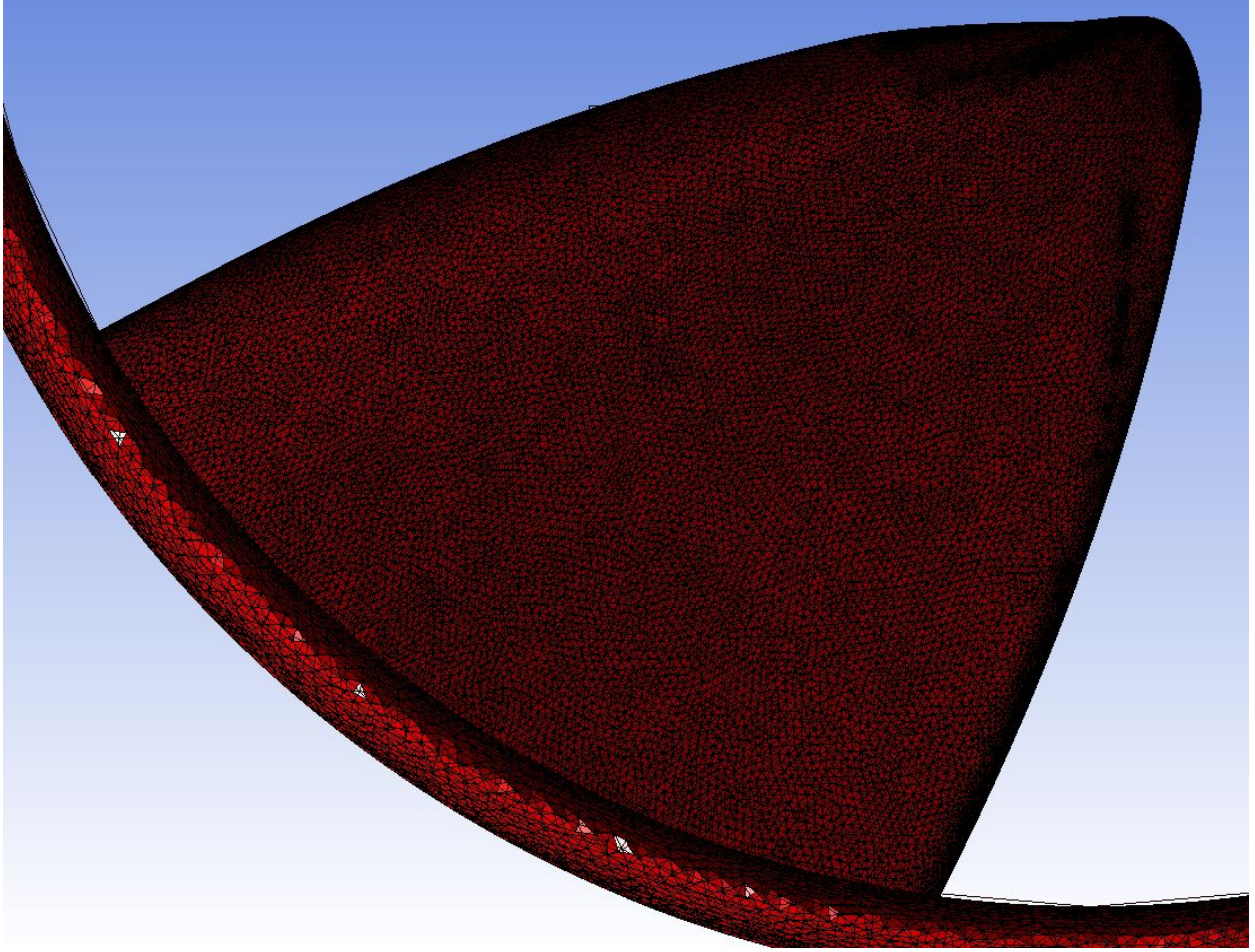


Figure 4.15: Ducted rotor mesh: rotor blade view

$$\frac{\partial}{\partial t}(\rho\omega) + \frac{\partial}{\partial x_i}(\rho\omega u_i) = \frac{\partial}{\partial x_j}(\Gamma\omega \frac{\partial\omega}{\partial x_j}) + G_\omega - Y_\omega + D_\omega + S_\omega \quad (4.8)$$

The boundary conditions were set as: velocity inlet (at 1 m/s), a pressure-outlet (at zero gauge), and the other outer domain surfaces were set to symmetry conditions, to simulate a turbine far away from the free surface or river walls. The spatial and temporal finite difference schemes were all evaluated at second order, and the pressure-velocity variables were coupled, with a Courant number of 2. To model the motion of the rotor, a sliding mesh technique was implemented. A multiple frame of reference model was used, providing the cylinder of fluid that represented the turbine-turned flow a mesh motion at 2.09 rad/s, and the same treatment was given to the walls associated with that fluid zone. The flow domain was initialized with the inlet conditions, and was solved implicitly with a time step

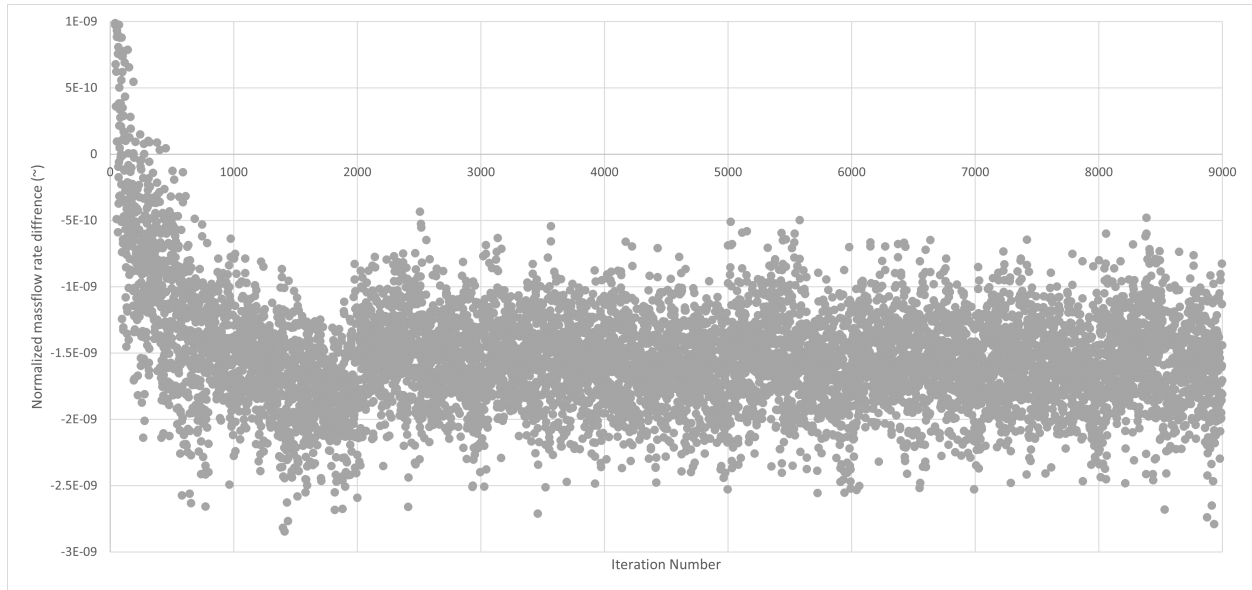


Figure 4.16: Massflow rate difference between inlet and outlet normalized by inlet massflow rate over iteration count

of one millisecond. The solution was allowed to time-step for at least two full blade rotations (6000 time steps), and was allowed 100 iterations at each time step to converge the tracked variables to a residual of  $1E-5$ . The simulation is considered converged once the massflow rate difference between inlet and outlet reached a semi-steady level, and the torque coefficient on the blades reaches a quasi-steady level (fluctuations are about a constant mean value), as is shown in Figures 4.16 and 4.17.

### 4.8.3 Results

The initial design case was simulated at a TSR of approximately 0.65. The TSR was varied from 1.87 towards 0 by varying the inflow velocity, mimicking large changes in seasonal river flow rates, while the generator maintains constant RPM. The performance of the turbine design was measured in terms of its ability to meet the aforementioned fish-friendly criteria as well as its ability to produce power. The shaft power is reported in terms of the power coefficient, and the ‘fish-friendliness’ of the design is measured in terms of the maximum strain rate and the minimum pressure encountered in the flow. The results calculated from

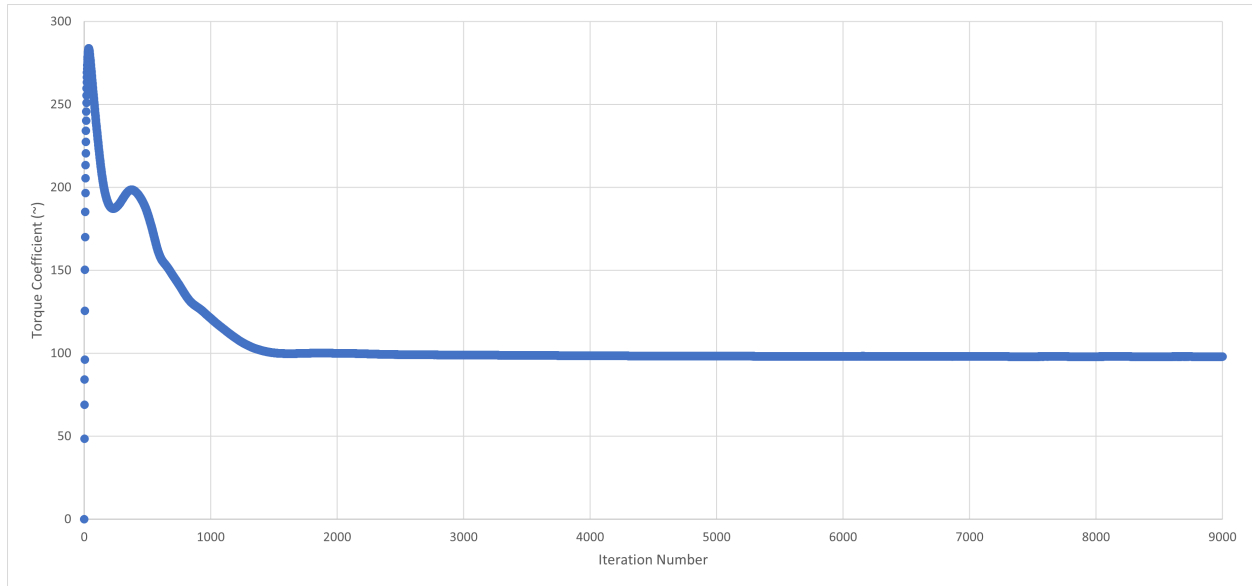


Figure 4.17: Torque coefficient over iteration count

Fluent are shown in Figures 4.18-4.22.

#### 4.8.3.1 Power Coefficient

Figure 4.18 shows the range of the typical performance metric for in-stream devices, the power coefficient, over the investigated tip speed ratio. The maximum found power coefficient is 0.239 using the rotor diameter as the basis for maximum kinetic flux, or 0.208 when considering the duct outermost diameter, occurring at a TSR of approximately 0.871. Comparing this peak power coefficient to the so-called Betz limit yields a relative efficiency of 35-40%, comparing to a bare rotor, 1-D momentum basis. However, as was mentioned in Section 4.2.3, this concept of a maximum power of free-flowing devices has been investigated in the literature for various device-environment configurations, with no clear answer yet as to the true upper limit, or the most accurate basis for calculation. Taking the analysis of Betz one step further, using the results of the rotor disk model, equations (4.9) and (4.10) can be used to evaluate a somewhat more realistic value for maximum power coefficient than

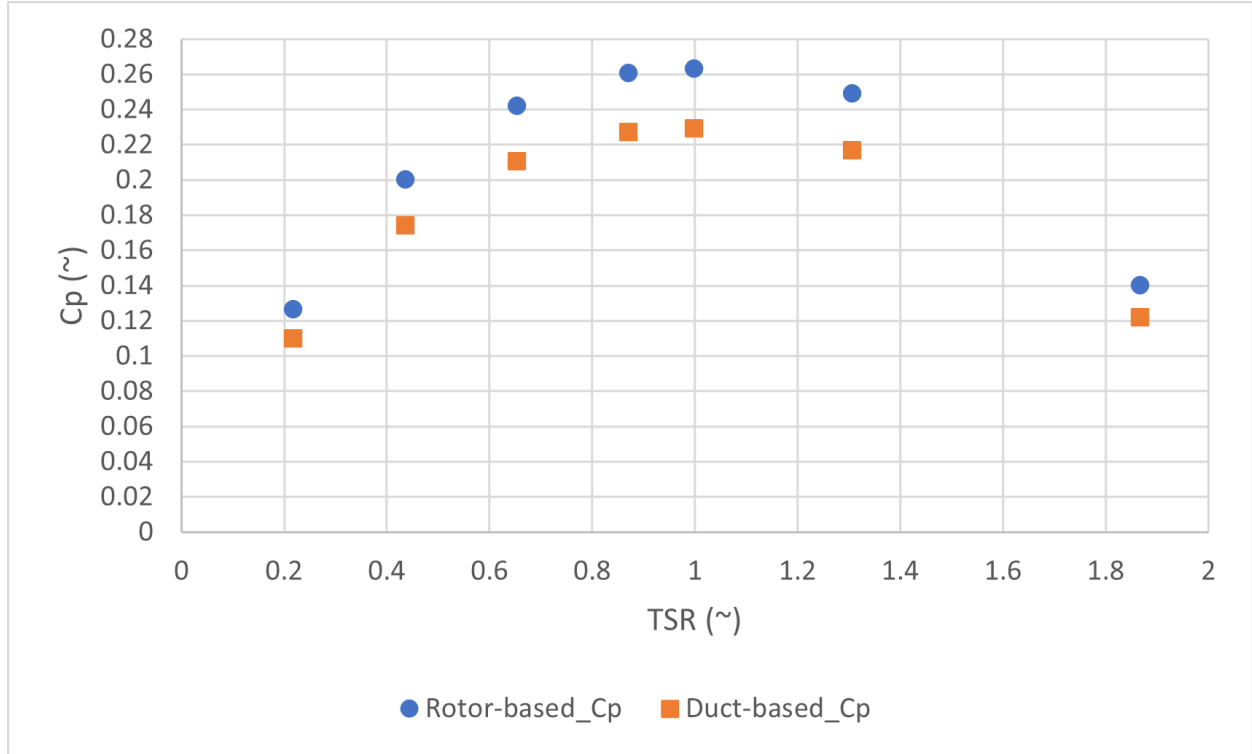


Figure 4.18: Plot of power coefficient over tip speed ratio, based on the rotor and duct areas

Betz [102]:

$$\lambda^2 = \frac{(1 - a_2)(4a_2 - 1)^2}{(1 - 3a_2)} \quad (4.9)$$

$$C_{p,max} = \frac{8}{729\lambda} \left[ \frac{64}{5}x^5 + 72x^4 + 124x^3 + 38x^2 - 63x - 12\ln(x) - 4x^{-1} \right] \Big|_{x=(1-3a_2)}^{x=0.25} \quad (4.10)$$

Using these two equations allows for the calculation of a maximum power coefficient equal to 0.391 at the same tip speed ratio as the peak power from CFD. This increases the efficiency of the design to around 53-61% when utilizing rotor disk theory over pure actuator disk theory; however, this is still inaccurate basis as no duct is considered in either disk analysis.

### 4.8.3.2 Pressure

Figure 4.19 shows the pressure ratio of the minimum (or nadir) pressure encountered in the flow to various hypothetical acclimation pressures of fish. The pressure ratio remains lower than 2 over the range of acclimation pressures for most of the design points considered. At

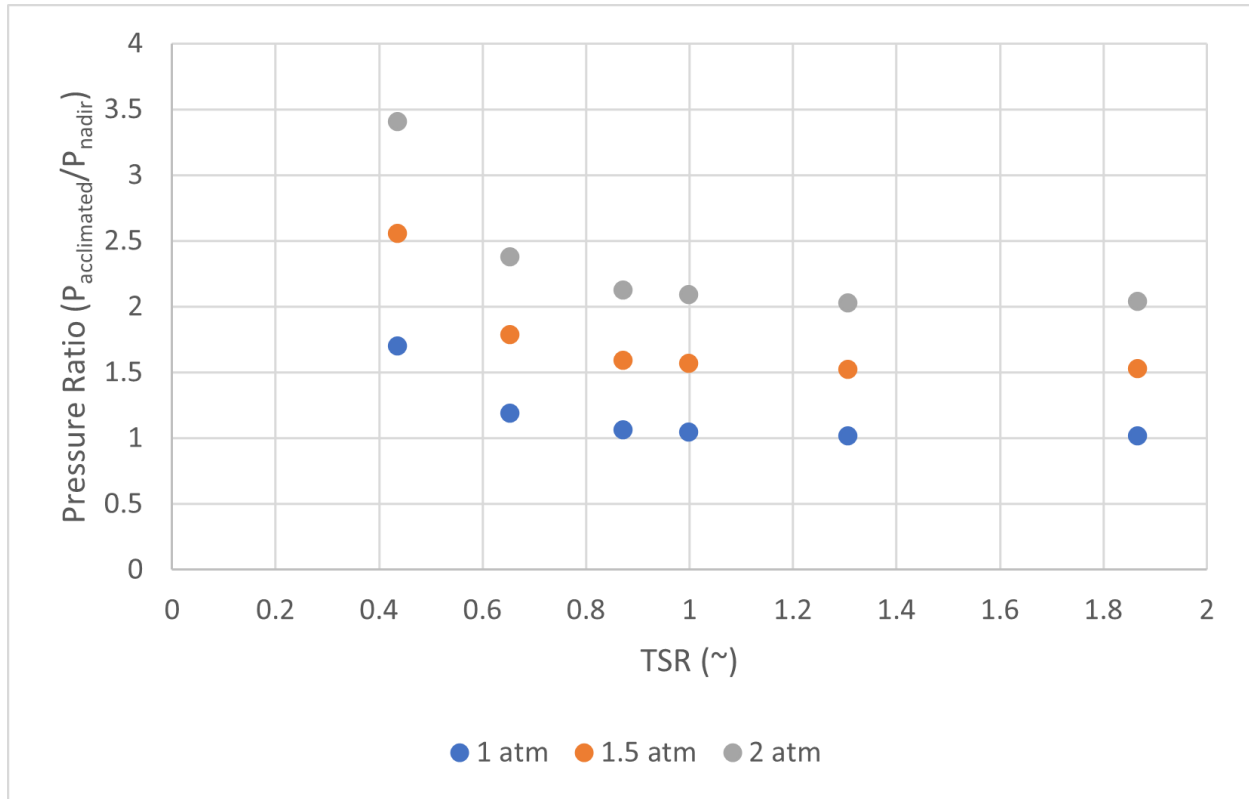


Figure 4.19: Plot of pressure ratio over tip speed ratio, at three acclimation pressures: 1 atm, 1.5 atm, and 2 atm

acclimation pressures higher than 2 atm, the peak performance point and higher velocities would present too high of a pressure ratio to keep injury probabilities at a minimum. This may not be a problem, however, depending on the placement of the turbine within a river channel, because a bottom-dwelling fish may not move quickly or close enough towards the surface to swim through the turbine-affected flow if the turbine was not placed on/very near to the bottom. Similarly, the maximum negative rate of pressure change is shown to be acceptable when compared with the industry-used 550 kPa/s criteria [118], down to a TSR of approximately 0.65.

#### 4.8.3.3 Strain Rate

Figures 4.21 and 4.22 show the maximum strain rate (or shear rate) in the flow, and the percent of the blade surfaces above the maximum criteria. Figure 4.21 shows that on a hyper-

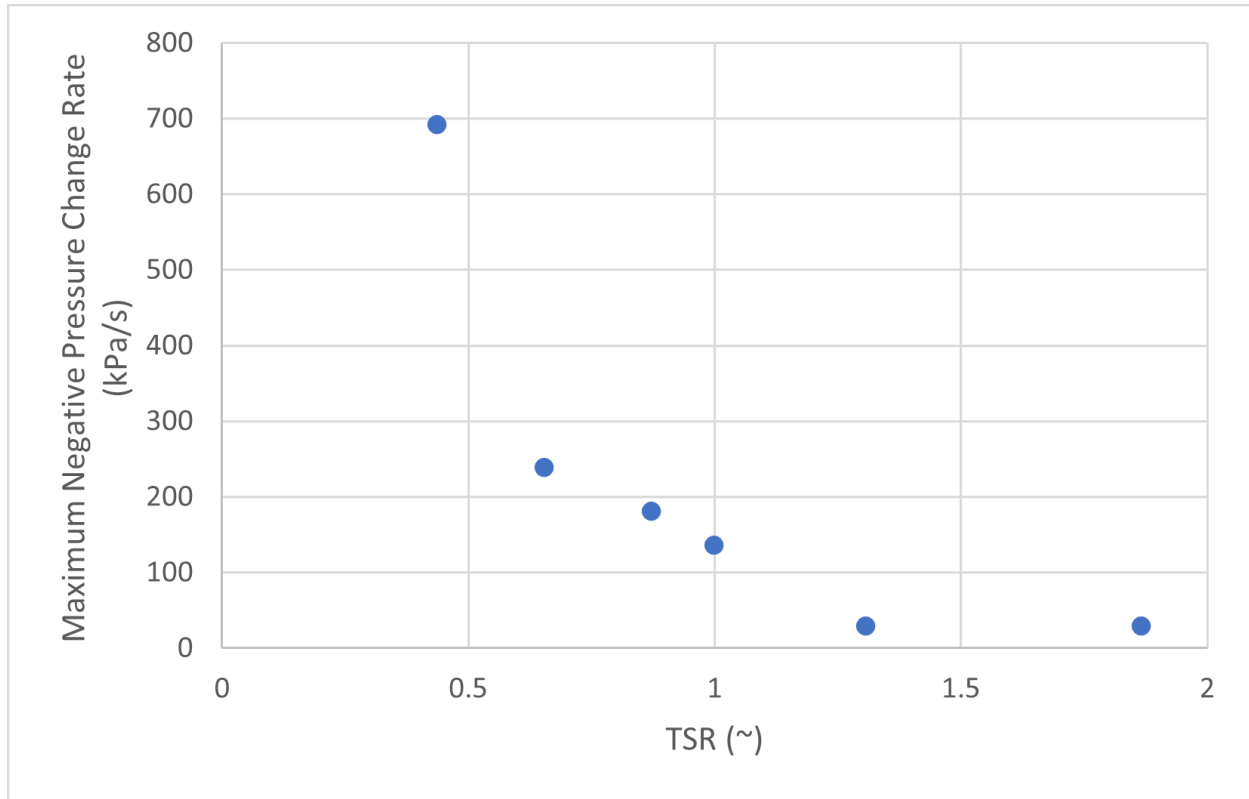


Figure 4.20: Plot of maximum negative pressure rate of change over tip speed ratio.

local maximum strain basis, none of the examined design conditions have an acceptably low level of shear; in other words, even if one mesh element experiences over-criteria strain rate, then the design fails. However, Figure 4.22 tells a different story by examining the entire high-strain region, namely, near to the blade surface, and the percent of the blade surface that is above the criteria. It is found that at a tip speed ratio of 0.871 and above, the percent of the blade surface (calculated by element volume) that is above the criteria is nearly null; only a very small number of elements near the blade "tip" (the blade root for the hubless, rim-driven design considered here) could present risk. To further avoid risk, the presence of the duct can mitigate fish's access to the tip, and the hubless open center can encourage (by lower pressure change and flow resistance) fish to swim through without needing to swim past the blades.

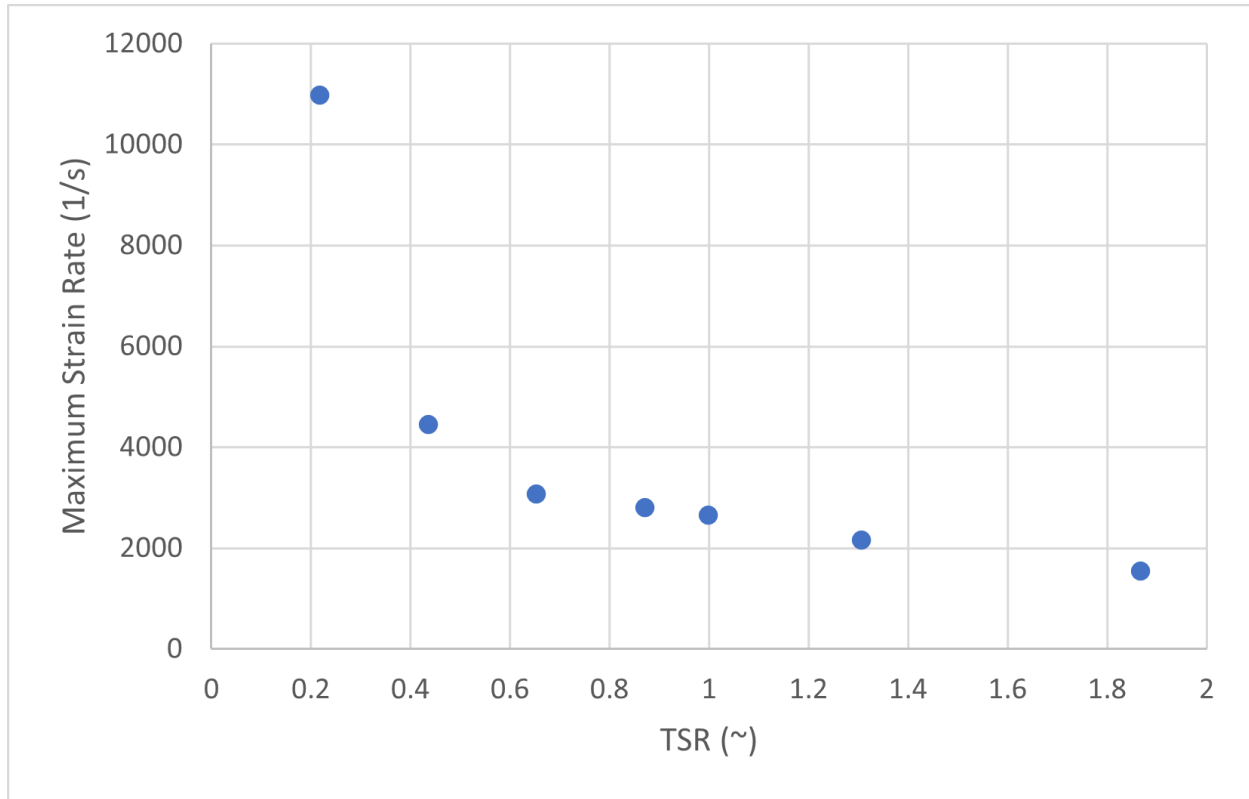


Figure 4.21: Plot of maximum domain strain rate over tip speed ratio

#### 4.8.4 Postprocessing Routine

After the initial results were calculated using ANSYS Fluent’s GUI-based routines, a separate analysis was done using MATLAB to analyze the CFD results to compare to the design.

##### 4.8.4.1 Method

To better visualize and analyze the performance of the simulated machine, it was desired to examine the flow and turbomachine variables qualitatively and quantitatively. ANSYS Fluent does not easily allow full-wheel 3D environment simulation within the turbomachinery toolset (only a repeated flow passage with a traditional hub and case). Therefore, any analysis needs to be done with general Fluent visualization/evaluation tools (simple geometry-bound plotting, postprocessing of elemental flow values, etc.), or needs to be developed externally, and provided the simulation result data. In this case, an "unwrapped“ view of

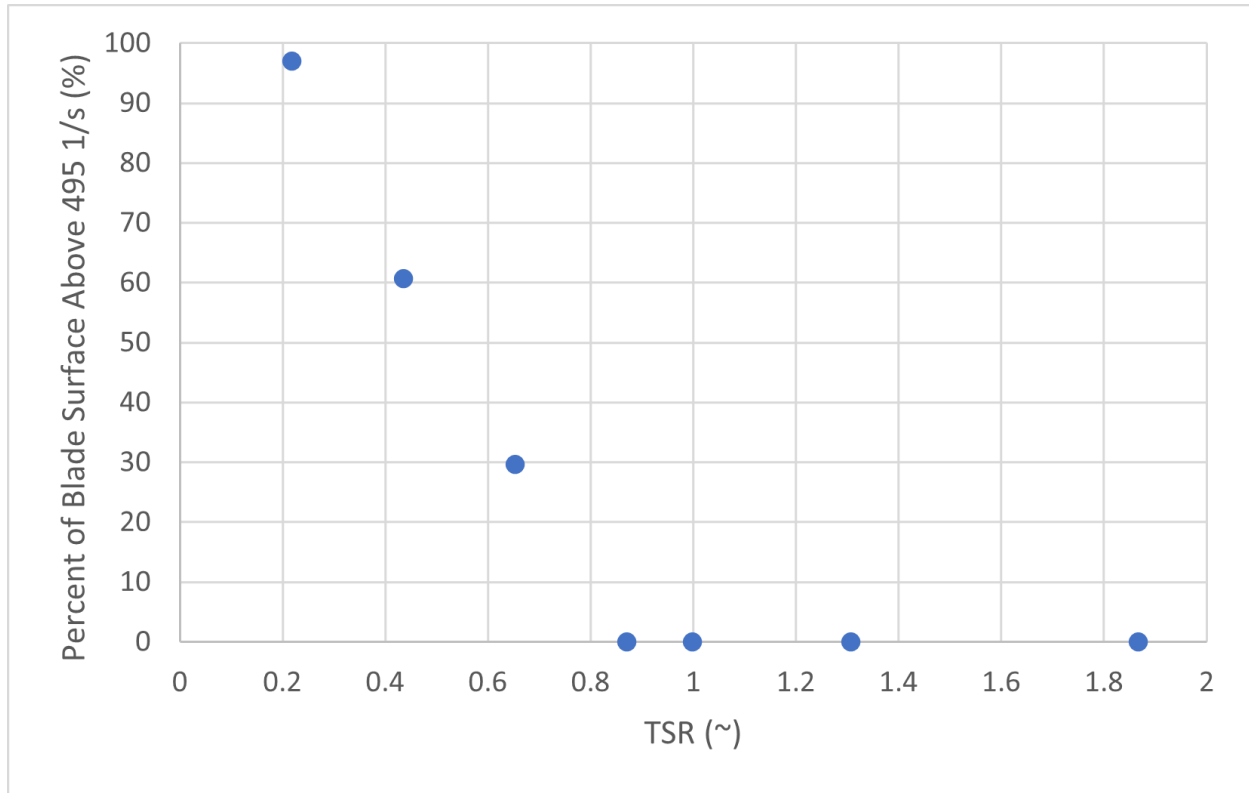


Figure 4.22: Plot of percent of blade surrounding volume above criteria of 495 1/s over tip speed ratio

the flow passages was desired (visualization on a 2D axial-tangential directional plane), so MATLAB was chosen as the best environment for analysis for its strong visualization toolset, see Appendix B. The simulation results were exported from Fluent for the entirety of the rotational domain, exporting cell-center evaluated values (because Fluent is a volumetric approach, these values are not interpolated like nodal values) of all variables. This was also done for the blade wall regions as well, to capture only the near-to-blade regions for the most accurate turbomachinery calculations.

#### 4.8.4.2 Output

Figures 4.23-4.32 show the output from the MATLAB script. Figures 4.23-4.26 show the initial free-vortex blade velocity triangle design, and the comparison with the near-blade data output from Fluent. Figures 4.27 - 4.32 focus on the 2D visualization of a flow passage

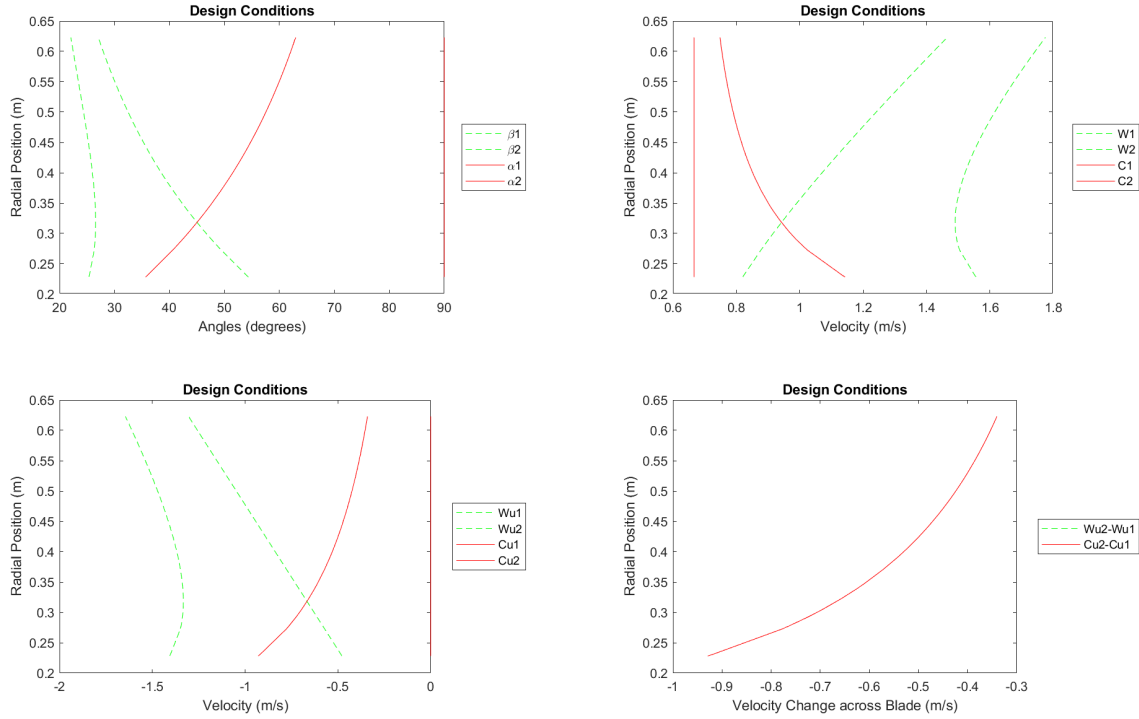


Figure 4.23: Designed triangle velocities over blade span

on either side of one blade, in terms of the relative flow velocities: vectors, contours, and streamlines, at three root-of-the-sum-of-the-square (RSS) radial span locations: 10%, 50% and 90%.

#### 4.8.4.3 Discussion

As can be seen from Figures 4.27-4.32, the relative flow velocity contours did not calculate as were expected when using cell-centered exported values from Fluent. Starting at a tangential arc length position of approximately 0 meters, there are periodic-looking (some multiplicative interval of  $\pi \cdot \text{radius}$ ) line disturbances to the data. This can be most easily seen in Figures 4.27 and 4.30, where it can be seen that there are physical data points within the meshless blade interior volume. This issue was attempted to be resolved, however, no fix was found during the time of this work; the interpolation function (other than `ScatteredInterpolant`) and technique was changed (linear, nearest neighbor, natural neighbor) to no avail. It

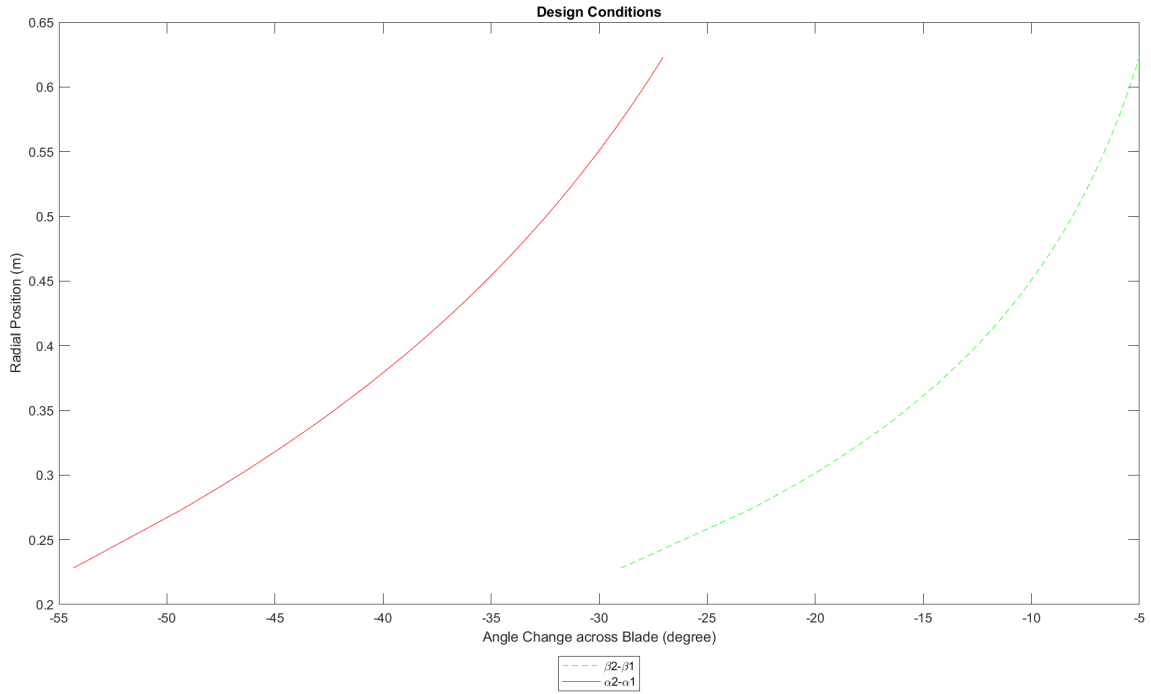


Figure 4.24: Designed blade angle difference across blade over blade span

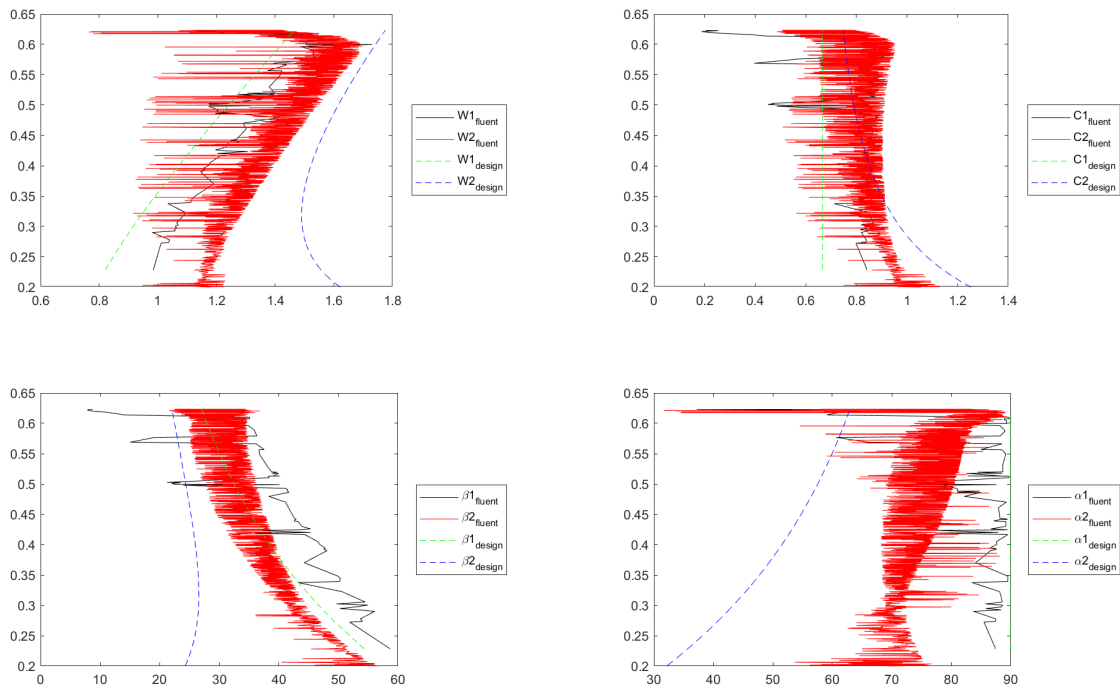


Figure 4.25: Comparison of designed blade triangle velocities with CFD output

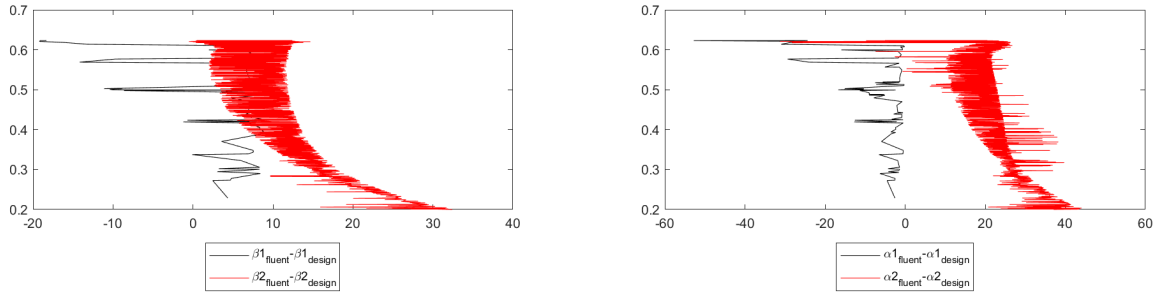


Figure 4.26: Spanwise profiles of angular difference between design and CFD output

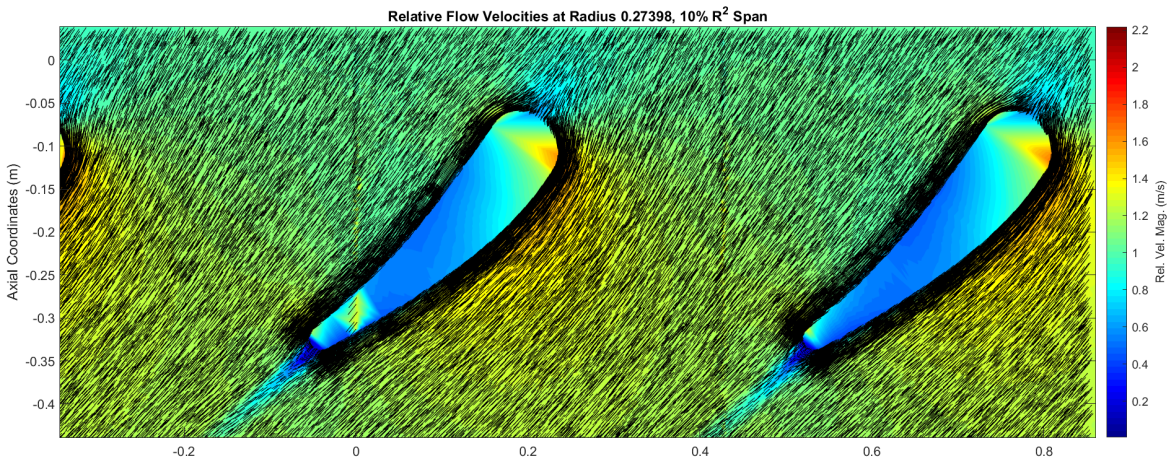


Figure 4.27: Relative flow velocity vectors and contours at 10% square radial span

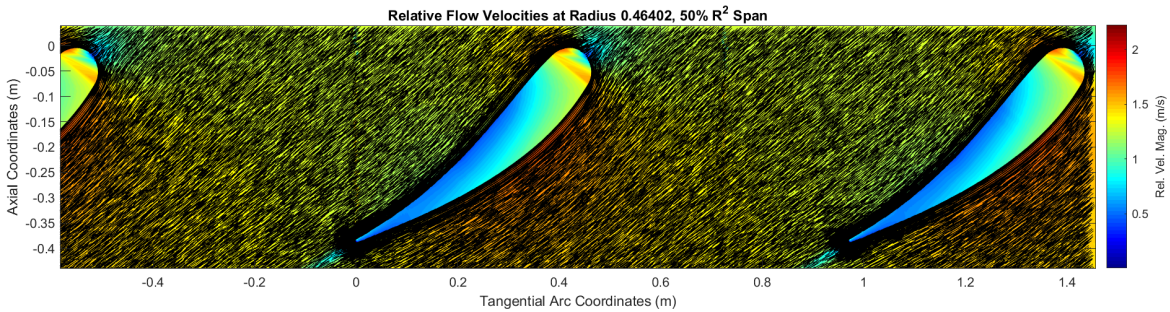


Figure 4.28: Relative flow velocity vectors and contours at 50% square radial span

was deemed that this issue is embedded within Fluent’s export routine, and so the node-based values (interpolated by Fluent from the cell centers) were exported to assist in the visual representation of the flow passages. The cell-centered values were retained for any quantitative calculations (such as the span-average angular difference from design), but the

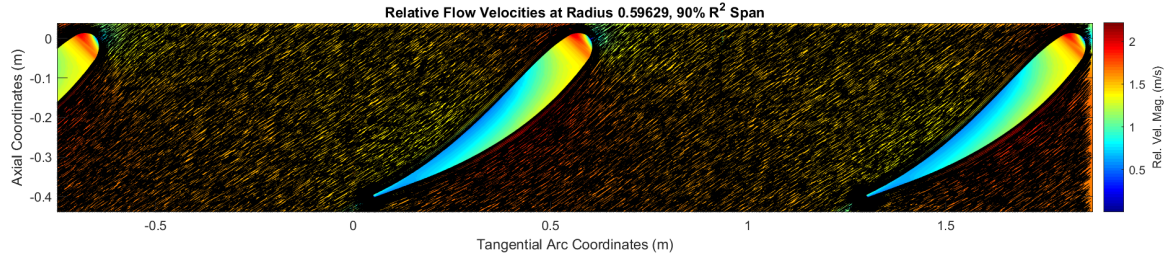


Figure 4.29: Relative flow velocity vectors and contours at 90% square radial span

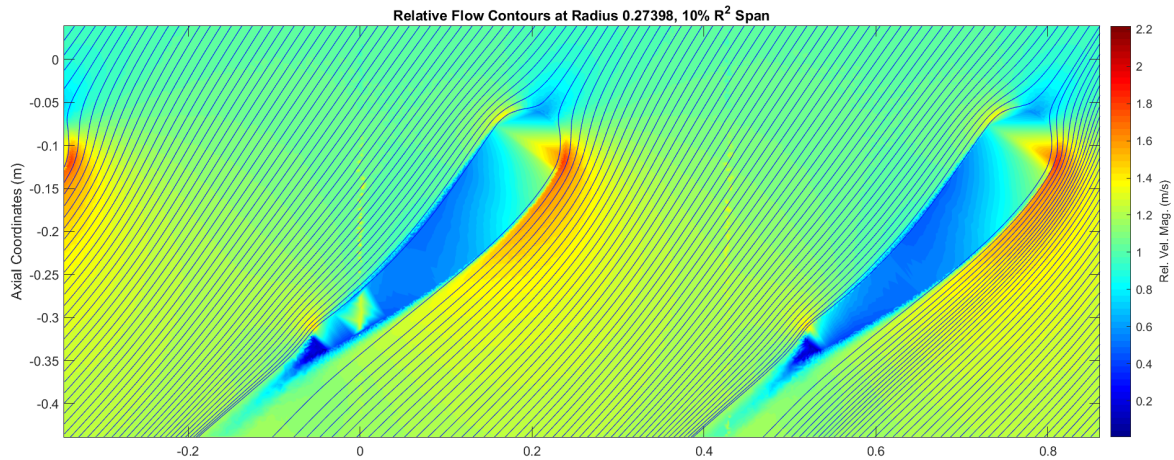


Figure 4.30: Relative flow velocity streamlines and contours at 10% square radial span

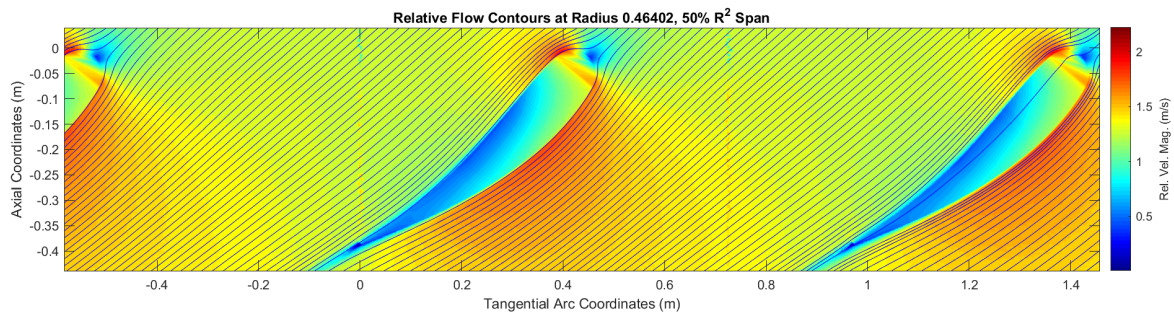


Figure 4.31: Relative flow velocity streamlines and contours at 50% square radial span

values are examined with a sense of conservative caution. Figures 4.33-4.35 show some of the relative vector and contour outputs calculated using the nodal data export from Fluent. It can be seen from Figures 4.27-4.35 that the relative velocity vectors align fairly well with the blade shapes through the flow passages. Figure 4.26 indicates that, when calculated using the cell-centered values, the mass-average span difference between the designed relative velocity

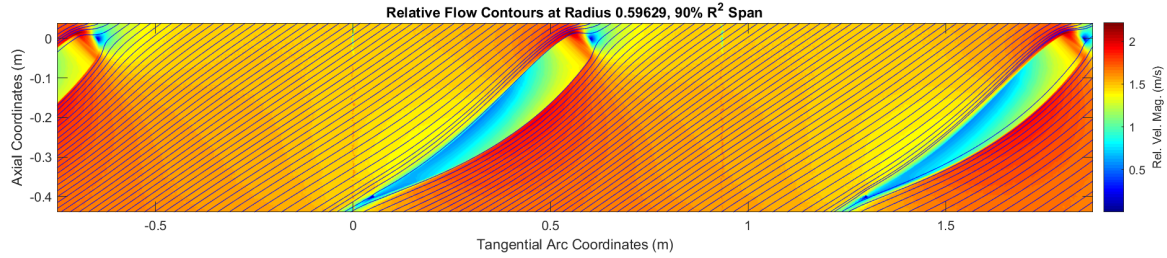


Figure 4.32: Relative flow velocity streamlines and contours at 90% square radial span

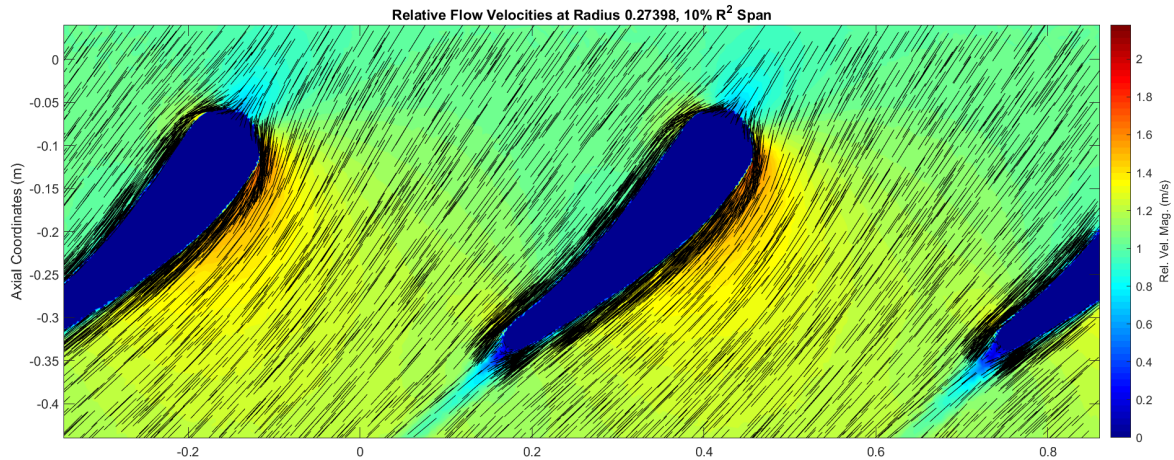


Figure 4.33: Relative flow velocity vectors and contours at 10% square radial span, using nodal values

angles ( $\beta$ ) and the CFD calculated angles are approximately 4 and 11 degrees, at the leading and trailing edges, respectively. For the absolute velocity angles ( $\alpha$ ), the calculated mass-averaged differences are approximately 5 and 22 degrees, at the leading and trailing edges. The relative angle difference can be qualitatively seen in Figures 4.27-4.35 in that the relative flow is well-aligned with the blade surfaces, with a noticeable difference of a few degrees at the leading and trailing edges, leading to reduced efficiency via less swirl difference (“unswirling”) than designed.

#### 4.8.5 Conclusion

Considering the results shown in Section 4.8.3, the designed in-stream device achieves the goal of being fish friendly based on the findings in Section 4.3, with the caveats mentioned

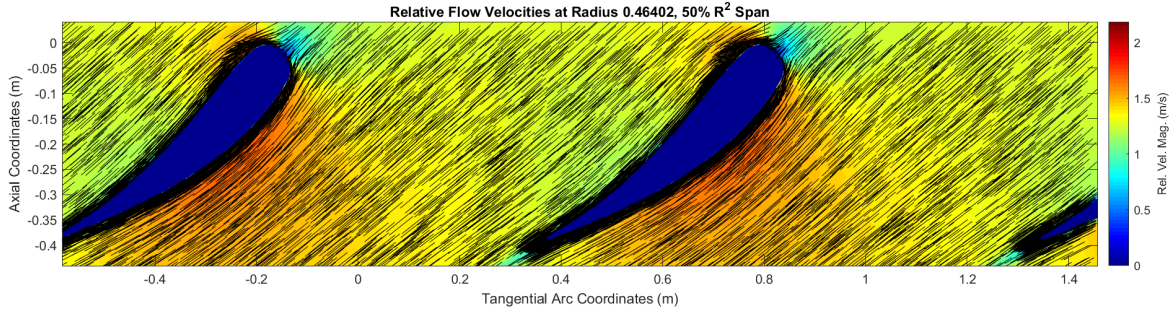


Figure 4.34: Relative flow velocity vectors and contours at 50% square radial span, using nodal values

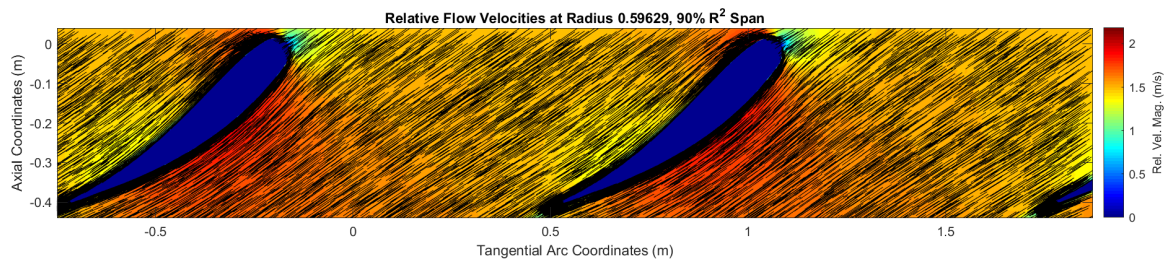


Figure 4.35: Relative flow velocity vectors and contours at 90% square radial span, using nodal values

over the tip speed ratio range investigated here. It is noteworthy to mention an interesting point that the literature mentioned herein yielded essentially two different sets of criteria and thus two different designs for "fish-friendly" turbines: MJ2's very-low-head (VLH) turbine based predominantly on the review work of Odeh et al. and the Alden turbine, with work and support by Alden Labs, Voith, the Environmental Power Research Institute (EPRI), and the Department of Energy (DoE) based on the newer experimentation and innovation. The work presented here is mainly based on the foundation of the latter design, with the addition of other novel research documented in the literature in an attempt to accumulate the mass of current knowledge into a design that is capable of being placed naturally into a free flowing river without significantly disturbing or harming the marine life present. Based on the criteria compiled and documented by Odeh and utilized by MJ2, it could be said that the design presented here uses conservative criteria, and could possibly use less restrictive values for pressure, strike velocity, etc. and maintain a high level of fish safety. Neverthe-

less, until the design would be manufactured and deployed in solo and farm configurations, the true behavioral impact on the marine life can only be stipulated on, which can hopefully someday add to the knowledge base on marine energy extraction interaction with the surrounding environment, or at least benefit from and be enhanced by future work. It is noted that the emitted sound levels of this particular design were not calculated during the simulation process. This is left for future to work to investigate for further understanding of the interaction of this turbine design with the surrounding environment. Additionally, the design was simulated in an effectively open environment (a blockage ratio less than 0.01); future work would involve simulating the turbine with a specific (“real”) channel geometry or an equivalent significant blockage ratio, while also examining the effect on a dynamic open-channel surface.

## CHAPTER 5

### CLOSING REMARKS AND GLOBAL IMPLICATIONS

The lessons learned from the Amazon can also be generalized to other regions of the world, such as Africa and India, where access to a national power grid and an abundance of natural energy sources may be limited by geographic, financial, or social situations. There are several challenges that need to be planned for and overcome when utilizing the technologies and energy generation strategies presented here, including:

- Guiding viewpoints towards global environmental and social safety and health over financial interests
- Overcoming local people's opinion of "not-in-my-backyard", often coming from experience with large hydro
- Creating interest of the local people as well the governing bodies and industry to accept "something new"
- Working with the appropriate government agencies and industries to fund the projects
- Sharing the benefits of distributed, renewable power with the public

These issues take time and multi-disciplinary planning to overcome, however, with enough public interest and involvement, working between all interested and benefitting parties is possible. Embracing decentralized renewable power generation, such as rooftop and floating solar, as well as in-stream technologies could be a key factor in improving global quality of life and meeting environmental goals towards a future-friendly global energy market.

## APPENDICES

## APPENDIX A

### GIS FILE SOURCES

Shapefile and GIS sources utilized:

- Background: Natural Earth: <http://www.naturalearthdata.com/>
- South America with boundaries: <https://tapiquen-sig.jimdofree.com/english-version/free-downloads/south-america/>
- Brazil with boundaries: IBGE: <https://www.ibge.gov.br/estatisticas/downloads-estatisticas.html>
- GIS software: QGIS: <https://www.qgis.org/en/site/>
- Brazilian energy generation locations: ANEEL: <https://www.aneel.gov.br/informacoes-geograficas>
- Brazilian transmission lines: ONS: <http://www.ons.org.br/paginas/sobre-o-sin/mapas>

**APPENDIX B**  
**MATLAB SAMPLE SCRIPT**

```
%BEGIN SCRIPT  
  
%This script takes ASCII output data from the rotating region  
around the  
turbine and extracts data necessary to examine the flow through  
the blade  
passages.  
clear all  
clc  
close all  
%Inputs  
%User must input R^2 locations as well as machine tip and hub  
diameters.  
R_squared_locs = [0.1,0.5,0.9]; %number of radial samples desired  
or from file  
tip_diameter = 1.25; %m  
hub_diameter = 0.4; %m  
N_blades = 3; %~, to calculate blade spacing  
blade_face_mesh_size = 0.005; %in meters  
rotating_body_mesh_size = 0.01; %in meters  
beta2_mean = 25.82; %at R=0.41, geometric mean  
alpha1 = 90; %no pre-swirl  
N = 20; %RPM  
c_inf = 1; %m/s
```

```

%Blade triangle knowns and calcs
tip_radius = tip_diameter/2;
hub_radius = hub_diameter/2;
R_mean_geometric = (tip_radius+hub_radius)/2;
R_mean_square = sqrt(tip_radius^2+hub_radius^2);
omega = N*pi/30; %rad/s
c1 = (2/3)*c_inf; %from Betz derivation, alpha
%Initialize data
for i = 1:length(R_squared_locs)
    sq_radii(i) = sqrt(R_squared_locs(i)*(tip_radius^2 -
        hub_radius^2) + hub_radius^2);
end
%Import data file of interest
blades = importdata("...");
turbine = importdata("...");
[num_rows,num_cols] = size(turbine.data);
[num_rows_blades,num_cols_blades] = size(blades.data);
blade_spacing = 2*pi*sq_radii/N_blades;
%Extract Desired Data into Matrices, turbine region
radii_data_loc = find(strcmp(turbine.colheaders, 'radial-
    coordinate'));
radial_coord_unsorted = turbine.data(:,radii_data_loc);
tangential_data_loc = find(strcmp(turbine.colheaders, 'angular-
    coordinate'));
tangential_coord_unsorted = turbine.data(:,tangential_data_loc);
axial_data_loc = find(strcmp(turbine.colheaders, 'axial-coordinate
    '));

```

```

axial_coord_unsorted = turbine.data(:,axial_data_loc);
rel_tan_vel_data_loc = find(strcmp(turbine.colheaders, 'rel-
    tangential-velocity'));
rel_tan_vel_mag_unsorted = turbine.data(:,rel_tan_vel_data_loc);
tan_vel_data_loc = find(strcmp(turbine.colheaders, 'tangential-
    velocity'));
tan_vel_mag_unsorted = turbine.data(:,tan_vel_data_loc);
axial_vel_data_loc = find(strcmp(turbine.colheaders, '_axial-
    velocity'));
axial_vel_mag_unsorted = turbine.data(:,axial_vel_data_loc);
radial_vel_data_loc = find(strcmp(turbine.colheaders, '_radial-
    velocity'));
radial_vel_mag_unsorted = turbine.data(:,radial_vel_data_loc);
rel_vel_mag_data_loc = find(strcmp(turbine.colheaders, 'rel-
    velocity-magnitude'));
rel_vel_mag_unsorted = turbine.data(:,rel_vel_mag_data_loc);
rel_vel_ang_data_loc = find(strcmp(turbine.colheaders, 'relative-
    velocity-angle'));
rel_vel_ang_unsorted = turbine.data(:,rel_vel_ang_data_loc);
vel_ang_data_loc = find(strcmp(turbine.colheaders, '_velocity-
    angle'));
vel_ang_unsorted = turbine.data(:,vel_ang_data_loc);
%Extract Desired Data into Matrices, on blades
radii_data_loc_blades = find(strcmp(blades.colheaders, 'radial-
    coordinate'));
radial_coord_blades_unsorted = blades.data(:,radii_data_loc_blades
    );

```

```

tangential_data_loc_blades = find(strcmp(blades.colheaders, '
    angular-coordinate'));
tangential_coord_blades_unsorted = blades.data(:,
    tangential_data_loc_blades);
axial_data_loc_blades = find(strcmp(blades.colheaders, 'axial-
    coordinate'));
axial_coord_blades_unsorted = blades.data(:,axial_data_loc_blades)
    ;
%Sort and index matrices based on radii
%turbine
[radial_coord,sortindex] = sort(radial_coord_unsorted, 'ascend');
tangential_coord = tangential_coord_unsorted(sortindex);
axial_coord = axial_coord_unsorted(sortindex);
rel_tan_vel_mag = rel_tan_vel_mag_unsorted(sortindex);
tan_vel_mag = tan_vel_mag_unsorted(sortindex);
axial_vel_mag = axial_vel_mag_unsorted(sortindex);
rel_vel_mag = rel_vel_mag_unsorted(sortindex);
radial_vel_mag = radial_vel_mag_unsorted(sortindex);
rel_vel_angle = rad2deg(rel_vel_ang_unsorted(sortindex));
vel_angle = rad2deg(vel_ang_unsorted(sortindex));
%blades
[radial_coord_blades,sortindex_blades] = sort(
    radial_coord_blades_unsorted);
axial_coord_blades = axial_coord_blades_unsorted(sortindex_blades)
    ;
tangential_coord_blades = tangential_coord_blades_unsorted(
    sortindex_blades);

```

```

clear("blades")
clear("turbine")
%Only include data at hub or above to compare to meanline design
%turbine
hub_loc= find(abs(radial_coord - hub_radius) == ...
    min(abs(radial_coord - hub_radius)));
radial_coord_hubup= radial_coord(hub_loc:end);
axial_coord_hubup = axial_coord(hub_loc:end);
tangential_coord_hubup = tangential_coord(hub_loc:end);
rel_tan_vel_mag_hubup = rel_tan_vel_mag(hub_loc:end);
tan_vel_mag_hubup = tan_vel_mag(hub_loc:end);
axial_vel_mag_hubup = axial_vel_mag(hub_loc:end);
rel_vel_mag_hubup = rel_vel_mag(hub_loc:end);
radial_vel_mag_hubup = radial_vel_mag(hub_loc:end);
rel_vel_angle_hubup = rel_vel_angle(hub_loc:end);
vel_angle_hubup = vel_angle(hub_loc:end);
%blades
hub_loc_blades = find(abs(radial_coord_blades - hub_radius) == ...
    min(abs(radial_coord_blades - hub_radius)));
radial_coord_blades_hubup = radial_coord_blades(hub_loc_blades:end
);
axial_coord_blades_hubup = axial_coord_blades(hub_loc_blades:end);
tangential_coord_blades_hubup = tangential_coord_blades(
    hub_loc_blades:end);
leading_edge_axial = max(axial_coord_blades_hubup);
trailing_edge_axial = min(axial_coord_blades_hubup);
crit = 0.1; %PICK range of axial locations to use (higher crit,

```

```

    likely higher radial variation)
leading_dist_error = 100*abs((leading_edge_axial -
    axial_coord_hubup)/leading_edge_axial);
trailing_dist_error = 100*abs((trailing_edge_axial -
    axial_coord_hubup)/trailing_edge_axial);
sep_locs_nonzero_leading = find(leading_dist_error <= crit);
sep_locs_nonzero_trailing = find(trailing_dist_error <= crit);
%Calculate from Fluent and compare to design
%Find leading and trailing edge points from data for blade inlet
    and outlet
%station 1, inlet
radial_coord_analysis1_nonunique = radial_coord_hubup(
    sep_locs_nonzero_leading);
axial_coord_analysis1_nonunique = axial_coord_hubup(
    sep_locs_nonzero_leading);
tang_vel_analysis1_nonunique = tan_vel_mag_hubup(
    sep_locs_nonzero_leading);
rel_tang_vel_analysis1_nonunique = rel_tan_vel_mag_hubup(
    sep_locs_nonzero_leading);
axial_vel_analysis1_nonunique = axial_vel_mag_hubup(
    sep_locs_nonzero_leading);
radial_vel_analysis1_nonunique = radial_vel_mag_hubup(
    sep_locs_nonzero_leading);
rel_vel_ang_analysis1_nonunique = rel_vel_angle_hubup(
    sep_locs_nonzero_leading);
vel_ang_analysis1_nonunique = vel_angle_hubup(
    sep_locs_nonzero_leading);

```

```

%only use unique values for interpolation later
[radial_coord_analysis1 , uniqueindex] = unique(
    radial_coord_analysis1_nonunique);
axial_coord_analysis1 = axial_coord_analysis1_nonunique(
    uniqueindex);
tang_vel_analysis1 = tang_vel_analysis1_nonunique(uniqueindex);
rel_tang_vel_analysis1 = rel_tang_vel_analysis1_nonunique(
    uniqueindex);
axial_vel_analysis1 = axial_vel_analysis1_nonunique(uniqueindex);
radial_vel_analysis1 = radial_vel_analysis1_nonunique(uniqueindex
);
rel_vel_ang_analysis1 = rel_vel_ang_analysis1_nonunique(
    uniqueindex);
vel_ang_analysis1 = vel_ang_analysis1_nonunique(uniqueindex);
Wu1_analysis = rel_tang_vel_analysis1;
Wm1_analysis = sqrt(axial_vel_analysis1.^2 + radial_vel_analysis1
.^2);
Cu1_analysis = tang_vel_analysis1;
Cm1_analysis = sqrt(axial_vel_analysis1.^2 + radial_vel_analysis1
.^2);
W1_analysis = sqrt(Wu1_analysis.^2 + Wm1_analysis.^2);
C1_analysis = sqrt(Cu1_analysis.^2 + Cm1_analysis.^2);
U1_analysis_check = Cu1_analysis - Wu1_analysis;
beta1_analysis = asind(-axial_vel_analysis1./W1_analysis); %-axial
    b/c flow in -z direction
alpha1_analysis = asind(-axial_vel_analysis1./C1_analysis); %-
    axial b/c flow in -z direction

```

```

%station 2, outlet
radial_coord_analysis2_nonunique = radial_coord_hubup(
    sep_locs_nonzero_trailing);
axial_coord_analysis2_nonunique = axial_coord_hubup(
    sep_locs_nonzero_trailing);
tang_vel_analysis2_nonunique = tan_vel_mag_hubup(
    sep_locs_nonzero_trailing);
rel_tang_vel_analysis2_nonunique = rel_tan_vel_mag_hubup(
    sep_locs_nonzero_trailing);
axial_vel_analysis2_nonunique = axial_vel_mag_hubup(
    sep_locs_nonzero_trailing);
radial_vel_analysis2_nonunique = radial_vel_mag_hubup(
    sep_locs_nonzero_trailing);
rel_vel_ang_analysis2_nonunique = rel_vel_angle_hubup(
    sep_locs_nonzero_trailing);
vel_ang_analysis2_nonunique = vel_angle_hubup(
    sep_locs_nonzero_trailing);
%only use unique values for interpolation later
[radial_coord_analysis2, unique2index] = unique(
    radial_coord_analysis2_nonunique);
axial_coord_analysis2 = axial_coord_analysis2_nonunique(
    unique2index);
tang_vel_analysis2 = tang_vel_analysis2_nonunique(unique2index);
rel_tang_vel_analysis2 = rel_tang_vel_analysis2_nonunique(
    unique2index);
axial_vel_analysis2 = axial_vel_analysis2_nonunique(unique2index);
radial_vel_analysis2 = radial_vel_analysis2_nonunique(unique2index);

```

```

    );
rel_vel_ang_analysis2 = rel_vel_ang_analysis2_nonunique(
    unique2index);
vel_ang_analysis2 = vel_ang_analysis2_nonunique(unique2index);
Wu2_analysis = rel_tang_vel_analysis2;
Wm2_analysis = sqrt(axial_vel_analysis2.^2 + radial_vel_analysis2
    .^2);
Cu2_analysis = tang_vel_analysis2;
Cm2_analysis = sqrt(axial_vel_analysis2.^2 + radial_vel_analysis2
    .^2);
W2_analysis = sqrt(Wu2_analysis.^2 + Wm2_analysis.^2);
C2_analysis = sqrt(Cu2_analysis.^2 + Cm2_analysis.^2);
U2_analysis_check = Cu2_analysis - Wu2_analysis;
beta2_analysis = asind(-axial_vel_analysis2./W2_analysis); %-axial
    b/c flow in -z direction
alpha2_analysis = asind(-axial_vel_analysis2./C2_analysis); %-
    axial b/c flow in -z direction
%Separate data by radial locations
%Calculate Blade Triangles, use radii from fluent analysis
radii_span1 = radial_coord_analysis1;
radii_span2 = radial_coord_analysis2;
blade_velocity1 = omega*radii_span1;
blade_velocity2 = omega*radii_span2;
r_geo_loc = find(abs(radii_span2-R_mean_geometric) == min(abs(
    radii_span2-R_mean_geometric)));
r_geo = radii_span2(r_geo_loc);
if isempty(r_geo_loc)

```

```

r_geo_loc = find((radii_span2 >= 0.999*R_mean_geometric) & ...
                (radii_span2 <= 1.001*R_mean_geometric));
r_geo = radii_span2(r_geo_loc);
end
if length(r_geo_loc) > 1
    distance_error = r_geo - R_mean_geometric;
    error_min_loc = find(abs(distance_error) == min(abs(
        distance_error)), 'first');
    r_geo_loc_min_error = r_geo_loc(error_min_loc);
    r_geo = radii_span2(r_geo_loc_min_error);
else
    r_geo_loc_min_error = r_geo_loc;
end
%Location 1, turbine inlet
alpha1_span = alpha1*ones(length(radii_span1),1);
c1_span = c1*ones(length(radii_span1),1);
cm1_span = sind(alpha1_span).*c1_span;
cu1_span = cosd(alpha1_span).*c1_span;
U1_span = blade_velocity1; %assume constant rpm and radii
w1_span = sqrt(c1_span.^2 + U1_span.^2);
wu1_span = -(U1_span - cu1_span);
wm1_span = cm1_span;
beta1_span = asind(wm1_span./w1_span);
%Location 2, turbine outlet
cm2_span = interp1(radii_span1,cm1_span,radii_span2,'linear','
    extrap'); %assume constant massflow through
%use extrap in case radii dont line up exactly

```

```

U2_span = blade_velocity2; %constant blade rpm and radius
wm2_span = cm2_span; %cm=wm
w2_mean = wm2_span(r_geo_loc_min_error)/sind(beta2_mean);
wu2_mean = sqrt(w2_mean^2 - wm2_span(r_geo_loc_min_error)^2);
cu2_mean = U2_span(r_geo_loc_min_error) - wu2_mean;
cu2_span = cu2_mean*(R_mean_geometric./radii_span2); %should be
    square mean, but not used in orig. design
c2_span = sqrt(cu2_span.^2 +cm2_span.^2);
alpha2_span = asind(cm2_span./c2_span);
wu2_span = -(U2_span - cu2_span);
w2_span = sqrt(wm2_span.^2 + wu2_span.^2);
beta2_span = asind(wm2_span./w2_span);
%interpolate variables at station 2 to 1 for difference
    calculations
w2_resamp = interp1(radii_span2,w2_span,radii_span1);
c2_resamp = interp1(radii_span2,c2_span,radii_span1);
wu2_resamp = interp1(radii_span2,wu2_span,radii_span1);
cu2_resamp = interp1(radii_span2,cu2_span,radii_span1);
beta2_resamp = interp1(radii_span2,beta2_span,radii_span1);
alpha2_resamp = interp1(radii_span2,alpha2_span,radii_span1);
%plot design variables
ab1 = figure('Position', get(0, 'ScreenSize'));
subplot(2,2,1)
plot(beta1_analysis,radial_coord_analysis1)
hold on
plot(rel_vel_ang_analysis1,radial_coord_analysis1)
legend('\beta1_{calc}','\beta1_{fluent}')

```

```

subplot(2,2,2)
plot(beta2_analysis , radial_coord_analysis2)
hold on
plot(rel_vel_ang_analysis2 , radial_coord_analysis2)
legend( '\beta2_{calc}' , '\beta2_{fluent}' )
subplot(2,2,3)
plot(alpha1_analysis , radial_coord_analysis1)
hold on
plot(vel_ang_analysis1 , radial_coord_analysis1)
legend( '\alpha1_{calc}' , '\alpha1_{fluent}' )
subplot(2,2,4)
plot(alpha2_analysis , radial_coord_analysis2)
hold on
plot(vel_ang_analysis2 , radial_coord_analysis2)
legend( '\alpha2_{calc}' , '\alpha2_{fluent}' )
saveas(ab1 , " AngleDifference_fluenttome.png")
ab2 = figure('Position' , get(0 , 'ScreenSize'));
subplot(2,2,1)
plot(beta1_analysis , radial_coord_analysis1)
hold on
plot(rel_vel_ang_analysis1 -90 , radial_coord_analysis1)
legend( '\beta1_{calc}' , '\beta1_{fluent}' )
subplot(2,2,2)
plot(beta2_analysis , radial_coord_analysis2)
hold on
plot(rel_vel_ang_analysis2 -90 , radial_coord_analysis2)
legend( '\beta2_{calc}' , '\beta2_{fluent}' )

```

```

subplot(2,2,3)
plot(alpha1_analysis , radial_coord_analysis1)
hold on
plot(-vel_ang_analysis1-90, radial_coord_analysis1)
legend( '\alpha1_{calc}', '\alpha1_{fluent}')
subplot(2,2,4)
plot(alpha2_analysis , radial_coord_analysis2)
hold on
plot(-vel_ang_analysis2-90, radial_coord_analysis2)
legend( '\alpha2_{calc}', '\alpha2_{fluent}')
saveas(ab2, " AngleDifference_fluenttome_adjusted.png")
ad1 = figure('Position', get(0, 'ScreenSize'));
subplot(2,2,1)
plot(beta1_analysis-rel_vel_ang_analysis1 , radial_coord_analysis1)
legend( '\beta1_{calc}-\beta1_{fluent}', 'location', 'southoutside')
subplot(2,2,2)
plot(beta2_analysis-rel_vel_ang_analysis2 , radial_coord_analysis2)
legend( '\beta2_{calc}-\beta2_{fluent}', 'location', 'southoutside')
subplot(2,2,3)
plot(alpha1_analysis-vel_ang_analysis1 , radial_coord_analysis1)
legend( '\alpha1_{calc}-\alpha1_{fluent}', 'location', 'southoutside'
)
subplot(2,2,4)
plot(alpha2_analysis-vel_ang_analysis2 , radial_coord_analysis2)
legend( '\alpha2_{calc}-\alpha2_{fluent}', 'location', 'southoutside'
)
saveas(ad1, " BladeAngleDifference.png")

```

```

bl1 = figure('Position', get(0, 'Screensize'));
subplot(2,2,1)
plot(beta1_span, radii_span1, 'g—')
hold on
plot(beta2_resamp, radii_span1, 'g—')
plot(alpha1_span, radii_span1, 'r-')
plot(alpha2_resamp, radii_span1, 'r-')
hold off
legend('\beta1', '\beta2', '\alpha1', '\alpha2', 'location', '
    eastoutside')
xlabel('Angles_(degrees)')
ylabel('Radial_Position_(m)')
title('Design_Conditions')
%bl2 = figure;
subplot(2,2,2)
plot(w1_span, radii_span1, 'g—')
hold on
plot(w2_resamp, radii_span1, 'g—')
plot(c1_span, radii_span1, 'r-')
plot(c2_resamp, radii_span1, 'r-')
hold off
legend('W1', 'W2', 'C1', 'C2', 'location', 'eastoutside')
xlabel('Velocity_(m/s)')
ylabel('Radial_Position_(m)')
title('Design_Conditions')
%bl3 = figure;
subplot(2,2,3)

```

```

plot(wu1_span, radii_span1, 'g—')
hold on
plot(wu2_resamp, radii_span1, 'g—')
plot(cu1_span, radii_span1, 'r—')
plot(cu2_resamp, radii_span1, 'r—')
hold off
legend('Wu1', 'Wu2', 'Cu1', 'Cu2', 'location', 'eastoutside')
xlabel('Velocity_(m/s)')
ylabel('Radial_Position_(m)')
title('Design_Conditions')
%bl4 = figure;
subplot(2,2,4)
plot(wu2_resamp-wu1_span, radii_span1, 'g—')
hold on
plot(cu2_resamp-cu1_span, radii_span1, 'r—')
hold off
legend('Wu2-Wu1', 'Cu2-Cu1', 'location', 'eastoutside')
xlabel('Velocity_Change_across_Blade_(m/s)')
ylabel('Radial_Position_(m)')
title('Design_Conditions')
saveas(bl1, "DesignConditions.png")
bl20 = figure('Position', get(0, 'ScreenSize'));
plot(beta2_resamp-beta1_span, radii_span1, 'g—')
hold on
plot(alpha2_resamp-alpha1_span, radii_span1, 'r—')
hold off
legend('\beta2-\beta1', '\alpha2-\alpha1', 'location', 'southoutside')

```

```

)
xlabel('Angle_Change_across_Blade_(degree)')
ylabel('Radial_Position_(m)')
title('Design_Conditions')
saveas(bl20,"DesignAngleDifference.png")
%plot blade velocity check
blch1 = figure('Position', get(0, 'Screensize'));
plot(U1_analysis_check, radial_coord_analysis1, 'k-')
hold on
plot(U2_analysis_check, radial_coord_analysis2, 'r-')
plot(U1_span, radii_span1, 'go-')
plot(U2_span, radii_span2, 'b.-')
legend('U1_{fluent}', 'U2_{fluent}', 'U1_{design}', 'U2_{design}', '
location', 'southoutside')
saveas(blch1,"UvelCheck.png")
%plot fluent vs. design variables
bl5 = figure('Position', get(0, 'Screensize'));
subplot(2,2,1)
plot(W1_analysis, radial_coord_analysis1, 'k-')
hold on
plot(W2_analysis, radial_coord_analysis2, 'r-')
plot(w1_span, radii_span1, 'g—')
plot(w2_span, radii_span2, 'b—')
hold off
legend('W1_{fluent}', 'W2_{fluent}', 'W1_{design}', 'W2_{design}', '
location', 'eastoutside')
%bl6 = figure;

```

```

subplot(2,2,2)
plot(C1_analysis,radial_coord_analysis1,'k-')
hold on
plot(C2_analysis,radial_coord_analysis2,'r-')
plot(c1_span,radii_span1,'g—')
plot(c2_span,radii_span2,'b—')
hold off
legend('C1_{fluent}','C2_{fluent}','C1_{design}','C2_{design}','
    location','eastoutside')
%bl7 = figure;
subplot(2,2,3)
plot(beta1_analysis,radial_coord_analysis1,'k-')
hold on
plot(beta2_analysis,radial_coord_analysis2,'r-')
plot(beta1_span,radii_span1,'g—')
plot(beta2_span,radii_span2,'b—')
hold off
legend('\\beta1_{fluent}','\\beta2_{fluent}','\\beta1_{design}','\\
    beta2_{design}','location','eastoutside')
%bl8 = figure;
subplot(2,2,4)
plot(alpha1_analysis,radial_coord_analysis1,'k-')
hold on
plot(alpha2_analysis,radial_coord_analysis2,'r-')
plot(alpha1_span,radii_span1,'g—')
plot(alpha2_span,radii_span2,'b—')
hold off

```

```

legend( '\alpha1_{fluent}', '\alpha2_{fluent}', '\alpha1_{design}', '\alpha2_{design}', 'location', 'eastoutside')
saveas(bl5, "FluentDesignComparison.png")
%Calculate average differences between Fluent and design
deltaBeta1 = beta1_analysis - beta1_span;
deltaBeta2 = beta2_analysis - beta2_span;
deltaAlpha1 = alpha1_analysis - alpha1_span;
deltaAlpha2 = alpha2_analysis - alpha2_span;
cumulative_avg_beta1 = 0;
cumulative_avg_beta2 = 0;
cumulative_avg_alpha1 = 0;
cumulative_avg_alpha2 = 0;
for i = 2:length(radial_coord_analysis1)
    cumulative_avg_beta1 = cumulative_avg_beta1 + 0.5*(deltaBeta1(i) + deltaBeta1(i-1))*(radial_coord_analysis1(i)^2 - radial_coord_analysis1(i-1)^2);
    cumulative_avg_alpha1 = cumulative_avg_alpha1 + 0.5*(deltaAlpha1(i) + deltaAlpha1(i-1))*(radial_coord_analysis1(i)^2 - radial_coord_analysis1(i-1)^2);
end
for i = 2:length(radial_coord_analysis2)
    cumulative_avg_beta2 = cumulative_avg_beta2 + 0.5*(deltaBeta2(i) + deltaBeta2(i-1))*(radial_coord_analysis2(i)^2 - radial_coord_analysis2(i-1)^2);
    cumulative_avg_alpha2 = cumulative_avg_alpha2 + 0.5*(deltaAlpha2(i) + deltaAlpha2(i-1))*(radial_coord_analysis2(i)^2 - radial_coord_analysis2(i-1)^2);

```

```

end
beta1_diff_area_avg = cumulative_avg_beta1/(tip_radius^2 -
    hub_radius^2);
beta2_diff_area_avg = cumulative_avg_beta2/(tip_radius^2 -
    hub_radius^2);
alpha1_diff_area_avg = cumulative_avg_alpha1/(tip_radius^2 -
    hub_radius^2);
alpha2_diff_area_avg = cumulative_avg_alpha2/(tip_radius^2 -
    hub_radius^2);
fprintf('Area_Averaged_Quantities:\n')
fprintf('\n_beta1diff=%g,\n_beta2diff=%g,\n_alpha1diff=%g,\n_
    alpha2diff=%g,\n', ...
    [beta1_diff_area_avg, beta2_diff_area_avg,
    alpha1_diff_area_avg, alpha2_diff_area_avg])
cumulative_mass_avg_beta1 = 0;
cumulative_mass_avg_beta2 = 0;
cumulative_mass_avg_alpha1 = 0;
cumulative_mass_avg_alpha2 = 0;
for i = 2:length(radial_coord_analysis1)
    cumulative_mass_avg_beta1 = cumulative_mass_avg_beta1 + 0.5*(
        deltaBeta1(i) + deltaBeta1(i-1))*((radial_coord_analysis1(i)
        )^2 - radial_coord_analysis1(i-1)^2).*cm1_span(i));
    cumulative_mass_avg_alpha1 = cumulative_mass_avg_alpha1 +
        0.5*(deltaAlpha1(i) + deltaAlpha1(i-1))*((
        radial_coord_analysis1(i)^2 - radial_coord_analysis1(i-1)
        ^2).*cm1_span(i));
end

```

```

for i = 2:length(radial_coord_analysis2)
    cumulative_mass_avg_beta2 = cumulative_mass_avg_beta2 + 0.5*(
        deltaBeta2(i) + deltaBeta2(i-1))*((radial_coord_analysis2(i)
        )^2 - radial_coord_analysis2(i-1)^2).*cm2_span(i));
    cumulative_mass_avg_alpha2 = cumulative_mass_avg_alpha2 +
        0.5*(deltaAlpha2(i) + deltaAlpha2(i-1))*((
        radial_coord_analysis2(i)^2 - radial_coord_analysis2(i-1)
        ^2).*cm2_span(i));
end

beta1_diff_mass_avg = cumulative_mass_avg_beta1/((tip_radius^2 -
    hub_radius^2).*c1);
beta2_diff_mass_avg = cumulative_mass_avg_beta2/((tip_radius^2 -
    hub_radius^2).*c1);
alpha1_diff_mass_avg = cumulative_mass_avg_alpha1/((tip_radius^2 -
    hub_radius^2).*c1);
alpha2_diff_mass_avg = cumulative_mass_avg_alpha2/((tip_radius^2 -
    hub_radius^2).*c1);
fprintf('Mass_Averaged_Quantities:\n')
fprintf('_beta1diff_=%g,\n_beta2diff_=%g,\n_alpha1diff_=%g,\n_
    alpha2diff_=%g,\n', ...
        [beta1_diff_mass_avg, beta2_diff_mass_avg,
            alpha1_diff_mass_avg, alpha2_diff_mass_avg])
bl9 = figure('Position', get(0, 'ScreenSize'));
subplot(2,2,1)
plot(deltaBeta1, radial_coord_analysis1, 'k-')
hold on
plot(deltaBeta2, radial_coord_analysis2, 'r-')

```

```

hold off
legend( '\beta1_{fluent}-\beta1_{design}', '\beta2_{fluent}-\beta2_{
    design}', 'location', 'southoutside')
%bl10 = figure;
subplot(2,2,2)
plot(deltaAlpha1,radial_coord_analysis1,'k-')
hold on
plot(deltaAlpha2,radial_coord_analysis2,'r-')
hold off
legend( '\alpha1_{fluent}-\alpha1_{design}', '\alpha2_{fluent}-\
    alpha2_{design}', 'location', 'southoutside')
subplot(2,2,3)
text(0,1, strcat( '\beta_1_{mass}_{average}_{difference}:', {'_'}, num2str
    (beta1_diff_mass_avg), '_degrees'))
text(0,0, strcat( '\beta_2_{mass}_{average}_{difference}:', {'_'}, num2str
    (beta2_diff_mass_avg), '_degrees'))
xlim([-1,2])
ylim([-1,2])
axis off
subplot(2,2,4)
text(0,1, strcat( '\alpha_1_{mass}_{average}_{difference}:', {'_'},
    num2str(alpha1_diff_mass_avg), '_degrees'))
text(0,0, strcat( '\alpha_2_{mass}_{average}_{difference}:', {'_'},
    num2str(alpha2_diff_mass_avg), '_degrees'))
xlim([-1,2])
ylim([-1,2])
axis off

```

```

saveas(bl9,"FluentCalcBladeAngleDifference.png")
%Find radii of interest
%for turbine region
sep_locs = zeros(num_rows,length(sq_radii));
for k = 1:length(sq_radii)
    for i = 1:num_rows
        if radial_coord(i) > sq_radii(k) - rotating_body_mesh_size
            /2 && ...
                radial_coord(i) < sq_radii(k) +
                    rotating_body_mesh_size/2
            sep_locs(i,k) = i;
        else
            sep_locs(i,k) = 0;
        end
    end
end
end
%for blades
sep_locs_blades = zeros(num_rows_blades,length(sq_radii));
for k = 1:length(sq_radii)
    for i = 1:num_rows_blades
        if radial_coord_blades(i) > sq_radii(k) -
            blade_face_mesh_size/2 && ...
                radial_coord_blades(i) < sq_radii(k) +
                    blade_face_mesh_size/2
            sep_locs_blades(i,k) = i;
        else
            sep_locs_blades(i,k) = 0;
        end
    end
end

```

```

        end
    end
end
%Plot
skip_approx = 3; %1 = show vectors at all available points
scaled = 3; %1 = automatic scaling
for k = 1:length(sq_radii)
    Q = figure('Position', get(0, 'Screensize'));
    %set up vectors for plotting and calculations
    %turbine
    sep_locs_nonzero_preminimize = nonzeros(sep_locs(:,k));
    sep_locs_nonzero = sep_locs_nonzero_preminimize(1:skip_approx:
        end,:);
    sep_locs_nonzero_noskip = sep_locs_nonzero_preminimize(1:end
        ,:);
    sep_locs_nonzero_preminimize2 = nonzeros(sep_locs(:,k));
    sep_locs_nonzero2 = sep_locs_nonzero_preminimize2(1:
        skip_approx:end,:);
    sep_locs_nonzero_noskip2 = sep_locs_nonzero_preminimize2(1:end
        ,:);
    tang_arc_coord = sq_radii(k)*tangential_coord(sep_locs_nonzero
        );
    tang_arc_coord2 = sq_radii(k)*tangential_coord(
        sep_locs_nonzero2);
    tang_arc_coord_noskip = sq_radii(k)*tangential_coord(
        sep_locs_nonzero_noskip);
    tang_arc_coord_noskip2 = sq_radii(k)*tangential_coord(

```

```

    sep_locs_nonzero_noskip2);
%blades
sep_locs_nonzero_preminimize_blades = nonzeros(sep_locs_blades
    (:,k));
sep_locs_nonzero_blades = sep_locs_nonzero_preminimize_blades
    (1:skip_approx:end,:);
tang_arc_coord_blades = sq_radii(k)*tangential_coord_blades(
    sep_locs_nonzero_blades);
axial_coord_blades_nonzero = axial_coord_blades(
    sep_locs_nonzero_blades);
tang_arc_range = max(tang_arc_coord_blades) - min(
    tang_arc_coord_blades);
tang_arc_bins = tang_arc_range/N_blades;
%others
spacing_backward = -blade_spacing(k)/2 - blade_spacing(k)/10;
spacing_forward = blade_spacing(k)/2 + blade_spacing(k);
%set up evenly spaced, only increasing grid to sample data
points_count = 2000;
x_points = linspace(spacing_backward, spacing_forward,
    points_count);
y_points = linspace(min(axial_coord), max(axial_coord),
    points_count);
[x_grid, y_grid] = meshgrid(x_points, y_points);
%duplicate vectors fore and aft of real data range to help
interpolation
num_dups = 3; %pick an odd number
axial_dup = repvec(axial_coord(sep_locs_nonzero_noskip2),

```

```

    num_dups,1);
rel_vel_dup = repvec(rel_vel_mag(sep_locs_nonzero_noskip2),
    num_dups,1);
for j = 1:num_dups
    for i = 1:length(tang_arc_coord_noskip2)
        tang_dup(i + (j-1)*length(tang_arc_coord_noskip2)) =
            tang_arc_coord_noskip2(i) +...
            ((j-((num_dups+1)/2))*(max(tang_arc_coord_noskip2)
                - min(tang_arc_coord_noskip2))));
    end
end
interpdata = scatteredInterpolant(tang_dup',axial_dup,
    rel_vel_dup);
%plots
[C,m] = contourf(x_points,y_points,interpdata(x_grid,y_grid)
    ,100);
set(m,'LineColor','none');
colormap(jet)
p = colorbar;
caxis ([min(rel_vel_mag),max(rel_vel_mag)])
set(get(p,'label'),'string','Rel. Vel. Mag. (m/s)')
hold on
q = quiver(tang_arc_coord,...
    axial_coord(sep_locs_nonzero),...
    rel_tan_vel_mag(sep_locs_nonzero),...
    axial_vel_mag(sep_locs_nonzero),scaled,'Color','black');
q.ShowArrowHead='off';

```

```

titleblock = strcat("Relative Flow Velocities at Radius ",
    num2str(sq_radii(k)) ,...
    ", ", num2str(100*R_squared_locs(k)) ,"% R^2 Span ");
title(titleblock)
xlabel("Tangential Arc Coordinates (m)")
ylabel("Axial Coordinates (m)")
axis equal %gives right blade shape, flow passage size, etc.
ylim([min(axial_coord),max(axial_coord)])
xlim([spacing_backward,spacing_forward])
savefig(Q, strcat("Relative_Flow_Velocities_at_Radius_",
    num2str(sq_radii(k)) ,...
    "_", num2str(100*R_squared_locs(k)) ,"%_R^2_Span_", ".fig"))
saveas(Q, strcat("Relative_Flow_Velocities_at_Radius_", num2str
    (sq_radii(k)) ,...
    "_", num2str(100*R_squared_locs(k)) ,"%_R^2_Span_", ".png"))
hold off
clf
q2 = quiver(tang_arc_coord ,...
    axial_coord(sep_locs_nonzero) ,...
    rel_tan_vel_mag(sep_locs_nonzero) ,...
    axial_vel_mag(sep_locs_nonzero) ,scaled , 'Color' , 'red');
q2.ShowArrowHead='off';
hold on
titleblock = strcat("Relative Flow Vectors at Radius ",
    num2str(sq_radii(k)) ,...
    ", ", num2str(100*R_squared_locs(k)) ,"% R^2 Span ");
title(titleblock)

```

```

xlabel("Tangential Arc Coordinates (m)")
ylabel("Axial Coordinates (m)")
axis equal %gives right blade shape, flow passage size, etc.
ylim([min(axial_coord),max(axial_coord)])
xlim([spacing_backward, spacing_forward])
savefig(Q, strcat("Relative_Flow_Vectors_at_Radius_", num2str(
    sq_radii(k)), ...
    "_", num2str(100*R_squared_locs(k)), "%R^2_Span", "
    NOCONTOUR", ".fig"))
saveas(Q, strcat("Relative_Flow_Vectors_at_Radius_", num2str(
    sq_radii(k)), ...
    "_", num2str(100*R_squared_locs(k)), "%R^2_Span", "
    NOCONTOUR", ".png"))
hold off
clf
[C2,m2] = contourf(x_points, y_points, interpdata(x_grid, y_grid)
    ,100);
set(m2, 'LineColor', 'none');
colormap(jet)
p2 = colorbar;
caxis ([min(rel_vel_mag),max(rel_vel_mag)])
set(get(p2, 'label'), 'string', 'Rel. Vel. Mag. (m/s)')
hold on
titleblock = strcat("Relative Flow Contours at Radius ",
    num2str(sq_radii(k)), ...
    ", ", num2str(100*R_squared_locs(k)), "%R^2_Span");
title(titleblock)

```

```

xlabel("Tangential Arc Coordinates (m)")
ylabel("Axial Coordinates (m)")
axis equal %gives right blade shape, flow passage size, etc.
ylim([min(axial_coord),max(axial_coord)])
xlim([spacing_backward, spacing_forward])
savefig(Q, strcat("Relative_Flow_Contours_at_Radius_", num2str(
    sq_radii(k)), ...
    "_", num2str(100*R_squared_locs(k)), "%_R^2_Span", "NOVECTOR
    ", ".fig"))
saveas(Q, strcat("Relative_Flow_Contours_at_Radius_", num2str(
    sq_radii(k)), ...
    "_", num2str(100*R_squared_locs(k)), "%_R^2_Span", "NOVECTOR
    ", ".png"))
points_count2 = 100;
x_points2 = linspace(spacing_backward, spacing_forward,
    points_count2);
y_points2 = linspace(min(axial_coord), max(axial_coord),
    points_count2);
[x_grid2, y_grid2] = meshgrid(x_points2, y_points2);
rel_tan_vel_dup = repvec(rel_tan_vel_mag(
    sep_locs_nonzero_noskip2), num_dups, 1);
axial_vel_dup = repvec(axial_vel_mag(sep_locs_nonzero_noskip2)
    , num_dups, 1);
interpdata_sep_axial = scatteredInterpolant(tang_dup',
    axial_dup, axial_vel_dup);
interpdata_sep_tang = scatteredInterpolant(tang_dup', axial_dup
    , rel_tan_vel_dup);

```

```

ys1 = ones(1,length(x_points2))*max(y_points2);
xs1 = linspace(min(x_points2),max(x_points2),length(y_points2)
);
ys2 = min(y_points2):range(xs1)/length(xs1):max(y_points2);
xs2 = ones(1,length(ys2))*max(x_points2);
xs = [xs1,xs2];
ys = [ys1,ys2];
[C3,m3] = contourf(x_points,y_points,interpdata(x_grid,y_grid)
,100);
set(m3,'LineColor','none');
colormap(jet)
p = colorbar;
caxis([min(rel_vel_mag),max(rel_vel_mag)])
set(get(p,'label'),'string','Rel. Vel. Mag. (m/s)')
hold on
streamline(x_grid2,y_grid2,...
interpdata_sep_tang(x_grid2,y_grid2),interpdata_sep_axial(
x_grid2,y_grid2),...
xs,ys);
hold off
axis equal %gives right blade shape, flow passage size, etc.
ylim([min(axial_coord),max(axial_coord)])
xlim([spacing_backward,spacing_forward])
savefig(Q, strcat("Relative_Streamlines_at_Radius_", num2str(
sq_radii(k)),...
"_", num2str(100*R_squared_locs(k)),"%_R^2_Span", ".fig"))
saveas(Q, strcat("Relative_Streamlines_at_Radius_", num2str(

```

```
sq_radii(k) , ...  
"_" , num2str(100*R_squared_locs(k)) , "%_R^2_Span " , ".png ")  
end  
clear ("c" , "m" , "p" , "q" , "q2" , "i" , "k" , "titleblock" , "turbine")  
%END OF SCRIPT
```

**APPENDIX C**  
**EXCEL VBA SAMPLE SCRIPT**

```
Attribute VB_Name = "Module1"  
Option Explicit  
Sub RunSolver()  
Dim num_input_rows As Integer  
Dim i As Integer  
Dim status As String  
Worksheets("SolverInputs").Activate  
num_input_rows = Cells.Find(What:="*", _  
    After:=Range("C1"), _  
    LookAt:=xlPart, _  
    LookIn:=xlFormulas, _  
    SearchOrder:=xlByRows, _  
    SearchDirection:=xlPrevious, _  
    MatchCase:=False).Row  
Worksheets("DistanceCostCurves").Range("B3:B" & num_input_rows).  
    Value = Worksheets("SolverInputs").Range("C3:C" &  
    num_input_rows).Value  
Worksheets("DistanceCostCurves_withbattery").Range("B3:B" &  
    num_input_rows).Value = Worksheets("SolverInputs").Range("C3:C"  
    & num_input_rows).Value  
Worksheets("Solver_withoutbatteries").Range("C3:C" &  
    num_input_rows).Value = Worksheets("SolverInputs").Range("C3:C"  
    & num_input_rows).Value
```

```

Worksheets("Solver_withoutbatteries").Range("D3:C" &
    num_input_rows).Value = Worksheets("SolverInputs").Range("D3:C"
    & num_input_rows).Value
Worksheets("Solver_withoutbatteries").Range("E3:C" &
    num_input_rows).Value = Worksheets("SolverInputs").Range("E3:C"
    & num_input_rows).Value
Worksheets("Solver_withoutbatteries").Range("F3:C" &
    num_input_rows).Value = Worksheets("SolverInputs").Range("F3:C"
    & num_input_rows).Value
Worksheets("Solver_withoutbatteries").Range("G3:C" &
    num_input_rows).Value = Worksheets("SolverInputs").Range("G3:C"
    & num_input_rows).Value
Worksheets("Solver_withbatteries").Range("C3:C" & num_input_rows).
    Value = Worksheets("SolverInputs").Range("C3:C" &
    num_input_rows).Value
Worksheets("Solver_withbatteries").Range("D3:C" & num_input_rows).
    Value = Worksheets("SolverInputs").Range("D3:C" &
    num_input_rows).Value
Worksheets("Solver_withbatteries").Range("E3:C" & num_input_rows).
    Value = Worksheets("SolverInputs").Range("E3:C" &
    num_input_rows).Value
Worksheets("Solver_withbatteries").Range("F3:C" & num_input_rows).
    Value = Worksheets("SolverInputs").Range("F3:C" &
    num_input_rows).Value
Worksheets("Solver_withbatteries").Range("G3:C" & num_input_rows).
    Value = Worksheets("SolverInputs").Range("G3:C" &
    num_input_rows).Value

```

```

For i = 1 To num_input_rows
    status = Worksheets("SolverInputs").Range("F" & i + 2)
    If status = "Unpowered" Then
        UnpoweredCommSolver_withbatteries (i)
        UnpoweredCommSolver (i)
    ElseIf status = "Powered" Then
        PoweredCommSolver_withbatteries (i)
        PoweredCommSolver (i)
    Else
    End If
Next i
Application.Wait (Now + 1E-05)
Worksheets("SolverInputs").Activate
End Sub

Attribute VB_Name = "Module3"
Option Explicit
Sub UnpoweredCommSolver(i As Integer)
Dim datamsg As String
Dim j As Integer
Dim k As Integer
Dim CHKTime As Integer
Dim InfoBox As Object
Dim householdcost As Double
Dim householdcost_minimum As Double
Dim distance_at_min As Double
Dim distance_min As Double
Dim turbinerating As Double

```

**Dim** numberhouseholds As Double  
**Dim** num\_velocity\_rows As Integer  
**Dim** num\_velocity\_cols As Integer  
**Dim** rRow As Integer  
**Dim** cCol As Integer  
**Dim** row\_select As Integer  
**Dim** column\_select As Integer  
**Dim** highestvalue As Double  
**Dim** row\_final As Integer  
**Dim** column\_final As Integer  
**Dim** row\_inter As Integer  
**Dim** column\_inter As Integer  
**Dim** lat\_val As Double  
**Dim** long\_val As Double  
**Dim** lat\_min\_loc As Integer  
**Dim** long\_min\_loc As Integer  
**Dim** loopnum As Integer  
**Dim** loopnum\_max As Double  
**Dim** loopnum\_double As Double  
**Dim** number\_generators\_minimum As Double  
**Dim** number\_panels\_minimum As Double  
**Dim** diff\_minimum As Double  
**Dim** River\_loc\_col\_pre As Integer  
**Dim** River\_loc\_row\_pre As Integer  
**Dim** River\_flow\_pre As Double  
**Dim** River\_loc\_col\_post As Integer  
**Dim** River\_loc\_row\_post As Integer

```

Dim River_flow_post As Double
Dim Elevation_site As Double
Dim Elevation_pre As Double
Dim Elevation_post As Double
Dim Depth_site As Double
Dim Depth_pre As Double
Dim Depth_post As Double
Dim Velocity_site As Double
Dim Velocity_pre As Double
Dim Velocity_post As Double
Dim Head_site As Double
Dim Head_pre As Double
Dim Head_post As Double
Dim Dam_potential_site As Double
Dim PV_oversize As Double
Dim result As Integer
Dim j_inter As Double
Dim k_inter As Double

Application.Wait (Now + 1E-05)
Worksheets("case2_gen").Activate
'Set NOCT value for PV panel power
Worksheets("case2_gen").Range("$L$2").Value = 260
Worksheets("case2_gen").Range("E6").Value = 1
Worksheets("case2_gen").Range("J8").Value = 1
'Set number of households, near infinity=theoretical max.
Worksheets("case2_gen").Range("$D$2").Value = Worksheets("
    Solver_withoutbatteries").Range("G" & i + 2).Value

```

```

'Calculate PV for desired location
Application.Wait (Now + 1E-05)
Worksheets("PV_Hourly").Activate
'Change latitude for lookup
Worksheets("PV_Hourly").Range("$C$7").Value = Worksheets("
    Solver_withoutbatteries").Range("D" & i + 2).Value
'Change longitude for lookup
Worksheets("PV_Hourly").Range("$C$8").Value = Worksheets("
    Solver_withoutbatteries").Range("E" & i + 2).Value
'Run PV data retrieval
Worksheets("PV_Hourly").Range("B21").Value = 1
Application.Run Worksheets("PV_Hourly").Shapes("Button_5").
    OnAction
'Wait for retrieval to complete and sheets to update
Application.Wait (Now + 5E-05)
Do Until datamsg = "Complete:"
datamsg = CStr(Worksheets("PV_Hourly").Range("B21").Value)
Loop
Application.Wait (Now + 5E-05)
' Adjusted for Application.Run() to avoid Reference problems
    with Solver
' Peltier Technical Services, Inc., Copyright _ 2007. All rights
    reserved.
' reset solver
Worksheets("Solver_withoutbatteries").Range("L" & i + 2).Value =
    Worksheets("PV_Hourly").Range("$N$29").Value
Worksheets("Solver_withoutbatteries").Range("M" & i + 2).Value =

```

```

Worksheets("PV_Hourly").Range("$N$32").Value
' set up LOOP
Application.Wait (Now + 1E-05)
Worksheets("DistanceCostCurves").Activate
Cells(i + 2, 3).Value = 1
householdcost_minimum = 9999999999999#
loopnum_max = 30
' Begin LOOP
For loopnum = 1 To loopnum_max
' up to 60 km, 2km*30 cells
' Calculate flow velocity (table lookup)
lat_val = Worksheets("Solver_withoutbatteries").Range("D" & i +
2).Value
long_val = Worksheets("Solver_withoutbatteries").Range("E" & i +
2).Value
Worksheets("RiverVelocities_Q90").Activate
num_velocity_rows = Cells.Find(What:="*", _
After:=Range("A1"), _
LookAt:=xlPart, _
LookIn:=xlFormulas, _
SearchOrder:=xlByRows, _
SearchDirection:=xlPrevious, _
MatchCase:=False).Row
num_velocity_cols = Cells.Find(What:="*", _
After:=Range("A1"), _
LookAt:=xlPart, _
LookIn:=xlFormulas, _

```

```

        SearchOrder:=xlByColumns, _
        SearchDirection:=xlPrevious, _
        MatchCase:=False).Column
cCol = 2
For j = 2 To num_velocity_cols - 1
    If (Cells(1, cCol).Value <= long_val And Cells(1, cCol +
        1).Value >= long_val) Then
        Exit For
    Else
        cCol = cCol + 1
    End If
Next j
column_select = cCol

rRow = 2
For j = 2 To num_velocity_rows - 1
    If (Cells(rRow, 1).Value >= lat_val And Cells(rRow + 1,
        1).Value <= lat_val) Then
        Exit For
    Else
        rRow = rRow + 1
    End If
Next j
row_select = rRow
'Find highest velocity within (loopnum*2)km
Application.Wait (Now + 1E-05)
Worksheets("FlowRates_Q90").Activate

```

```

cCol = column_select
rRow = row_select
highestvalue = Cells(rRow, cCol).Value
For j = -loopnum To loopnum
    For k = -loopnum To loopnum
        If Cells(rRow + k, cCol + j).Value >= highestvalue Then
            highestvalue = Cells(rRow + k, cCol + j).Value
            column_inter = cCol + j
            row_inter = rRow + k
            j_inter = Abs(j)
            k_inter = Abs(k)
        Else
        End If
    Next k
Next j
If CStr(column_inter) = "0" Then
    column_final = column_select
    row_final = row_select
    distance_at_min = 0
Else
    column_final = column_inter
    row_final = row_inter
    distance_at_min = (4 * j_inter * j_inter + 4 * k_inter *
        k_inter) ^ 0.5
End If
If distance_at_min > 2 * loopnum_max Then
Exit For

```

**End If**

*'Change flow velocity*

Application.Wait (Now + 1E-05)

Worksheets("Solver\_withoutbatteries").Activate

Worksheets("Solver\_withoutbatteries").Range("\$H" & i + 2).Value  
= Worksheets("RiverVelocities\_Q90").Cells(row\_final,  
column\_final).Value

Worksheets("Solver\_withoutbatteries").Range("\$R" & i + 2).Value  
= Worksheets("RiverVelocities\_Q90").Cells(row\_final, 1).Value

Worksheets("Solver\_withoutbatteries").Range("\$S" & i + 2).Value  
= Worksheets("RiverVelocities\_Q90").Cells(1, column\_final).  
Value

Worksheets("Solver\_withoutbatteries").Range("\$T" & i + 2).Value  
= Worksheets("FlowRates\_Q90").Cells(row\_final, column\_final).  
Value

*'use 2.8 m/s limit for smart hydro monofloat turbine, change for  
others*

*'input rounding logic*

Worksheets("Solver\_withoutbatteries").Activate

**If** Worksheets("Solver\_withoutbatteries").Range("H" & i + 2).  
Value > 2.8 **Then**

Worksheets("Solver\_withoutbatteries").Range("I" & i + 2).Value =  
2.8

**Else**

Worksheets("Solver\_withoutbatteries").Range("I" & i + 2).Value =  
Worksheets("Solver\_withoutbatteries").Range("H" & i + 2).  
Value

**End If**

```
Worksheets("case2_gen").Range("$F$2").Value = Worksheets("
    Solver_withoutbatteries").Range("I" & i + 2).Value
Application.Wait (Now + 1E-05)
Worksheets("case2_gen").Activate
Application.Run "Solver.xlam!SolverReset"
' set up new analysis
' SolverOk ( SetCell, MaxMinVal, ValueOf, ByChange, Engine,
    EngineDesc)
' 1 Maximize
' 2 Minimize
' 3 Match a specific value
Application.Run "Solver.xlam!SolverOk", "$Q$28", 2, , "$J$8,$E$6
    ", 2, "GRG_Nonlinear"
' SolverOptions( MaxTime, Iterations, Precision, AssumeLinear,
    StepThru,
' Estimates, Derivatives, SearchOption, IntTolerance, Scaling,
    Convergence, AssumeNonNeg,
' PopulationSize, RandomSeed, MultiStart, RequireBounds,
    MutationRate, MaxSubproblems,
' MaxIntegerSols, SolveWithout, MaxTimeNoImp)
Application.Run "Solver.xlam!SolverOptions", _
100000, 100000, 1E-12, False, False, _
2, 2, 1, 1, True, 1E-12, True, _
100, [], False, True, 0.075, 100000, _
100000, False, 30
' add constraints
```

```

' SolverAdd( CellRef, Relation, FormulaText)
' 1  <=
' 2  =
' 3  >=
' 4  Cells referenced by CellRef must have final values that
    are integers.
' 5  Cells referenced by CellRef must have final values of
    either 0 (zero) or 1.
' 6  Cells referenced by CellRef must have final values that
    are all different and integers.
Application.Run "Solver.xlam!SolverAdd", "$J$8", 4, 0
Application.Run "Solver.xlam!SolverAdd", "$E$6", 4, 0
Application.Run "Solver.xlam!SolverAdd", "$L$4:$L$28", 3, "$D$4:
    $D$28"
' run the analysis
' SolverSolve( UserFinish, ShowRef)
result = Application.Run("Solver.xlam!SolverSolve", True)
' finish the analysis
' SolverFinish(KeepFinal, ReportArray, OutlineReports)
Application.Run "Solver.xlam!SolverFinish"
' report on success of analysis
' Result = 0, Solution found, optimality and constraints
    satisfied
' 1, Converged, constraints satisfied
' 2, Cannot improve, constraints satisfied
' 3, Stopped at maximum iterations
' 4, Solver did not converge

```

- ' 5, *No feasible solution*
- ' 6 *Solver stopped at user's request.*
- ' 7 *The conditions for Assume Linear Model are not satisfied*  
*.*
- ' 8 *The problem is too large for Solver to handle.*
- ' 9 *Solver encountered an error value in a target or*  
*constraint cell.*
- ' 10 *Stop chosen when maximum time limit was reached.*
- ' 11 *There is not enough memory available to solve the*  
*problem.*
- ' 12 *Another Excel instance is using SOLVER.DLL. Try again*  
*later.*
- ' 13 *Error in model. Please verify that all cells and*  
*constraints are valid.*
- ' 14 – *Solver found an integer solution within tolerance. All*  
*constraints are satisfied (14).*
- ' 15 – *Stop chosen when the maximum number of [integer or*  
*feasible] solutions was reached (15).*
- ' 16 – *Stop chosen when the maximum number of [integer]*  
*subproblems was reached (16).*
- ' 17 – *Solver converged in probability to a global solution*  
*(17).*
- ' 18 – *All variables must have both upper and lower bounds*  
*(18).*
- ' 19 – *Variable bounds conflict in binary or alldifferent*  
*constraint (19).*
- ' 20 – *Lower and upper bounds on variables allow no feasible*

*solution (20).*

**If** result = 14 **Or** result = 0 **Then**

*'Set InfoBox = CreateObject("WScript.Shell")*

*'Set the message box to close after 10 seconds*

*'CHKTime = 0.5*

*'Select Case InfoBox.Popup("Solver found a solution, Result #" +*

*+ CStr(Result), \_*

*'CHKTime, "SOLUTION FOUND", 0)*

*'  Case 1, -1*

*'End Select*

*'MsgBox "Solver found a solution, Result #" + CStr(Result),*

*vbInformation, "SOLUTION FOUND"*

GoTo REPORTING

**Else**

*'MsgBox "Solver was unable to find a solution, Result #" +*

*CStr(Result), vbExclamation, "SOLUTION NOT FOUND"*

*'Exit For*

GoTo ERRORFOR

**End If**

ERRORFOR:

Application.Wait (Now + 1E-05)

Worksheets("case2\_gen").Range("E6").Value = 1

Worksheets("case2\_gen").Range("J8").Value = 10

Application.Wait (Now + 1E-05)

Worksheets("case2\_gen").Activate

Application.Run "Solver.xlam!SolverReset"

Application.Run "Solver.xlam!SolverOk", "\$Q\$28", 2, , "\$J\$8,

```

    $E$6", 2, "GRG_Nonlinear"
Application.Run "Solver.xlam!SolverOptions", _
100000, 100000, 1E-12, False, False, _
2, 2, 1, 1, True, 1E-12, True, _
100, [], False, True, 0.075, 100000, _
100000, False, 30
Application.Run "Solver.xlam!SolverAdd", "$J$8", 4, 0
Application.Run "Solver.xlam!SolverAdd", "$E$6", 4, 0
Application.Run "Solver.xlam!SolverAdd", "$L$4:$L$28", 3, "
    $D$4:$D$28"
result = Application.Run("Solver.xlam!SolverSolve", True)
Application.Run "Solver.xlam!SolverFinish"
If result = 14 Or result = 0 Then
GoTo REPORTING
Else
GoTo ERRORFOR2
End If

```

ERRORFOR2:

```

Application.Wait (Now + 1E-05)
Worksheets("case2_gen").Range("E6").Value = 10
Worksheets("case2_gen").Range("J8").Value = 1
Application.Wait (Now + 1E-05)
Worksheets("case2_gen").Activate
Application.Run "Solver.xlam!SolverReset"
Application.Run "Solver.xlam!SolverOk", "$Q$28", 2, , "$J$8,
    $E$6", 2, "GRG_Nonlinear"
Application.Run "Solver.xlam!SolverOptions", _

```

```

100000, 100000, 1E-12, False, False, _
2, 2, 1, 1, True, 1E-12, True, _
100, [], False, True, 0.075, 100000, _
100000, False, 30
Application.Run "Solver.xlam!SolverAdd", "$J$8", 4, 0
Application.Run "Solver.xlam!SolverAdd", "$E$6", 4, 0
Application.Run "Solver.xlam!SolverAdd", "$L$4:$L$28", 3, "
    $D$4:$D$28"
result = Application.Run("Solver.xlam!SolverSolve", True)
Application.Run "Solver.xlam!SolverFinish"
If result = 14 Or result = 0 Then
GoTo REPORTING
Else
GoTo ERRORFOR3
End If

```

ERRORFOR3:

```

Application.Wait (Now + 1E-05)
Worksheets("case2_gen").Range("E6").Value = 1
Worksheets("case2_gen").Range("J8").Value = 100
Application.Wait (Now + 1E-05)
Worksheets("case2_gen").Activate
Application.Run "Solver.xlam!SolverReset"
Application.Run "Solver.xlam!SolverOk", "$Q$28", 2, , "$J$8,
    $E$6", 2, "GRG_Nonlinear"
Application.Run "Solver.xlam!SolverOptions", _
100000, 100000, 1E-12, False, False, _
2, 2, 1, 1, True, 1E-12, True, _

```

```

100, [], False, True, 0.075, 100000, _
100000, False, 30
Application.Run "Solver.xlam!SolverAdd", "$J$8", 4, 0
Application.Run "Solver.xlam!SolverAdd", "$E$6", 4, 0
Application.Run "Solver.xlam!SolverAdd", "$L$4:$L$28", 3, "
    $D$4:$D$28"
result = Application.Run("Solver.xlam!SolverSolve", True)
Application.Run "Solver.xlam!SolverFinish"
If result = 14 Or result = 0 Then
GoTo REPORTING
Else
GoTo ERRORFOR4
End If

```

ERRORFOR4:

```

Application.Wait (Now + 1E-05)
Worksheets("case2_gen").Range("E6").Value = 100
Worksheets("case2_gen").Range("J8").Value = 1
Application.Wait (Now + 1E-05)
Worksheets("case2_gen").Activate
Application.Run "Solver.xlam!SolverReset"
Application.Run "Solver.xlam!SolverOk", "$Q$28", 2, , "$J$8,
    $E$6", 2, "GRG_Nonlinear"
Application.Run "Solver.xlam!SolverOptions", _
100000, 100000, 1E-12, False, False, _
2, 2, 1, 1, True, 1E-12, True, _
100, [], False, True, 0.075, 100000, _
100000, False, 30

```

```

Application.Run "Solver.xlam!SolverAdd", "$J$8", 4, 0
Application.Run "Solver.xlam!SolverAdd", "$E$6", 4, 0
Application.Run "Solver.xlam!SolverAdd", "$L$4:$L$28", 3, "
    $D$4:$D$28"
result = Application.Run("Solver.xlam!SolverSolve", True)
Application.Run "Solver.xlam!SolverFinish"
If result = 14 Or result = 0 Then
GoTo REPORTING
Else
GoTo REPORTING
End If

```

REPORTING:

```

turbinerating = Worksheets("case2_gen").Range("Q4").Value
numberhouseholds = Worksheets("Solver_withoutbatteries").Range("
    G" & i + 2).Value
loopnum_double = CDBl(loopnum)
Application.Wait (Now + 1E-05)
Worksheets("DistanceCostCurves").Activate
'Keep track of cost curve, and add 1000$USD per 1 km of cabling,
per 24 kW of hydro (40A*600V)
If turbinerating > 24000 Then
    householdcost = Worksheets("case2_gen").Range("$Q$12").Value +
        (1000 * distance_at_min) * (turbinerating / 24000) /
        numberhouseholds
Else
    householdcost = Worksheets("case2_gen").Range("$Q$12").Value +
        (1000 * distance_at_min) / numberhouseholds

```

**End If**

Cells(i + 2, loopnum + 2).Value = householdcost

Cells(i + 2 + 17 + 1, loopnum + 2).Value = distance\_at\_min

**If** householdcost < householdcost\_minimum **Then**

householdcost\_minimum = householdcost

number\_generators\_minimum = Worksheets("case2\_gen").Range("\$E\$6").Value

number\_panels\_minimum = Worksheets("case2\_gen").Range("\$J\$8").Value

diff\_minimum = Worksheets("case2\_gen").Range("\$M\$31").Value

distance\_min = distance\_at\_min

lat\_min\_loc = row\_final

long\_min\_loc = column\_final

PV\_oversize = Worksheets("case2\_gen").Range("\$Q\$31").Value

Worksheets("FlowRates\_Q90").Activate

**For** j = -1 To 1

**For** k = -1 To 1

**If** (Round(Cells(row\_final + k, column\_final + j).Value, 0) < 1.1 \* Round(Cells(row\_final, column\_final).Value, 0) **And** \_

Round(Cells(row\_final + k, column\_final + j).Value, 0) > 0.9 \* Round(Cells(row\_final, column\_final).Value, 0)) **Then**

**If** (j = -1 **Or** (j = 0 **And** k = -1)) **Then**

River\_loc\_col\_pre = column\_final + j

River\_loc\_row\_pre = row\_final + k

River\_flow\_pre = Cells(row\_final + k, column\_final

```

        + j).Value
End If
If (j = 1 Or (j = 0 And k = 1)) Then
    River_loc_col_post = column_final + j
    River_loc_row_post = row_final + k
    River_flow_post = Cells(row_final + k,
        column_final + j).Value
End If
If River_loc_col_pre = 0 Or River_loc_col_post = 0
    Then
        If (k = -1 Or (k = 0 And j = -1)) Then
            River_loc_col_pre = column_final + j
            River_loc_row_pre = row_final + k
            River_flow_pre = Cells(row_final + k,
                column_final + j).Value
        End If
        If (k = 1 Or (k = 0 And j = 1)) Then
            River_loc_col_post = column_final + j
            River_loc_row_post = row_final + k
            River_flow_post = Cells(row_final + k,
                column_final + j).Value
        End If
    End If
End If
End If
Next k
Next j
'calculate dam at IST insertion location

```

```

Application.Wait (Now + 1E-05)
Worksheets("Elevations").Activate
Elevation_site = Cells(row_final, column_final)
Elevation_pre = Cells(River_loc_row_pre, River_loc_col_pre)
Elevation_post = Cells(River_loc_row_post, River_loc_col_post)
Application.Wait (Now + 1E-05)
Worksheets("Depths").Activate
Depth_site = Cells(row_final, column_final)
Depth_pre = Cells(River_loc_row_pre, River_loc_col_pre)
Depth_post = Cells(River_loc_row_post, River_loc_col_post)
Application.Wait (Now + 1E-05)
Worksheets("RiverVelocities_Q90").Activate
Velocity_site = Cells(row_final, column_final)
Velocity_pre = Cells(River_loc_row_pre, River_loc_col_pre)
Velocity_post = Cells(River_loc_row_post, River_loc_col_post)
Head_site = Elevation_site + Depth_site + 0.5 * Velocity_site *
    Velocity_site / 9.81
Head_pre = Elevation_pre + Depth_pre + 0.5 * Velocity_pre *
    Velocity_pre / 9.81
Head_post = Elevation_post + Depth_post + 0.5 * Velocity_post *
    Velocity_post / 9.81
Dam_potential_site = highestvalue * 998.2 * 9.81 * (
    WorksheetFunction.Max(Abs(Head_pre - Head_site), Abs(
    Head_site - Head_post)))
End If
Next loopnum
Application.Wait (Now + 1E-05)

```

```

Worksheets("Solver_withoutbatteries").Activate
Worksheets("Solver_withoutbatteries").Range("$H" & i + 2).Value
    = Worksheets("RiverVelocities_Q90").Cells(lat_min_loc ,
        long_min_loc).Value
If Worksheets("Solver_withoutbatteries").Range("H" & i + 2).
    Value > 2.8 Then
Worksheets("Solver_withoutbatteries").Range("I" & i + 2).Value =
    2.8
Else
Worksheets("Solver_withoutbatteries").Range("I" & i + 2).Value =
    Worksheets("Solver_withoutbatteries").Range("H" & i + 2).
    Value
End If
Worksheets("Solver_withoutbatteries").Range("$R" & i + 2).Value
    = Worksheets("RiverVelocities_Q90").Cells(lat_min_loc , 1).
    Value
Worksheets("Solver_withoutbatteries").Range("$S" & i + 2).Value
    = Worksheets("RiverVelocities_Q90").Cells(1 , long_min_loc).
    Value
Worksheets("Solver_withoutbatteries").Range("$T" & i + 2).Value
    = Worksheets("FlowRates_Q90").Cells(lat_min_loc , long_min_loc
    ).Value
Worksheets("Solver_withoutbatteries").Range("J" & i + 2).Value =
    householdcost_minimum
Worksheets("Solver_withoutbatteries").Range("K" & i + 2).Value =
    householdcost_minimum * numberhouseholds
Worksheets("Solver_withoutbatteries").Range("N" & i + 2).Value =

```

```

    number_generators_minimum
Worksheets("Solver_withoutbatteries").Range("O" & i + 2).Value =
    number_panels_minimum
Worksheets("Solver_withoutbatteries").Range("P" & i + 2).Value =
    diff_minimum
Worksheets("Solver_withoutbatteries").Range("Q" & i + 2).Value =
    result
Worksheets("Solver_withoutbatteries").Range("J" & i + 2).
    NumberFormat = "###,###,###,###"
Worksheets("Solver_withoutbatteries").Range("K" & i + 2).
    NumberFormat = "###,###,###,###"
Worksheets("Solver_withoutbatteries").Range("L" & i + 2).
    NumberFormat = "###,###,###,###"
Worksheets("Solver_withoutbatteries").Range("M" & i + 2).
    NumberFormat = "###,###,###,###"
Worksheets("Solver_withoutbatteries").Range("N" & i + 2).
    NumberFormat = "###,###,###,##0"
Worksheets("Solver_withoutbatteries").Range("O" & i + 2).
    NumberFormat = "###,###,###,##0"
Worksheets("Solver_withoutbatteries").Range("P" & i + 2).
    NumberFormat = "###,###,###,##0"
'output km away to place turbine
Worksheets("Solver_withoutbatteries").Range("U" & i + 2).Value =
    distance_min
Worksheets("Solver_withoutbatteries").Range("V" & i + 2).Value =
    Dam_potential_site
Worksheets("Solver_withoutbatteries").Range("W" & i + 2).Value =

```

PV\_oversize

**End Sub**

Credit for base solver structure from various sources:

- Peltier Tech: <https://peltiertech.com/Excel/SolverVBA.html>
- Microsoft: <https://docs.microsoft.com/en-us/office/vba/api/overview/>

## BIBLIOGRAPHY

## BIBLIOGRAPHY

- [1] Abril, Gwenaél, Frédéric Guérin, Sandrine Richard, Robert Delmas, Corinne Galy-Lacaux, Philippe Gosse, Alain Tremblay, Louis Varfalvy, Marco Aurelio Dos Santos & Bohdan Matvienko. 2005. Carbon dioxide and methane emissions and the carbon budget of a 10-year old tropical reservoir (petit saut, french guiana). *Global Biogeochemical Cycles* 19.
- [2] Agostinho, Carlos Sergio, Fernando Mayer Pelicice, Elineide Eugenio Marques, Anderson Brito Soares & Deusimar Augusto Alves de Almeida. 2011. All that goes up must come down? absence of downstream passage through a fish ladder in a large amazonian river. *Hydrobiologia* 675. 1–12.
- [3] Allan, Ronald N et al. 2013. *Reliability evaluation of power systems*. Springer Science & Business Media.
- [4] Amaral, Stephen, Daniel Giza & Paul Jacobson. 2014. Survival and behavior of fish interacting with hydrokinetic turbines. Tech. rep. Alden Laboratory.
- [5] Amaral, Stephen V., Sterling M. Watson, Abraham D. Schneider, Jenna Rackovan & Andrew Baumgartner. 2020. Improving survival: injury and mortality of fish struck by blades with slanted, blunt leading edges. *Journal of Ecohydraulics* 2470–5357.
- [6] Amaral, Steve. 2014. Turbines and fish: The status of fish-friendly hydropower turbines. Tech. rep. Alden Laboratory.
- [7] ANEEL. 2003. Energia hidraulica [www.aneel.gov.br/aplicacoes/atlas/energia\\_hidraulica/4\\_3.htm](http://www.aneel.gov.br/aplicacoes/atlas/energia_hidraulica/4_3.htm).
- [8] ANEEL. 2019. Relatórios de consumo e receita de distribuição. Tech. rep. ANEEL. <https://www.aneel.gov.br/relatorios-de-consumo-e-receita>.
- [9] ANEEL. 2019. Sigel. <https://sigel.aneel.gov.br/portal/home/index.html>.
- [10] Ansar, Atif, Bent Flyvbjerg, Alexander Budzier & Daniel Lunn. 2014. Should we build more large dams? the actual costs of 477 hydropower megaproject development. *Energy Policy* 69. 43–56.
- [11] Antonioli, Andriago Filippo, André M Nobre, Thomas Reindl & R RUTHER. 2014. A review on grid-connected pv systems in brazil including system performance. In *European photovoltaic solar energy conference (eu pvsec)*, 2747–2752.
- [12] Armaroli, Nicola & Vincenzo Balzani. 2007. The future of energy supply: challenges and opportunities. *Angewandte Chemie International Edition* 46(1-2). 52–66.
- [13] Bacellar, Atlas Augusto & Brigida R.P. Rocha. 2010. Wood-fuel biomass from the madeira river: A sustainable option for electricity production in the amazon region. *Energy Policy* 38. 5004–5012.

- [14] Bank, World. 2016. Pump price for diesel fuel used per liter. <https://data.worldbank.org/indicator/EP.PMP.DESL.CD?locations=BR>.
- [15] Baring-Gould, E. Ian, Corrie Christol, Al LiVecchi, Sharon Kramer & Anna West. 2016. A review of the environmental impacts for marine and hydrokinetic projects to inform regulatory permitting. Tech. rep. NREL.
- [16] Barroso, LA, F Porrua, MV Pereira & B Bezerra. 2009. Solving the major challenges in transmission asset investment in the competitive environment: The brazilian case. In *Power & energy society general meeting, 2009. pes'09. ieee*, 1–8. IEEE.
- [17] Barroso, Luiz Augusto, José Marcos Bressane, Luiz M Thomé, Max Junqueira, Ivan Camargo, Gerson Oliveira, Silvio Binato & Mario Veiga Pereira. 2004. Transmission structure in brazil: organization, evaluation and trends. In *Power engineering society general meeting, 2004. ieee*, 1301–1306. IEEE.
- [18] Barroso, Luiz Augusto, José Rosenblatt, André Guimarães, Bernardo Bezerra & Mario Veiga Pereira. 2006. Auctions of contracts and energy call options to ensure supply adequacy in the second stage of the brazilian power sector reform. In *Power engineering society general meeting, 2006. ieee*, 8–pp. IEEE.
- [19] seals (*Phoca vitulina*) around an operational tidal turbine in Strangford Narrows: No barrier effect but small changes in transit behaviour, Harbour. 2018. Carol sparling and mike lonergan and bernie mcconnell. *Aquatic Conservation: Marine Freshwater Ecosystems* 28. 194–204.
- [20] Benchimol, Maíra & Carlos A Peres. 2015. Widespread forest vertebrate extinctions induced by a mega hydroelectric dam in lowland amazonia. *PloS one* 10(7). e0129818.
- [21] Bevelhimer, Mark S., Z. Daniel Deng & Constantin Scherelis. 2016. Characterizing large river sounds: Providing context for understanding the environmental effects of noise produced by hydrokinetic turbine. *The Journal of the Acoustical Society of America* 139(1). 85–92.
- [22] Bilgili, Ozbek A. Sahin B., M. & A. Kahraman. 2015. An overview of renewable electric power capacity and progress in new technologies in the world. *Renewable and Sustainable Energy Reviews* 49(7). 323–334.
- [23] Billinton, R., C. L. Wee & G. Hamoud. 1982. Digital computer algorithms for the calculation of generating capacity reliability indices. *IEEE Power Eng. Rev.* PAS–101(1). 34–35.
- [24] Billinton, R. & C. Singh. 1971. Generating capacity reliability evaluation in interconnected systems using a frequency and duration approach part I. mathematical analysis. *IEEE Trans. Power App. Syst.* PAS-90(4). 1646–1654.
- [25] Billinton, Roy & Guang Bai. 2004. Generating capacity adequacy associated with wind energy. *IEEE transactions on energy conversion* 19(3). 641–646.

- [26] Billinton, Roy, Hua Chen & R Ghajar. 1996. A sequential simulation technique for adequacy evaluation of generating systems including wind energy. *IEEE Transactions on Energy Conversion* 11(4). 728–734.
- [27] Billinton, Roy & Yi Gao. 2008. Multistate wind energy conversion system models for adequacy assessment of generating systems incorporating wind energy. *IEEE Trans. on Energy Conv.* 23(1). 163–170.
- [28] Billinton, Roy & Rajesh Karki. 1999. Application of monte carlo simulation to generating system well-being analysis. *IEEE Transactions on Power systems* 14(3). 1172–1177.
- [29] Billinton, Roy & Wenyuan Li. 1994. Basic concepts of power system reliability evaluation. In *Reliability assessment of electric power systems using monte carlo methods*, 9–31. Springer.
- [30] Brazilian Electricity Regulatory Agency. 2018. Agência Nacional de Energia Elétrica–ANEEL. <http://www.aneel.gov.br/>.
- [31] Brown, Alan. 2019, <https://www.asme.org/topics-resources/content/fish-safe-turbines-empower-small-dam-hydro-projects>. Fish-safe turbines empower small-dam hydro projects.
- [32] Brown, Richard Steven. 2012. Quantifying mortal injury of juvenile chinook salmon exposed to simulated hydro turbine passage. *Transactions of the American Fisheries Society* 141. 147–157.
- [33] Bui, Samantha, Frode Oppedal, Øyvind J. Korsøen, Damien Sonny & Tim Dempster. 2013. Group behavioural responses of atlantic salmon (*salmosalar* l.) to light, infrasound and sound stimuli. *PLoS ONE* 8(5). e63696.
- [34] Čada, Glenn, Charles C. Coutant & Richard R Whitney. 1997. Development of biological criteria for the design of advanced hydropower turbines. Tech. rep. U.S. Department of Energy Idaho Operations Office.
- [35] Čada, Glenn, James Loar, Laura Garrison, Jr. Richerd Fisher & Duane Neitzel. 2006. Efforts to reduce mortality to hydroelectric turbine-passed fish: Locating and quantifying damaging shear stresses. *Environmental Management* 37(6). 898–906.
- [36] Čada, Glenn F. 2001. The development of advanced hydroelectric turbines to improve fish passage survival. Tech. rep. Oak Ridge National Laboratory.
- [37] CapeSharpTidal. 2015. <http://capesharptidal.com/faqs/>.
- [38] Castro-Diaz, Laura, Maria Claudia Lopez & Emilio Moran. 2018. Gender-differentiated impacts of the belo monte hydroelectricdam on downstream fishers in the brazilian amazon. *Human Ecology* 46. 411–422.
- [39] Cazzaniga, R, M Cicu, M Rosa-Clot, P Rosa-Clot, GM Tina & C Ventura. 2018. Floating photovoltaic plants: Performance analysis and design solutions. *Renewable and Sustainable Energy Reviews* 81. 1730–1741.

- [40] Charity, S., N. Dudley, D. Oliveira & S. Stolton (editors). 2016. Living amazon report 2016: A regional approach to conservation in the amazon. *WWF Living Amazon Initiative, Brasília and Quito* [http://d2ouvy59p0dg6k.cloudfront.net/downloads/wwf\\_living\\_amazon\\_\\_report\\_2016\\_mid\\_res\\_spreads.pdf](http://d2ouvy59p0dg6k.cloudfront.net/downloads/wwf_living_amazon__report_2016_mid_res_spreads.pdf).
- [41] Chaudhari, Suyog, Yadu Pokhrel, Emilio Moran & Gonzalo Miguez-Macho. 2019. Multi-decadal hydrologic change and variability in the amazon river basin: understanding the terrestrial water storage variations and drought characteristics. *Hydrology Earth System Sciences* 23. 2841–2862.
- [42] Chaurey, Akanksha & Tara Chandra Kandpal. 2010. Assessment and evaluation of pv based decentralized rural electrification: An overview. *Renewable and Sustainable Energy Reviews* 14(8). 2266–2278.
- [43] Copping, Andrea. 2018. The state of knowledge for environmental effects: Driving consenting/permitting for the marine renewable energy industry. Tech. rep. Pacific Northwest National Laboratory (PNNL).
- [44] Copping, Andrea, Luke Hanna, Brie Van Cleve, Kara Blake & Richard M. Anderson. 2015. Environmental risk evaluation system—an approach to ranking risk of ocean energy development on coastal and estuarine environments. *Estuaries and Coasts* 38(Suppl 1). S287–S302.
- [45] Coutant, Charles C. & Richary R. Whitney. 1997. Fish behavior in relation to modeling fish passage through hydropower turbines: A review. Tech. rep. Oak Ridge National Laboratory.
- [46] Deichmann, Uwe, Craig Meisner, Siobhan Murray & David Wheeler. 2011. The economics of renewable energy expansion in rural sub-saharan africa. *Energy Policy* 39. 215–227.
- [47] Deichmann, Uwe, Craig Meisner, Siobhan Murray & David Wheeler. 2011. The economics of renewable energy expansion in rural sub-saharan africa. *Energy Policy* 39. 215–227.
- [48] Emea, L. C., J. A. Ulasi, A. I. Alade Tunde & A. C. Odunze. 2019. Hydrokinetic turbines for power generation in nigerian river basins. *Water Practice and Technology* 14(1). 71–80.
- [49] Endrenyi, John. 1978. *Reliability modeling in electric power systems*. Wiley New York.
- [50] Engineering, Civil. 1991. Sound may steer fish clear of dam turbines. ProQuest.
- [51] EPE. 2019. Webmap epe. <https://gisepe.epe.gov.br/WebMapEPE/>.
- [52] EPRI. 2011. Evaluation of fish injury and mortality associated with hydrokinetic turbines. Tech. rep. Electric Power Research Institute.
- [53] EPRI. 2013. Epr workshop on emf and aquatic life. Tech. rep. Electric Power Research Institute.

- [54] EPRI. 2014. Evaluation of survival and behavior of fish exposed to an axial-flow hydrokinetic turbine. Tech. rep. Electric Power Research Institute.
- [55] (ESMAP), ENERGY SECTOR MANAGEMENT ASSISTANCE PROGRAMME. 2000. Reducing the cost of grid extension for rural electrification. Tech. rep. NRECA International, Ltd.
- [56] Esteves, Victor Paulo Pecanha, Elisa Maria Mano Esteves, Davi Jose Bungenstab, Daniel Gomes dos Santos Wendriner Loebmann, Daniel de Castro Victoria, Luiz Eduardo Vicente, Ofelia de Queiroz Fernandes Araujo & Claudia do Rosario Vaz Morgado. 2016. Land use change (luc) analysis and life cycle assessment (lca)of brazilian soybean biodiesel. *Clean Technology Environmental Policy* 18. 1655–1673.
- [57] Fargione, Joseph, Jason Hill, David Tilman, Stephen Polasky & Peter Hawthorne. 2008. Land clearing and the biofuel carbon debt. *Science* 319(5867). 1235–1238.
- [58] Fearnside, Philip M. 1997. Greenhouse-gas emissions from amazonian hydroelectric reservoirs: The example of brazil’s tucuruí dam as compared to fossil fuel alternatives. *Environmental conservation* 24(1). 64–75.
- [59] Fearnside, Philip M. 1997. Greenhouse gases from deforestation in brazilian amazonia: net committed emissions. *Climatic Change* 35(3). 321–360.
- [60] Fearnside, Philip M. 1999. Social impacts of brazil’s tucuruí dam. *Environmental Management* 24(4). 483–495.
- [61] Fearnside, Philip M. 1999. Social impacts of brazil’s tucuruí dam. *Environmental Management* 24(4). 483–495.
- [62] Fearnside, Philip M. 2005. Brazil’s samuel dam: Lessons for hydroelectric development policy and the environment in amazonia. *Environmental Management* 35(1). 1–19.
- [63] Fearnside, Philip M. 2013. Carbon credit for hydroelectric dams as a source of greenhouse-gas emissions: The example of brazil’s teles pires dam. *Mitigation and Adaptation Strategies for Global Change* 18(5). 691–699.
- [64] Fearnside, Philip M. 2014. Impacts of brazil’s madeira river dams: Unlearned lessons for hydroelectric development in amazonia. *Environmental Science and Policy* 38. 164–172.
- [65] Fearnside, Philip M. 2015. Emissions from tropical hydropower and the ipcc. *Environmental Science and Policy* 50. 225–239.
- [66] Fearnside, Philip M. 2015. Tropical hydropower in the clean development mechanism: Brazil’s santo antônio dam as an example of the need for change. *Climatic Change* 131(4). 575–589.
- [67] Ferguson, John W. 2007. Bypass system modification at the bonnevillie dam on the columbia river improved the survival of juvenile salmon. *Transactions of the American Fisheries Society* 136. 1487–1510.

- [68] Filhoa, Pedro Anselmo & Ossama Badr. 2004. Biomass resources for energy in north-eastern brazil. *Applied Energy* 77. 51–67.
- [69] Fox, Clive J., Steven Benjamins, Elizabeth A. Masden & Raeanne Miller. 2018. Challenges and opportunities in monitoring the impacts of tidal-stream energy devices on marine vertebrates. *Renewable and Sustainable Energy Reviews* 81. 1926–1938.
- [70] Fundacion Proteger, International Rivers & ECOA. 2019. Dams in amazonia. <http://dams-info.org/en>.
- [71] Galdino, Marco Antonio Esteves & Marta Maria de Almeida Olivieri. 2017. Some remarks about the deployment of floating pv systems in brazil. *J. Electr. Eng* 1. 10–19.
- [72] Garcia, Letícia Couto, Danilo Bandini Ribeiro, Fabio Oliveira Roque, Jose Manuel Ochoa-Quintero & William F Laurance. 2017. Brazil’s worst mining disaster: corporations must be compelled to pay the actual environmental costs. *Ecological applications* 27(1). 5–9.
- [73] Garrett, Chris & Patrick Cummins. 2007. The efficiency of a turbine in a tidal channel. *Journal of Fluid Mechanics* 588. 243–251.
- [74] Gibbs, Holly K & Martin Herold. 2007. Tropical deforestation and greenhouse gas emissions. *Environmental Research Letters* 2.
- [75] Gorban, Alexander N., Alexander M. Gorlov & Valentin M. Silantyev. 2001. Limits of the turbine efficiency for free fluid flow. *Journal of Energy Resources Technology* 123. 311–317.
- [76] Gorlov, Alexander. 2010. Helical turbine and fish safety.
- [77] Goswami, Anik, Paromita Sadhu, Utpal Goswami & Pradip Kumar Sadhu. 2019. Floating solar power plant for sustainable development: A techno-economic analysis. *Environmental Progress and Sustainable Energy* e13268.
- [78] Gurshin, Christopher W. D., Matthew P. Balge & Michael M. Taylor. 2014. Importance of ultrasonic field direction for guiding juvenile blueback herring past hydroelectric turbines. *North American Journal of Fisheries Management* 34. 1242–1258.
- [79] Hammar, Linus, Martin Gullström, Jimmy Ehnberg & Sverker Molander. 2013. Hydrokinetic turbine effects on fish swimming behavior. *PLoS ONE* 8(12). e84141.
- [80] Hastie, Gordon D., Debbie J. F. Russell, Paul Lepper, Jim Elliot, Ben Wilson, Steven Benjamins & Dave Thompson. 2018. Harbour seals avoid tidal turbine noise: Implications for collision risk. *Journal of Applied Ecology* 55. 684–693.
- [81] Hill, Craig, Jessica Kozarek, Fotis Sotiropoulos & Michele Guala. 2016. Hydrodynamics and sediment transport in a meandering channel with a model axial-flow hydrokinetic turbine. *Water Resources Research* 52. 860–879.

- [82] Hill, Craig, Mirko Musa, Leonardo P. Chamorro, Chris Ellis & Michele Guala. 2014. Local scour around a model hydrokinetic turbine in an erodible channel. *Journal of Hydraulic Engineering* 140(8).
- [83] Hogan, Timothy W., Glenn F. Cada & Stephen V. Amaral. 2014. The status of environmentally enhanced hydropower turbines. *Fisheries* 39(4). 164–172.
- [84] Holdermann, Claudius, Johannes Kissel & Jürgen Beigel. 2014. Distributed photovoltaic generation in Brazil: An economic viability analysis of small-scale photovoltaic systems in the residential and commercial sectors. *Energy Policy* 67. 612–617.
- [85] Huld, Thomas, Rapha Gottschalg, Hans Georg Beyer & Marko Topic. 2010. Mapping the performance of PV modules, effects of module type and data averaging. *Solar Energy* 84. 324–338.
- [86] IBGE. 2010. Downloads <https://www.ibge.gov.br/estatisticas-novoportal/downloads-estatisticas.html>.
- [87] IEA/NEA. 2010. Projected costs of generating electricity 2010 edition. Tech. rep. IEA/NEA.
- [88] IEEE Task Force. 1979. IEEE Reliability Test System. *IEEE Trans. Power App. Syst* PAS-98(6). 2047–2054.
- [89] J. F. Manwell, J. G. McGowan & A. L. Rogers. 2010. *Wind energy explained: theory, design and application*. John Wiley & Sons.
- [90] Jamieson, Peter M. 2009. Beating betz: Energy extraction limits in a constrained flow field. *Journal of Solar Energy Engineering* 131. 031008–1 – 031008–6.
- [91] Katezhnikova, Maria & Thomas M. Ravens. 2014. Hydraulic impacts of hydrokinetic devices. *Renewable Energy* 66. 425–432.
- [92] Kessler, Rebecca. 2014. Mimicking nature, new designs ease fish passage around dams. *Yale Environment* 360.
- [93] Khatod, Dheeraj Kumar, Vinay Pant & Jaydev Sharma. 2010. Analytical approach for well-being assessment of small autonomous power systems with solar and wind energy sources. *Energy Conversion, IEEE Transactions on* 25(2). 535–545.
- [94] Killgore, Jack K., Steve T. Maynard, Matthew D. Chan & Raymond P. Morgan II. 2011. Evaluation of propeller-induced mortality on early life stages of selected fish species. *North American Journal of Fisheries Management* 21(4). 947–955.
- [95] Killgore, Jack K., Andrew C. Miller & Kenneth C. Conley. 2011. Effects of turbulence on yolk-sac larvae of paddlefish. *Transactions of the American Fisheries Society* 116(4). 670–673.
- [96] Lasdon, Leon S., Richard L. Fox & Margery W. Ratner. 1973. Nonlinear optimization using the generalized reduced gradient method. Tech. rep. Office of Naval Research.

- [97] Lasdon, Leon S., A. D. Waren, A. Jain & Margery W. Ratner. 1978. Design and testing of a generalized reduced gradient code for nonlinear programming. *ACM Transactions on Mathematical Software* 4(1). 34–50.
- [98] Laurance, William F, Anna Peletier-Jellema, Bart Geenen, Harko Koster, Pita Verweij, Pitou Van Dijck, Thomas E Lovejoy, Judith Schleicher & Marijke Van Kuijk. 2015. Reducing the global environmental impacts of rapid infrastructure expansion. *Current Biology* 25(7). R259–R262.
- [99] Levin, Todd & Valerie M. Thomas. 2016. Can developing countries leapfrog the centralized electrification paradigm? *Energy for Sustainable Development* 31. 97–107.
- [100] Magrin, GO, JA Marengo, JP Boulanger, MS Buckeridge, E Castellanos, G Poveda et al. 2014. Central and south america in climate change 2014: Impacts, adaptation, and vulnerability. *Part B: Regional Aspects. Contribution of Working Group II to the Fifth Assessment Report of the Intergovernmental Panel of Climate Change (eds. Barros, VR et al.)* 1499–1566.
- [101] Malinka, Chloe E., Douglas M. Gillespie, Jamie D. J. Macaulay, Ruth Joy & Carol E. Sparling. 2018. First in situ passive acoustic monitoring for marine mammals during operation of a tidal turbine in ramsey sound, wales. *Marine Ecology Progress Series* 590. 247–266.
- [102] Manwell, James, Jon McGowan & Anthony Rogers. 2009. *Wind energy explained : theory, design, and application*, vol. 2nd ed. ISBN 978-0-470-01500-1. John Wiley and Sons Ltd.
- [103] Martins, Fernando Ramos, R R  ther, Enio Bueno Pereira & SL Abreu. 2008. Solar energy scenarios in brazil. part two: Photovoltaics applications. *Energy Policy* 36(8). 2865–2877.
- [104] Masson, G. & I. Kaizuka. 2019. The international energy agency (IEA).
- [105] Mirzaei, Perham A. 2016. Development of a fish leaping framework for low-head barriers. *Journal of Hydro-Environment Research* 14. 34–43.
- [106] Mitra, J & C Singh. 1999. Pruning and simulation for determination of frequency and duration indices of composite power systems. *Power Systems, IEEE Transactions on* 14(3). 899–905.
- [107] Miyamoto, Robert T. 1989. Underwater noise generated by columbia river hydroelectric dams. *The Journal of the Acoustical Society of America* 85. S127.
- [108] MJ2. 2018, <http://www.vlh-turbine.com/products/vlh-turbine/>. Vlh turbine fish friendly.
- [109] MJ2. 2018, <http://www.vlh-turbine.com/products/vlh-turbine/fish-friendliness/>. Fish friendliness.

- [110] Moran, Emilio F, Maria Claudia Lopez, Nathan Moore, Norbert Müller & David W Hyndman. 2018. Sustainable hydropower in the 21st century. *Proceedings of the National Academy of Sciences* 115(47). 11891–11898.
- [111] NASA. 2019. Power. <https://power.larc.nasa.gov/>.
- [112] Neitzel, D. A., D. D. Dauble, G. F. Čada, M. C. Richmond, G. R. Guensch, R. P. Mueller, C. S. Abernathy & Brett Amidan. 2004. Survival estimates for juvenile fish subjected to a laboratory-generated shear environment. *Transactions of the American Fisheries Society* 133. 447–454.
- [113] Nestler, John M. 1992. Responses of blueback herring to high-frequency sound and implications for reducing entrainment at hydropower dams. *North American Journal of Fisheries Management* 12(4). 667–683.
- [114] Neto, MR Borges, PCM Carvalho, JOB Carioca & FJF Canafístula. 2010. Biogas/photovoltaic hybrid power system for decentralized energy supply of rural areas. *Energy Policy* 38(8). 4497–4506.
- [115] Nobre, Carlos A., Gilvan Sampaio, Laura S. Borma, Juan Carlos Castilla-Rubio, José S. Silva & Manoel Cardoso. 2016. Land-use and climate change risks in the amazon and the need of a novel sustainable development paradigm. *PNAS* 113(39). 10759–10768.
- [116] Nobre, Carlos A, Gilvan Sampaio, Laura S Borma, Juan Carlos Castilla-Rubio, José S Silva & Manoel Cardoso. 2016. Land-use and climate change risks in the amazon and the need of a novel sustainable development paradigm. *Proceedings of the National Academy of Sciences* 113(39). 10759–10768.
- [117] Noonan, Michael J. 2012. A quantitative assessment of fish passage efficiency. *Fish and Fisheries* 13. 450–464.
- [118] Odeh, Mufeed. 1999. A summary of environmentally friendly turbine design concepts. Tech. rep. U.S. Department of Energy Idaho Operations Office.
- [119] Odeh, Mufeed. 2011. Facilitating fish passage at ultra low head dams: An alternative to dam removal. Extended abstract only World Water Congress.
- [120] Oertel, Cornelius, Jörg Matschullata, Kamal Zurba, Frank Zimmermann & Stefan Erasmib. 2016. Greenhouse gas emissions from soils - a review. *Chemie der Erde* 76. 327–352.
- [121] Oliveira-Pinto, Sara & Jasper Stokkermans. 2020. Assessment of the potential of different floating solar technologies—overview and analysis of different case studies. *Energy Conversion and Management* 211. 112–747.
- [122] ONS. 2016. Par 2017-2019 plano de ampliações e reforços nas instalações de transmissão do sin. Tech. rep. ONS.
- [123] ONS. 2018. Balanco de energia .

- [124] ONS. 2018. Histórico da operação. <http://www.ons.org.br/paginas/resultados-da-operacao/historico-da-operacao>.
- [125] ONS. 2018. Mapas <http://ons.org.br/paginas/sobre-o-sin/mapas>.
- [126] ONS. 2018. O sistema em numeros <http://ons.org.br/paginas/sobre-o-sin/o-sistema-em-numeros>.
- [127] ONS. 2018. Par/pel executivo 2019-2023. Tech. rep. ONS.
- [128] ONS. 2018. Sistemas isolados <http://ons.org.br/paginas/sobre-o-sin/sistemas-isolados>.
- [129] ONS. 2019. Par/pel executivo 2020-2024. Tech. rep. ONS.
- [130] Operator of the National Electricity System. 2018. Operator of the national electricity system. <http://www.ons.org.br>.
- [131] Orchard, Bryan. 2011, <http://www.renewableenergyfocus.com/view/16785/case-study-river-turbines-provide-ecologically-acceptable-power/>. Case study: river turbines provide ecologically acceptable power. Renewable Energy Focus.
- [132] Pangala, Sunitha R., Alex Enrich-Prast, Luana S. Basso, Roberta Bittencourt Peixoto, David Bastviken, Edward R. C. Hornibrook, Luciana V. Gatti, Humberto Marotta, Luana Silva Braucks Calazans, cassia Mônica Sakuragui, Wanderley Rodrigues Bastos, Olaf Malm, Emanuel Gloor, John Bharat Miller & Vincent Gauci. 2017. Large emissions from floodplain trees close the amazon methane budget. *Nature* 552. 230–234.
- [133] Parshall, Lily, Dana Pillai, Shashank Mohan, Aly Sanoh & Vijay Modib. 2009. National electricity planning in settings with low pre-existing grid coverage: development of a spatial model and case study of kenya. *Energy Policy* 37. 2395–2410.
- [134] Pelc, Robin & Rod M. Fujita. 2002. Renewable energy from the ocean. *Marine Policy* 26. 471–479.
- [135] Petheram, C & T.A. McMahon. 2019. Dams, dam costs and damnable overruns. *Journal of Hydrology X* 3.
- [136] Pfenninger, Stefan & Iain Staffell. 2016. Long-term patterns of european pv output using 30 years of validated hourly reanalysis and satellite data. *Energy* 114. 1251–1256.
- [137] Pimentel Da Silva, Gardenio Diogo, Alessandra Magrini & David Alves Castelo Branco. 2020. A multicriteria proposal for large-scale solar photovoltaic impact assessment. *Impact Assessment and Project Appraisal* 38(1). 3–15.
- [138] Pine, Matthew K., Andrew G. Jeffs & Craig A. Radford. 2012. Turbine sound may influence the metamorphosis behaviour of estuarine crab megalopae. *PLoS ONE* 7(12).
- [139] Pine, Matthew K., Andrew G. Jeffs & Craig A. Radford. 2014. The cumulative effect on sound levels from multiple underwater anthropogenic sound sources in shallow coastal waters. *Journal of Applied Ecology* 51. 23–30.

- [140] Popper, Arthur N. & Thomas J. Carlson. 2011. Application of sound and other stimuli to control fish behavior. *Transactions of the American Fisheries Society* 127(5). 673–707.
- [141] Power, Northwest & Conservation Council. 2019. Fish passage at dams. <https://www.nwcouncil.org/>.
- [142] Powers, Patrick, Thomas Bumstead & John Orsborn. 1984. New concepts in fish ladder design, volume iii of iv; assessment of fishway development and design. 1982-1984 Final Report Project No. 198201400 BPA Report DOE/BP-36523-4.
- [143] Pracheil, Brenda M., C. R. DeRolph, M. P. Schramm & M. S. Bevelhimer. 2016. A fish-eye view of riverine hydropower systems: the current understanding of the biological response to turbine passage. *Reviews in Fish Biology and Fisheries* 26. 153–167.
- [144] Quintas, Marlus C., Claudio J. C. Blanco & Andre L. Amarante Mesquita. 2012. Analysis of two schemes using micro hydroelectric power (mhps) in the amazon with environmental sustainability and energy and economic feasibility. *Environment, Development and Sustainability* 14. 283–295.
- [145] Ranjbaran, Parisa, Hossein Yousefi, GB Gharehpetian & Fatemeh Razi Astarai. 2019. A review on floating photovoltaic (FPV) power generation units. *Renewable and Sustainable Energy Reviews* 110. 332–347.
- [146] Rei, Andrea M & Marcus Theodor Schilling. 2008. Reliability assessment of the brazilian power system using enumeration and monte carlo. *IEEE Transactions on Power Systems* 23(3). 1480–1487.
- [147] renewables ninja . 2018. Global solar and wind energy estimator. <https://www.renewables.ninja/>.
- [148] Richey, Jeffrey E., John M. Melack, Anthony K. Aufdenkampe, Victoria M. Ballester & Laura L. Hess. 2002. Outgassing from amazonian rivers and wetlands as a large tropical source of atmospheric co2. *Nature* 416. 617–620.
- [149] Richmond, Marshall C., John A. Serkowski, Laurie L. Ebner, Mirjam Sick, Richard S. Brown & Thomas J. Carlson. 2014. Quantifying barotrauma risk to juvenile fish during hydro-turbine passage. *Fisheries Research* 154. 152–164.
- [150] Robb, Drew. 2011. Hydro’s fish friendly turbines. *Renewable Energy Focus*.
- [151] Rodrigues, Italo Sampaio, Geraldo Luis Bezerra Ramalho & Pedro Henrique Augusto Medeiros. 2020. Potential of floating photovoltaic plant in a tropical reservoir in brazil. *Journal of Environmental Planning and Management* 1–24.
- [152] Rosa-Clot, Marco, Giuseppe Marco Tina & Sandro Nizetic. 2017. Floating photovoltaic plants and wastewater basins: an australian project. *Energy Procedia* 134. 664–674.

- [153] R  ther, Ricardo & MM Dacoregio. 2000. Performance assessment of a 2 kwp grid-connected, building-integrated, amorphous silicon photovoltaic installation in brazil. *Progress in Photovoltaics: Research and Applications* 8(2). 257–266.
- [154] Sahu, Alok, Neha Yadav & K Sudhakar. 2016. Floating photovoltaic power plant: A review. *Renewable and Sustainable Energy Reviews* 66. 815–824.
- [155] Sanoh, Aly, Lily Parshall, Ousmane Fall Sarr, Susan Kum & Vijay Modi. 2012. Local and national electricity planning in senegal: Scenarios and policies. *Energy for Sustainable Development* 16. 13–25.
- [156] Schilling, M Th, AM Leite Da Silva, Roy Billinton & MA El-Kady. 1990. Bibliography on power system probabilistic analysis (1962-88). *IEEE Transactions on Power Systems* 5(1). 1–11.
- [157] Schilling, M Th, JCG Praca, JF De Queiroz, C Singh & H Ascher. 1988. Detection of ageing in the reliability analysis of thermal generators. *IEEE transactions on power systems* 3(2). 490–499.
- [158] Schilling, Marcus Theodor, Julio Cesar Stacchini de Souza & Milton Brown Do Coutto Filho. 2008. Power system probabilistic reliability assessment: Current procedures in brazil. *IEEE Transactions on Power Systems* 23(3). 868–876.
- [159] Schilt, Carl R. 2007. Developing fish passage and protection at hydropower dams. *Applied Animal Behaviour Science* 104. 295–325.
- [160] Schmutz, Stefan & Carina Mielach. 2013. Measures for ensuring fish migration at transversal structures. Tech. rep. ICPDR – International Commission for the Protection of the Danube River.
- [161] Schneider, A.W., J. Raksany, R.O. Gunderson, C.C. Fong, R. Billington, P.M. O’Neill & B. Silverstein. 1989. Bulk system reliability-measurement and indices. *IEEE Transactions on Power Systems* 4(3). 829–835.
- [162] Schramm, Michael P., Mark Bevelhimer & Constantin Scherelis. 2017. Effects of hydrokinetic turbine sound on the behavior of four species of fish within an experimental mesocosm. *Fisheries Research* 190. 1–14.
- [163] Schweizer, Peter E. 2011. Estimation of the risks of collision or strike to freshwater aquatic organisms resulting from operation of instream hydrokinetic turbines. Tech. rep. Oak Ridge National Laboratory.
- [164] SERIS. 2018. Where sun meets water floating solar market report. Tech. rep. World Bank Group and ESMAP and SERIS.
- [165] da Silva, Armando M. Leite, Reinaldo A.G. Fern  ndez & Chanan Singh. 2010. Generating capacity reliability evaluation based on monte carlo simulation and cross-entropy methods. *IEEE Transactions on Power Systems* 25(1). 129–137.

- [166] da Silva, Armando M Leite, Muriell R. Freire, Fernando A Assis & Luiz AF Manso. 2016. Transmission expansion planning based on relaxed n-1 criteria and reliability indices. In *2016 international conference on probabilistic methods applied to power systems (pmaps)*, 1–6. IEEE.
- [167] da Silva, Rodrigo Corrêa, Ismael de Marchi Neto & Stephan Silva Seifert. 2016. Electricity supply security and the future role of renewable energy sources in brazil. *Renewable and Sustainable Energy Reviews* 59. 328–341.
- [168] Silva, Sergio B, Marco AG De Oliveira & Mauro M Severino. 2010. Economic evaluation and optimization of a photovoltaic–fuel cell–batteries hybrid system for use in the brazilian amazon. *Energy Policy* 38(11). 6713–6723.
- [169] da Silva Soito, João Leonardo & Marcos Aurélio Vasconcelos Freitas. 2011. Amazon and the expansion of hydropower in brazil: Vulnerability, impacts and possibilities for adaptation to global climate change. *Renewable and Sustainable Energy Reviews* 15(6). 3165–3177.
- [170] Silvério, Naidion Motta, Regina Mambeli Barros, Geraldo Lúcio Tiago Filho, Miguel Redón-Santafé, Ivan Felipe Silva dos Santos & Victor Eduardo de Mello Valério. 2018. Use of floating PV plants for coordinated operation with hydropower plants: Case study of the hydroelectric plants of the são francisco river basin. *Energy Conversion and Management* 171. 339–349.
- [171] Singh, C & A Lago-Gonzalez. 1985. Reliability modeling of generation systems including unconventional energy sources. *IEEE Transactions on Power Apparatus and Systems* (5). 1049–1056.
- [172] Slabbekoorn, Hans, Niels Bouton, Ilse von Opzeeland, Aukje Coers, Carel ten Cate & Arthur N. Popper. 2010. A noisy spring: the impact of globally rising underwater sound levels on fish. *Trends in Ecology and Evolution* 25. 419–427.
- [173] SmartHydro. 2019. Smart prices and products overview. <https://www.smart-hydro.de/renewable-energy-systems/prices-hydrokinetic-photovoltaic/>.
- [174] Smith, David L., R. Andrew Goodwin & John M. Nestler. 2014. Relating turbulence and fish habitat: A new approach for management and research. *Reviews in Fisheries Science and Aquaculture* .
- [175] Spencer, Robert Sterling, Jordan Macknick, Alexandra Aznar, Adam Warren & Matthew O Reese. 2018. Floating pv: Assessing the technical potential of photovoltaic systems on man-made water bodies in the continental us. *Environmental science & technology* .
- [176] St. Louis, Vincent L, Carol A Kelly, Éric Duchemin, John WM Rudd & David M Rosenberg. 2000. Reservoir surfaces as sources of greenhouse gases to the atmosphere: A global estimate: Reservoirs are sources of greenhouse gases to the atmosphere, and their surface areas have increased to the point where they should be included in global

- inventories of anthropogenic emissions of greenhouse gases. *AIBS Bulletin* 50(9). 766–775.
- [177] Sternberg, Rolf. 2008. Hydropower: dimensions of social and environmental coexistence. *Renewable and Sustainable Energy Reviews* 12(6). 1588–1621.
- [178] Stickler, Claudia M, Michael T Coe, Marcos H Costa, Daniel C Nepstad, David G McGrath, Livia CP Dias, Hermann O Rodrigues & Britaldo S Soares-Filho. 2013. Dependence of hydropower energy generation on forests in the amazon basin at local and regional scales. *Proceedings of the National Academy of Sciences* 110(23). 9601–9606.
- [179] Stiubiener, Uri, Thadeu Carneiro da Silva, Federico Bernardino Morante Trigoso, Ricardo da Silva Benedito & Julio Carlos Teixeira. 2020. PV power generation on hydro dam’s reservoirs in Brazil: A way to improve operational flexibility. *Renewable Energy* .
- [180] Stokes, PM & C. D. Wren. 1987. Bioaccumulation of mercury by aquatic biota in hydroelectric reservoirs: a review and consideration of mechanisms. *Lead, mercury, cadmium and arsenic in the environment* 255–257.
- [181] Sulaeman, Samer, Mohammed Benidris, Joydeep Mitra & Chanan Singh. 2017. A wind farm reliability model considering both wind variability and turbine forced outages. *IEEE Transactions on Sustainable Energy* 8(2). 629–637.
- [182] Trumbo, Bradley A., Martin L. Ahmann, Jon F. Renholds, Richard S. Brown, Alison H. Colotelo & Z. D. Deng. 2014. Improving hydroturbine pressures to enhance salmon passage survival and recovery. *Reviews in Fish Biology and Fisheries* 24. 955–965.
- [183] Turbulent. 2019. Technology. <https://www.turbulent.be/technology>.
- [184] Vennell, Ross. 2015. Designing large arrays of tidal turbines: A synthesis and review. *Renewable and Sustainable Energy Reviews* 41. 454–472.
- [185] Viehman, Haley A. & Gayle Barbin Zydlewski. 2015. Fish interaction with a commercial-scale tidal energy device in the natural environment. *Estuaries and Coasts* 38(Suppl 1). S241–S252.
- [186] Vision, Wind. 2015. A new era for wind power in the united states. *US Department of Energy* .
- [187] Vowles, Andrew S., James J. Anderson, Michael H. Gessel, John G. Williams & Paul S. Kemp. 2014. Effects of avoidance behavior on downstream fish passage through areas of accelerating flow when light and dark. *Animal Behavior* 92. 101–109.
- [188] Waldman, John. 2013. Blocked migration: Fish ladders on u.s. dams are not effective. *Yale Environment* 360.
- [189] WaybackMachine. 2018. Dams in amazonia. <https://web.archive.org/web/20181230133801/https://dams-info.org/en>.

- [190] Weston, Eve. 2019, <https://www.ge.com/news/reports/go-with-the-flow-these-engineers-are-building-a-fish-friendly-hydropower-plant>. Go with the flow: These engineers are building a fish-friendly hydropower plant.
- [191] Williams, J.G. 2012. Thinking like a fish: a key ingredient for development of effective fish passage facilities at river obstructions. *River Research and Applications* 28. 407–417.
- [192] Wilson, B., R. S. Batty, F. Daunt & C. Carter. 2007. Collision risks between marine renewable energy devices and mammals, fish and diving birds. *Report to the Scottish Executive*. .
- [193] World Bank Group. 2018. Solar and wind resource maps and data. <http://solargis.com/maps-and-gis-data/download/brazil/>.
- [194] World Bank Group, ESMAP and SERIS. 2018. Where sun meets water: Floating solar market report–executive summary.
- [195] worldatlas. 2019. The world’s tallest dams. <https://www.worldatlas.com/>.
- [196] Yadav, Neha, Manju Gupta & K Sudhakar. 2016. Energy assessment of floating photovoltaic system. In *Electrical power and energy systems (icepes), international conference on*, 264–269. IEEE.
- [197] Yale. 2018. The amazon basin forest <https://globalforestatlas.yale.edu/region/amazon>.
- [198] Zangiabadi, E., I. Masters, Alison J. Williams, T. N. Croft, R. Malki, N. Edmunds, A. Mason-Jones & I. Horsfall. 2017. Computational prediction of pressure change in the vicinity of tidal stream turbines and the consequences for fish survival rate. *Renewable Energy* 101. 1141–1156.
- [199] Zhang, Junbo, Daisuke Kitazawa, Sayuri Taya & Yoichi Mizukami. 2017. Impact assessment of marine current turbines on fish behavior using an experimental approach based on the similarity law. *Journal of Marine Science and Technology* 22. 219–230.
- [200] Zhou, Yanlai, Fi-John Chang, Li-Chiu Chang, Wei-De Lee, Angela Huang, Chong-Yu Xu & Shenglian Guo. 2020. An advanced complementary scheme of floating photovoltaic and hydropower generation flourishing water-food-energy nexus synergies. *Applied Energy* 275. 115389.